การปรับปรุงคุณภาพน้ำมันชีวภาพโดยการเร่งปฏิกิริยาจากการไพโรไลซิสอย่างรวดเร็วของกากสบู่ดำ
โดยเครื่อง PY-GC/MS และเครื่องปฏิกรณ์แบบปล่อยหล่น

นางสาวปรางค์ทิพย์ แก้วเพ็งกรอ

วิทยานิพนธ์นี้เป็นส่วนหนึ่งของการศึกษาตามหลักสูตรปริญญาวิศวกรรมศาสตรดุษฎีบัณฑิต
สาขาวิชาวิศวกรรมสิ่งแวดล้อม ภาควิชาวิศวกรรมสิ่งแวดล้อม
คณะวิศวกรรมศาสตร์ จุฬาลงกรณ์มหาวิทยาลัย
ปีการศึกษา 2559

CATALYTIC UPGRADING BIO-OILS FROM FAST PYROLYSIS OF JATROPHA RESIDUE USING
PY-GC/MS AND DROP TUBE PYROLYZER

Miss Prangtip Kaewpengkrow

A Dissertation Submitted in Partial Fulfillment of the Requirements

for the Degree of Doctor of Philosophy Program in Environmental Engineering

Department of Environmental Engineering

Faculty of Engineering

Chulalongkorn University

Academic Year 2016

| | |
|---|---|
| Thesis Title | CATALYTIC UPGRADING BIO-OILS FROM FAST PYROLYSIS OF JATROPHA RESIDUE USING PY-GC/MS AND DROP TUBE PYROLYZER |
| By | Miss Prangtip Kaewpengkrow |
| Field of Study | Environmental Engineering |
| Thesis Advisor | Associate Professor Dr.Viboon Sricharoenchaikul |
| Thesis Co-Advisor | Dr. Duangduen Atong |

Accepted by the Faculty of Engineering, Chulalongkorn University in Partial Fulfillment of the Requirements for the Doctoral Degree

⋯⋯⋯⋯⋯⋯⋯⋯⋯⋯⋯⋯⋯Dean of the Faculty of Engineering

(Associate Professor Dr.Supot Teachavorasinskun)

THESIS COMMITTEE

⋯⋯⋯⋯⋯⋯⋯⋯⋯⋯⋯⋯⋯Chairman

(Associate Professor Dr. Sirima Panyametheekul)

⋯⋯⋯⋯⋯⋯⋯⋯⋯⋯⋯⋯⋯Thesis Advisor

(Associate Professor Dr.Viboon Sricharoenchaikul)

⋯⋯⋯⋯⋯⋯⋯⋯⋯⋯⋯⋯⋯Thesis Co-Advisor

(Dr. Duangduen Atong)

⋯⋯⋯⋯⋯⋯⋯⋯⋯⋯⋯⋯⋯Examiner

(Assistant Professor Dr. Manaskorn Rachakornkij)

⋯⋯⋯⋯⋯⋯⋯⋯⋯⋯⋯⋯⋯Examiner

(Assistant Professor Dr.Pichaya Rachdawong)

⋯⋯⋯⋯⋯⋯⋯⋯⋯⋯⋯⋯⋯External Examiner

(Dr. Supawan Vichaphund)

ปรางค์ทิพย์ แก้วเพ็งกรอ : การปรับปรุงคุณภาพน้ำมันชีวภาพโดยการเร่งปฏิกิริยาจากการ
ไพโรไลซิสอย่างรวดเร็วของกากสบู่ดำโดยเครื่อง PY-GC/MS และเครื่องปฏิกรณ์แบบปล่อย
หล่น (CATALYTIC UPGRADING BIO-OILS FROM FAST PYROLYSIS OF JATROPHA
RESIDUE USING PY-GC/MS AND DROP TUBE PYROLYZER) อ.ที่ปรึกษาวิทยานิพนธ์
หลัก: รศ. ดร.วิบูลย์ ศรีเจริญชัยกุล, อ.ที่ปรึกษาวิทยานิพนธ์ร่วม: ดร. ดวงเดือน อาจองค์,
297 หน้า.

งานวิจัยนี้ทำการศึกษาผลของการใช้ตัวเร่งปฏิกิริยาต่อผลผลิตและคุณภาพของน้ำมัน
ชีวภาพจากการไพโรไลซิสอย่างรวดเร็วของกากสบู่ดำที่อุณหภูมิ 400-700 °C โดยทำการทดลอง
เปรียบเทียบในเครื่องปฏิกรณ์สองเครื่องคือ Py-GC/MS (µg-scale) และเตาปฏิกรณ์แบบท่อปล่อย
หล่น (g-scale) ในการศึกษาการไพโรไลซิสด้วยเครื่อง Py-GC/MS โดยใช้ตัวเร่งปฏิกิริยาโลหะ (Ni
หรือ Pd) 5% โดยน้ำหนัก บนตัวรองรับอะลูมินา ($Al_2O_3$) และตัวรองรับคาร์บอน (Ac) พบว่าสามารถ
ปรับปรุงไอผลิตภัณฑ์ของสารประกอบ มีการเร่งปฏิกิริยาและมีความสามารถในการคัดเลือกสารที่
ต้องการสูงกว่าตัวรองรับเซรามิกอื่นๆอีก 3 กลุ่ม ($ZrO_2$, $TiO_2$ (rutile) และ $TiO_2$ (anatase)) ดังนั้น
ตัวเร่งปฏิกิริยา $Al_2O_3$ และ Ac จึงเหมาะสมสำหรับศึกษาการไพโรไลซิสอย่างรวดเร็วต่อไปด้วยเตา
ปฏิกรณ์ขนาดใหญ่แบบท่อปล่อยหล่น โดยจากการไพโรไลซิสกากสบู่ดำขนาด 0.125-0.425 mm ที่
อุณหภูมิ 600 °C ด้วยตัวเร่งปฏิกิริยา Ac ทำให้ได้ปริมาณน้ำมันสูงถึง 39% โดยน้ำหนัก ในขณะที่
ตัวเร่งปฏิกิริยา Ni/Ac ทำให้ได้น้ำมันชีวภาพที่มีค่าความร้อนสูงถึง 29.20 MJ/kg และค่า pH เท่ากับ
6.78 จากการวิเคราะห์การกระจายตัวของผลิตภัณฑ์น้ำมันชีวภาพโดยใช้ GC-MS พบว่าผลิตภัณฑ์
หลัก ได้แก่ ฟีนอล อะโรมาติกส์และไฮโดรคาร์บอนที่เพิ่มขึ้นจาก 39 % เป็น 50-65% (% พื้นที่ใต้
กราฟ) โดยตัวเร่งปฏิกิริยา Ni/Ac และ Pd/Ac น้ำมันชีวภาพที่ได้มีสารประกอบออกซิเจนที่ต่ำ
สารประกอบไฮโดรคาร์บอนและอะโรมาติกส์สูงซึ่งเป็นคุณสมบัติที่ต้องการสำหรับการไพโรไลซิสจาก
กากสบู่ดำ จากผลการทดลองพบว่าน้ำมันชีวภาพที่สภาวะที่เหมาะสมสามารถนำไปใช้เป็นเชื้อเพลิง
ชีวภาพได้ นอกจากนี้ยังศึกษาพัฒนาแบบจำลองเพื่อทำนายสารระเหยในรูปของน้ำมันทาร์ แก๊สเบา
ต่างๆ และถ่านชาร์จากการไพโรไลซิสสบู่ดำโดยใช้แบบจำลอง CFD ผลการทำนายเปรียบเทียบกับ
การทดลองในแง่ของเปอร์เซนต์ความเบี่ยงเบนพบว่าสัดส่วนของแก๊ส ของเหลว (bio-oil) และของแข็ง
(char) มีค่าอยู่ในช่วง 6.67-28.9%, 0.26-11.26% และ 16.67-24.59% ตามลำดับ

| | | | |
|---|---|---|---|
| ภาควิชา | วิศวกรรมสิ่งแวดล้อม | ลายมือชื่อนิสิต | ................................ |
| สาขาวิชา | วิศวกรรมสิ่งแวดล้อม | ลายมือชื่อ อ.ที่ปรึกษาหลัก | ................................ |
| ปีการศึกษา | 2559 | ลายมือชื่อ อ.ที่ปรึกษาร่วม | ................................ |

# # 5571413021 : MAJOR ENVIRONMENTAL ENGINEERING

KEYWORDS: BIO-OIL, CATALYTIC, JATROPHA WASTES, FAST PYROLYSIS, METAL-CATALYSTS

PRANGTIP KAEWPENGKROW: CATALYTIC UPGRADING BIO-OILS FROM FAST PYROLYSIS OF JATROPHA RESIDUE USING PY-GC/MS AND DROP TUBE PYROLYZER. ADVISOR: ASSOC. PROF. DR.VIBOON SRICHAROENCHAIKUL, CO-ADVISOR: DR. DUANGDUEN ATONG, 297 pp.

Effects of activity of catalysts on the yield and quality of bio-oil from rapid pyrolysis of Jatropha waste were investigated. Pyrolytic conversion of Jatropha wastes was performed at 400-700°C. The reactions were conducted and compared in two reactors, an analytical pyroprobe GC-MS (µg-scale) and a drop tube pyrolyzer (g-scale). In the catalytic trial using Py-GC/MS, alumina ($Al_2O_3$) and activated carbon (Ac) catalysts powder with 5 wt% metal loading (Ni or Pd) exhibited high catalytic activities when compared to those of three other ceramic supporters, $ZrO_2$, $TiO_2$ (rutile), and $TiO_2$ (anatase). Therefore, $Al_2O_3$ and Ac catalysts are suitable for further investigation with a scaled up drop tube reactor. The maximum bio-oil of 39.38 wt% was obtained at 600°C and particle size of 0.125-0.425 mm with the presence of Ac. Reaction at 600°C with Ni/Ac catalyst yielded bio-oil with the highest HHV of 29.20 MJ/kg with a pH of 6.78. Analysis of bio-oil by GC/MS reveals the main products as phenols, aromatics, and hydrocarbons which increased from 39 to 50-65% (peak area) with Ni/Ac and Pd/Ac catalysts. Since low oxygenated compounds, high aromatics and hydrocarbon compounds of bio-oil are desirable for the pyrolysis of Jatropha wastes, the results indicate that the bio-oil at the optimize condition can be readily applied as biofuel. Moreover, a CFD based model was developed to estimate the volatiles in terms of tar, light gas and char fraction released during in conversion. Comparison with experimental data yielded % deviation for gas species, liquid and solid in the range of 6.67-28.9%, 0.26-11.26%, and 16.67-24.59%, respectively.

| | | | |
|---|---|---|---|
| Department: | Environmental Engineering | Student's Signature | ........................................ |
| Field of Study: | Environmental Engineering | Advisor's Signature | ........................................ |
| Academic Year: | 2016 | Co-Advisor's Signature | ........................................ |

# ACKNOWLEDGEMENTS

# CONTENTS

# List of figures

# List of Table

# CHAPTER 1

# INTRODUCTION

## 1.1 Thesis Topic

ภาษาไทย: การปรับปรุงคุณภาพน้ำมันชีวภาพโดยการเร่งปฏิกิริยาจากการไพโรไลซิสอย่าง
รวดเร็วของกากสบู่ดำโดยเครื่อง PY-GC/MS และเตาปฏิกรณ์ไพโรไลซิสแบบท่อปล่อยหล่น

ภาษาอังกฤษ: CATALYTIC UPGRADING BIO-OIL FROM FAST PYROLYSIS OF
JATROPHA RESIDUE USING PY-GC/MS AND DROP TUBE PYROLYZER

## 1.2 Keywords

Catalysts

Jatropha residues

Fast Pyrolysis

Bio oil upgrading

## 1.3 Background

Biomass derived fuels could be the probable fuel of future which can be
produced within a relatively short cycle and are considered sound for the environment
(Mortensen et al., 2011). These renewable sources can become partial alternative of
crude oil to produce high quality transportation fuels. They also help on reducing the
dependence on petroleum as well as mitigating carbon dioxide emissions which are
responsible for the greenhouse effect (Graça et al., 2013). In recent years, Jatropha,
due to its usable oil, is widely receiving attentions as a potential renewable energy
crop which may be used directly with slow speed diesel engine or upgraded via
transesterification to conventional biodiesel (Murata et al., 2012). However, Jatropha
residues from biodiesel production process are needed to be collected and disposed

of. Pyrolysis is a process developed to directly convert biomass feedstock into liquid products. Thus, fast pyrolysis can be a promising residue management that is possible to convert these wastes to fuel products such as bio-oil.

Bio-oil constitutes an alternative energy sources. It has several potential applications such as heat and power generation and also as a feedstock for various chemical processes. But they cannot be directly used as transportation fuels due to some of their undesired properties such as oxygen-rich composition, low heating value, immiscibility with hydrocarbon fuels, thermal and chemical instability, high density, corrosiveness, etc. However, bio-oil, in its present form, may be upgraded to be used as a liquid transportation fuel (Srinivasan et al., 2012). There are several methods of upgrading and improving bio-oils quality. Some proposed methods are the catalytic cracking through hydrotreatment (HDT), deoxygenation (DO) or hydrodeoxygenation (HDO), performed at high temperature and hydrogen pressure which are similar to petroleum refining with conventional metal catalysts (Co, Mo, and Ni). This method can produce oil with low oxygen content and a heating value corresponding to crude oil (Thangalazhy-Gopakumar et al., 2011). However, the practicality and economic possibility of such methods are still being debated(French & Czernik, 2010). The catalytic cracking is the most probable route to remove the oxygen containing functional groups of bio-oils at atmospheric pressure and hence convert the oxygenated compounds to a lighter hydrocarbon fraction and higher aromatic contents (Graça et al., 2013). Moreover, the most promising processes for the continuous biomass catalytic conversion to bio-oil requires catalyst regeneration in order to reuse in the pyrolysis catalytic process. Consequently, upgrading of bio-oil by catalytic reforming of pyrolytic vapors product was to be studied in this work.

Researches on upgrading of bio-oil from fast pyrolysis vapors have been carried out by several researches using Py-GC/MS. Recently, zeolites have been widely studied, such as HZSM-5 and Al/SBA-15 (Murata et al., 2012; Pattiya et al., 2008; Qiang et al., 2009; Thangalazhy-Gopakumar et al., 2011) and found that they are effective to convert the highly oxygenated compounds to aromatic hydrocarbons. Murata et al. (2012) studied fast pyrolysis of Jatropha residues in the absence and presence of

catalysts. The result showed that aromatics are largely formed above 90% of peak area by using catalysts (H-ZSM-5 and zeolites). However, zeolites are difficult to synthesized and also inherit high production cost. Alumina is one of the best-known catalyst support materials and is often used in both research and industrial applications. It is not only for its relatively high surface area, but active metal atoms also can spread out as reaction sites on their surface area. Zhang et al. (2013) added mesoporous catalysts ($\gamma$-$Al_2O_3$) in the microporous catalyst (LOSA-1) for biomass catalytic pyrolysis, and found that these catalysts can significantly improve the selectivity of low-carbon components with the maximum aromatic and olefin yield of 25.3%. In addition, some transition metal based catalysts on ceramic supports such as Ni, Co, Pt, Pd and Ru catalysts are utilized for deoxygenated reactions which were reported by several researches (Bulushev & Ross, 2011; Choudhary & Phillips, 2011; Lu et al., 2010; Ying et al., 2012; Zhang et al., 2013). Modifications of the metal catalysts on ceramic support were generally performed by the impregnation method. These works were reported by Lu et al. (2012) who studied catalytic upgrading of biomass fast pyrolysis vapors by noble metal with titania and zirconia/anatase based catalysts. The highest hydrocarbon content was obtained by the zirconia/anatase based catalysts. Therefore, modification of the metal catalysts by the impregnation method has not only low production cost, but also fine hydrothermal stability which makes them possible for treating biomass pyrolysis vapor (Kaewpengkrow et al., 2013). There have been some works using ceria ($CeO_2$) based catalysts, mostly for promotion of hydrogen production and prevention of coke deposition during the gasification and pyrolysis process (Bulushev and Ross, 2011; Kaewpengkrow et al., 2013). Metals such as Ni, Pd, Pt and Ru have been added to the ceria-based catalyst system to improve the catalytic performance. For this reason, Ce-based modified catalysts were synthesized in this study.

Moreover, the use of mesoporous catalysts has attracted a lot of interest due to their potential ability to convert large complex compounds into simpler liquid products. In particular, the meso-pores of activated carbon are thought to play an important role in the effective conversion of heavy hydrocarbon compounds into lighter fractions (Wang et al., 2016a; Zhang et al., 2013). Due to their highly porous

structures, ACs have been widely used as catalyst supports in the conversion of hydrocarbons and tar cracking, because their mesopores greatly improve the dispersion of metal ions and also facilitate transport of reactant molecules (Shen & Yoshikawa, 2013). Cheng et al., (2016) studied the bio-oil upgraded through hydrodeoxygenation with 6%wt. Ni based activated carbon (Ni/AC, Ni-Fe/AC, Ni-Mo/AC and Ni-Cu/AC). It was found that the Ni/AC catalysts produced the highest content of gasoline range hydrocarbons (C6–C12) at 32.63% area in the upgraded bio-oil. Recently, bio-char from biomass pyrolysis/gasification have been greatly attracted (Jin et al., 2015). Bio-char can be employed to adsorb heavy metals or organic pollutants as a promising alternative. Char has also been studied as an inexpensive catalyst in tar removal and also an excellent adsorbent (Shen, 2015). There were several studies on char and char-supported nickel catalysts for secondary syngas clean-up (Jurarat et al., 2015; Wang et al., 2011; Shen, 2015) which indicated that char-supported plays a better role in improving the reactivity of deoxygenation. Consequently, the superior activity and stability of these catalysts would further enhance the fast pyrolysis sequential process.

In the in-situ continuous process, the biomass is cracked to produce pyrolytic vapors which then passed through catalyst beds where they are converted into bio-oil as well as gaseous and solid byproducts. Catalytic vapor cracking is generally considered superior to other catalytic upgrading technologies, such as hydrotreating, esterification and deoxygenation. There are several researches studied the pyrolysis of biomass (such as Jatropha, palm shell, pine wood and sawdust) for produced bio-oil. They found that the obtained pyrolytic liquid product was 30-60 wt%, 15–25 wt% of solid char, and 10–20 wt. % of gas products, which depending on the feedstock used (Kim, 2013; Biradar, 2014; Bosong, 2014; Kim, 2014; Zhang, 2014). Usually pyrolysis of Jatropha waste was performed at 400-600°C due to the main thermal decomposition of Jatropha residues generally occurred over the temperature range of 250–450°C (Sricharoenchaikul et al., 2009). In this research, pyrolysis fixed-bed catalytic reactor was designed and used for continuous pyrolysis and catalytic upgrading of Jatropha waste and metal catalyst was evaluated for catalytic cracking. A number of research studies have indicated the potential of Jatropha residues as pyrolysis feedstock

(Manurung, 2009; Kim, 2014; Biradar, 2014 Jourabchi, 2014). The effect of temperature on the bio-oil yield has been reported on fixed-bed reactor setups. The optimization of pyrolysis parameters to maximum not only Jatropha residues bio-oil yield, but also its quality has yet to be carried out. Several kinds of catalysts (i.e. CaO, MgO, MCM-41, and HZSM-5) were used to upgrade the properties of bio-oil from continuous process (Jae et al., 2014; Mortensen et al., 2011; Murata et al., 2016; Murata et al., 2013). Because of coke deposit on the surface, activity of these catalysts deteriorates rapidly, results in lower hydrocarbon yields which limit their application to catalytic fast pyrolysis (CFP) technology. Therefore, the metal activated carbon catalysts were developed to mitigate the problem and tested for bio-oil upgrading using drop tube pyrolyzer.

Furthermore, to accurately predict the process performances, reliable kinetic models and associated product distribution profile are needed. Here, computational fluid dynamics (CFD) modeling techniques are becoming prevalent tool in the biomass thermochemical conversion field. Researchers have been using CFD to simulate and analyze the performance of thermochemical conversion instrument such as, fixed beds, fluidized beds, combustion furnaces, firing boilers, rotating cones and rotary kilns (Wang & Yan, 2008). Therefore, pyrolysis of Jatropha waste is simulated in a lab-scale drop tube reactor using the developed CFD (ANSYS FLUENT v.17.0 program) protocol. The model was developed to predict the volatiles in terms of tar and light gas as well as char fraction released during Jatropha waste conversion. Due to complex nature of tar species evolved during this process, phenol was considered as tar representative while the main gas species were individually determined ($H_2$, CO, $CO_2$, $CH_4$ and steam). CFD method is one approach which was used to predict the product yields and gain a better understanding of the product evolution pathways of pyrolysis with various feedstocks and reactors (Borello et al., 2014; Tabet & Gökalp, 2015; Xue et al., 2011). Several researches studied the CFD model of biomass thermochemical processes to predict the products from fluidized bed reactor (Liu et al., 2016; Xue et al., 2011; Zhong et al., 2016). There are a few researches using CFD model of a biomass packed bed system to predict products from pyrolysis process. Borello et al., (2014) developed a

CFD model of biomass packed porous bed system to predict the volatiles in terms of tar, light gas and char fraction released during the pyrolysis process. The predicted data using proposed kinetic parameters were able to reduce the % error to almost negligible values (0.00-0.08%), except for the water content. For this reason, the predictions of product distributions of Jatropha residues pyrolysis based on this technique were applied and compared to the experimental yield profile in this study.

The objectives of this research are to investigate the effect of Jatropha to catalyst ratios (J/C), the catalytic activity of metal as well as the influence of six supporters on the distribution of pyrolytic vapors product in order to produce quality bio-oil and synthesize advanced catalyst for reforming/upgrading pyrolysis vapors from Jatropha waste by reducing the bio-oil oxygen content to below 30 wt%. Pyrolysis experiments on Jatropha residues were carried out using Py-GC-MS to allow direct real-time analysis of the evolved pyrolytic vapors product which would assist on screening of the catalysts for bio-oil upgrading. The selected catalysts from Py-GC-MS experiments were then tested in a drop tube reactor (semi continuous feeding) to determine their activities on Jatropha residues decomposition in a larger and more realistic environment. Therefore, the focus of this study is also to determine the effects of pyrolysis parameters on the yield and quality of bio-oil from Jatropha residues. Moreover, CFD model were used to investigate and predict the effect of operating conditions on the product distribution.

## 1.4 Plan of the Thesis

This thesis comprises seven chapters in total. The content of each chapter was divided as the following:

1.4.1 Chapter 1 Introduction: This chapter sets the background to the research project. An overview of the need for biomass as a renewable energy source, fast pyrolysis, bio-oil upgrading, as well as efficiency of catalysts. The research objective, hypothesis, scope and benefit of research are also presented.

1.4.2 Chapter 2 Theory and Literature Review: A review of related research works on biomass fast pyrolysis, its production and characterization, bio-oil upgrading as well as catalyst activity.

1.4.3 Chapter 3 Methodology: This chapter focuses on the method of catalyst synthesized, Lab-pyrolyzer apparatus, fast pyrolysis process, and setting up of CFD boundaries for fast pyrolysis process model.

1.4.4 Chapter 4 Result and Discussion for biomass prepared catalyst properties: This chapter revealed the characterization of biomass and catalyst synthesized.

1.4.5 Chapter 5 Result and Discussion of catalytic fast pyrolysis using Py-GC/MS: Effect of metal-based ceramic, activated carbon and char-supported catalysts on pyrolytic product in micro scale by Py-GC/MS were discussed in this chapter.

1.4.6 Chapter 6 Result and Discussion of catalytic fast pyrolysis using a drop tube reactor: Effect of operating condition and catalytic fast pyrolysis of Jatropha residues in large scale by drop tube reactor was investigated. In addition, CFD model was used to predict the product distribution from fast pyrolysis of Jatropha residue.

1.4.7 Conclusions: The final chapter of this thesis presents the main outcomes of the study which are in line with the specific objectives. The chapter concludes by suggesting potential of research for future work.

## 1.5 Research objective

1.5.1 To determine the operating conditions for optimum bio-oil composition and production of fast pyrolysis Jatropha residue by Py-GC/MS

1.5.2 To improve catalysts for reducing oxygen content of bio-oil to below 40 wt%

1.5.3 To evaluate bio-oil quality and predict product distributions from fast pyrolysis of Jatropha residue using drop tube pyrolyzer

## 1.6 Research Hypothesis

1.6.1 Reducing of oxygen content in bio-oil can be accomplished using fast pyrolysis process with addition of synthesized catalyst

1.6.2 Computational fluid dynamics (CFD) model can be used to predict the distribution of product from fast pyrolysis of Jatropha residue

## 1.7 Scope of research

In order to study the effect of synthesized catalysts on product distributions of bio-oil from fast pyrolysis process. The scope of research was as follows:

1.7.1 Py-GC/MS was applied to investigate four particle sizes of Jatropha residues (125-850 µm) at 400- 700°C.

1.7.2 Synthesis of 1% metals was performed by impregnation method on ceramic supports, alumina, zirconia, rutile and anatase with cerium (Ce) as a promoter. Active sites of the catalysts include Nickel (Ni), Palladium (Pd) and Ruthenium (Ru).

1.7.3 Synthesis of 5% metals was performed by impregnation method on alumina, activated carbon and bio-char. Active sites of the catalysts were Cerium (Ce), Cobalt (Co), Lanthanum (La), Molybdenum (Mo) Nickel (Ni), Palladium (Pd) and Ruthenium (Ru).

1.7.4 Jatropha to catalyst ratios (J: C) of 1:1, 1:5 and 1:10 was used for catalytic fast pyrolysis with Py-GC/MS.

1.7.5 Fast pyrolysis of Jatropha residues was investigated using a drop tube pyrolyzer at 400 - 700°C, gas flow rate of 2-4 L/min and particle sizes of 125-850 µm.

1.7.6 Catalytic fast pyrolysis of Jatropha residues was investigated using drop tube pyrolyzer selected operating condition of 600°C and particle sizes of 125-425 µm with 5% metals/$Al_2O_3$ extruded and 5% metals/Ac.

1.7.7 CFD model was applied to obtain essential modeling parameter for prediction of product distributions from fast pyrolysis of Jatropha residue.

## 1.8 Benefit of research

1.8.1 Bio-oil upgrading is an innovation on production and automotive utilization of biofuels from non-edible agricultural source

1.8.2 Conversion of biomass using pyrolysis reactor and the catalytic one-step process can produce and upgrade the bio-oil suitable for using as biofuels.

1.8.3 Computational fluid dynamics model of fast pyrolysis can be modified to benefit the designing of commercial scale pyrolyzer.

# CHAPTER 2

# THEORY AND LITERATURE REVIEWS

## 2.1 Biomass

Biomass consists of organic materials including derivatives from plants and animals. The main elements of biomass are carbon, hydrogen, oxygen and nitrogen. Biomass can be divided into two groups which are primary biomass and biomass waste. Primary or virgin biomass comes directly from plants or animals. Waste or derived biomass comes from different biomass-derived products.

- Virgin biomass includes wood, plants, leaves (ligno-cellulose), crops and vegetables.
- Biomass waste includes solid and liquid wastes (municipal solid waste (MSW)); sewage, animal, and human waste; gases derived from landfilling (mainly methane); and agricultural wastes.

A main representative for biomass in term of a renewable energy resource is woody biomass including forest products, agricultural crops, and their residues. In addition, wood biomass consists of three main components involving extractives, cell wall, and ash as shown in Fig. 2.1.
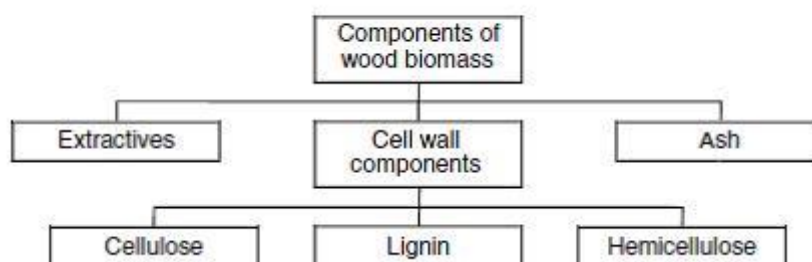


**Fig. 2.1** Main components of a woody biomass (Basu, 2010)

Extractives such as protein, oil, starch, sugar, and etc., are the soluble part which can be dissolved in solvents. Cell wall including cellulose, lignin, and hemicelluloses provides a structural strength to plant. Ash is the inorganic component

of biomass that does not burn. Lignocellulosic biomass consists of three main compositions including cellulose, hemicelluloses, and lignin. Actually, bio-oil is produced from rapidly pyrolysis and simultaneously depolymerizing and fragmenting of the cellulose, hemicellulose, and lignin of biomass. In a typical operation, biomass is subjected to a rapid increase temperature (high heating rate) resulted in degradation the cellulose and hemicellulose of biomass. Therefore, amount of cellulose and hemicellulose suggesting that it can be effectively converted into bio-oil.

### 2.1.1 Cellulose

Cellulose of wood provides strength and comprises 40-50 wt. % of dry wood (Mohan et al., 2006). Cellulose $(C_6H_{12}O_5)_n$, is the main constituents of cell walls and consists of a linear chain polysaccharide with $\beta$-1, 4 linkages of D-glucopyranose monomers. The degree of polymerization is approximately 10,000 with the high molecular weight of 500,000. Cellulose has a crystalline structure with an extended, flat, 2-fold helical conformation.
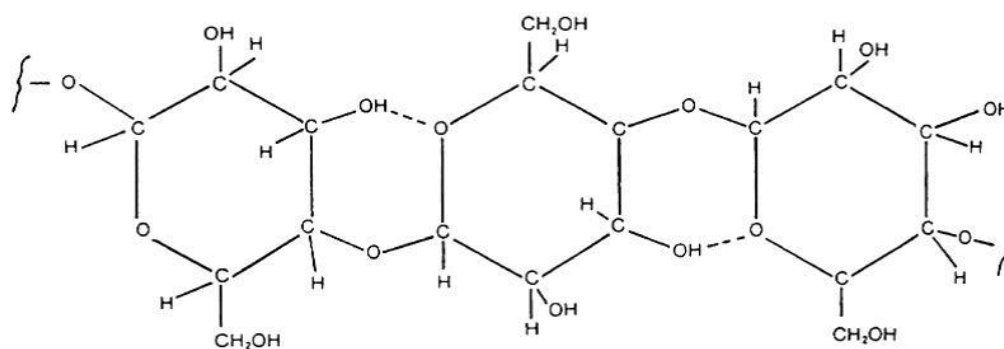


**Fig. 2.2** Molecular structure of cellulose (Basu, 2010)

### 2.1.2 Hemicellulose

Hemicelluloses is commonly account for 25%-35% of the mass of dry wood, 28% in softwoods, and 35% in hardwoods (Mohan et al., 2006). In contrast to cellulose, hemicellulose is a polymer of five different sugars and has an amorphous structure. It contains a group of carbohydrates with a branched structure and lower degree of

polymerization (∼100-200). Therefore, it is easy to hydrolyze compared to cellulose. The most representative building block of hemicelluloses is xylan as shown in Fig. 2.3.
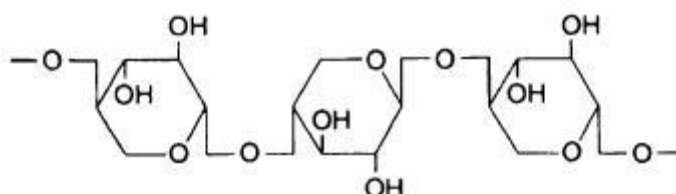


**Fig. 2.3** Molecular structure of typical hemicelluloses, xylan (Basu, 2010)

2.1.3 Lignin

Lignin is a highly irregular polymer synthesized by free radical polymerization of the alcohol precursors such as coumaryl, coniferyl and sinapyl alcohols, which include phenol, 2-methoxy phenol (guaiacol), and 2,6-dimethoxy phenol (syringol) aromatic unit as illustrated in Fig. 2.4. A hardwood contains 10-25 wt. % of lignin, whereas softwood has 25-35 wt. % of lignin by dry weight.



coumaryl alcohol          coniferyl alcohol          sinapyl alcohol
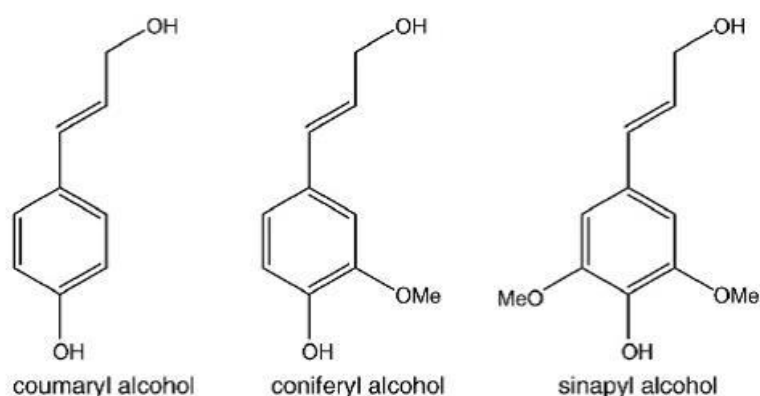
**Fig. 2.4** Typical of lignin monomers (Basu, 2010)

Generally, pyrolysis of biomass is significantly dependent on its main components of cellulose, hemicelluloses and lignin. Comparison between characteristics of Jatropha residue and other biomass is shown in table 2.1. Jatropha

residue contains large amount of cellulose (59.20%) with much lesser hemicellulose and lignin of 18.00% and 22.80%, respectively. Obviously, cellulose composition in Jatropha seed cake is higher than other woody biomass; it is suggesting that this waste can be effectively converted into liquid fuel by pyrolysis process at relatively low temperature (400-600℃). According to Abnisa et al. (2013), hemicellulose decomposes first, and the decomposition of cellulose and then lignin follows. These phases were identified as the temperature increased during the pyrolysis.

**Table 2.1** Comparison between chemical composition of Jatropha waste and other biomass

| Biomass feedstock | poplar wood[a] | Pine wood[b] | JR[c] | Cedar[c] | Jatropha Seed cake[d] | Palm leaf[d] | Jatropha Residue[e] |
|---|---|---|---|---|---|---|---|
| Cellulose | 49.70 | 43.8 | 26.2 | 34.2 | 36.64 | 46.1 | 59.20 |
| Hemicellulose | 24.10 | 19.9 | 16.2 | 15.3 | 4.82 | 23.17 | 18.00 |
| Lignin | 23.55 | 24.3 | 20.2 | 32.1 | 39.61 | 29.31 | 22.80 |
| Other* | - | - | 23.1 | 4.8 | 18.94 | - | n/a |

[b]Thangalazhy-Gopakumar et al., 2011, [c]Mochizuki et.al., 2013, [a] Lu et al., 2010, [d]Kim et al., 2013, [e]Kaewpengkrow et al., 2014

 *By difference

## 2.2 Biomass Characteristics

Design of a biomass thermal utilization system needs the composition of the fuel as well as its energy content. The following three primary properties describe its composition and energy content: (1) ultimate analysis, (2) proximate analysis, and (3) heating values. Experimental determination of these properties is covered by ASTM standard E-870-06.

### 2.2.1 Ultimate Analysis

The composition of biomass is expressed in terms of its basic elements except for its moisture, $M$, and inorganic constituents. A typical ultimate analysis is

$$C + H + O + N + S + ASH + M = 100\% \qquad (2\text{-}2)$$

Here, C, H, O, N, and S are the weight percentages of carbon, hydrogen, oxygen, nitrogen, and sulfur, in solid fuels, respectively. Fig. 2-5 is a scheme of the atomic ratios (H/C) and (O/C) determined from the ultimate analysis of different fuels. It shows that biomass; cellulose in particular, has very high relative amounts of oxygen and hydrogen. This results in relatively low heating values.
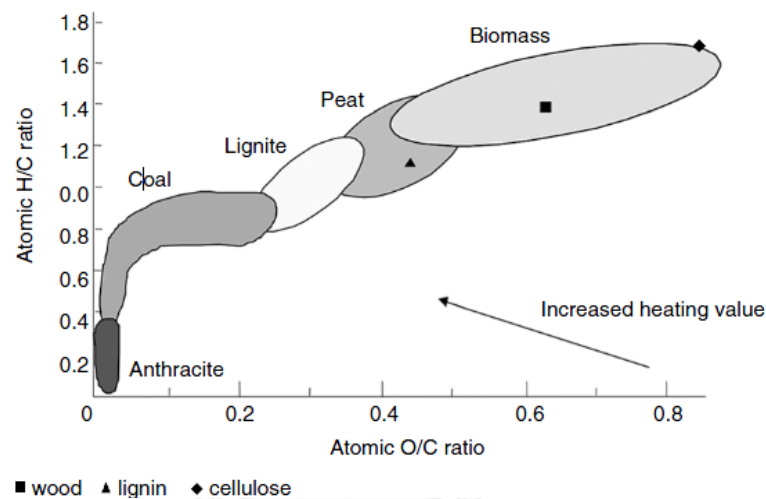


**Fig. 2.5** Classification of hydrogen/carbon and oxygen/carbon ratios of solid fuels

2.2.2 Proximate Analysis

Proximate analysis gives the composition of the biomass in terms of gross components such as moisture (M), volatile matter (VM), ash (ASH), and fixed carbon (FC). It is a relatively simple and economical process. For wood fuels, ASTM standard E-870-06 may be used. The moisture and ash content determined in proximate analysis refer to the same things as reported by ultimate analysis. However, the fixed carbon in proximate analysis is different from the carbon in ultimate analysis. In proximate analysis, it does not include the carbon in the volatile matter and is often referred to as the char yield after devolatilization. The volatile matter of a fuel is the condensable and non-condensable vapor released when the fuel is heated. The amount depends

on the rate of heating and the temperature. For the determination of volatile matter, the fuel is heated to a standard temperature and at a standard rate in a controlled environment. The ASTM standard was use for determination of volatile matter is E-872 for wood fuels, and D-3175-07 for coal and coke. The ash is the inorganic solid residue (silica, aluminium, iron, and calcium; small amounts of magnesium, titanium, sodium, and potassium) after the fuel completely burned. Ash content is determined by ASTM of E-1755-01 for other biomass. It is generally very small, but may play a significant role in biomass utilization especially those containing alkali metals. Straw, grasses, and demolition wood are particularly liable to this problem. These components can lead to serious agglomeration, fouling, and corrosion in boilers or gasifiers.

In addition, high moisture is a major characteristic of biomass. This important input design parameter must be known for assessment of the cost or energy penalty in drying the biomass. The moisture in biomass can remain in two forms: (1) free or external; and (2) inherent or equilibrium. Moisture content (M) is determined by the test procedure given in ASTM standards D-871-82 for wood in which weighed sample of the fuel is heated in an air oven at 103°C and weighed after cooling. The difference in weight between a dry and a fresh sample gives the moisture content in the fuel. Fixed carbon (FC) in a fuel is determined from the following equation, where M, VM, and ASH stand for moisture, volatile matter, and ash, respectively.

$$FC = 1 - M - VM - ASH \qquad (2\text{-}3)$$

This represents the solid carbon in the biomass that remains in the char in the pyrolysis process after devolatilization. During the determination of VM, a part of the organic carbon is transformed into a carbonaceous material called pyrolytic carbon. Since FC depends on the amount of VM, it is not determined directly (Basu, 2010).

## 2.3 Biomass conversion

Biomass conversion technologies can be broadly classified into primary conversion technologies and secondary conversion technologies. The primary

conversion technologies such as combustion, gasification and pyrolysis involve the conversion of biomass directly into heat, or into a more useful form which can serve as an energy carrier such as gases (methane and hydrogen), liquid fuels (methanol and ethanol), and solids (char). The secondary technologies convert these products of primary conversion into the desired form which may be an energy product such as transportation fuel or a form of energy such as electricity. (Pande & Bhaskarwar, 2012). Biomass or lignocellulosic can be converted to valuable fuels and chemicals via a number of processes including biological and thermochemical processes as display in Fig.2.6.
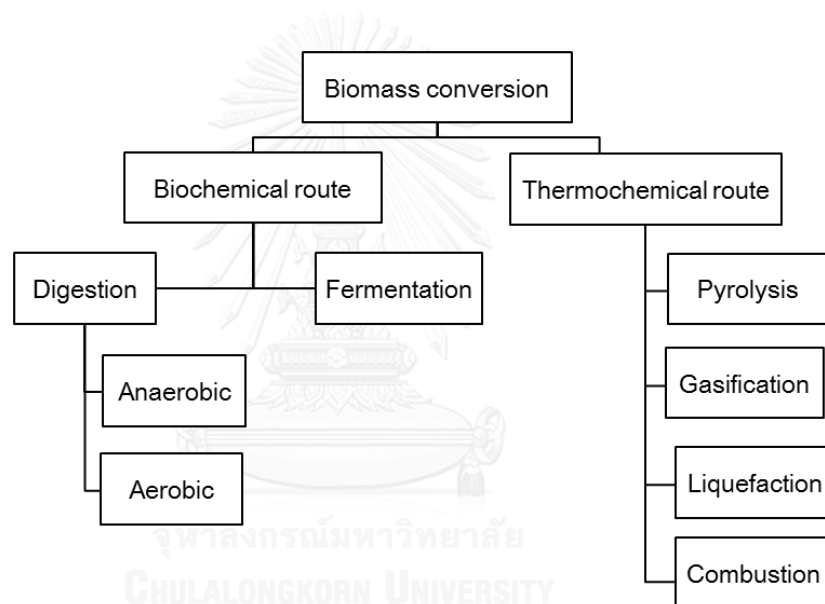


**Fig. 2.6** Two routes, bio- and thermochemical conversion of biomass

In biological conversion, biomass is digested to smaller substances by bacterial or enzyme. It can be classified as fermentation, digestion by anaerobic or aerobic. However, this process is slower than thermochemical conversion. In case of later method, the three principle processes are combustion, gasification and pyrolysis. Combustion is defined as the biomass conversion at high temperature and excess air. The two major products are carbon dioxide and water. Gasification is a thermal process that solid or liquid material react with partial oxygen to produce syngas (carbon

monoxide and hydrogen) as well as carbon dioxide and methane whereas pyrolysis is the thermal decomposition process of the feedstock with the absence of oxygen and liquid is a major product.

## 2.4 Jatropha curcas

Jatropha curcas or physic nuts which will be called ''Jatropha'', is a small tree or large shrub that normally reaches a height of 3–5 m, but can reach a height of 8–10 m under favorable conditions. Jatropha plant is widely distributed in the wild and cultivated tropical areas of Central America, South America, Africa, India, South Eastern Asia, and Australia. Therefore, it typically grows between 15 and 40°C and is more altered by lower temperatures than by altitude or day length (Carels, 2009). It is one of the renewable resources, not only as bioenergy, but also for medical, food, and non-food application. In addition, Jatropha is a multi-purpose species with many attributes and considerable potential.

As biomass, Jatropha is attracting great attention over the world as a source of renewable energy as well as an alternative to fossil fuels. Moreover the Jatropha plant is currently receiving a lot of attention as an energy plant (Khalil et al., 2013). Different plant parts of Jatropha are shown in Fig. 2.7. Dry Jatropha fruit contains about 35–40% shell and 60–65% seed by weight. The seed is made up of about 42% husks and 58% kernel. Jatropha contains about 17–18% oil and seeds contain up to 34% oil. The fatty acids found common in all the oil samples were oleic, linoleic, palmitic and stearic. In recent years, the biofuels industry is growing rapidly as a result of high petroleum prices and increasing concerns about global climate change. Jatropha oil from the seed can be used as fuel in diesel engines directly and by blending it with methanol. Most importantly, it is significant to point out that the oil of Jatropha is a viable alternative to diesel fuel since it has desirable physico-chemical and performance characteristics as diesel. The obtained biodiesel from Jatropha oil after transesterification conforms to the standard requirements of American and European countries.
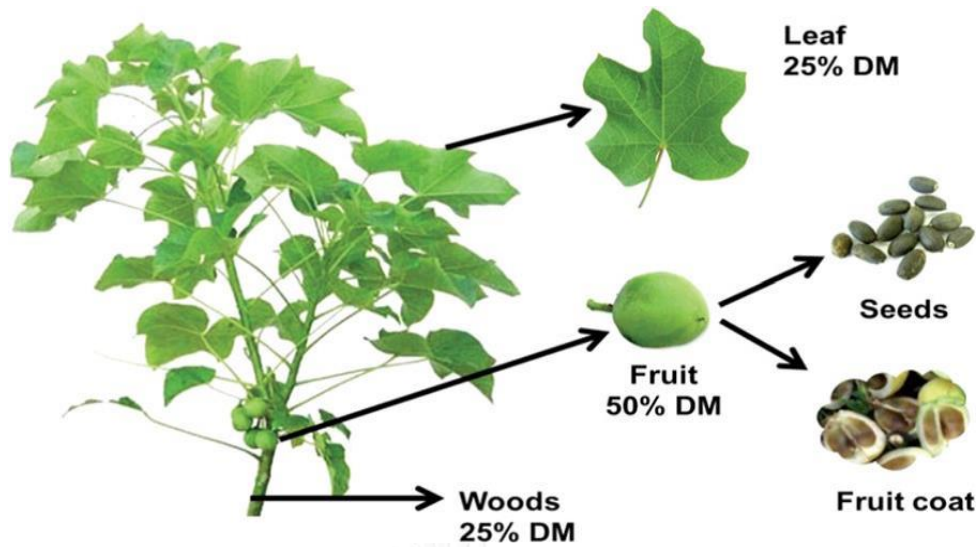
**Fig. 2.7** Different components of Jatropha (Khalil et al., 2013)

However, Jatropha generates approximately 1 ton of seed cake per hectare. Taking India as an example, it is expected that Jatropha will be grown on more than 20 million hectares in the few coming years and will generate around 20 million tons of seed cake per year. This is a significant biomass potential; however, at the moment, seed cake is devolved to the crop field for mulching. Otherwise, it can be fermented for biogas production. It releases more energy than cattle dung. Seed cake can also be converted to briquettes for domestic or industrial combustion. One kilogram of briquettes can be combusted completely in 35 min at 525–780°C. In addition, Jatropha oil is toxic and as such, it does not compete directly with food applications. This is of prime importance as the non-food biomass. Without efficient utilization of Jatropha waste byproducts, large amounts of waste products will be produced at the processing units, leading to negative impacts on the environment.

In Thailand, Jatropha plantations has 16,000 ha (100,000 rais), but only 3200 ha are managed commercially. Jatropha oil yields of 1.2 tons/ha, it generated Jatropha residue (seed cake) approximately 3.6 tons/ha (Siriwardhana et al., 2009). In order to make Jatropha business more feasible, a conversion of Jatropha wastes into liquid products is highly desirable (Murata et al., 2012). Therefore, Jatropha seed cakes are needed to be collected and disposed which may create environmental problem. The

environmental impacts discussed are lower than the fossil alternative as long as no natural ecosystems are removed in favor of Jatropha as it occurs along with sugarcane and palm oil.

## 2.5 Pyrolysis

Pyrolysis is the thermal decomposition process with the absence of oxygen. Pyrolysis of biomass is usually carried out with the temperature in the range of 300 to 1000°C. During pyrolysis of biomass, large hydrocarbon complex molecules (cellulose, hemicelluloses and lignin) are decomposed by high temperature to smaller molecules. Three main products are achieved such as liquid (tar, water, and heavier hydrocarbon compounds), permanent gases ($H_2O$, $CO$, $CO_2$, other hydrocarbon) and solid char as shown in equation (2-4).

$$C_n H_m O_p \text{ (Biomass)} + \text{Heat} \rightarrow \sum_{liquid} C_a H_b O_c + \sum_{gas} C_x H_y O_z + \sum_{solid} C \qquad (2\text{-}4)$$
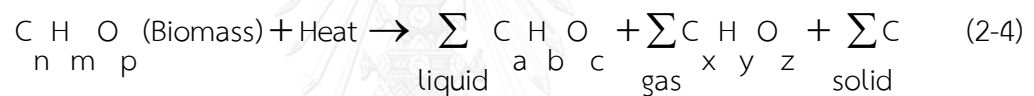
The yield of each product depends on the characteristics of biomass, heating rate, pyrolysis temperature, and residence time. The types of pyrolysis are commonly classified as conventional, fast and flash pyrolysis (Basu, 2010). The pyrolysis conditions and products of woody biomass are illustrated in Table 2.2.

**Table 2.2** The pyrolysis conditions and products of woody biomass

| Pyrolysis processes | Conditions | | | | Products (wt%) | | |
|---|---|---|---|---|---|---|---|
| | Temperature (°C) | Heating rate (°C/s) | Particle size (mm) | Residence time (s) | Liquid | Solid | Gas |
| Conventional (slow) | ~300-500 | 0.1-1 | 5-0 | 450-550 | 30 | 35 | 35 |
| Fast | ~600-1000 | 10-200 | <1 | 0.5-10 | 75 | 12 | 13 |
| Flash | ~800-1000 | > 1000 | <0.2 | <0.5 | >70 | | |

In case of biomass pyrolysis, the main components of pyrolysis vapors are acid, furan, phenol, carbonyl, linear hydrocarbon, aromatic hydrocarbon, and sugar. The formation of these organic compounds results from three pyrolytic pathways. Firstly, the decomposition of lignin leads to phenolic compound (Phenol, Guaiacols and syringols). Secondly, the depolymerization of holocellulose (cellulose and hemicellulose) generated anhydroglucose (Levoglucosan), related derivatives and furan. The pyrolytic ring scission of holocellulose produced various light products such as acids, esters, aldehydes, ketones, alcohols, esters as shown in Fig.2.8 (Asadieraghi et al., 2014). It suggested that main chemical compounds obtained from hemicellulose and cellulose degradation.
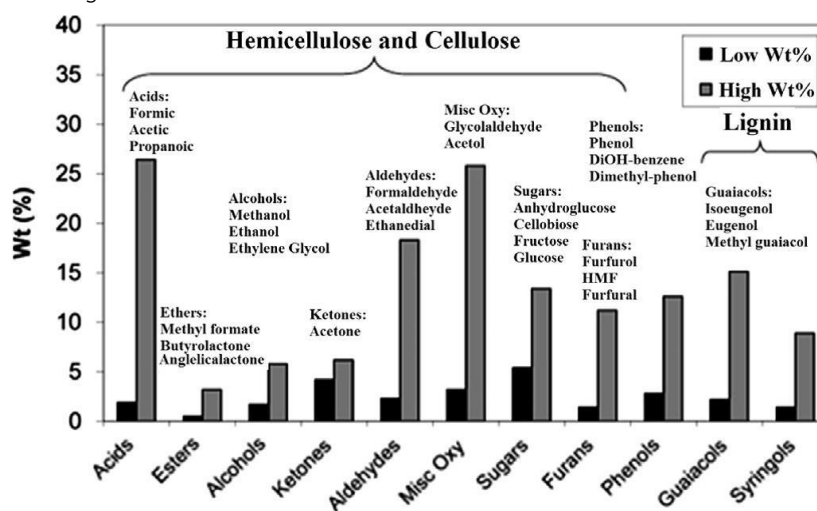


**Fig. 2.8** The chemical compositions of bio-oils (Asadieraghi et al., 2014)

A schematic of a typical pyrolysis plant is shown in Fig. 2.9. Biomass is fed into a pyrolysis chamber containing hot solids (fluidized bed) that heat the biomass and the decomposition starts. The condensable and non-condensable vapors released from the biomass leave the chamber, while the solid char produced remains partly in the chamber and partly in the gas. The gas is separated from the char and cooled downstream of the reactor. The condensable vapor condenses as bio-oil or pyrolysis oil; the non-condensable gases leave the chamber as product gas. These gases may be fired in a burner to heat the pyrolysis chamber or used for other energy purposes. Similarly, the solid char may be collected as a commercial product or burned in a separate chamber to produce heat that is necessary for pyrolysis. As this gas is free from oxygen, part of it may be recycled into the pyrolysis chamber as a heat carrier or fluidizing medium.
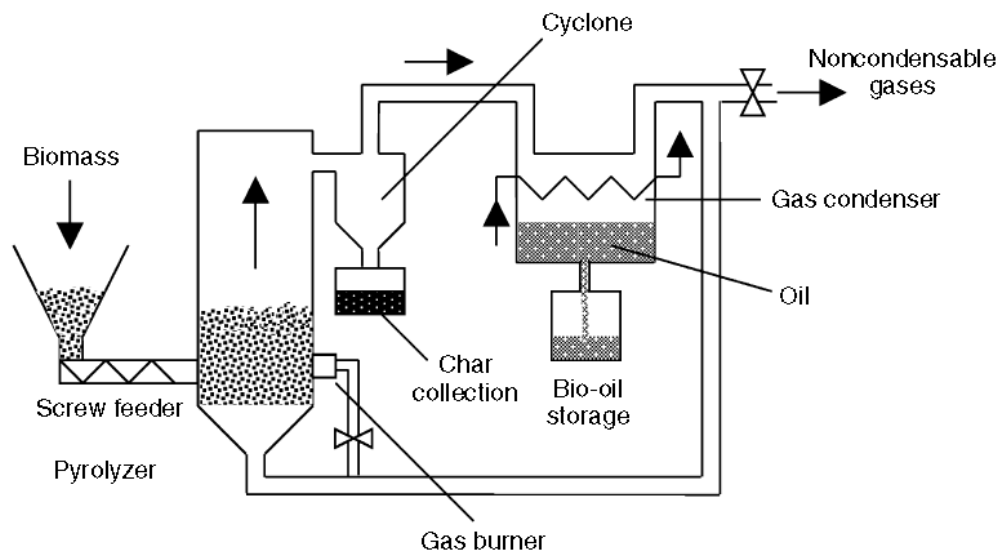


**Fig. 2.9** Simplified layout of a pyrolysis plant (Basu, 2010)

## 2.6 Pyrolyzer Types

Recently the objective of pyrolysis was to produce the maximum yield of liquid or gas more than to produce charcoal. Therefore, the rate of heating, the peak pyrolysis temperature, and the duration of pyrolysis had to be chosen accordingly. These

choices also decided what kind of reactor was to be used. The yield is maximized for different choices of heating rate, temperature, and gas residence time.

Operations of modern pyrolyzers are more concerned with gas and liquid products, and require a continuous process. A number of different types of pyrolysis reactor have been developed. Based on the gas–solid contacting mode, they can be broadly classified as fixed bed, fluidized bed, and entrained bed, and then further subdivided depending on design configuration. Commonly-used pyrolyzers, such as bubbling fluidized bed (BFB), circulating bed (CFB), ablative, auger, entrained flow, rotating cone and vacuum reactor, as well as their characteristics are shown in Table 2.2 (Zhang, 2010) and Fig. 2.10 (Basu, 2010).
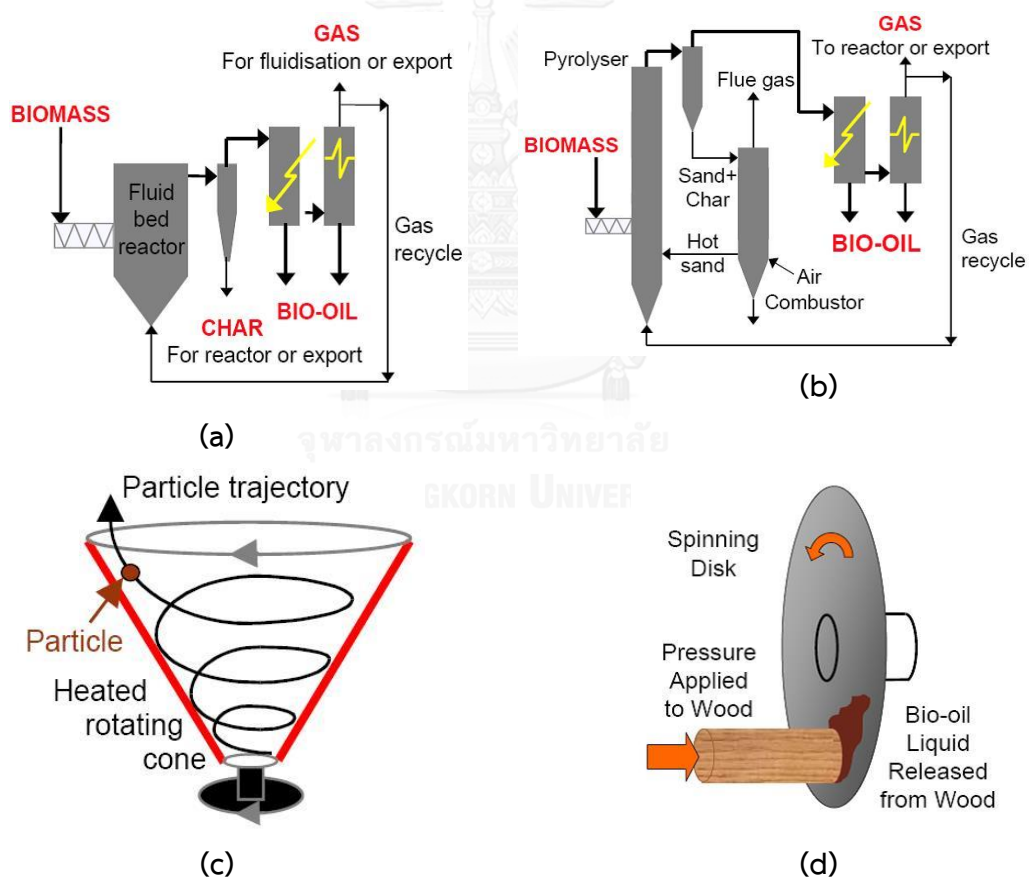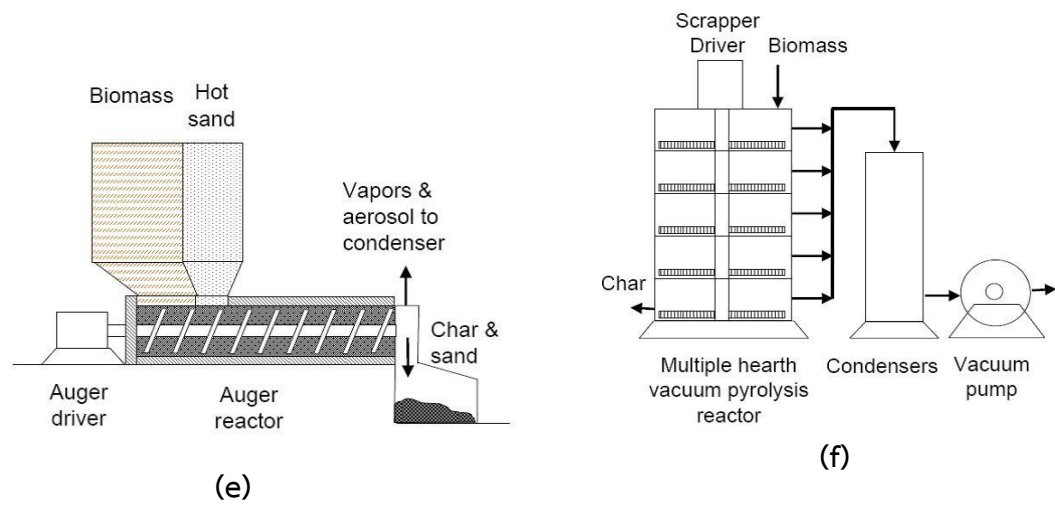
**Fig. 2.10** Commonly-used pyrolyzers such as (a) bubbling fluidized bed, (b) circulating bed (CFB), (c) rotating cone (d) ablative (e) auger and (f) vacuum

Fixed-bed reactors have mainly been used to identify governing parameters affecting pyrolysis products, due its ease of operation than other reactors. Therefore, this work used the fixed bed for studies effect of operating condition on bio-oil production. Within the scope of this work, the focus is on upgrading bio-oil, which sometimes can be referred to as pyrolysis oil (or crude bio-oil).

**Table 2.3** Commonly-used pyrolyzers with own characteristics

| Reactor | Fixed bed | Ablative | BFB | CFB |
|---|---|---|---|---|
| Carrier gas | Yes | No | Yes | Yes |
| Heating method | Temperature is not uniform inside the sample, and low heat transfer | Reactor wall/disc | • Heated recycle gas<br>• Hot inert gas<br>• Partial gasification<br>• Fire tubes | In-bed gasification of char to heat sand |
| Primary heat transfer | • Gas-solid | Solid-solid | • Solid-solid<br>• Gas-solid | • Solid-solid<br>• Gas-solid |
| Main features | • Almost no requirements except for energy-saving purpose<br>• Maintenance requirement is low, but batch by batch operation demanding manual labor<br>• Excellent flexibility to operate parameter changes | • Accepts large size feed stock<br>• Very high mechanical char abrasion from biomass<br>• Compact design<br>• Heat supply problematical<br>• Particulate transport gas not always required | • High heat transfer rates<br>• Heat supply to fluidizing gas or to bed directly<br>• Limited char abrasion<br>• Very good solid mixing<br>• Particle size <2mm in smallest dimension<br>• Simple reactor configuration<br>• Residence time of solids and vapors controlled by the fluidizing gas | • High heat transfer rates<br>• Heat char abrasion from biomass and char erosion leading to high char in product<br>• Char/solid heat carrier separation required<br>• Solid cycle required<br>• Increased complexity of system<br>• Maximum particle size up to 6mm<br>• Possible catalytic activity from hot char |

This crude bio-oil has an irritating smell, its color is dark-brown for flash pyrolysis or dark for slow pyrolysis. With rather high oxygen content in the range of 35-40% compared to fossil fuel, crude bio-oil has quite lower energy density and suffers from immiscibility with fossil fuel blending. Furthermore, high acidity, which would cause instability, as well as large number of components (over 300 types), which causes wide distillation temperature range, make crude bio-oil not suitable for direct

combustion usage. Hence, upgrading is necessary which will be described in the next section.

## 2.7 Bio-oil properties and its applications

Bio-oils are composed of differently sized molecules derived primarily from the depolymerization and fragmentation reactions of biomass. Generally, as-received bio-oil produced by biomass pyrolysis process can be directly applied in boilers, industrial kilns, and generator. Unfortunately, the properties of bio-oil are obviously different from that of petroleum oil (Heavy fuel oil) as displayed in Table 2.4.

**Table 2.4** Comparison properties of bio-oil and heavy fuel oil

| Physical properties | Bio-oil[a] from wood | Bio-oil From palm shell[b] | Bio-oil From Jatropha[c] | Bio-oil From palm[d] (Upgraded) | Heavy fuel oil[d] |
|---|---|---|---|---|---|
| Moisture content (wt.%) | 15-30 | 53 | 25 | - | 0.10 |
| pH | 2.5 | 2.5 | - | - | - |
| Density (g/cm$^3$) | 1.2 | 1.05 | - | 1.03 | 0.98 |
| HHV (MJ/Kg) | 16-19 | 6.58 | 17.00 | 23.2-31.3 | 43.4 |
| Viscosity (cP, at 50°C) | 40-100 | 3.2 | - | - | 180 |
| Elemental (wt.%) | | | | | |
| C | 54-58 | 19.48 | 55.25 | 51.59-69.20 | 82.79 |
| H | 5.5-7.0 | 8.92 | 4.3 | 6.98-9.04 | 12.98 |
| O | 35-40 | 71.4 | 39.36 | 14.50-34.60 | 0.48 |
| N | 0-0.2 | 0.2 | 1.01 | 6.49-9.43 | 0.20 |
| S | 0-0.3 | - | 0.08 | - | 3.55 |
| Solid (wt%) | 0.2-1 | - | - | - | 1.0 |

[a]Bridgewater, 2012, [b]Abnisa et al., 2011, [c]Biradar et al., 2014, [d]Kim et al., 2014

In fact, bio-oil contains high oxygen contents of almost 35-40 wt% due to oxygen-rich compounds such as water, organic acid, ketone, aldehyde and phenolic as well as anhydro sugars. Whereas Beste & Buchanan Iii (2012) suggested that the oxygen content is dependent on the bio-oil's water content (Beste & Buchanan Iii, 2012). These components are responsible for poor fuel quality of bio-oils which are low heating value, incompatibility with conventional fuel, high viscosity, chemical instability and acidity (Bridgwater, 2012). Bio-oil from biomass pyrolysis showed low pH, it is due to the high concentration of acidic compounds from the degradation of hemicellulose and lignin during pyrolysis. In term of high heating value, the heating value of bio-oil is range from 16-19 MJ/kg. However, high water and oxygen contents are mainly responsible for the low bio-oil HHV.

Bio-oils produced were analyzed the elemental in term of carbon, hydrogen, oxygen, nitrogen, and sulfur. Bio-oil from Jatropha and bio-oil upgraded showed higher carbon than bio-oil from other biomass. Heavy fuel oil as petroleum fuel oils was chosen for comparison properties, and bio-oils produced showed lower HHV than heavy fuel oil. The higher HHV value of the upgraded bio-oil (23.2-31.3 MJ/kg) as compared to 43.4 MJ/kg of heavy fuel oil, it was due to higher moisture content and higher oxygen content than that of Heavy fuel oil. These data suggested that bio-oil from Jatropha waste could be used as alternative feedstocks for biodiesel production using hydrotreating process (Kim et al., 2014), However, these properties demonstrate that the bio-oil upgraded necessary to determine in order to apply as biofuel.

## 2.8 Bio-oil upgrading

Upgrading bio-oil to transport fuel such as diesel, gasoline, require deoxygenation process two major routes: (1) hydrodeoxygenation and (2) catalytic vapor cracking by catalysts.

(1) Hydrodeoxygenation (HDO) or hydrotreating includes treating bio-oils at moderate temperature (300-600°C) with high hydrogen pressure in the presence of catalysts, which are normally sulfide CoMo and NiMo-based catalysts. In addition, $Pt/SiO_2-Al_2O_3$, vanadium nitride, and ruthenium have been

applied for hydrotreating. During the reaction, the oxygen in bio-oil reacts with $H_2$ to form water and saturated C-C bonds. However, hydrogenation of aromatics in bio-oil should be avoided, because it can reduce the octane number and increase hydrogen consumption.

(2) Upgrading pyrolysis vapors by using cracking catalysts is an emerging technology to convert oxygenated compounds produced during biomass pyrolysis directly to hydrocarbons which can improve bio-oil quality. In contrast to hydrotreating, catalytic vapor cracking can be processed without the requirement of high hydrogen pressure leading to the reduction of operating cost (Czernik & Bridgwater, 2004). Several catalysts were applied for this application such as metal oxides, mesoporous materials, and shape-selectivity zeolites. Among them, zeolites, particularly ZSM-5, have been successfully used for the deoxygenation of biomass-derived oxygenates to enhance aromatic production.

## 2.9 Supported Catalysts

### 2.9.1 Ceramic support

Catalysis plays an important role in modern energy conversion, chemical manufacture, and environmental technology. Approximately 85% of all chemical processes are concerned with the use of catalyst. In modern transport fuels, all molecules are inevitably involved in one or more solid catalyst. The original solid catalyst naturally consists of support and active phase. Catalysts have various forms, ranging from atoms or molecules to large structure such as zeolites or enzymes. They also can be used in varied operating environments: in liquids, gases or at surface of solids. The specialization in studying composition and shape of particular catalyst, including preparing its optimum form, is very vital. With high surface area, the support particle also acts as a thermal stabilizer and eases the accessibility of the reactive gas. Under the same condition, the distribution of the metal within the porous support dominantly influences the performance of supported catalyst (P.de Jong, 2009). Support catalysts normally are thermally stable and chemically relatively inert.

Alumina silica and carbon are commonly used. Magnesia, titania, zirconia, zinc oxide, silicon carbide and zeolite also can be utilized in some specific applications.

Many studies dealing with the preparation of supported catalysts have been concerned with the control of the metal profile within the solid support. A uniform metal distribution is desirable. The choice of the optimal metal profile is determined by the required activity, selectivity, and other characteristics of the chemical reaction. Catalyst stability is also an important factor, the four main categories of catalyst profiles, namely uniform, egg-shell, egg-white, and egg-yolk, are shown in Fig.2.11. Several reported that under isothermal conditions, the egg-yolk catalysts have the best activity at low values of Thiele's modulus (no mass transfer limitation). Clearly, egg-shell catalysts, where the catalyst layer is concentrated close to the external pellet surface, are advantageous in the case of fast reactions with strong diffusional limitations. Additionally, egg-shell catalysts give higher selectivity for reactions, where diffusion is the limiting step. When the external surface of the catalyst is exposed to poisoning or intense abrasion and attrition, as seen in fluidized or moving beds, the egg-white and egg-yolk distributions have a longer lifetime because the active layer is not impacted (Regalbuto, 2011).



(I) Uniform     (II) Egg-shell

(III) Egg-white     (IV) Egg-yolk
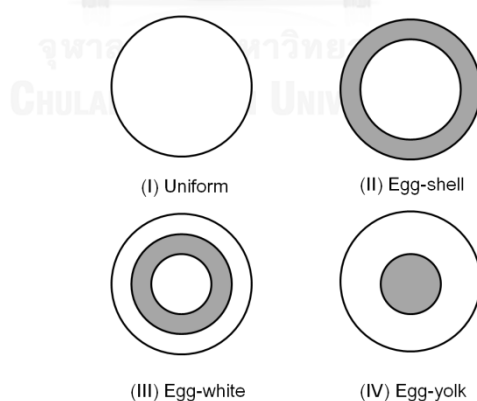
**Fig. 2.11** Main types of metal distribution in supported catalysts

Uniform metal profiles are advantageous for reactions that are kinetically controlled. Depending on the environment under which the catalyst will operate, different types of solid support materials are used. The most common supports in industry are solid oxide supports. Typically, these materials include alumina ($Al_2O_3$),

silica ($SiO_2$), and titania ($TiO_2$). Oxide surfaces are generally covered with hydroxyl groups, which are usually represented as S-OH, where S stands for alumina, silica, or titanium. When contacted with water (during the impregnation step), these groups can behave as Brønsted acids or bases by exchanging a proton with the liquid solution, which gives them the ability to interact with several catalytic precursors (Regalbuto & ENGnetBASE Supplement, 2007).

Owing to its excellent thermal and mechanical stability and its rich chemistry, alumina ($Al_2O_3$) is the most widely used support in catalysis. As a support, $\gamma$-$Al_2O_3$ offers high surface areas (50–300 $m^2g^{-1}$), mesopores of between 5 and 15 nm, pore volumes of about 0.6 $cm^3g^{-1}$, high thermal stability and the ability to be shaped into mechanically stable extrudates and pellets. The thermal stability of $\gamma$-$Al_2O_3$ can be significantly improved by lanthanum oxide additives, which reduce the rate of sintering and retard the conversion into other phases of alumina. Its surface contains several hydroxyls, between 10 and 15 OH per $nm^2$, the linear ones being Brønsted bases ($H^+$ acceptors), and the bridged ones Brønsted acids ($H^+$ donor) (Chorkendorff and Niemantsverdriet, 2006).

2.9.2 Activated Carbons

The surprising usefulness of the core chemical element, carbon, has given rise to a wide diversity of structural forms of solid carbon, which well known as polymorphs. These are composed entirely of carbon but have different physical structures. Two variants are amorphous carbons and crystalline carbons as shown in Fig. 2.12 (Yang et al, 2011).



**Fig. 2.12** Polymorphs of carbon (Yang et al, 2011)

As the other major form of carbon, amorphous carbon is primarily made of graphitic sheetlets with no regular order. They are characterized by strong covalent bonding in the basal plane. Activated carbon is one of the most common amorphous carbons which manufacture and use date back to the 19th century. The usefulness of activated carbon mainly derives from its high micropore and mesopore volumes and the resulting high surface area. Modern activated carbon manufacturing process basically comprises three main steps, which are: raw material preparation, low-temperature carbonization, and activation. The raw materials are carbonaceous matter such as wood, peat, coals (anthracite and bituminous coals), petroleum coke, coconut shell, fruit nuts, and other biomass derived sources. Because the presence of favorable pore geometries and volumes, activated carbons have been used in the areas of gas separation and storage, water purification, catalysis, and electrochemistry.

The activated carbons are the supports for most study on hydrogenation reaction. These materials do not present electronic effect like the partially reducible oxides, or graphite which could enhance the selectivity towards un-saturated alcohols. Due to the high surface areas, there're much interested in the preparation of bimetallic catalyst with activated carbon as supporter (Esther Bailón-Garcaí, 2013). However, the use of micro-mesoporous supports may not be suitable for hydrogenation reactions in liquid phase where hydrogen solubility in the solvent is small, because when very active metals are used, isomerization reactions may occur to a greater extent than the desired ones due to an immediate decrease of the hydrogen concentration on the active site.

## 2.10 Impregnation

Preparation of supported metal oxides for heterogeneous catalysis can be carried out through several routes. This work will focus on finding suitable catalyst for bio-oil upgrading route via catalytic cracking of pyrolysis vapors, the catalysts will be synthesized by impregnate method. The following primary steps are common to all procedures for support metal oxides: preparation of the support precursor, contact of

the surface and support precursors, and thermal decomposition of the precursors (through calcination) to their oxide form (Regalbuto & ENGnetBASE Supplement, 2007). During impregnation, the dissolved precursor migrates in the pores of the support, on which it may adsorb. The impregnation solution contains several chemical species: the metal precursor of the active phase, it is also selected according to their physicochemical properties and cost.

The simplest way to achieve impregnation by contacting a previously dried support, the solution is drawn into the pores by capillary suction (capillary impregnation). In the case of proper wetting, no excess of solution remains outside the pore space and the procedure is also called dry or incipient wetness impregnation. It can also be carried out in diffusional conditions, by dipping a water-filled support in the precursor solution (wet impregnation). Wet impregnation should be avoided when the interaction between precursor and support is too weak to promise the deposition of the former (P. de Jong, 2009). The catalysts are produced by impregnation of a porous, catalytically inert support material with a solution of the active catalyst, which is adsorbed onto the support surface. The reason for using support materials is that in many cases the active catalytic material, i.e., the precursor, is an expensive metal (e.g., Pt, Pd, Rh, Au), which needs to be used economically. This can be achieved by using supported catalysts, where the active metal or the metal oxide is dispersed on a porous solid support with a high surface area with a predefined pore structure and particle shape. The precursor is deposited on the support from a liquid solution, which in most cases is water-based. If the support surface is hydrophobic or if hydrolysis of the support must be avoided, a nonaqueous solution is used. Typically, the support is immersed in a solution that contains the inert precursor as a metal salt (Regalbuto, 2011).
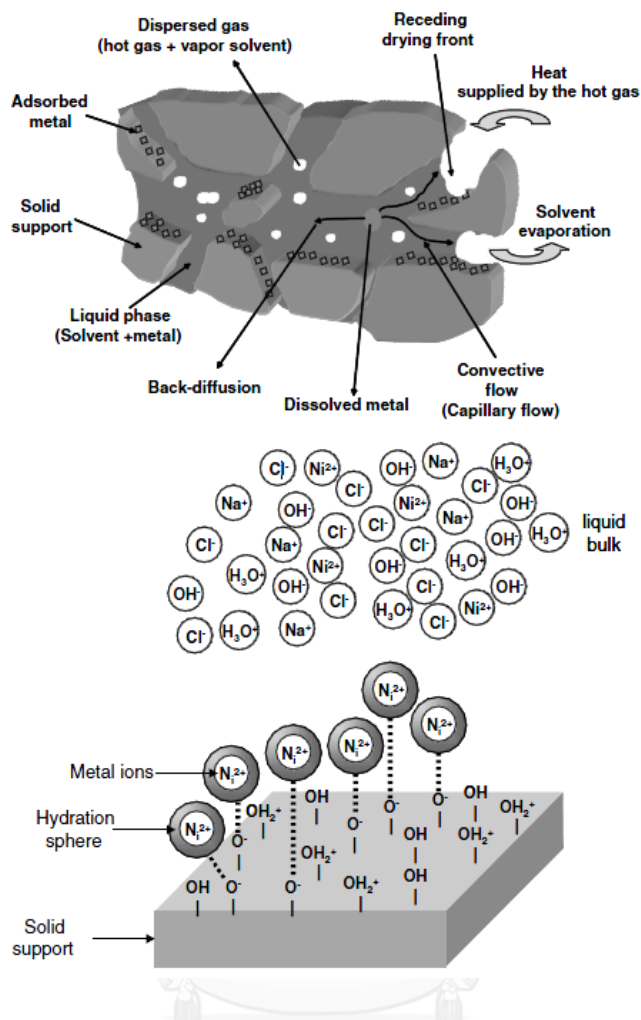
**Fig. 2.13** Transport mechanisms during drying of supported catalysts and
metal adsorption on an oxide support

The rearrangement of the active metal to the support is supervised by several processes in physical and chemical. The most important ones, which determine the final metal profile, are (1) adsorption of the active metal onto the support, (2) transport of the solvent, (3) transport of various dissolved species in the solvent, (4) heat transport, and (5) mass and heat transfer at the surface of the support particle (Fig.2.13).

In catalytic conversion reaction, noble-metal catalysts are commonly applied. Hydrogeneration reactions on noble metals catalysts are widely used in the refining, pharmaceutical, specialty chemical and food industries. Added either by incipient wetness or cation exchange and subsequently dried and calcined to form the correlated oxide or the metal itself, noble-metal precursor salts are usually used to

prepare supported noble-metal catalysts. This is because some noble-metal oxides, such as those of Pt and Au, are decomposed to metal at below 500°C. As impregnated catalysts, the dispersion and deduction of the supported noble metal are influenced by the interaction strength between the metal precursor and support. Usually, the moderate precursor-support interaction is most preferable due to the improvement of dispersibility of the metal precursor on the support. However, it easily reduces the metal precursor-support interaction strength. The noble-metal catalysts are more expensive than the base-metal catalysts, but they normally have higher site activity. Therefore, their loading is much lower than supported base metals. With lower-loading, they contain metal particles (1-3 nm) at much smaller than those found in base-matal catalysts (> 10 nm) (P. de Jong, 2009).

## 2.11 Metal active sites

This section is focused on the important principles and concepts of heterogeneous catalysts. The Sabatier principle is concerned with linear free energy relationships, for instance, the Brønsted relation. These relations are defined by the heat of reaction q (thermodynamic quantity) and the activation barrier E (kinetic quantity) of an elementary step in the exothermic direction (q>0). Regardless of entropy effects, a Brønsted relation can be expressed as

$$\Delta E = a \, \Delta q$$

where $\Delta E$ is the decrease in activation energy, $\Delta q$ is the increase in the heat of reaction and a (0<a<1) is an empirical parameter. Consequently, in exothermic direction, when q (the heat of reaction) increases, an elementary step will have a high rate constant. On the contrary, in the endothermic direction, the rate constant will reduce with increasing q because the activation barrier is equivalent to the sum of the activation energy E and the heat of reaction. In addition, the Brønsted relationship represents a bridge between thermodynamics and kinetics and, with the Sabatier principle, permits an interpretation of the so-called volcano plots. These volcano curves result when a quantity correlated with the reaction rate under consideration is plotted against a measure of the intermediate compound stability.
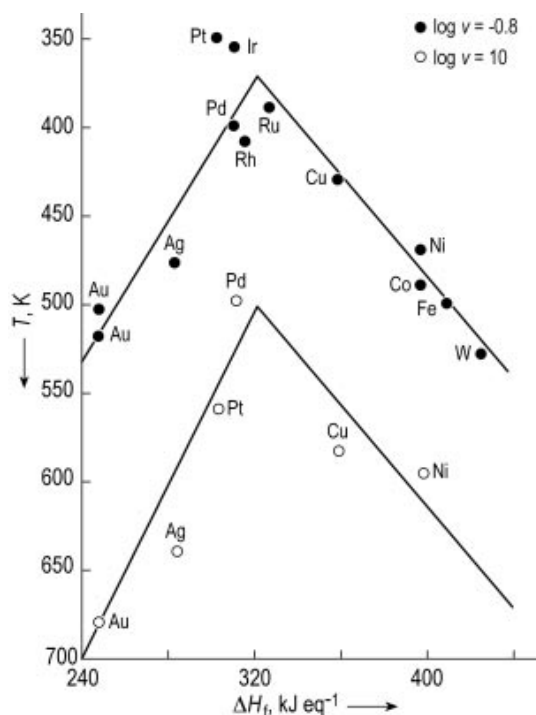
**Fig. 2.14** Volcano plot for the decomposition of formic acid. The temperature Tat which the rate of decomposition has a fixed value is plotted against the heat of formation $\Delta H_f$ of the metal formate.

The volcano plot for the decomposition of formic acid on transition metal is shown in Fig. 2.14. In this reaction, a surface formate acts as the intermediate, so $\Delta H_f$ (the heat of formation) of the bulk metal formates were used to gauge the stability of the intermediate. At low values of $\Delta H_f$, the low reaction rate corresponds to the absorption rate. The absorption rate increases with rising heat of formation of bulk formates. As mention previously, this heat can represent the stability of the surface compound. On the other hand, at high values of $\Delta H_f$, the reaction rate is also low, but corresponds to the desorption rate, increasing with reducing $\Delta H_f$. For this reason, a maximum rate of reaction (decomposition of formic acid) can be observed at intermediate $\Delta H_f$ value which leads to both optimal rates of absorption and desorption.

In supported catalysts, the active phase (metal, oxide, sulfide) expose to active support interactions, mostly relied on the surface free energies of the support and

active phase material as well as the interfacial free energy between the two components. Compared to typical oxide support materials, such as g-$Al_2O_3$, $TiO_3$ (anatase) and $SO_2$, active transition metal oxides (e.g., $V_2O_5$, $MoO_3$, $WO_3$) own comparatively low surface free energy. In the absence of $SiO_2$-supported transition metal oxide, the interaction between active phase and support seems to be advantageous, even though their interfacial free energies are unknown. Consequently, spreading and wetting phenomena are allowed, if the oxide mixtures are thermally treated at the temperature that is high enough to bring about mobility of the active oxide. Referred to a rule of thumb, mobility of a solid theoretically appears above the Tammann temperature, equivalent to half the melting point of the bulk solid. For this reason, the active transition metal oxide is prone to wet the support surface and form a monolayer (monolayer-type catalysts). Due to high surface energies of transition and nodel metals, small particles or crystallites are likely to agglomerate in order to reduce their surface area. As a result, on the surface of supports, deposition which causes favorable metal-support interaction (MSI) is necessary to stabilize nano size metal particles. The smaller particles the more effect of these interactions on their own physical properties and morphology. The characteristics of support metal for designated metal therefore vitally influences the catalytic properties of the metal particles.

Unstable supported metals still tend to agglomerate at properly high temperature in reducing atmosphere. As metal surface area reduces, deactivation is inevitable. With oxidized active metal, thermal treatment in an atmosphere is a typical process for regeneration. Compared to the parent metal, the surface free energies of transition and noble metal are significantly low. Their spreading on the support surface becomes more advantageous. Under certain moderate condition, subsequent reduction can regenerate the high degree of metal dispersion which can be defined as the ratio of number of metal atoms, exposed to the particle surface (NS), o the total number of metal atoms (NT) in the particle (D = NS/NT) (Deutschmann et al., 2000).

Besides metals, the principle of active sites can be extended to metal cation, anion, Lewis and Bronsted acid-base pairs (acid and base simultaneously acting in chemisorption). In many thermal catalyst reaction studies, Nickel (Ni) was used to be

an active site because of cheapness. With comparable activity and selectivity, Ni is the most practical option. In the field of heterogeneous non-noble metal catalyzed organic synthesis, Ni-containing solids have been used as a promoter or heterogeneous catalyst for hydrogenation of various compounds (Shimizu et al., 2013).

## 2.12 Kinetic Models of Pyrolysis

Based on classical approach to liquid oil (bio-oil) production in fixed bed reactor, this research aims to develop model that mathematically considers the physical characteristics of solids, liquids and gases of pyrolysis products in order to obtain the solution and interpretation the pyrolysis reaction. The principal of kinetics of pyrolysis is mandatorily applied to gain the optimal process parameters and maximal yields. In fact, the reliable data of kinetic rate constants which are valid for a broad range of biomass and different heating rate are difficult to acquire. Additionally, in a non-equilibrium and non-steady state process, these data are much more difficult to determine, so designers can use classical approach as a guideline to define the first approximation. The following section presents a qualitative interpretation of process, referred to data from comparatively slow heating rate. The pyrolysis kinetic models of lingo-cellulosic fuel (biomass) can be generally categorized into three types which are:

- One-stage global single reaction model. This model is developed by a one-step reaction and experiment data of weight-loss rate and will be described later.

-One-stage, multiple reactions, several reactions model. This model describes the degradation of biomass into char and several gases. A one-stage simplified kinetic model is applied for these parallel reactions. The model is applicable to determine a product distribution.

- Two-stage semi-global model. Both primary and secondary reactions are serially reckoned in this model.

This research particularly applies One-stage global single reaction model. The reaction model is based on a single overall reaction:

$$\text{Biomass} \rightarrow \text{Volatile} + \text{Char} \tag{2-5}$$

The rate of pyrolysis leans on the non-pyrolyzed mass of the biomass. Therefore, in primary pyrolysis process, the decomposition rate of mass, $m_b$, can be written as

$$\frac{dm_b}{dt} = -k(m_b - m_c) \qquad (2\text{-}6)$$

where $m_c$ is the mass of char residual after complete conversion (kg), $k$ is the first-order reaction rate constant (s$^{-1}$) and $t$ is time (s). The fraction change, $X$, in the mass of biomass can be non-dimensionally written as

$$x = \left(\frac{m_b - m_c}{m_0 - m_c}\right) \qquad (2\text{-}7)$$

where $m_0$ is the initial mass of biomass. Combining Eq. (2-6) and Eq. (2-7) lead to

$$\frac{dx}{dt} = -k(1-x) \qquad (2\text{-}8)$$

Solving this equation to obtain

$$x = 1 - A exp^{-kt} \qquad (2\text{-}9)$$

where A is the pre-exponential coefficient, E is the activation energy (J/mol), R is the gas constant (J/mol·K) and T is temperature (K). For fast pyrolysis, A and E cannot be simply determined due to the difficulties in extracting data from dynamic thermogravimetric analysis (TGA). However, both can be reasonably obtained for slow heating. Without the effect of secondary cracking and heat-transfer limitation, an irreversible one-stage global first-order equation can represent the weight-loss rate of cellulose during pyrolysis (Basu, 2010).

## 2.13 Computational fluid dynamics (CFD)

In biomass thermochemical conversion field, computational fluid dynamics (CFD) modeling techniques are widely used to simulate and analyze the performance of thermochemical conversion implements, such as fixed beds, fluidized beds, combustion furnace, firing boilers, rotating cones and rotary kilns. The developed model is not only to simulate the solid biomass pyrolysis in an operating drop tube reactor under stable conditions, but also to forecast the volatiles in term of tar, light

gas and char fractions which were released from biomass. $H_2$, $CO_2$, $CO$ and $CH_4$ and steam were considered as separate species of gases. The boundary conditions of the simulation are described in Chapter 4.

2.13.1 Basic governing equations

For the thermochemical processes, the developed CFD model considers the characteristics of fluid flow, heat transfer, mass transfer and chemical reactions. Fundamentally the governing equations, concerning the conservation laws of mass momentum, energy and species, are presented respectively by following equations:

$$\frac{\partial \rho}{\partial t} + \nabla \bullet (\rho \vec{u}) = S_p \tag{2-10}$$

$$\frac{\partial (\rho \vec{u})}{\partial t} + \nabla \bullet (\rho \vec{u} \vec{u}) = -\nabla p + \nabla \bullet (\mu \nabla \vec{u}) + S_u \tag{2-11}$$

$$\frac{\partial (\rho H)}{\partial t} + \nabla \bullet (\rho \vec{u} H) = \nabla \bullet (\lambda \nabla T) + S_H \tag{2-12}$$

$$\frac{\partial (\rho Y_i)}{\partial t} + \nabla \bullet (\rho \vec{u} Y_i) = \nabla \bullet (D \nabla (\rho Y_i)) + S_Y + R_f \tag{2-13}$$

where $\rho$ is the static pressure, T is the stress tensor and $\rho \vec{u}$ are the gravitational body force. The source $S_p$ is the added mass from the dispersed secondary phase to the continuous phase, for example the vaporization of liquid droplet.

2.13.2 Thermochemical reaction submodels

The biomass thermal conversion involves complicate chemical and physical processes, for instance vaporization, devolatilization, volatile secondary reactions and char oxidation as well as transport phenomena (Wang & Yan, 2008).

*2.13.2.1 Devolatilization submodels*

Once the critical temperature of biomass is reached, the devolatilization process is initiated. Many biomass devolatilization models have been developed and reviewed. One-step global mechanisms and a semi-global multi-step mechanism is obviously separable (ref). Devolatilization rates are simplified by single or two-step Arrhenius reaction schemes. The one-step global mechanisms can be represented as:

$$\textbf{\textit{Biomass}} \xrightarrow{k} \textbf{\textit{Volatiles}} + \textbf{\textit{Char or Biomass}} \xrightarrow{k} \textbf{\textit{Tar}}(\textbf{\textit{bio}} - \textbf{\textit{oil}}) + \textbf{\textit{Gases}} + \textbf{\textit{Char}} \tag{2-14}$$

*2.13.2.2. Secondary cracking submodels*

The devolatilized tar is a condensable hydrocarbon mixture. The secondary tar crack reaction appears homogeneously in gas phase, but heterogeneous at the surface of biomass or char particles. Tar is a complex multi-component mixture and the cracking mechanism is very comprehensive. Recently, tar cracking can be considered through the overall reaction schemes such as:

$$\text{Tar} \rightarrow \ \tilde{v}_{co}CO + \tilde{v}_{CO_2}CO_2 + \ \tilde{v}_{H_2}H_2 + \tilde{v}_{CH_4}CH_4 + \tilde{v}_{tar_{inert}}tar_{inert} \qquad (2\text{-}15)$$
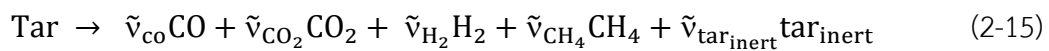
Where $\tilde{v}$ is stoichiometric coefficients, many experimental investigation and model studies have been done on the cracking process. The model stoichiometric coefficients and kinetics data can be found in the literatures.

*2.13.2.3 Homogenous gas-phase reactions submodels*

Both the biomass devolatilization and the cracking gas species will react with the supplied oxidizer and interact with each other, such as water gas shift reaction. The exothermic reactions generate heat which is necessary for the release of volatiles and the ignition of char. The typical homogeneous reactions are:

$$H_2 + \tfrac{1}{2}O_2 \rightarrow H_2O + 242 \ kJ/mol \qquad (2\text{-}16)$$
$$CO + \tfrac{1}{2}O_2 \rightarrow CO_2 + 283 \ kJ/mol \qquad (2\text{-}17)$$
$$CH_4 + \ 2O_2 \rightarrow CO_2 + 2H_2O + 35.7 \ kJ/mol \qquad (2\text{-}18)$$
$$CH_4 + \ H_2O \ \rightarrow CO + \ 3H_2 - 206 \ kJ/mol \qquad (2\text{-}19)$$
$$CO + \ H_2O \ \leftrightarrow CO_2 + H_2 + 41.1 \ kJ/mol \qquad (2\text{-}20)$$
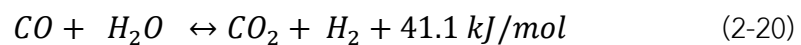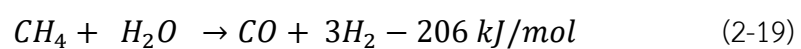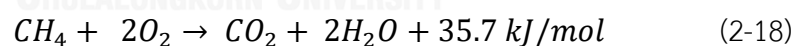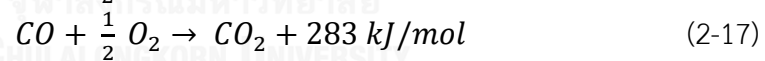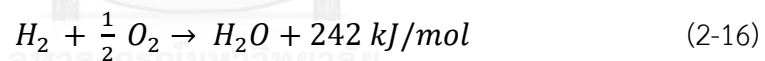
More reaction mechanisms and the kinetic parameters can be found from the literature (Boateng & Mtui, 2012; Mellin et al., 2013).

*2.13.2.4 Heterogeneous reaction submodels*

Char is the solid residue from thermochemical reaction after devolatilization. These reactions involve balancing the rate of mass diffusion of the oxidizing chemical species to the particle surface of biomass with the surface reaction of gas species with the char. The overall rate of a char particle depends on the temperature and composition of the gaseous environment and the size, porosity and temperature of

the particle. It is determined by the oxygen diffusion and particle surface reaction rate. The simplified reactions models consider the following overall reactions:

$$C + CO_2 \rightarrow 2CO \qquad -172 \; kJ/mol \qquad (2\text{-}21)$$

$$C + \frac{1}{2} O_2 \rightarrow CO \qquad +122.9 \; kJ/mol \qquad (2\text{-}22)$$

$$C + \; H_2O \; \rightarrow CO + H \; -131 \; kJ/mol \qquad (2\text{-}23)$$
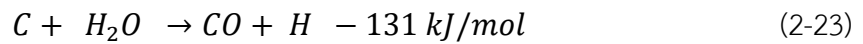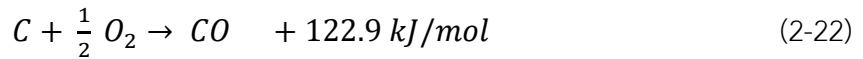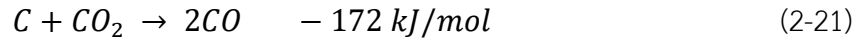
### 2.13.3 Additional physical models

Even though Navier-Stokes equations are known as the basis of fluid mechanics describing the conservation laws of mass, momentum, and energy, they have a limited amount of biomass thermochemical conversion applications. The additional processes may be effected the dynamics of the thermochemical reactor system. Accordingly, the basic governing equations need to be supported with special additional physical models in order to completely represent the physical process. The important physical models include turbulence models, porous media and multiphase models, heat transfer with radiation models, and mass transfer and diffusion.

#### 2.13.3.1 Turbulent flow

Turbulent flows are considered the fluctuating velocity fields since the complex of geometry and/or high flow rates. It affects to the heat and mass transfer and plays an important role in some processes such as biomass gasification/pyrolysis in fluidized bed and non-premixed combustion in furnaces. Although the Navier-Stokes equations can be solved directly for laminar flows, the turbulent flows can be solved using the direct numerical simulation (DNS) with full solution of the transport equations. At all length and time scales of turbulent flows, the computation is too exhaustive due to the fluctuations can be of small scale and high frequency.

#### 2.13.3.2 Radiation modeling

The radiative transfer equation (RTE) for an absorbing, emitting, and scattering medium at position $\vec{r}$ in the direction $\vec{s}$ can be written as follows:

$$\frac{dI(\vec{r},\vec{s})}{ds} + (a + \sigma_s)I(\vec{r},\vec{s}) = an^2 \frac{\sigma T^4}{\pi} + \frac{\sigma_s}{4\pi} \int_0^{4\pi} I(\vec{r},\vec{s}')\Phi(\vec{r},\vec{s}')d\,\Omega \qquad (2\text{-}24)$$

Where

$\vec{r}$ = position vector $\qquad$ $\vec{s}$ = direction vector

$\vec{s}'$ = scattering direction vector $\qquad$ $S$ = path length

$a$ = absorption coefficient $\qquad$ $n$ = refractive index

$\sigma_s$ = scattering coefficient $\qquad$ $\Phi$ = phase function

$\Omega'$ = solid angle

$\sigma$ = Stefan-Boltzmann constant (5.669 × 10-8 W/m$^2$-K$^4$)

$I$ = radiation intensity, which depends on position $\vec{r}$ and direction $(\vec{s})$

A semi-transparent medium is considered; and the refractive index is equal to unity. The optical thickness $aL$ where $L$ is an appropriate length scale is a good indicator of which model to use.

*2.13.3.3 Mixture fraction model*

The reaction chemistry in the probability density function (PDF) method were presented the reaction chemistry in the mixture fraction model for solving turbulent-chemistry interaction. The equilibrium model was applied which assumes that the chemistry is rapid enough for chemical equilibrium to exist at the molecular level. As the simplifying assumptions, the immediate thermo chemical state of the fluid related with the mixture fraction f. Algorithms based on the minimization of Gibbs free energy are applied to compute species mole fractions from f. The mixture fraction f is presented in terms of the atomic mass fraction as:

$$f = \frac{Z_j - Z_{j,ox}}{Z_{j,fuel} - Z_{j,ox}}$$
(2-25)

where $Z_j$ is the mass fraction for element *j*. The subscript *ox* and *fuel* are the value at the oxidizer stream inlet and the fuel stream inlet respectively. Under the equal diffusivities, the species equations can be reduced to a single equation for the mean (time-averaged) mixture fraction *f*. While the mean mixture fraction variance *f* '2 is used in the closure model, to describe the turbulence-chemistry interactions

*2.13.3.4 Porous media and two-phase model*

The porous media is generally used in biomass pyrolysis by fixed bed. The biomass particles arrangement in the fixed bed forms void spaces. The volatiles and gases pass through the particle voids and can flow through a porous media. The particle position was changed during the conversion for the devolatilization and combustion of biomass particles. In this process, to create the mesh of geometry with a complex unstructured is out of both computational power and CFD algorithms levels, so Darcy's law was applied to the simplified porous media. The relationship on pressure drop and volume averaged velocity caused by viscous drag are presented in the equation:

$$\nabla p = -\frac{U}{\alpha} \; \vec{v}$$

(2-26)

## 2.14 Literature reviews for cracking catalysts

In recent year, the catalytic upgrading of bio-oil is widely practiced. The use of a suitable catalyst during the fast pyrolysis can not only improve the quality of bio-oil but also increase its yield. Therefore, an important step in the success of the pyrolytic catalytic upgrading process of bio-oil is the selection of a suitable catalyst (Kanaujia et al., 2014) . Thus, fast pyrolysis can be a promising residue management that is possible to convert these wastes to fuel products such as bio-oil.

There are several methods of upgrading and improving bio-oils quality as mention above. They can produce oil with low oxygen content and a heating value corresponding to crude oil (Thangalazhy-Gopakumar et al., 2011). Catalysis is important to modern energy conversion, chemicals manufacture, and environmental technology. From the start, oil refining and bulk chemicals manufacture have relied largely on the application of solid catalysts. In the meantime, in specialty and fine-chemicals production, catalysis is used frequently too. According to current estimates, about 85% of all chemical processes make use of catalysis, while all molecules in modern transportation fuels have been confronted with one or more solid catalysts (Graça et al., 2013). Catalysts are the workhorses of chemical transformations in the industry.

Approximately 85–90% of the products of chemical industry require manufacturing processes that involve the use of catalysts (Srinivasan et al., 2012).

Catalytic cracking is the most probable route to remove the oxygen containing functional groups of bio-oils at atmospheric pressure and hence convert the oxygenated compounds to a lighter hydrocarbon fraction and higher aromatic contents (Graça et al., 2013). Moreover, the most promising processes for the continuous biomass catalytic conversion to bio-oil, requires catalyst regeneration in order to reuse in the pyrolysis catalytic process.

2.14.1 Biomass pyrolysis using analytical Py-GC/MS

Upgrading of bio-oil by catalytic reforming of pyrolytic vapors product was to be performed in this work. Zeolites have been widely studied, such as HZSM-5 and Al/SBA-15 which are effective to convert the highly oxygenated compounds to aromatic hydrocarbons (Murata et al., 2012). Several catalysts applied in this upgrading technology are metal oxide, microporous, and mesoporous materials via both lab scale-pyrolyzer and pyroprobe-GC/MS instruments. Pattiya et al. (2008) tested the catalytic effects of zeolites by Py–GC/MS, the results showed that all the catalysts produced aromatic hydrocarbons and reduced oxygenated lignin derivatives. Zhang et al. (2013) added mesoporous catalysts ($\gamma$-$Al_2O_3$) in the microporous catalyst (LOSA-1) for biomass catalytic pyrolysis, and found that these catalysts can significantly improve the selectivity of low-carbon components with the maximum aromatic and olefin yield of 25.3% (Zhang et al., 2013). However, zeolites are difficult to synthesized and also inherit high production cost. They are difficult to be industrially utilized for upgrading biomass pyrolysis vapors. Recently, some transition metal based catalysts such as Ni, Co, Pt, Pd and Ru catalysts are utilized for deoxygenated reactions which were reported by several researches (Shen & Yoshikawa, 2013)

Modifications of the metal catalysts on ceramic support were generally performed by the impregnation method. These works were reported by Lu et al. (2010) who studied catalytic upgrading of biomass fast pyrolysis vapors by noble metal with titania and zirconia/anatase based catalysts. The highest hydrocarbon content (13.1%) was obtained by the zirconia/anatase based catalysts. Kaewpengkrow et al. (2014) who

studies effect of metal catalysts (Ce, Ni, Pd and Ru) on selective deoxygenation, reported relatively higher catalytic activity toward deoxygenation reactions and enhanced yields of aliphatic and aromatic hydrocarbons to 40%. Therefore, modification of the metal catalysts by the impregnation method has not only lower production cost, but also improving hydrothermal stability which makes them possible for treating biomass pyrolysis vapor. There have been some works using ceria ($CeO_2$) based catalysts, mostly for promotion of hydrogen production and prevention of coke deposition during the gasification and pyrolysis process. Metals such as Ni, Pd, Pt and Ru have been added to the ceria-based catalyst system to improve the catalytic performance. For this reason, Ce-based modified catalysts were synthesized in this study. In addition, there are reports of the use of M/AC as catalysts for the deoxygenation of fatty acids in supercritical water and for upgrading heavy oils or bio-oil with added $H_2$ high pressure  (Duan et al., 2016; Luo et al., 2010; Spadaro et al., 2015; Wang et al., 2016b).  Cheng et al., (2016) studied the bio-oil upgraded through hydrodeoxygenation with 6 wt%. Ni based activated carbon (Ni/AC, Ni-Fe/AC, Ni-Mo/AC and Ni-Cu/AC) (Cheng et al., 2016). It was found that the Ni/AC catalysts produced the highest content of gasoline range hydrocarbons ($C_6$–$C_{12}$) at 32.63% (% area) in the upgraded bio-oil. However, there're only a few studies of M/AC catalysts on upgrading of bio-oil from pyrolysis vapors phase. Murata et al., (2016) studied the effect of metal modified carbon catalysts on pyrolytic product by Py–GC/MS. They found that these catalysts enhanced yields of aromatic to 40–60% (Murata et al., 2016; Murata et al., 2013). Comparison of the effect of catalytic fast pyrolysis vapors on product selectivity is shown in Table 2.5.

**Table 2.5** The effect of catalytic fast pyrolysis vapors of biomass on product selectivity

| Biomass | Type of catalyst | B:C ratio | Pyrolysis product (%Peak area) | | | Ref. |
|---|---|---|---|---|---|---|
| | | | Hydro-carbon | Aromatic | Phenol | |
| cassava rhizome | ZSM-5 | 1:1 | - | 7.0 | 0.55 | (Pattiya et al., 2008) |
| Sawdust | SBA-15, Al/SBA-15 | 1:1 | 0.14 | - | 7.5-16.0 | (Qiang et al., 2009) |
| poplar wood | Pd, Ru, Ce/ZrO$_2$ | 1:2 | 0.10-13.10 | - | 10.6-37.2 | (Lu et al., 2010) |
| Biomass (oak,corn cob,) | H-ZSM5 | 1:5 | - | 9-14 | 0.087-0.22 | (Mihalcik et al., 2011) |
| Jatropha wastes | H-ZSM5 | 1:6.25 | - | 90 | - | (Murata et al., 2012) |
| Jatropha wastes | Noble metal on AC | 1:6.25 | 2.45-29.5 | 40.7-73.9 | 1.78-26.2 | (Murata et al., 2013) |
| Jatropha residue | Pd, Ru, or Ni on Ce/Al$_2$O$_3$, Ce/ZrO$_2$ | 1:1 and 1:5 | 12.71-40.60 | 0.99-16.80 | 1.49-4.51 | (Kaewpengkrow et al., 2014b) |
| Sawdust | Fe(III)/CaO | 1:1 | aromatic hydrocarbons increased | Light heavy phenols, | - | (Zhang et al., 2014) |
| Corn stover | ZSM-5 | 1:2 | 39 | - | - | (Zhang et al., 2015) |

**Table 2. 6** The effect of catalytic fast pyrolysis vapors of biomass on product selectivity

| Biomass | Type of catalyst | B:C ratio | Pyrolysis product (% Peak area) | | | References |
|---------|------------------|-----------|-------------|----------|--------|------------|
| | | | Hydro-carbon | Aromatic | Phenol | |
| agricultural wastes | - | - | - | 5-7 | 10-25 | (Chen et al., 2015) |
| Pine, sawdust, Microalgae | H-ZSM5 | 1:10 | >60 | - | - | (Lorenzetti et al., 2016) |

Moreover, char-catalyzed was used to the upgrading of bio-oil from pyrolysis vapors phase in this work. In a partial or absence of oxygen, thermal decomposition of biomass (pyrolysis) is manipulated to yield a carbon-rich biochar. Char derived from biomass pyrolysis/gasification can be employed to adsorb heavy metals or organic pollutants as a promising alternative to commercial absorbents. Char has also been studied as an inexpensive catalyst with fair performance in tar removal and an excellent adsorbent (Shen, 2015). Consequently, the superior activity and stability of these catalysts would enhance the further fast pyrolysis sequential process.

2.14.2 Pyrolysis Lab scale

Based on the positioning of the catalyst within the reactor, catalytic pyrolysis can be divided into two different processes: in-situ and in-bed. In the in-situ process, the biomass is cracked to produce pyrolytic vapors which pass through catalyst beds where they are converted into bio-oil as well as gaseous and solid byproducts. Catalytic vapor cracking is generally considered superior to other catalytic upgrading technologies, such as hydrotreating, esterification and deoxygenation. There have been a few studies on catalytic pyrolysis to bio-oil production using drop tube reactor.

Therefore, this review summarizes the current status of research concerning the catalytic pyrolysis of biomass using the various catalysts, focusing on the specific catalysts employed, as well as bio oil properties and reaction mechanisms.

**Table 2.7** Summaries of fast pyrolysis reaction systems for liquid products

| Reactor | Biomass types | Catalyst | Temp. (°C) | Bio-oil (%) | Reference |
|---|---|---|---|---|---|
| Rotating cone fast pyrolyser | Jatropha curcas L. | - | 450 | 40-65% | (Manurung et al., 2009) |
| free-fall reactor | sugarcane and cassava | - | 350-450 | 70% | (Pattiya et al., 2012) |
| Fluidized bed | Jatropha seed shell cake, palm | - | 380–530 | 32-48 | (Kim et al., 2013) |
| Fluidized bed | palm kernel shell | zsm-5, FCC | 400 and 485 | 11.7-23.1 | (Kim et al., 2014) |
| Fluidized bed reactor | pine sawdust | ZSM-5, Ga-ZSM- | 600 | - | (Jae et al., 2014) |
| Fluidized bed | Jatropha curcas de-oiled seed cake | - | 450 | 48% | (Biradar et al., 2014) |
| Fixed bed | sugarcane bagasse and palm empty | - | 460–600 | 53.4% | (Vecino Mantilla et al., 2014) |
| Lab-scale pyrolysis | Rice straw | - | 300-700 HR10 | 30-40% | (Park et al., 2014 |
| Fixed bed | Jatropha curcas de-oiled seed cake | - | 300-800 | 30-50% | (Jourabchi et al., 2014) |
| Bench-scale auger, batch, fluidized bed | Rice straw | - | 400-600°C | 30-43% | Nam et al., 2015) |

**Table 2.8** Summaries of fast pyrolysis reaction systems for liquid products

| Reactor | Biomass types | Catalyst | Temp. (°C) | Bio-oil (%) | Reference |
|---------|---------------|----------|-----------|-------------|-----------|
| Drop tube | Coal, wood | - | 600-1400 | - | (Zellagui et al., 2016) |
| Drop tube | Jatropha waste | $Al_2O_3$ and AC | 400-700 | 30-40% | This work 2017 |

Pyrolysis of Jatropha waste for bio-oil production was investigated by other research. Kim et al. (2013) studied the pyrolysis of Jatropha seedshell cake (JSC) in a fluidized bed. The effects of bed temperature and gas flow rate on the product yields and properties of pyrolytic liquid have been determined (Kim et al., 2013). They found that the pyrolytic liquid product and fractionated oil yields of JSC were maximized at 48 wt. % and 32 wt. % with increase of bed temperature. Biradar et al., (2014) studied the conversion of non-edible Jatropha curcas de-oiled seed cake into bio-oil and bio-char via pyrolysis process. A fluidized bed pyrolysis system with maximum feed rate, particle size range, sweep gas flow rate and operating temperature were optimized as 12 g/min, 0.5 mm–0.99 mm, 8 L/min and 450°C, respectively. The maximum obtained yields were 48% for bio-oil and 35.1% for bio-char. The crude bio-oil has lower viscosity (1.98 cSt), higher moisture content (31%) and higher density (1040 kg/m$^3$) as compared to commercial petro-diesel. In addition, Jourabchi et al., (2014) explored the effects of pyrolysis parameters on the yield and quality of bio-oil from Jatropha curcas pressed cake. It was pyrolysed in a fixed-bed reactor over a temperature range of 573.15 K to 1073.15 K and a nitrogen flow of 7.8 $\times10^{-5}$ m/s to 6.7$\times10^{-2}$ m/s. They found that at optimum pyrolysis conditions, above 50% of the waste is converted to bio-oil with less than 30% water content, a gross calorific value of 15.12 MJ/kg and a pH of 6.77. It was demonstrated that the bio-oil can be used in burners without any modifications, if the rest of its specifications match that of the ASTM D7554-10 bio-fuel standard.

Others types of biomass and pyrolysis reactor for bio-oil production were shown in Table 2.5. Park et al., (2014) investigated the slow pyrolysis of rice straw at

300–700°C to characterize the yields and detailed composition of the biochar, bio-oil and non-condensable gases using batch reactor. The result suggested that biochar was the primary product of pyrolysis containing 40% of energy and 45% of carbon from the straw. The utilization of by-products (bio-oil and gases) as energy resources was essential, since the sum of energy yield was about 60%. The gases could be burned to produce the heat for an auto-thermal pyrolysis process, but the heat balance was significantly influenced by the moisture content of the raw material.

Nam et al., (2015) investigated the energy conversion efficiencies of three pyrolysis reactors (bench-scale auger, batch, and fluidized bed) using rice straw as the feedstock at 500°C. It was found that the highest bio-oil yield of 43% was obtained from the fluidized bed reactor, while the maximum bio-char yield of 48% was achieved from the batch reactor. Heating value of high quality bio-oil and bio-char from the batch reactor was 31 MJ/kg and 19 MJ/kg, respectively. The energy conversion efficiencies of the three reactors indicated that the majority of the energy (50-64%) was in the bio-char products from the auger and batch reactors, while the bio-oil from the fluidized bed reactor contained the highest energy (47%).

Several kinds of catalysts (i.e. CaO, MgO, MCM-41, and HZSM-5) were used to upgrade the properties of bio-oil from continuous process [12]. Because of coke deposit on the surface, activity of these catalysts deteriorates rapidly, results in lower hydrocarbon yields which their application to catalytic fast pyrolysis (CFP) technology. Yildiz et al. 2016 who investigated the effect of catalyst type and reactor type on the products of pine wood in a micro-pyrolysis setup and a continuously operated bench-scale fast pyrolysis unit. The result suggested that CFP increased the water, coke, and NCGs of CFP-oil. For all catalysts, the acidity of CFP-oils remarkably decreased with an increased deoxygenation. The best performance was obtained with the lower redox-metal containing acidic catalyst and freshly calcined metal doped basic mixed-metal oxide catalysts. (Yildiz et al., 2016)

In recent year, Zellagui et al., 2016 studied the fast pyrolysis of pulverized coal and woody biomass in a drop tube furnace at several temperatures (600°C–1400°C) and under two atmospheres ($N_2$ and $CO_2$). The drop tube furnace is accurately equipped to record gas and wall temperature profiles. For the woody biomass, a single

first-order reaction model is successfully used. The results show that the maximum yields of volatile matter is clearly affected by the temperature set point for coal, while no significant influence is observed for woody biomass.

2.14.3 Modeling of biomass pyrolysis

The pyrolysis of biomass particles is a complex phenomenon which involves many physical and chemical processes such as momentum, heat and mass transfer, and variations of physical properties. There has already been a substantial amount of experiments and models into biomass pyrolysis as reviewed by several researches. Dufour (2011) studied the model accounts for a simplified multi-step chemical decomposition with the formation of tars at liquid phase inside the particle. The tars at liquid phase are then competitively converted into a secondary char and gases and evaporated, a Clausius–Clapeyron law for tar evaporation and a Darcy's law for mass transfer by convection. Masnadi et al. (2014) who studied the influences of temperature on the physical and chemical properties of char produced from biomass and non-biomass fuels, and the kinetics of atmospheric-pressure pyrolysis. They found that the Coats–Redfern method can be described by multi-step reactions; the model was able to identify likely reaction mechanisms and activation energies of each pyrolysis stage.

In order to understand the degradation behavior of Jatropha waste, separate components of this residue should be examined. Actually, the chemistry of biomass very complicated, simplification may be done by considering only major constituents such as hemicellulose, cellulose and lignin. The result found that the main thermal decomposition of physic nut waste generally occurred over the temperature range of 250–450℃. The three-parallel reactions model was applied for simulating the degradation of physic nut waste. From the model equation, the activation energy of hemicelluloses, cellulose and lignin was in the range of 41–68, 187–235, and 97–150 kJ/mol, respectively. The model agreed relatively well with the experimental data, the reaction orders of those fractions were in the range of 2.4–3.2 (Sricharoenchaikul & Atong, 2009). The result corresponded well with Gottipati and Mishra (2011) who used the differential method to obtain the pyrolysis kinetic parameters from the

thermogravimetric data.  The reaction rate constant $k$ was expressed by the Arrhenius equation and taking a natural logarithm, the above equation yields as:

$$\ln\frac{dx}{dt} = lnA + n\ln(1-x) - \frac{E}{RT} \tag{2-29}$$

Moreover Zhou, 2013 who studied the thermogravimetric curve overlap ratio was applied to evaluate the simulation of biomass by hemi-cellulose, cellulose and lignin. The results indicated that biomass pyrolysis characteristics could be well simulated by its components and the results from the overlap ratio were compared with the content derived from chemical separation.

**Table 2.9** Summaries of model for pyrolysis reaction

| Pyrolysis reactor/ Instrument | Biomass types | Model/ Equation/ method | Result | Reference |
|---|---|---|---|---|
| Fixed bed quartz reactor/ TGA | Physic nut waste | Arrhenius equation | Reaction orders of those fractions were in the range of 2.4–3.2 | (Sricharoench aikul & Atong, 2009) |
| Entrained flow reactor | rice husk and sawdust | Arrhenius equation | The predicted yields of produced gases agreed reasonably with the experimental data | (Sun et al., 2010) |
| Furnaces higher heating rates | pistachio shells | Discrete Particle Method | Predicted results yielded good agreement. | (Peters, 2011) |
| TGA | co-feeding of coal and biomass | Arrhenius equation | The pyrolysis of the samples containing biomass exhibited approximately first-order reaction kinetic control | (Masnadi et al., 2014) |

**Table 2. 10** Summaries of model for pyrolysis reaction

| Pyrolysis reactor/ Instrument | Biomass types | Model/ Equation /method | Result | Reference |
|---|---|---|---|---|
| TGA | Jatropha waste | Arrhenius equation | Kinetic parameters can be utilized to predict its thermal decomposition behavior for a wide range of heating rates (10℃/min to 60℃/min). Reaction orders was 0.5-2.5 | (Sharma et al., 2016) |

       Summaries of model for pyrolysis reaction and CFD model are shown in Table 2.8. The mainly researches used the Arrhenius equation to study the reaction orders of biomass fractions from pyrolysis. Furthermore, kinetic model using CFD technique is interested in this work because it was positively applied to predict the product distributions, chemical composition and the product yields of pyrolysis in many researches. Therefore, it is possible to apply this model to predict the product distributions, and gain a better understanding that agreed reasonably with the experimental data. Several researches developed a chemically reactive fluidized bed process to predicted major species in the product gas composition using CFD model (Boateng & Mtui, 2012).

       Boateng & Mtui (2012) studied the simulation of a chemically reactive fluidized bed process. The effect of heavily-loaded gas-particle hydrodynamics, heat transfer and complex fast pyrolysis reactions by applying the single-step chemical kinetics to the pyrolysis of biomass were investigated. They found that the predicted results compare reasonably well with measurements. Xue et al., 2014 studied the CFD model of fluidized bed reactor by using Euler–Euler multi-phase model. The velocity of produced gas, biomass density profile, axial temperature of gases phase, partial density distribution, and the gas temperature in reactor outlet were predicted in the model.

The result suggested that the CFD model can be applied and validated with experimental data.

In fixed bed system, Borello et al., (2014) developed a CFD model of biomass packed porous bed system to predict the volatiles in terms of tar, light gas and char fraction released during the pyrolysis process. Phenol was considered as tar representative while each single component were considered (in particular $H_2$, CO, $CO_2$, $CH_4$ and steam) for gas species. The result indicated that the kinetic parameters proposed here allow reduction of % error to almost negligible values (except for water). Tabet et al., (2015) reviewed a CFD based co-firing tools consist of models for turbulent flow, gas phase combustion, particles dispersion by turbulent flow, coal/biomass particles devolatilization, heterogeneous char reaction and radiation. The result indicated that CFD based modelling can be used to predicted and validated with experimental data.

Recently, Weber et al. (2017) developed CFD model of biomass pyrolysis and gasification in a drop tube reactor at high temperatures (1000–1400°C). The influence of reactor temperature, steam/carbon-ratio and air ratio on the production rate of the gas components ($H_2$, CO, $CO_2$ and $CH_4$) were investigated. The results are compared with published experiments and detailed CFD simulations. This approach is able to predict all major species in the product gas composition very well for only a fraction of the computational time as needed for comprehensive CFD (Weber et al., 2017).

**Table 2.11** Summaries of CFD model for pyrolysis reaction

| Application | Aim/Outcome | Model/Extra Model | Agreement with Exp. | Ref. |
|---|---|---|---|---|
| Entrained flow gasifier | Products mass fraction distribution; temperature contours; swirl velocity distribution | Std k $\varepsilon$– RSM/ Lagrangian | Acceptable | (Wang & Yan, 2008). |
| Horizontal entrained flow reactor | Predictions of flow, temperature and conversion; sensitivity of the kinetic parameters of corn stalk fast pyrolysis | Lagrangian | Reasonable | Xiu, et al, 2008 |
| Fluidized bed | To predict the pyrolysis vapors, char and non-condensable gases | Eularian-Eularian multiphase | Reasonable | (Boateng & Mtui, 2012) |
| Fixed bed pyrolysis | Pyrolysis models were able to describe the mass loss behavior of the fuels | species conservation equation | Reasonable | (Borello et al., 2014) |
| Fluidized bed | Predicted pyrolysis products on the major products; liquid, char and gas. | Eularian-Eularian multiphase | satisfactory | (Mellin et al., 2014) |
| Drop tube | To study kinetic of pyrolysis wood biomass | Arrhenius | satisfactory | (Zellagui et al., 2016) |
| Fluidized bed reactor | To predict all major species in the product gas composition | Eularian-Eularian multiphase | Acceptable | (Weber et al., 2017) |
| Drop tube reactor | To predict gas species CO, $CO_2$, $CH_4$, $H_2$, $H_2O$, Char | Eddy dispersion/ | Reasonable | (this work) |

# CHAPTER 3

# PROCEDURE

The objectives of this research are to produce bio-oil and synthesize advanced catalyst for reforming/upgrading pyrolysis vapors from Jatropha pyrolysis by reducing the oxygen content below 30 wt%.  Therefore, the experiment was divided into six parts;

1) Biomass preparation and characterization

2) Synthesis of transition metal-based ceramic catalysts and characterization

3) Synthesis of transition metal-based carbon catalysts and characterization

4) Catalytic fast pyrolysis of Jatropha residues in micro scale by Py-GC/MS

5) Continuous catalytic fast pyrolysis of Jatropha residues by Drop tube reactor

6) Setting up of CFD boundaries of for fast pyrolysis process model

## 3.1. Biomass preparation and characterization

### 3.1.1. Raw materials: Jatropha residues

The Jatropha residues used as raw material for fast pyrolysis were obtained from local plants in Chiangrai. They were left after extraction of oil from biodiesel production process.



**Fig. 3.1** Physical appearance of extracted Jatropha residues

3.1.2 Biomass preparation

Firstly, extracted Jatropha residues (grain mill with Hatz engine) were separated from physical impurities and dried at $60^{\circ}$C for 24 hours to reduce their moisture content. The dried samples were crushed with a grinder (Thai kitchen Mart, 3HP, 380V) equipped with 3mm-mesh (Fig. 3.2). The entireties of samples were then passed through a 20, 40, and 120 mesh sieves and were subsequently divided into four size fractions: 0.85-3mm, 0.425-0.85mm, 0.125-0.425m and <0.125 mm (125 microns), respectively. Jatropha waste after size reduction was shown in fig. 3.3.



**Fig. 3.2** Instruments for preparation the Jatropha residues (a) Grinding machine (b) Sieve shaker

**Fig. 3.3** Physical appearance of extracted Jatropha residues with four sizes (<0.125, 0.125-0.425, 0.425-0.850 and 0.850-2.0 mm.)

### 3.1.3 Biomass characterization

The issue of the variation of chemical with particle size is explored in this part. Jatropha residues were subjected to analysis by various testing techniques including proximate analysis (moisture, ash, volatiles, and fixed carbon), ultimate analysis (C, H, N, O and S), heating value, toxic element analysis, and composition analysis (cellulose, hemicellulose and lignin). In addition, thermal degradation of Jatropha residues was also investigated.

#### 3.1.3.1 Proximate analysis

The proximate analysis was performed followed ASTM to classify the sample in terms of moisture (ASTM E871), volatile matter (ASTM E872), fixed carbon (ASTM E872) and ash (ASTM D1102).

#### 3.1.3.2 Ultimate analysis

The ultimate analysis carried out using Leco TruSpec® CHNS (micro) analyzer gives the composition of Jatropha in weight percentages of carbon, hydrogen and oxygen as well as sulfur and nitrogen. The oxygen content was calculated by difference.

### 3.1.3.3 Heating value

Bomb calorimeter (Leco model AC-350, Table. 3.2) was used to determine the higher (gross) heating value of raw material following ASTM D240. High heating value can be estimated from LHV by equation 3.1.

$$HHV = LHV + 23.95\times (9H+M) \qquad (MJ/kg) \qquad (3.1)$$

where

HHV = higher heating value $(MJ/m^3)$

LHV = lower heating value $(MJ/m^3)$

H = hydrogen content in biomass (%)

M = moisture content in biomass (%)

### 3.1.3.4 Component analysis

Chemical components of Jatropha waste sample were also identified using Tappi T203 and T222 standard methods and AOAC2000 standard and shown in Chapter 4.

### 3.1.3.5 Thermal degradation

Thermal degradation characteristics of Jatropha residue were studied using a thermogravimetric method. Experiments were performed on a Mettler Toledo TGA/STDA851 analyzer. Thermogravimetric analysis (TGA) is one of the most common techniques for the investigation of thermal events and their associated kinetics during pyrolysis of solid raw materials such as coal, biomass, and plastic. It provides a measurement of weight loss of the sample as a function of time and temperature. In this work, each sample of 10-20 mg was heated from room temperature to a final temperature of 1000°C at various heating rate (10 -200°C/min) under nitrogen atmosphere, flowing at 20 ml/min. Variation of sample mass with respect to temperature change (TG data) and its first derivative (DTG data) was continuously collected. Effect of particle size of Jatropha residue and heating rate on the thermal degradation behavior were discussed. The combined TG and derivative TG (DTG) profiles showing the thermal degradation characteristics of extracted Jatropha at

various heating rates. These plots show the typical degradation profile for biomass with regions of moisture release, devolatilization and char degradation.

## 3.2 Synthesis of metal catalysts with ceramic support

The objective of this part is to synthesize advanced cracking catalyst for reforming/upgrading pyrolysis vapors from Jatropha pyrolysis by reducing the oxygen content to be less than 30 wt%. The upgraded product would be used as reactants for down-stream process before applying them in any application; heat, power, transportation fuel, etc. This part will be focused on (1) the metals doped various supports with $CeO_2$ promoter and (2) the metals doped on $Al_2O_3$, Activated carbon, and char support without $CeO_2$ promoter. The results will be compared to those obtained with typical cracking catalysts. The modification of metal on ceramic supports was performed by the impregnated method of transition metals with the aim to investigation how these metals would affect the catalytic activity and aromatic selectivity. The assumption of loading metal was to improve the activity of the catalyst in term of eliminating oxygenated compounds, increasing hydrocarbon and aromatic hydrocarbon yields as well as solving the coke formation during pyrolysis. The diagram of methodologies of catalytic pyrolysis by Py-GCMS is shown in Fig.3.4.
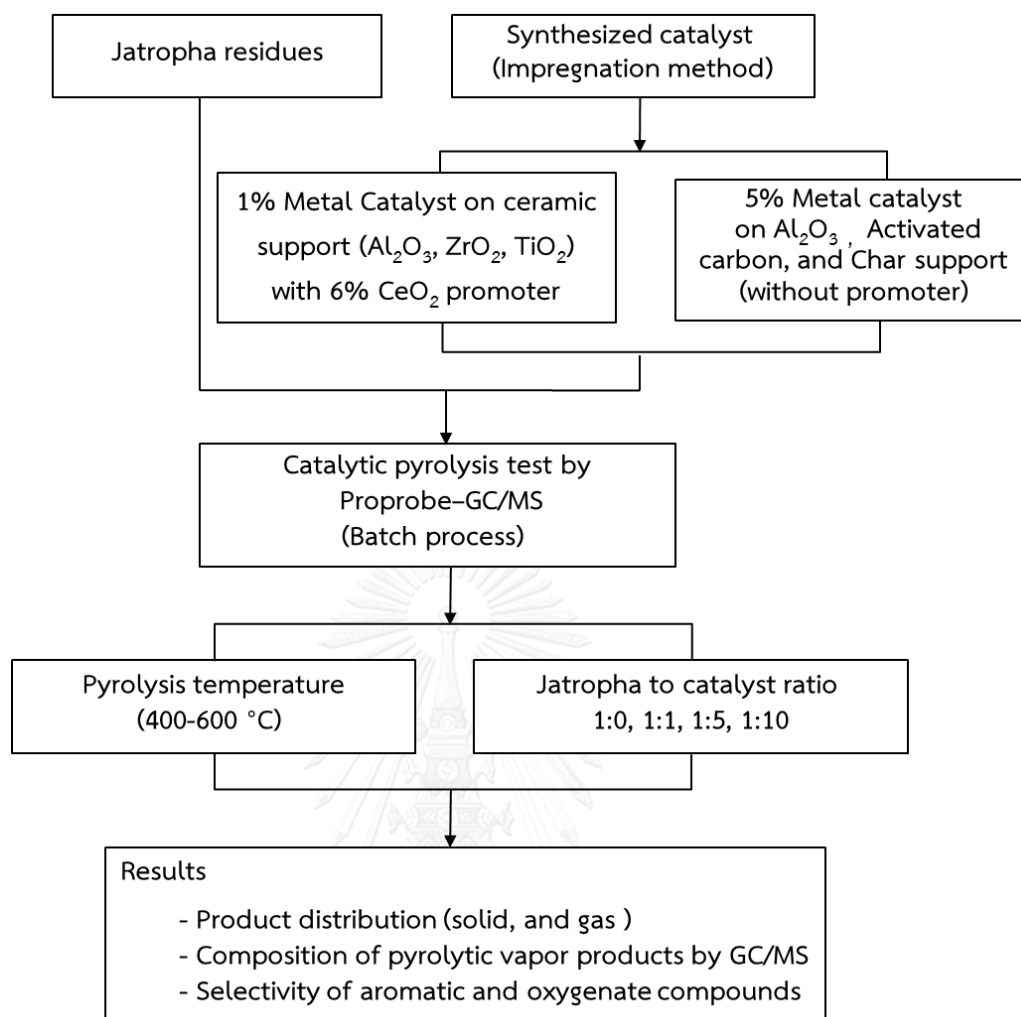
**Fig. 3.4** Flow chart of methodologies of catalytic pyrolysis by Py-GCMS

### 3.2.1 Chemical reagents and apparatus

The catalyst supports employed in this research were titanium (IV) oxide (anatase and rutile), aluminium oxide and zirconium (IV) oxide. The metals used as active species were nickle (II) nitrate hexahydrate, ruthenium (III) chloride hydrate and palladium (II) nitrate hydrate whereas the promoter was cerium (III) nitrate hexahydrate. The specific properties of the support given by the company are shown in Table 3.1. Instruments for characterization the biomass and synthesized catalysts are shown in Table 3.2.

**Table 3.1** Specific properties of the catalyst supporter

| | Material | Company | Purity (%) | Particle size (nm) | Density (g/cm³) |
|---|---|---|---|---|---|
| Ceramic Support (*μm) | Aluminum oxide ($\gamma$-Al$_2$O$_3$) | Sigma-Aldrich | 99.8 | ~13 | 4.18 |
| | Aluminum oxide ($\alpha$-Al$_2$O$_3$) | Showa denko | 99.0 | 10* | 1.3 |
| | Titanium (IV) oxide (Anatase) | Sigma-Aldrich | 99.7 | <25 | 3.53 |
| | Titanium (IV) oxide (Rutile) | Sigma-Aldrich | 99.5 | <100 | 4.32 |
| | Zirconium (IV) oxide | Alfa-Aesar | 99.0 | 15-25 | 5.89 |
| Activated carbon (*μm,**mm.) | Activated carbon powder | Sigma-Aldrich | ≥99.0 | 149* | - |
| | Activated carbon granule | Wako | ≥99.0 | 2-5** | - |
| Promoter | Cerium (III) nitrate hexahydrate | Alfa-Aesar | ≥99.0 | - | - |
| Active species | Nickel (II) nitrate hexahydrate | Alfa-Aesar | ≥99.0 | - | - |
| | Ruthenium (III) chloride hydrate | Alfa-Aesar | ≥99.0 | - | - |
| | Palladium (II) nitrate hydrate | Alfa-Aesar | ≥99.0 | - | - |
| | Cobalt (II) nitrate hexahydrate | Wako | ≥99.0 | - | - |
| | Lanthanum nitrate hexahydrate | Fluka | ≥99.0 | - | - |
| | Ammonium molybdate tetra hydrate | Fluka | ≥99.0 | - | - |

**Table 3.2** Instruments for characterization the biomass and synthesized the catalysts

| List | Picture |
|---|---|
| a.) Bomb calorimeter (Leco model AC-350) |  |
| b.) Thermogravimetric analyses (TGA) |  |
| c.) CHON/S analyzer |  |
| d.) Furnace for calcine the catalysts |  |
| e.) X-ray diffractometer, PANalytical, model X' Pert Pro |  |
| f.) Scanning electron microscopy (SEM) |  |

3.2.2 Impregnation of transition metal catalysts on ceramic support

Catalytic testing included $Al_2O_3$, $ZrO_2$, $TiO_2$ (rutile) and $TiO_2$ (anatase) support catalysts and $TiO_2$ support referred to as $TiO_2$ ($T_1$) and $TiO_2$ ($T_2$) respectively. Method of impregnation the metal catalyst with $CeO_2$ promoter is shown in Fig. 3.5.

```
┌─────────────────────────────────────┐
│  Ce(NO₃)₂ was impregnated in         │
│  ceramic supporter (Al₂O₃ or ZrO₂    │
│  or TiO₂ )                           │
└─────────────────────────────────────┘
                  │
                  ▼
┌─────────────────────────────────────┐
│  Stirring at 80 °C with 300 rpm      │
│  for 3 h                             │
└─────────────────────────────────────┘
                  │
                  ▼
┌─────────────────────────────────────┐
│  Dried at 110 °C for 24h             │
└─────────────────────────────────────┘
                  │
                  ▼
┌─────────────────────────────────────┐
│  Calcined in air at 700 °C for 4 h   │
└─────────────────────────────────────┘
                  │
                  ▼
            ╱─────────────╲
           ╱   Obtained    ╲
          ╱  6%CeO₂/Al₂O₃   ╲
           ╲  as promoter   ╱
            ╲─────────────╱
                  │
                  ▼
┌─────────────────────────────────────┐
│  Metal (Pd, Ru, or Ni) solution      │
│  was impregnated in 6%CeO₂/Al₂O₃     │
└─────────────────────────────────────┘
                  │
                  ▼
┌─────────────────────────────────────┐
│  Dried at 110 °C for 24h and         │
│  calcined in air at 700 °C for 4 h   │
└─────────────────────────────────────┘
                  │
                  ▼
            ╱─────────────╲
           ╱   Obtained    ╲
          ╱  1% Pd (orRu,Ni)╲
           ╲ on6%CeO₂/Al₂O₃ ╱
            ╲─────────────╱
```
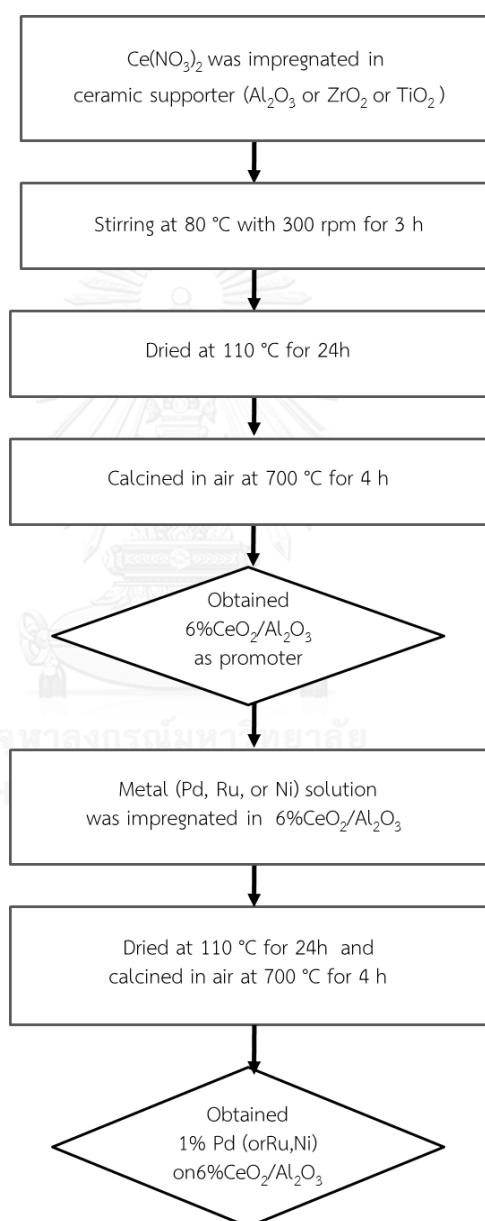
**Fig. 3. 5** Method of impregnation the 1 wt% metal catalysts with $CeO_2$ promoter

Catalyst preparation was initiated by stirring mixture of cerium (III) nitrate solution and $Al_2O_3$ support for 3 h at 80°C and 300 rpm, and then dried at 110°C for 24 h. The dried $Ce(NO_3)_2/Al_2O_3$ was calcined in air at 700°C for 4 h to obtain $6\%CeO_2/Al_2O_3$ as promoter to achieve well dispersion of the metal. After that, palladium nitrate (or ruthenium chloride hydrate, nickel nitrate) was then impregnated on $CeO_2/Al_2O_3$ catalyst by the same method. The catalysts contained 1.0 wt. % metal (Pd, Ru or Ni) on $6\%CeO_2/Al_2O_3$ catalyst. Physical appearances of metal on ceramic catalysts in various step of synthesis are show in Fig.3.7. By the same method, the Pd, Ru and Ni were impregnated in $CeO_2$ promoter with zirconia ($ZrO_2$), rutile ($TiO_2$; $T_1$) and anatase ($TiO_2$, $T_2$) supporter. Finally, the synthesized catalysts were $1\%Pd$-$6\%CeO_2/support$, $1\%Ru$-$6\%CeO_2/support$ and $1\%Ni$-$6\%CeO_2/support$, making a total of twenty prepared catalysts to be tested in this study. Physical appearances of all support catalysts are shown in Fig.3.6.



**Fig. 3. 6** Physical appearances of support catalysts (a) alumina ($Al_2O_3$) (b) $ZrO_2$ (c) rutile based ($TiO_2$) and (d) anatase ($TiO_2$)
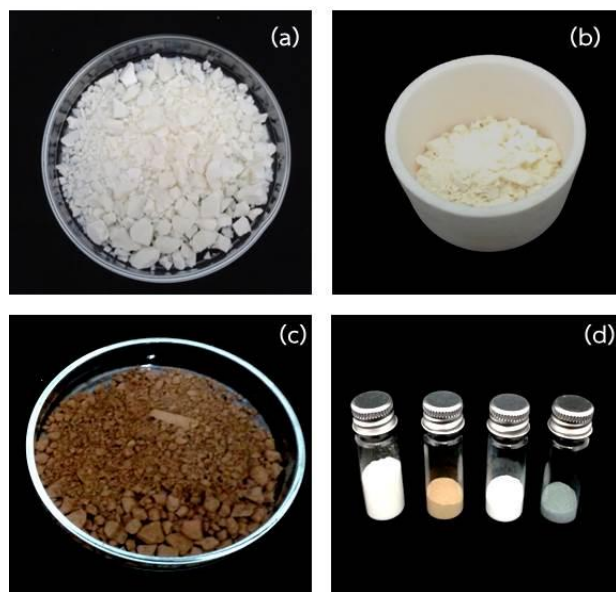
**Fig. 3. 7** Physical appearances of metal on ceramic catalysts in various step of synthesis (a) $CeO_2$/support after dried at 110°C (b) $CeO_2$ promoter calcined with ceramic crucible (c) Metal ($PdO_2$) on $CeO_2$ promoter (d) metal catalysts after calcined at 700℃

### 3.2.3 Impregnation of transition metal catalysts without promoter

The objective of this part is to synthesize catalyst for upgrading pyrolysis vapors from Jatropha pyrolysis by increasing metal to 5 wt% onto the alumina supported, in order to reduce the oxygen content to below 30 wt%. Methods of impregnation the metal catalysts on $Al_2O_3$ support are shown in Fig. 3.8. The metals used as active species were cerium (III) nitrate hexahydrate, ruthenium (III) chloride hydrate, palladium (II) nitrate hydrate, nickle (II) nitrate hexahydrate, cobalt (II) nitrate hexahydrate, lanthanum nitrate hexahydrate and ammonium molybdate tetra hydrate.

From previous section, the catalysts prepared included 1% of metal (Pd, Ru, and Ni) on 6%$CeO_2$/$Al_2O_3$; the metal catalysts were first impregnated with $CeO_2$ which was believed to promote the noble metal dispersion. It was found that the promoter ($CeO_2$) had not significantly effect for distribution the metal and pyrolytic product of Jatropha residue. Thus in this section, the metal content loading onto the $Al_2O_3$ support

by the impregnation were synthesized; the catalyst was not impregnated with $CeO_2$ as promoter and increased metal loading from 1% to 5 wt%.
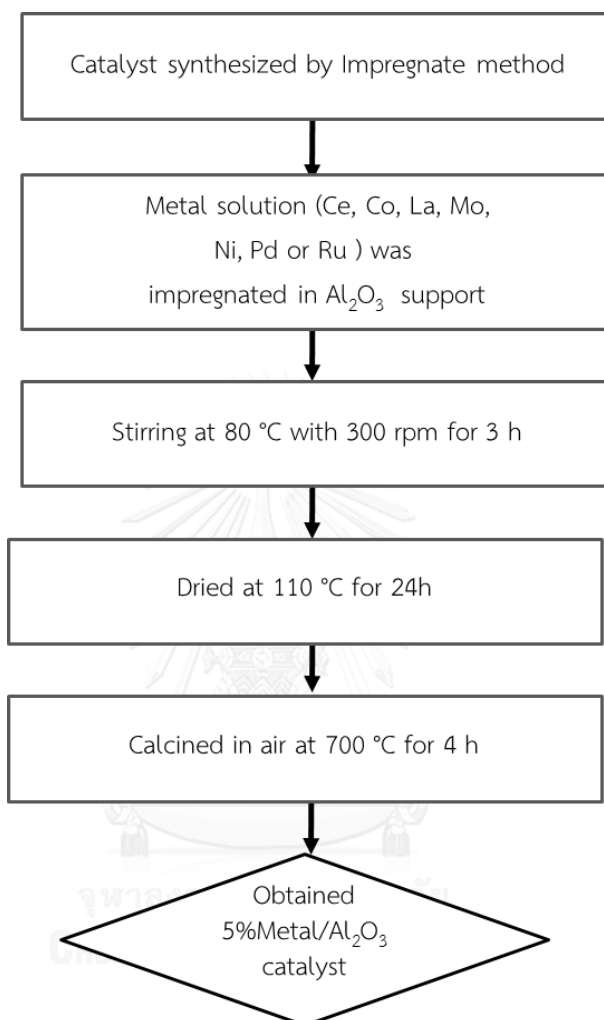


**Fig. 3. 8** Method of impregnation the metal catalysts on $Al_2O_3$ support

The $Al_2O_3$ was stirred in metal solution such as cerium nitrate for 3 h at 80°C with 300 rpm, and then dried at 110°C for 24 h. The sample was calcined in air at 700°C for 4 h in air atmosphere to obtain $CeO_2/Al_2O_3$ catalyst. Other metals (cobalt nitrate, palladium nitrate, ruthenium chloride, nickel nitrate, lanthanum nitrate and molybdate) were also prepared in the same method. Physical appearances of alumina based catalysts are shown in Fig.3.9. The catalysts prepared included 5% metal of $CeO_2/Al_2O_3$, $CoO_2/Al_2O_3$, $LaO/Al_2O_3$ $MoO_2/Al_2O_3$ $NiO/Al_2O_3$, $PdO_2/Al_2O_3$, and $RuO_2/Al_2O_3$.

**Fig. 3. 9** Physical appearances of 5% metal on $Al_2O_3$ support

3.2.4 Impregnation of transition metal catalysts on $Al_2O_3$ extruded

From previous section, $Al_2O_3$ catalyst powder with 5 wt. % metal (Ni or Pd) loading amount exhibited higher catalytic activity and selectivity than three ceramic supporters ($ZrO_2$, $TiO_2$ (rutile), and $TiO_2$ (anatase)). The result suggested that $Al_2O_3$ based catalysts are suitable for further investigation with a scaled up fast pyrolysis sequential process using a drop tube reactor. Consequently, added catalysts were modified metal catalysts (Ni and Pd) over Alumina ($Al_2O_3$) extruded support. $Al_2O_3$ support was modified by extrusion in pellet form to facilitate the usage in drop tube reactor. Added catalysts were modified 5 wt% metal catalysts (Ni and Pd) over $Al_2O_3$ support by impregnation method. Method of impregnation the metal catalyst with $CeO_2$ promoter is shown in Fig. 3.10.
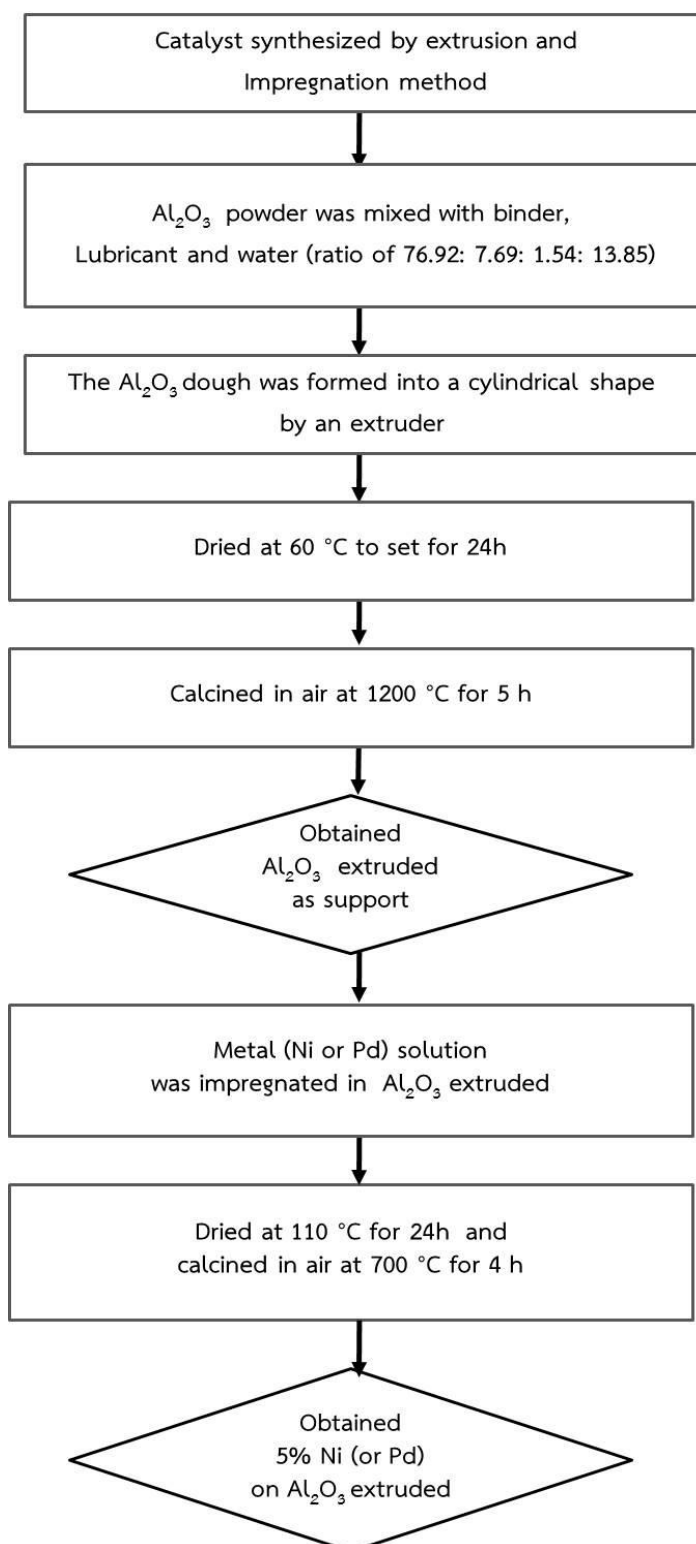
**Fig. 3. 10** Method of impregnation the metal catalysts on $Al_2O_3$ extruded support

Alumina ceramic powder ($\alpha$-Al$_2$O$_3$) 1.7 $\mu$m mixed with 7.69% organic binder, 1.54% lubricant and 13.85% distilled water was extruded through the die with an external diameter of 6.5 mm. The dough was then formed into a cylindrical shape by an extruder (FM-30-1, Miyazaki Iron Work). The extruded supports were dried at 80°C for 2 h and calcined in air at 1200°C for 4 h. The sintered alumina was of 36.48% porosity, with an average pore diameter of 0.32 $\mu$m. Finally, the alumina tube, 300 mm in length and 6.5 mm diameter, were used as supporter. The Alumina ceramic powder and extruder are presented in Fig.3.11.
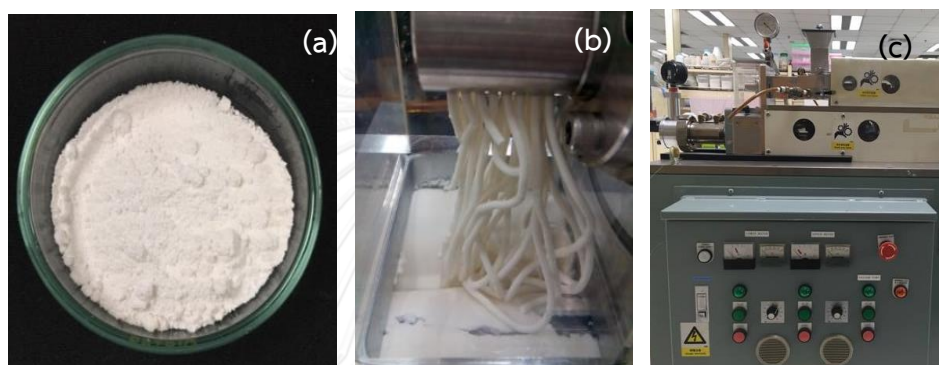


**Fig. 3. 11** Al$_2$O$_3$ extruded catalyst: (a) Alumina ceramic powder ($\alpha$-Al$_2$O$_3$) (b) Alumina dough mixing and (c) an extruder.

Catalyst preparation was commenced by stirring mixture of nickel (II) nitrate solution and alumina extruded pellet for 3 h at 80°C. They were shaken for 3 h in water bath to coat the nickel on alumina extruded pellet, and then dried at 110°C for 24 h. The dried Ni(NO$_3$)$_2$/Al$_2$O$_{3(ext.)}$ was calcined in air at 800°C for 4 h to obtain 5% Ni/Al$_2$O$_3$ which acts as active site of the catalyst. The palladium catalyst was synthesis by the same method. Finally, the catalysts contained 5.0 wt.% of metal on Al$_2$O$_3$ extruded pellets as shown in Fig. 3.12 (c-d).
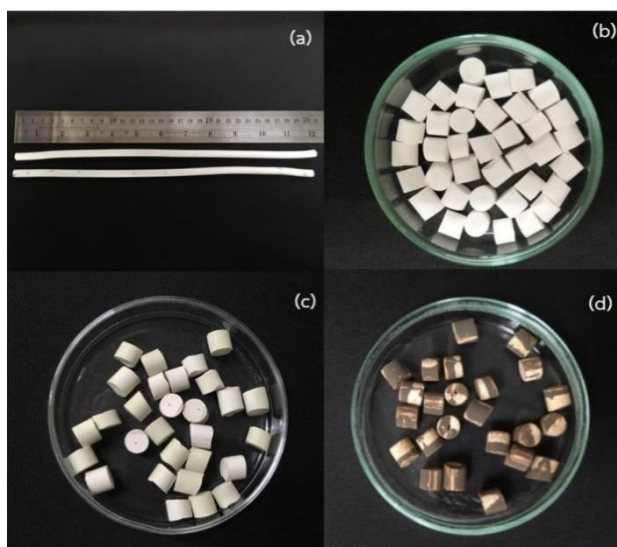
**Fig. 3. 12** $Al_2O_3$ extruded catalysts (a) $Al_2O_3$ extruded (300 mm); (b) $Al_2O_{3(ext.)}$ pellet (5 mm.); (c) 5% $Ni/Al_2O_{3(ext.)}$ pellet; (d) 5% $Pd/Al_2O_{3(ext.)}$ pellet

## 3.3 Impregnation of metal catalysts on Activated carbon

Method of impregnation the metal catalysts on activated carbon support are similar to those with $Al_2O_3$ supports as shown in Fig. 3.13.
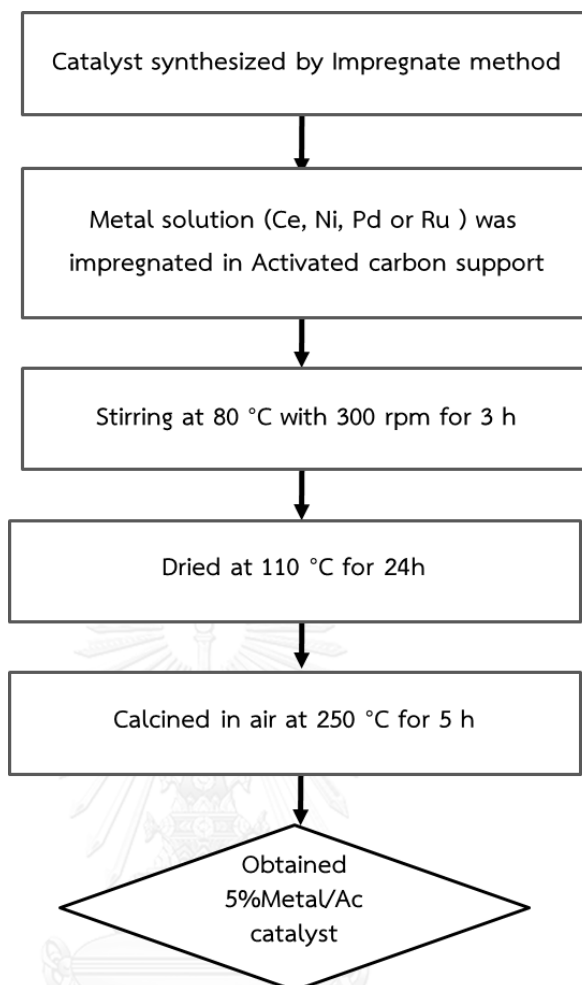
**Fig. 3. 13** Method of impregnation the metal catalysts on activated carbon support

Four metals used as active species were cerium (III) nitrate hexahydrate, ruthenium (III) chloride hydrate, palladium (II) nitrate hydrate and nickel (II) nitrate hexahydrate.
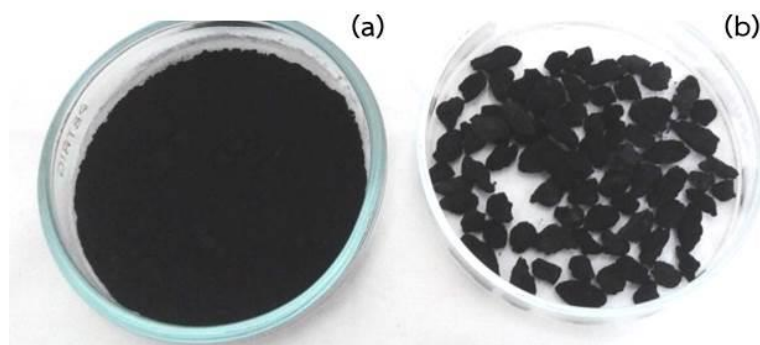
**Fig. 3. 14** Physical appearances of 5% metal on activated carbon support

(a) activated carbon powder and (b) activated carbon granules 2-5 mm

Both of AC support (Wako Pure Chemical Industries) was impregnated with the respective aqueous metal salt solution (Ce $(NO_3)_3 6H_2O$, $Pd(NO_3)_2$, $Cl_3Ru \cdot xH_2O$ and $Ni(NO3)2 \cdot 6H_2O$). Catalyst preparation was initiated by stirring mixture of 1.54 g $Ce(NO_3)_3$ with 200 mL distilled water, and 10 g of AC were then dispersed in metal salt solution. The mixture was stirred constantly for 3 h at 80°C to fill the pores completely, and then dried at 110°C for 24 h to evaporate the excess water. Palladium nitrate (or ruthenium chloride hydrate, nickel nitrate) was impregnated on AC catalyst by similar method. After that, the dried sample was calcined in air atmosphere at 250°C for 5 h to obtain the respective 5%$CeO_2$/AC, 5%PdO/AC, 5%$RuO_2$/AC and 5%NiO/AC catalysts, referred here simply as Ce/AC, Pd/AC, Ru/AC and Ni/AC, respectively. Physical appearances of activated carbon-based catalysts are shown in Fig.3.14.

## 3.4 Impregnation of transition metal catalysts on bio-char

Bio-char is a fine-grained, highly porous charcoal substance, typically produced as a product or byproduct of pyrolysis and gasification of biomass. The procedure of the bio-char catalysts preparation was illustrated in Fig. 3.15.
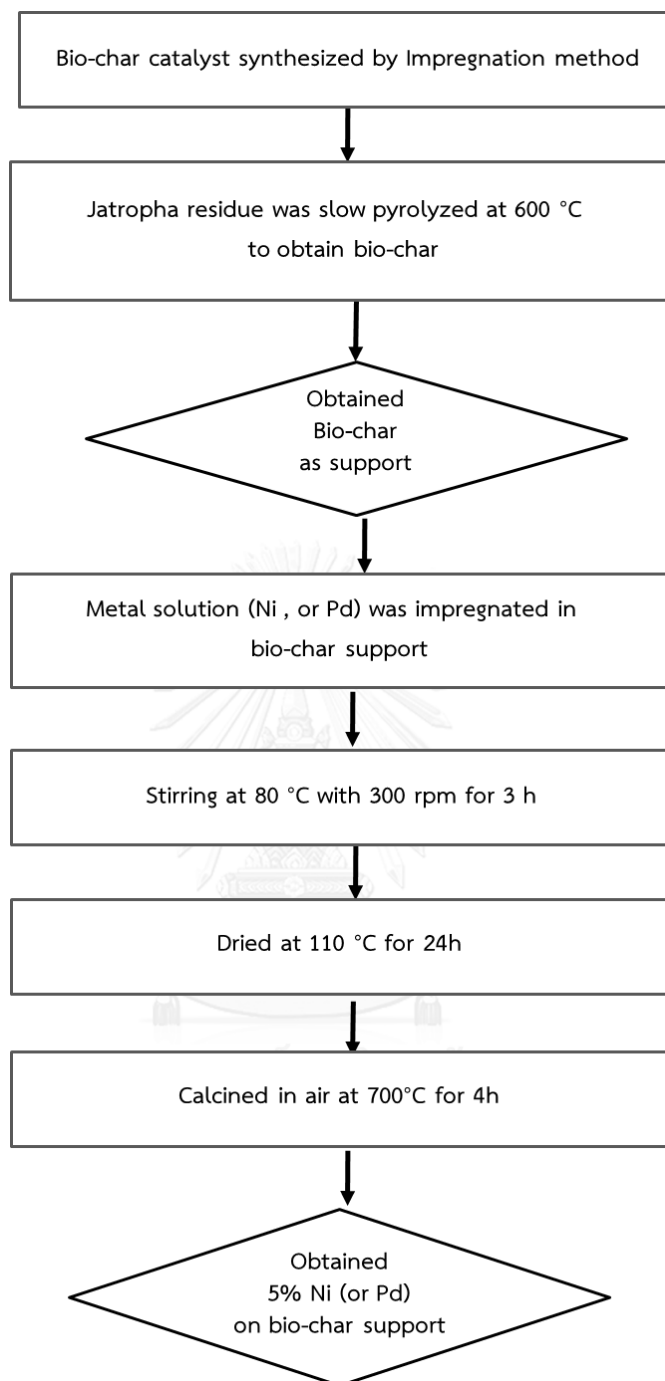
**Fig. 3. 15** Method of impregnation the metal on bio-char support

Firstly, the char support was prepared by slow pyrolysis from 25 to 600°C in the flow of 2 l/min $N_2$ atmosphere and then hold for 1 h. The catalysts were simply prepared by the wetness impregnation and calcination using the Ni $(NO_3)_2 \cdot 6H_2O$ and $Pd(NO_3)$ as and nickel and palladium precursors. The mixture was stirred constantly for

3 h at 80°C to fill the pores completely, and then dried at 110°C for 24 h to evaporate the excess water. The metal species in bio-char were calcined in air atmosphere at 700°C for 4 h to obtain the 5 wt.% of Ni/Char and Pd/Char. Physical appearances of bio-char catalysts are shown in Fig.3.16.
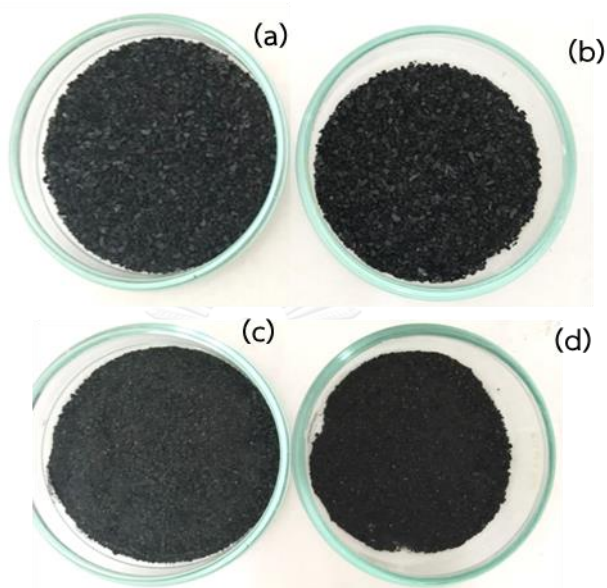


**Fig. 3. 16** Physical appearances of bio-char catalysts (a) Bio-char support (b) Bio-char calcined at 700°C, (c) Ni/char, and (d) Pd/Char

## 3.5 Characterization of synthesized catalysts

### 3.5.1. X-ray diffraction (XRD)

In order to determine the formation of crystalline materials, phase analysis of synthesized powder was performed by X-ray powder diffraction (XRD; JEOL, JDX-3530 and PANalytical, X' Pert Pro) with 40kV, 45 mA, CuK$\alpha$ radiation. The sample was scanned at $2\theta$ from 5 to 90° with a step size of 0.02. Crystalline phases of each sample were identified according to JCPDS.

### 3.5.2. Particle size and distribution

The average particle size and distribution of each sample were determined using laser diffraction by Mastersizer 2000 (Version 5.54 Serial Number: MAL 1021434, Malvern Instrument Ltd).

### 3.5.3. Surface area, pore size and pore volume

The specific surface area, pore volume and pore diameter were measured by nitrogen adsorption using Autosorb-1 (Quantachrome instruments). The samples were degassed for 8 h at 300°C prior to the analysis.

### 3.5.4. Scanning electron microscopy (SEM)

Scanning electron microscopy (SEM) is the technique that provides the morphology of samples. Microstructure was characterized by scanning electron microscope (SEM; JEOL, JSM-5410 and JSM-6301F). For analysis of metal dispersion of catalysts, energy dispersive X-ray spectroscope (EDS; model Oxford Inca 300) was used.

## 3.6 Catalyst test by analytical Pyrolysis-GC/MS

Pyrolysis Gas Chromatography (Py-GC/MS) allows analysis of almost all sorts of materials including insoluble materials and complex materials at trace levels without any pretreatment of samples, and information otherwise unobtainable by other techniques can be obtained; therefore, Py-GC technique is becoming more important technique in the area of polymer characterization. Flow chart of methodologies of catalytic pyrolysis experiments is shown in Fig.3.17.
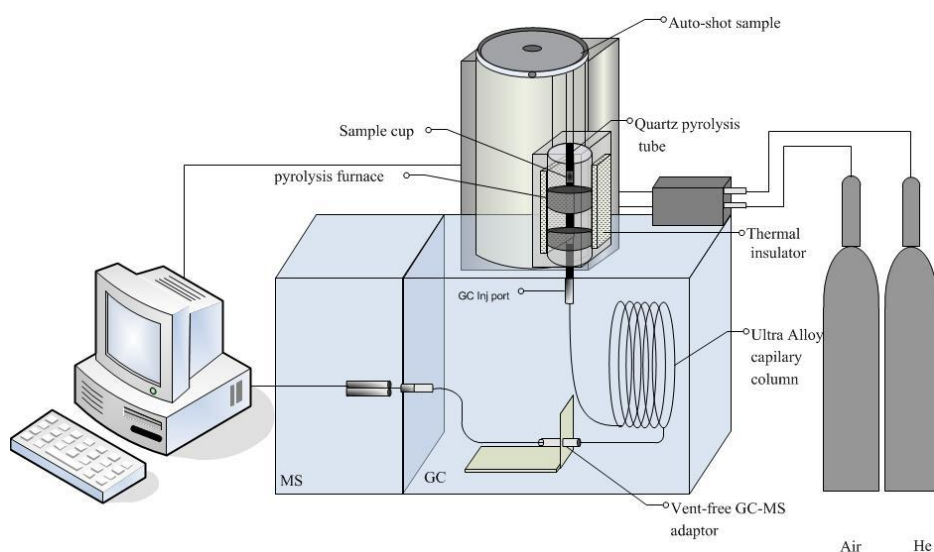
**Fig. 3. 17** Schematic diagram of the pyrolysis of Jatropha waste residue by Py-GC/MS

The experimental set-up is shown schematically in Fig. 3.17. Pyrolysis was performed using a Pyroprobe pyrolyzer (multi funtional pyrolyzer, PY-2020iD, Frontier Lab) with an auto-shot sampler AS-1020E interfaced to a gas chromatograph coupled to a mass selective detector (GCMS-QP2010, Shimudzu). Each experiment, approximately 0.4 mg Jatropha residues were used. In order to investigate the effect of catalysts to biomass ratios, catalysts were placed above the biomass layer in the amount of 0.4, 2.0, and 4.0 mg to obtain the biomass to catalyst ratios of 1:1, 1:5, and 1:10, respectively. Then, the sample was pyrolyzed with the pyroprobe set to 400-600°C and hold for 0.5 min. The sample was placed in a sample cup and the catalyst was placed above the Jatropha residues and then dropped into the heated zone, so that all the pyrolysis vapors would pass through the catalyst layer. The pyrolysis vapors were then identified by GC/MS (GCMS- QP2010, Shimadzu)

**Fig. 3. 18** A pyroprobe (multifunctional pyrolyzer, PY-2020iD, Frontier Lab) interfaced to a gas chromatograph coupled to a mass selective detector (GCMS- QP2010, Shimadzu)

The column used was a 30m×0.25 mm ultra-alloy 5 (i.d., 0.25μm film thickness). Helium (99.999%) was used as a carrier gas with a column flow of 1.3 ml/min, and the split injector ratio was 1:50. During the analysis of the pyrolytic products, the oven temperature was started from 50°C (3 min) to 200°C (heating rate of 5°C/min) then to 350°C (heating rate of 10°C/min, hold 10 min). The injector and detector temperature was kept at 280°C. The mass spectrometer was operated in EI mode at 70 eV. The mass spectra were obtained from m/z 20 to 800 with the scan speed of 625 amu/s. Identification of chromatographic peaks were achieved according to the NIST and Wiley mass spectrum library. For establishing of baseline measurement, a Jatropha residue without catalyst addition was also tested for comparison.

### 3.7 Lab-pyrolyzer apparatus: semi-continuous drop tube reactor

Pyrolysis of Jatropha residues were carried out via a drop tube pyrolyzer to investigate performance of catalyst in a more realistic bio-oil production scheme. This part will be focused on the effect of pyrolysis temperature and the effect of type of catalysts. The diagram of methodologies of catalytic pyrolysis is shown in Fig.3.19.
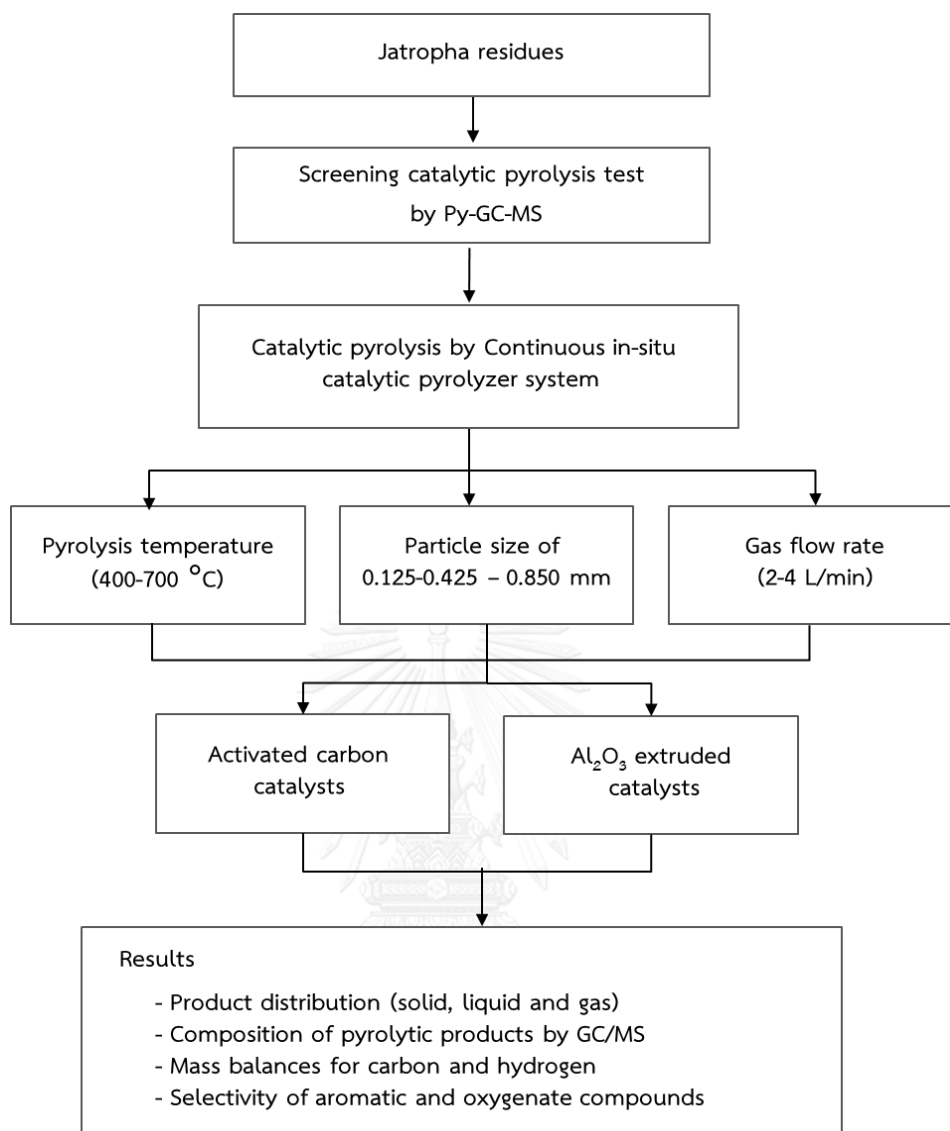
**Fig. 3. 19** Flow chart of methodologies of catalytic pyrolysis experiments

From previous part, the continuous in-situ catalytic rapid pyrolyzer was upgraded system of pyrolyzer as shown in Fig.3.20. The continuous in-situ catalytic rapid pyrolyzer system consists of several parts i.e., gas preheater, pyrolysis vapor producer, bio-oil condenser, and product collection and analysis. Details of each particular important parts are described in the next section. This set-up mainly consisted of a semi-continuous biomass feeder, fixed bed tube reactor with gas pre-heater, cyclone seperator, solid collector, water condensers with liquid collector, liquid nitrogen condenser, and cotton wool filter. All reactor parts were connected by

several flanges. High temperature gaskets were installed to prevent gas leakage. Ceramic fiber thermal insulation was used to minimize heat loss by wrapping them around a reactor and its pipe line. Tube line connecting equipment on the cold side for gas or condensed water flow were silicone rubber tubes.
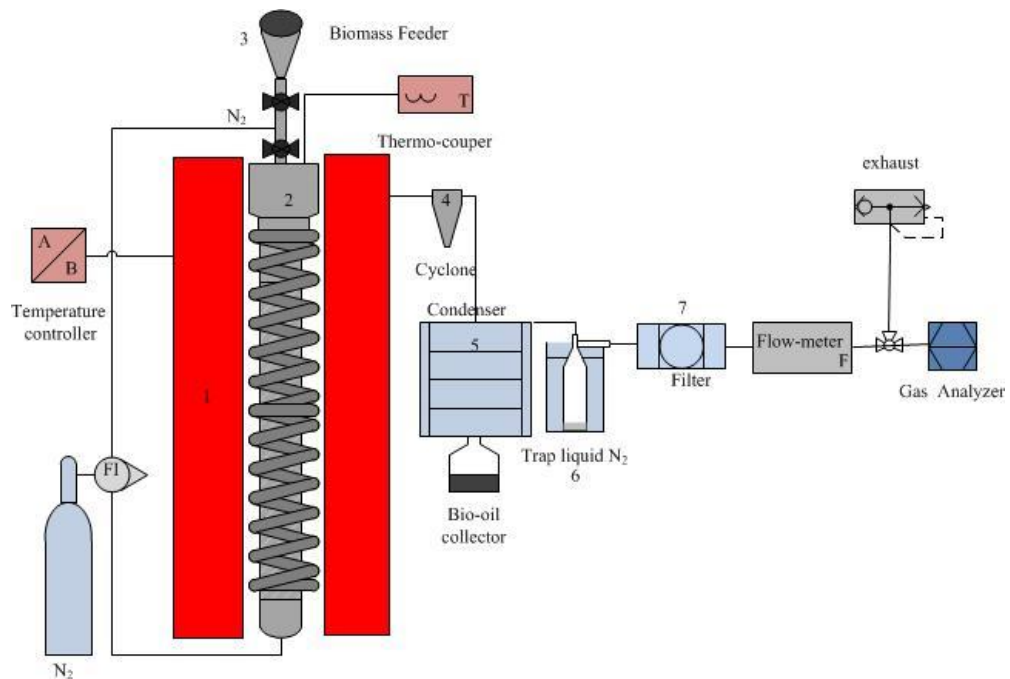


**Fig. 3. 20** Schematic of the fast pyrolysis unit

### 3.7.1 Drop tube reactor

The reactor unit consisted of three main parts, thermal decomposition zone, head zone and bottom zone. The body of reactor was constructed from a 310-stainless steel with a total height of about 190 cm, while the gas pre-heater was made of a stainless-steel SUS 316 with an internal diameter of 1.27 cm and its tube was bent into a spiral wrap around the heated cylinder and carrier gas first enters this spiral tube before entering the reactor as shown in Fig. 3.21.

The thermal decomposition zone of this stainless-steel cylinder has a length of 180 cm with an internal diameter of 7.62 cm. It is a zone which was directly heated by tubular electrical furnace and solid biomass was mainly decomposed in this zone. Condensable gas and non-condensable gas from pyrolysis will rise up on the top of

this zone and then leave from the head zone, whereas the solid products will fall down at bottom zone.
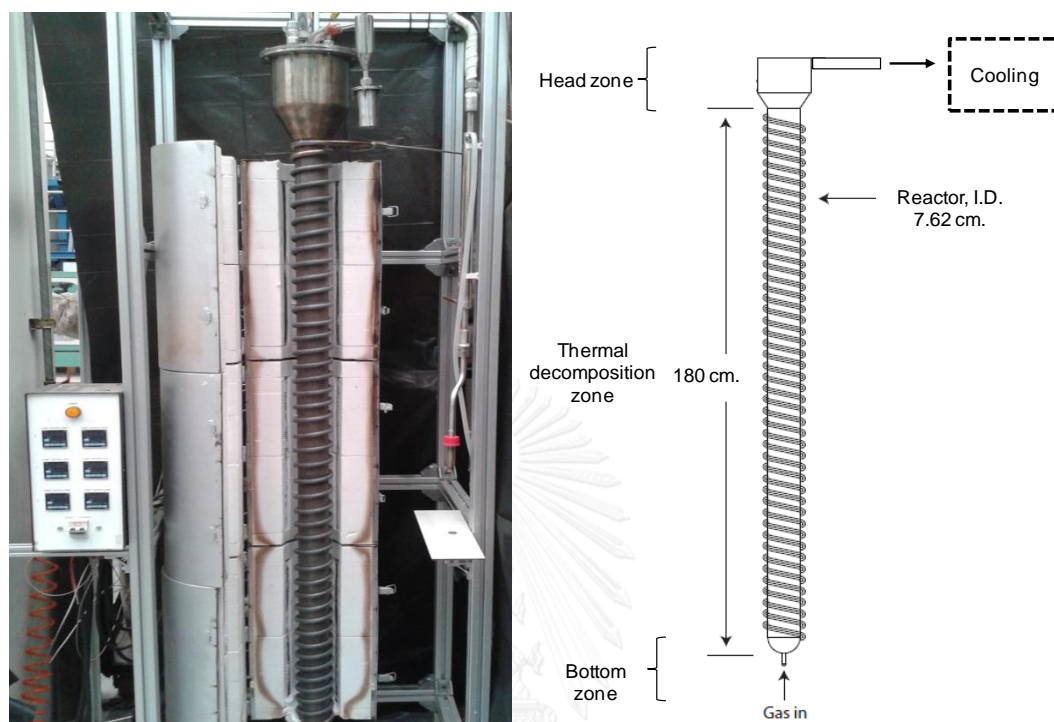


**Fig. 3.21** Upgraded size of continuous in-situ catalytic rapid pyrolyzer system

3.7.2 Pyrolysis vapor producer

The reactor consists of three main sections which are 1) Head section, 2) Thermal degradation section, and 3) Char collection section. Major product exits from this part are pyrolysis vapor which composes of both condensable and non-condensable gases as well as char.

3.7.2.1 The head section

The head section consists of a biomass hopper, and a biomass feeder line. The reactor is a 4-in. outer diameter 316 stainless-steel tube with a free board height of 30 inches (Fig. 3.22). Feeder is 1" OD a stainless-steel tubing cover with water cooled heat exchanger shell to prevent premature heating of fed biomass from convection and conduction of heat from reaction zone below.

The feeder tube connected to reactor opening by several ball valves to ensure oxygen starving condition inside the reaction zone.
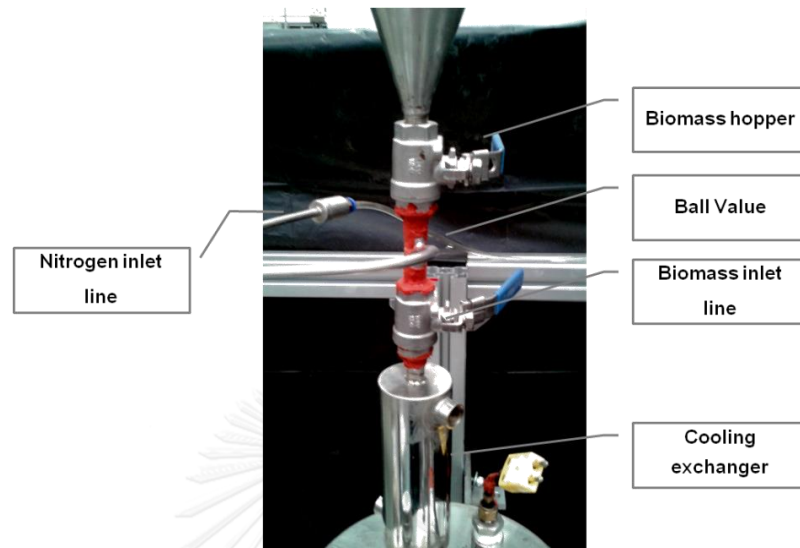


**Fig. 3. 22** Biomass feeder setup

Pyrolysis vapor upgrading part (Fig.3.23) is the freeboard section which wrap around biomass feeder tube in form of annulus. The catalyst bed was supported by a distributor made from a 316-stainless-steel wire mesh (50×250 mesh).
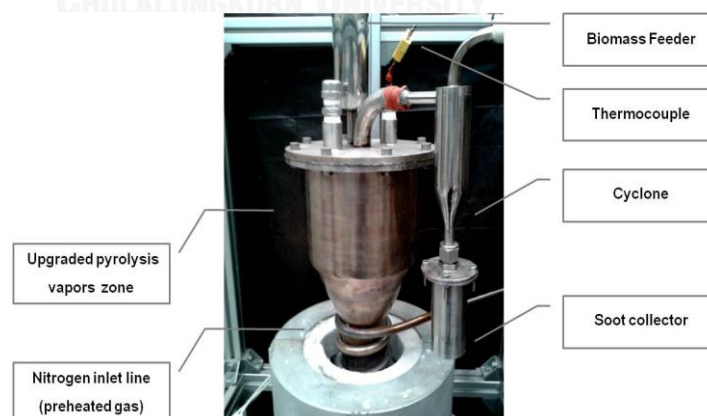


**Fig. 3. 23** Outside of pyrolysis vapor upgrading section

A stainless-steel mesh tubing is placed inside this vapor upgrading part to retain tested catalyst during catalytic vapor upgrading experiment as shown in Fig. 3.24.



**Fig. 3. 24** Catalytic upgrading tube

3.7.2.2 Thermal degradation zone

This part is a main pyrolysis reactor which composes of two major parts: carrier gas pre-heater which is a 0.25" OD stainless steel tube coiled around and along the length of reactor tube. The carrier gas enters at the bottom part then circling to the top then turn down to straight tube and into reactor at the bottom zone as shown in Fig. 3.25 (a). Reaction section is the cylinder tube where pyrolysis of biomass takes place. It is constructed from 60 mm OD stainless steel tube with the length of 1900 mm. The biomass enters in this zone by free fall from feeder and then pyrolyzed. Gas produces from thermal degradation would be entrained by carrier gas and flow up to the vapor upgrading section and through the catalytic bed where in-situ catalytic conditioning of product gas takes place. The product gas then exit from the upgrading section and further into condenser where bio-oil is collected.
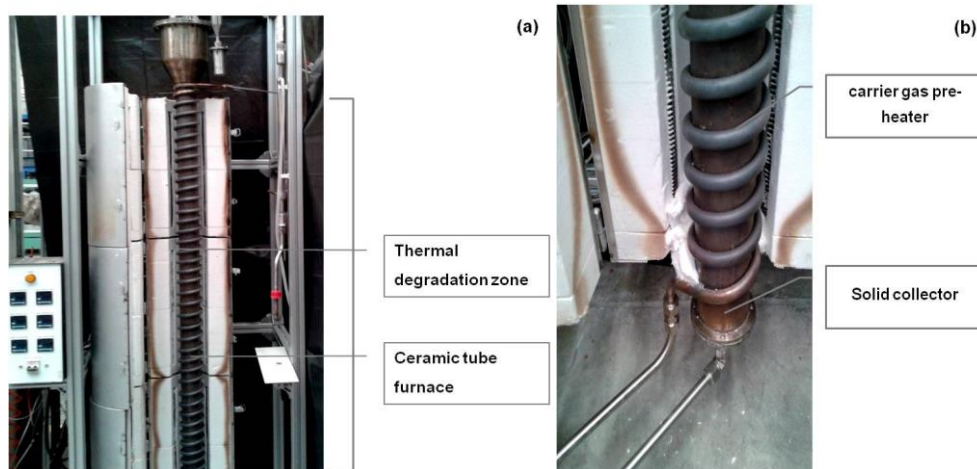
**Fig. 3. 25** Thermal degradation zone (a) pyrolysis reactor (b) solid collector

*3.7.2.3 Solid collection section*

This part is the conical shaped stainless-steel body below reaction zone where the carrier gas enters the reactor and the produced char is collected as shown in Fig. 3.25 (b). In addition, other auxiliary parts are required for completion of pyrolysis system which includes carrier gas feeder, ceramic tube furnace as well as temperature controller, rotameters, etc.

3.7.3 Pyrolysis experiment

The pyrolysis temperature of biomass wastes was set at 400, 500, and 600°C with monitoring by a K-type thermocouple located inside the reactor. In addition, the effect of ceramic catalyst was also investigated. In this work, Jatropha residues with the particle size of 125-425 micron were used as biomass feedstock. For any experiments, nitrogen gas was used as carrier gas at a flow rate of 3 L/min. Alumina ball with the size of 8 mm (250 g.) was applied on a distributor plate at the bottom of the reactor. The biomass feed rate was controlled approximately 1 g/min. The total time for each run was approximately 30 min.
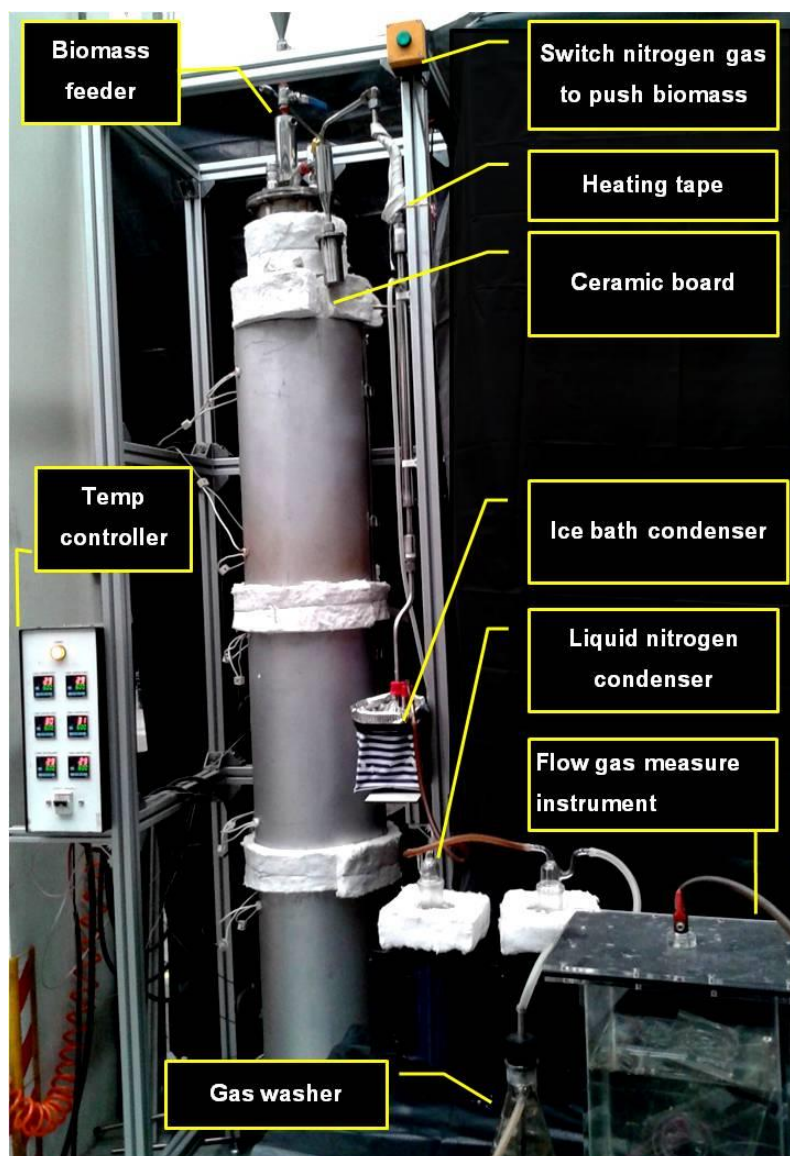
**Fig. 3. 26** Continuous in-situ catalytic rapid pyrolyzer system during test run

In typical run, catalyst will be placed over quartz wool in catalytic upgraded zone where reactive gas produced from pyrolysis reaction was directed to pass through. Condensable products such as water and heavy hydrocarbon compounds were collected in first condenser, which was cooled by chilled water, light hydrocarbons were trapped by liquid nitrogen. The condensing hydrocarbons system was shown in Fig. 3.26. Finally, product from rapid pyrolysis composes of three major fractions such as solid in form of char, liquid as bio-oil and gas; these products will be

further investigated by various methods. Gas product will also be analyzed for chemical species by online gas analyzer, which was measured as $CO_2$, $CO$, $H_2$, and $CH_4$ as mentioned earlier. Char will be collected and analyzed for C, H, O, N, and S. Bio-oil collected will be conditioned and separated into two parts, water soluble and water non-soluble parts. These liquid samples will also be analyzed for C, H, O, N, and S. All of the results will be discussed in next chapters.

## 3.8 Computational Scheme

Significant effort in both theoretical and experimental research activities is still required to formulate and validate truly comprehensive the CFD models coupled with pyrolysis models. In this chapter, describe in detail the CFD model for reacting biomass particles in a drop tube reactor. It is provided a description of the computational domain and boundary conditions used in our simulations.

### 3.8.1 Solution Methodology

There are three major steps for solving a CFD problem. These are included the pre-processing, solver, and post-processing.

*3.8.1.1 Preprocessing*

Solving of CFD problem is basically involves designing and building the domain. It involves the following steps:

- Definition of the geometry of the region: The computational domain as shown in Fig. 3.27.

- Mesh generation, the subdivision of the domain into a number of smaller, or control volumes or elements selection of physical or chemical phenomena that need to be modeled.

- Definition of fluid properties.

- Specification of proper boundary conditions at cells, which match with the boundary. The solution to a flow problem (velocity, pressure, temperature etc.) is defined at nodes inside each cell. The accuracy of a CFD solution is

governed by the number of cells in the grid. In general, the larger numbers of cells the better solution accuracy.
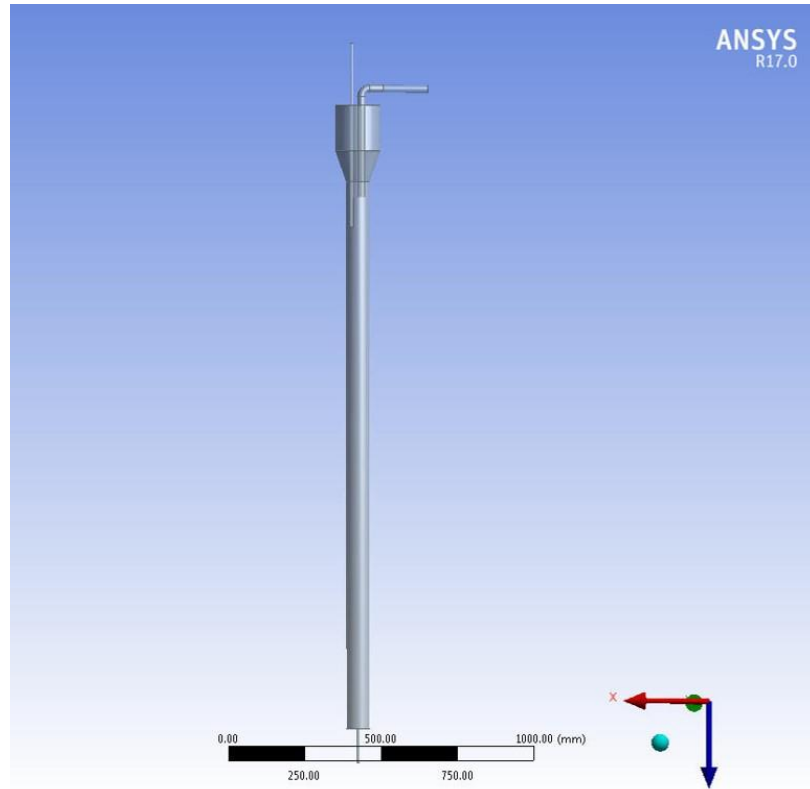


**Fig. 3. 27** Geometry of a drop tube reactor by Ansys R17.0

The CFD model was solved in three-dimensional coordinates using the ANSYS-FLUENT CFD code (Ver 17.0). The model formulation is presented with focus on the new equations added to the original hydrodynamic model developed in the first part of this study in order to take into consideration the thermo-chemical reaction associated with the biomass conversion. In this work, a numerical model for a fixed bed reactor is presented. Appropriate User Defined Functions (UDFs) have been implemented within the commercial software ANSYS Fluent 17.0 (license: 0061053). In the model, source terms were added to the species conservation equation to account for the formation/destruction of gaseous compounds, liquid compounds and water during the pyrolysis process. Furthermore, energy equation was considered to account for temperature variation. The validation of the numerical model was performed

comparing the simulation results with experimental data obtained in a drop tube laboratory scale reactor.

**Table 3. 3** Data used for the CFD simulation

| Boundary | Parameter (unit) | Value | | |
|---|---|---|---|---|
| | | Mellin et al. | (Borello et al.) | This work |
| Outlet | Pressure-outlet (Pa) | 101325 | 101325 | 101325 |
| Gas inlet | Mass inlet, $N_2$ (kg/s) | 4.5E-04 | - | 4.167E-06 |
| Feeding | Solid feed rate (kg/h) | 2 | 0.036 | 0.06 |
| line (25℃) | Gas flow rate, $N_2$ (Nl/min) | 6.19 | 0.4 | 3 |
| Material | Heat conductivity ($Wm^{-1}K^{-1}$) | 0.105 | 0.173 | 0.105 |
| parameter | Heat capacity ($J kg^{-1} K^{-1}$) | 1500 | 2310 | 1500 |
| | Density (kg $m^{-3}$) | 600 | 400 | 330 |
| | Char density (kg $m^{-3}$) | 200 | - | 100 |
| | Biomass Particle size (um) | 850 | 1000 | 233 |

The pyrolysis reaction was implemented in the CFD model based on one-step global reaction scheme for biomass pyrolysis (Wang & Yan, 2008; Basu, 2010). The initial temperatures of $N_2$ gas inside the reactor are 600℃, corresponding to steady- state conditions as will be explained later. The initial gas phase is pure nitrogen. Biomass is injected at the beginning of the simulation. All other initial and boundary conditions are summarized in Table 3.5. The nitrogen gas flows in at 600℃ from the bottom of the bed. The uniform gas velocity inlet is 3 L/min (1.1 cm/s). The biomass is entrained at a flow rate of 60 g/h at 25℃. At the outlet, an atmospheric pressure boundary condition is used. At the solid walls, no-slip wall conditions are specified for all phases, and a standard wall-function is applied for the gas phase. For the thermal boundary conditions, an isothermal wall of 600℃ is used for the reactor wall which is treated as adiabatic

*3.8.1.2 Solver*

After the geometry has been made, the flow was calculated to obtain the solution for the governing equations. CFD solver executes the flow calculations and displays the results obtained. Numerous iterations are performed until the solution converges and the results obtained. For performing the simulation in ANSYS FLUENT 17.0 the procedures are:

- Import geometry into ANSYS FLUENT 17.0
- Define the solver model
- Define the turbulence model
- Define the species model
- Define the materials and the chemical reactions
- Define phases: primary and secondary phase
- Define phase Interaction such as drag force, heterogeneous reaction, etc.
- Define the boundary conditions
- Initialize the calculations
- Iterate/calculate until convergence is achieved
- Post processes the results.

*3.8.1.3 Post processing*

In this case, the products were evaluated by integrating the reaction rate of all primary pyrolysis reactions and adding up all the product species. This is the final step in CFD analysis, and it involves the organization and interpretation of the predicted flow data and the production of CFD images and animations. The contour results can be employed to aid in understanding the physics of the solution. The results are presented in the form of contour plots (e.g. temperature contour), velocity vector plots, streamline plots, and animations via the built-in plotting software in ANSYS/Fluent.

# CHAPTER 4

# RESULT AND DISCUSSION OF BIOMASS BEHAVIOR AND
# SYNTHESIZED CATALYST

## 4.1 Biomass properties and its pyrolysis behavior

The Jatropha waste used as raw material for fast pyrolysis was obtained from local plants (Chiangrai province). They were left after extraction of oil from biodiesel production process. The main observable differences are particle size and homogeneity of sample color as shown in Fig. 4.1. Jatropha powders were kept in desiccators for further characterization. The large size distribution appeared in the first and second sample size range (0.85-2.0 mm and 0.425-0.85 mm). The Jatropha sample was further analyzed for particle size distribution. Characterization of four size fractions after passed through a 20, 40, and 120 mesh sieves to obtain of 0.850-2.0mm, 0.425-0.85mm, 0.125-0.425m and <0.125 mm (125 μm) as shown in Table 4.1. The results found that the particle size distribution analysis cannot be detected in larger particle size because of the limitation of laser diffraction instrument.



**Fig. 4.1** Jathropha residues obtained from Chiangrai province after size reduction; (a) 0.425-0.85 mm (b) 0.125-0.425 mm (c) < 0.125 mm

**Fig. 4.2** Particle size distribution analysis of Jatropha residues

| Particle size(mm) | Jatropha residues | | | |
|---|---|---|---|---|
| | Mean Diameter [d(4,3)] | D10% [d(v,0.1)] | D50% [d(v,0.5)] | D90% [d(v,0.9)] |
| 0.850-2.0 | ND | ND | ND | ND |
| 0.425-0.850 | ND | ND | ND | ND |
| 0.125-0.425 | 266.13 | 13.58 | 270.74 | 505.3 |
| <0.125 | 73.21 | 3.38 | 55.98 | 168.9 |

The Jatropha waste was analyzed using proximate analysis, ultimate analysis and component and bomb calorimeter and characteristics of four size fractions are shown in Table 4.2. Volatile matter and inherently bound water in Jatropha are released during pyrolysis starting at relatively low temperature forming a vapor consisting of water, oils and gases. High volatile matter in Jatropha generally increases liquid product. An elemental analysis was carried out using a TruSpec CHN, LECO Cooperation which reported the composition of Jatropha in weight percentage of carbon, hydrogen, sulfur, nitrogen and oxygen. The relative content of elements is in acceptable level though relatively higher amount of nitrogen and sulfur was reported for Jatropha waste. Similar to typical biomass, carbon (48.70-49.03 wt. %) is the main element of this waste. The oxygen content is also considerably high which could yield unfavorable oxygenated pyrolysis liquid products. The relatively higher presence of nitrogen and sulphur are shown in Jatropha with difference sizes which are not desired in combustion properties. Nitrogen and sulphur are the major contributing factor to ash formation and also form the corrosive compounds. These elements are also precursors to $NO_x$ and $SO_x$ formation during thermochemical conversion of raw materials (Sricharoenchaikul, 2009; Kaewpengkrow et al., 2014; Vichaphund et al., 2014). The determination of HHVs was carried out using a Leco model AC-350, Jatropha waste was within range of 18.83–20.15 MJ/kg, similar to that of typical biomass. In term of elemental atomic ratio which is based on the hydrogen, oxygen, and carbon content

of the fuel, generally biomass has much higher ratios of H/C and O/C than those of fossil fuels. The H/C ratio might be expressed as a linear function of the (O/C) ratio. The high oxygen and hydrogen content of biomass results in high volatile and liquid yields, and thus the high H/C biomass does not convert into high gas yield (Basu, 2010).

**Table 4.1** Characterizations of Jatropha residue in various sizes

| Characteristic (wt %) | Jatropha curcus (mm.) | | | |
|---|---|---|---|---|
| | 0.850-2.00 mm (S.D.) | 0.425-0.850 (S.D.) | 0.125-0.425 (S.D.) | < 0.125 (S.D.) |
| **Proximate Analysis** | | | | |
| Moisture | 4.38 (±1.72) | 4.46 (±1.94) | 4.70 (±1.80) | 5.17 (±1.64) |
| Ash | 4.85 (±1.65) | 5.08 (±1.38) | 5.45 (±1.15) | 6.16 (±0.36) |
| Volatile content | 70.74 (±1.24) | 71.38 (±1.58) | 71.43 (±0.13) | 72.36 (±1.44) |
| Fixed Carbon | 20.03 (±1.17) | 19.09 (±1.02) | 18.43 (±0.53) | 16.32 (±2.72) |
| **Element Analysis** | | | | |
| Carbon | 46.51 (±2.31) | 46.22 (±2.92) | 45.90 (±2.80) | 46.54 (±2.49) |
| Hydrogen | 6.72 (±0.49) | 6.72 (±0.38) | 6.60 (±0.50) | 6.70 (±0.35) |
| Oxygen | 35.80 (±1.30) | 37.10 (±1.25) | 36.29 (±1.73) | 35.24 (±2.00) |
| Nitrogen | 5.62 (±0.62) | 4.44 (±0.36) | 5.31 (±0.11) | 4.82 (±0.35) |
| Sulfur | 1.02 (±0.00) | 0.56 (±0.33) | 0.65 (±0.02) | 1.10 (±0.18) |
| Atomic H/C | 1.74 | 1.76 | 1.74 | 1.74 |
| Atomic O/C | 0.58 | 0.61 | 0.60 | 0.57 |
| HHV (MJ/kg) | 19.70 | 19.63 | 20.13 | 18.83 |
| **Chemical composition** | | | | |
| Hemicellulose | 17.47 | 17.39 | 18.00 | 17.60 |
| Cellulose | 56.31 | 56.44 | 57.88 | 57.00 |
| Lignin | 23.91 | 23.17 | 24.13 | 25.40 |

Moreover, chemical composition for macro components was determined according to the TAPPI (Technical Association of the Pulp and Paper Industry) of TAPPI T222 and T203 method. Jatropha waste contains large amount of cellulose (56.31-57.00%) with much lesser hemicellulose and lignin of 17.39-18.00% and 23.17-25.45%, respectively. The three components decomposed at different rates and within distinct temperature ranges during the pyrolysis.

**Table 4. 2** Characteristics of Jatropha wastes comparing with other works

| Biomass feedstock | JW[a] | JSC[b] | JR[c] | Cedar[c] | Pine wood[d] |
|---|---|---|---|---|---|
| **Proximate analysis (wt%)** | | | | | |
| Volatile | 73.80 | 79.80 | - | - | - |
| Fixed carbon | 13.60 | 14.13 | - | - | - |
| Moisture | 6.80 | 2.56 | - | - | 5.6 |
| Ash | 5.80 | 3.42 | - | - | 0.9 |
| **Elemental analysis (wt%)** | | | | | |
| C | 44.35 | 50.52 | 48.0 | 50.0 | 45.7 |
| H | 6.76 | 6.15 | 5.8 | 6.1 | 6.5 |
| O | 32.95 | 39.41 | 45.2 | - | 45.5 |
| N | 7.35 | 2.32 | 1.6 | 0.1 | 0.1 |
| S | 0.47 | - | 1.3 | - | - |
| **Component analysis (wt%)** | | | | | |
| Cellulose | 59.20 | 36.64 | 26.2 | 34.2 | 43.8 |
| Hemicellulose | 18.00 | 4.82 | 16.2 | 15.3 | 19.9 |
| Lignin | 22.80 | 39.61 | 20.2 | 32.1 | 24.3 |
| Other | n/a | 18.94 | 23.1 | 4.8 | - |
| HHV (MJ/kg) | 18.83 | 20.80 | - | - | - |

[a] Kaewpengkrow et al., [b] Kim et al., [c] Mochizuki et al., [d] Thangalazhy et al., *By difference

According to Basu (2010), hemicellulose decomposes first, and the decomposition of cellulose and then lignin follows. These phases were identified as

the temperature increased during the pyrolysis. The hemicellulose usually starts to decompose near 220°C, and the process is mostly complete by the time the temperature reaches 315°C. When hemicellulose had completely decomposed, cellulose then undergoes decomposition, which normally starts at a temperature of 315°C and is completed at 400°C. Therefore, the result suggested that this waste can be effectively converted into liquid fuel by pyrolysis process at relatively moderate temperature. The analysis findings show that extracted Jatropha residues have acceptable heating value with high content of volatiles, carbon, hydrogen and oxygen which are compared with other tropical biomasses as shown in Table 4.3. Heating value of 18.83-20.15 MJ/Kg for Jatropha waste was higher to that of cane trash (16.80 MJ/kg), palm shell (18.26 MJ/Kg), and much greater than some other biomass such as rice husk (14.75 MJ/Kg), corncob (11.3 MJ/kg), bagasse (9.24 MJ/kg), or tapioca rhizome (7.45 MJ/kg) (reference). Consequently, this waste has high potential of producing quality bio-fuel by thermal conversion process.

In addition, thermogravimetric analysis (TGA) is one of the most common techniques for the investigation of thermal events and their associated kinetics during pyrolysis of solid raw materials such as coal, biomass, and plastic. It provides a measurement of weight loss of the sample as a function of time and temperature. In this work, thermal degradation characteristics of Jatropha residue were studied using this method. Experiments were performed on a Mettler Toledo TGA/STDA851e analyzer.

The thermogravimetric (TG) data and its first derivative (DTG data) with various size of Jatropha residue at the heating rate of 100°C/min are plotted against the temperature in the same graph in order to show their degradation profile (Fig. 4.2). As observed, the particle size has no significant effect on the thermogram of extracted Jatropha at the initial stage of pyrolysis (lower than 200°C), after that the residual mass and the final yield of char increase with increasing of particle size. However, the decomposition of solid appears to start and end at approximately the same temperature range for all particle size. The DTG plots indicate that the first and second peaks of DTG curve occur at the similar temperature independent of particle sizes. However, the residual mass of particle sizes 0.425-0.85 and 0.85 mm are not

significantly different, this may be due to non-homogeneous property, typical to any biomass and the fact that these two size ranges are relatively large so that the heat transfer and temperature gradient would be relatively similar.
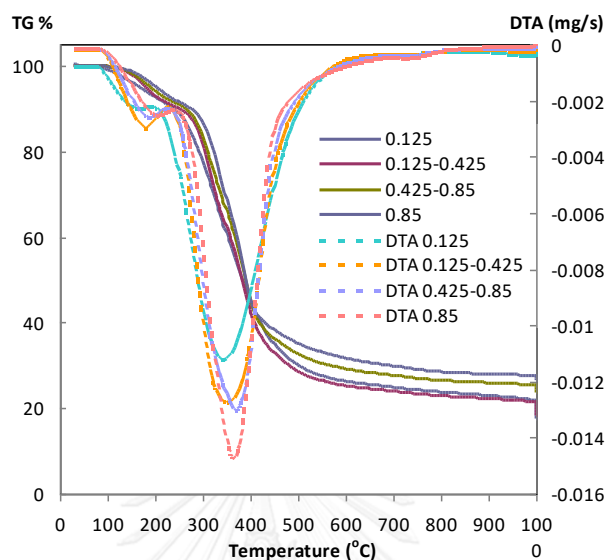


**Fig. 4. 3** DTA and TG of Jatropha residue from Chiangrai with various sizes at heating rate of 100$^{o}$C/min

In order to optimize the process parameters and maximize desired yields, the knowledge of associated kinetics of pyrolysis is important. Thermochemical conversion of Jatropha residue was performed by TGA analysis at various heating rates to study the kinetic parameters of the pyrolysis process. Each sample of 10 mg was heated from room temperature to a final temperature of 900°C at various heating rate (10-100°C/min) under nitrogen atmosphere at 20ml/min. Variation of sample mass with respect to temperature change (TG data) and its first derivative (DTG data) was continuously collected. TG and DTG curves of the thermal degradation characteristics of Jatropha residue at various heating rates are shown in Fig. 4.3 and Fig.4.4, respectively.

Final char yields at 900°C varied with heating rates from 22.28% to 24.88% at 10–100°C/min, respectively. Slower heating rates yield better separation among decomposition stages of Jatropha waste components as seen in DTG curve. The region

corresponds to the second mass loss rate in the DTG curves due to further slow thermal decomposition of lignin component of Jatropha residue.  It should be noted that the two maximum of decomposition rates occur at about 250 and 350°C which are lower than typical oil-palm shell and fiber at 300°C and 350°C, respectively (Jeong et al. 2016).
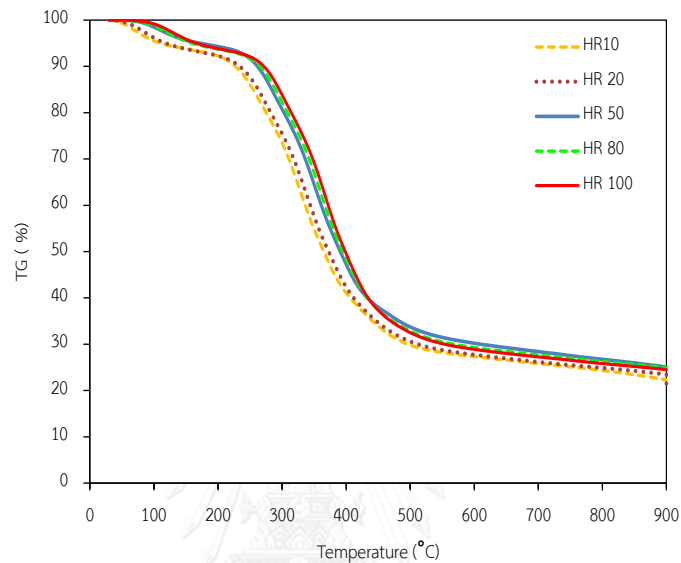


**Fig. 4.4** TGA of Jatropha residue with size of 0.125-0.425 mm at different heating rates between 10-100°C/min
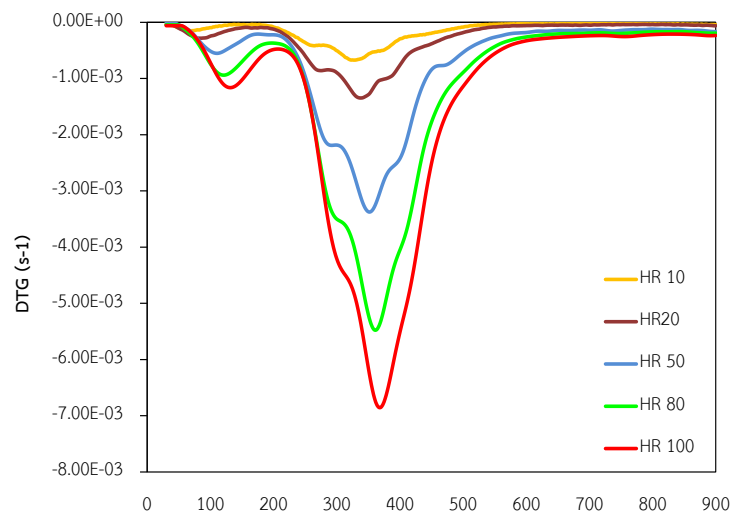


**Fig. 4.5** DTG of Jatropha residue with size of 0.125-0.425 mm at different heating rates between 10-100°C/min

The kinetics of these thermal events has been determined by the application of the Arrhenius equation corresponding to the separate slopes of constant mass degradation. The method is referred to as a model-free method. Therefore, the FWO method is able to calculate the activation energy ($E_a$) without prior knowledge of the reaction mechanism, the reaction rate in logarithmic form can be expressed as follows:

$$\ln(\beta) = \ln(\frac{AE_a}{Rg(\alpha)} - 5.331 - 1.052\frac{E_a}{R}\frac{1}{T} \tag{4-1}$$

where:

A pre-exponential factor, 1/s

T pyrolysis temperature, K

$E_a$ activation energy, kJ/mol

R universal gas constant = 8.314 J/mol K

$\alpha$ percent conversion of samples

$\beta$ Heating rates

The slope of ln ($\beta$) against 1/T at different heating rates determines the value of apparent activation energy $E_a$ when $\alpha$ is constant. The slope of such a plot gives the value of E/R. From this result, the activation energies and the pre-exponential factors are obtained in the range of 67.9-160.9 kJ/mol and $10^6$-$10^{13}$ s$^{-1}$, respectively. The range of activation energies of the samples increases with increasing conversion. Maximum activation energy of 160.9 kJ/mol is required for complete pyrolysis of the Jatropha residue. The result agreed well with Sharma et al. (2016) who study the kinetic parameters of Jatropha residue seed cake. The data can be utilized to predict thermal decomposition behavior for a wide range of heating rates (10°C/min to 60°C/min). The activation energies and the pre-exponential factors are obtained in the range of 33.7-160 kJ/mol and $10^4$-$10^{13}$ min$^{-1}$ (Sharma et al., 2016).
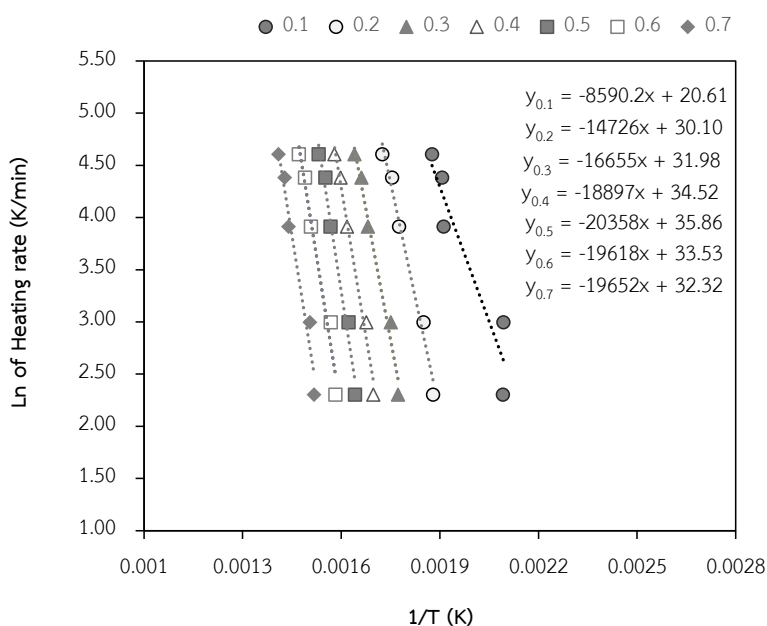
**Fig. 4.6** The slope of plot ln ($\beta$) against 1/T at different heating rates

## 4.2 The ceramic catalysts synthesis

### 4.2.1 Characterization of catalysts (ceramic catalysts with $CeO_2$ promoter)

The analyses of catalyst were done in term of particle size and size distribution, and specific surface area. The density was determined using ultrapycnometry technique (Ultrapycnometer 1000 Version 2.12, Quantachrome Corporation). The particle size and distribution was determined using laser diffraction by two instruments (Mastersizer S Version 2.19 Serial Number: 32734-89, Malvern Instrument Ltd and Zetasizer nano ZS Version 5.01 Serial Number: MAL500361, Malvern Instrument Ltd). Brunauer-Emmett-Teller (BET) specific surface area was determined from the nitrogen adsorption data using gas sorption analyzer (Autosorb-1, Version 1.19, Quantachrome Corporation). The results were listed in Table 4.4. After impregnation with promoter (Ce) and active phase on $Al_2O_3$ support, the particle sizes of prepared catalysts increased significantly from 11 mm to 27-65 mm.

**Fig. 4.7** Characteristics of metal catalyst on various supports

| Material | Density (g/cm$^3$) | Particle size (μm) * | Surface area (m$^2$/g) † | Porosity characteristics | | EDS (wt %) |
|---|---|---|---|---|---|---|
| | | | | Pore volume (cm$^3$/g) | Pore size (A) | |
| $Al_2O_3$ | 4.18 | 11.76 | 103.38 | 0.425 | 108.7 | - |
| Ce/ $Al_2O_3$ | | 65.89 | 90.35 | | | 7.3 |
| Pd/ Ce-$Al_2O_3$ | | 27.94 | 86.93 | | | 1.19 |
| Ru/ Ce-$Al_2O_3$ | | 30.73 | 85.81 | | | 1.68 |
| Ni/ Ce-$Al_2O_3$ | | 30.96 | 87.91 | | | 1.07 |
| $ZrO_2$ | 5.80 | 11.80 | 12.78 | 0.102 | 341.9 | - |
| Ce/ $ZrO_2$ | | 10.25 | 11.83 | | | - |
| Pd/ Ce-$ZrO_2$ | | 10.46 | 12.37 | | | 1.69 |
| Ru/ Ce-$ZrO_2$ | | 10.20 | 10.49 | | | 2.01 |
| Ni/ Ce-$ZrO_2$ | | 9.84 | 11.61 | | | 1.64 |
| $TiO_2$ (Rutile) | 4.32 | 8.51 | 4.15 | 0.017 | 91.59 | - |
| Ce/ $TiO_2$ | | 3.52 | 3.40 | | | - |
| Pd/ Ce-$TiO_2$ | | 4.31 | 3.57 | | | 0.81 |
| Ru/ Ce-$TiO_2$ | | 3.75 | 3.48 | | | 0.21 |
| Ni/ Ce-$TiO_2$ | | 3.69 | 3.29 | | | 0.82 |
| $TiO_2$ (Anatase) | 3.54 | 0.51 | 204.25 | 0.379 | 70.17 | - |
| Ce/ $TiO_2$ | | 0.50 | 45.91 | | | - |
| Pd/ Ce-$TiO_2$ | | 0.54 | 40.72 | | | 0.77 |
| Ru/ Ce-$TiO_2$ | | 0.54 | 35.18 | | | 1.32 |
| Ni/ Ce-$TiO_2$ | | 0.53 | 33.34 | | | 0.84 |

* Mastersizer-S Version 2.19 Serial Number: 32734-89, Malvern Instruments Ltd., UK

** Zetasizer Nano Zs Version 5.01, Malvern Instruments Ltd., UK † Autosorb-1 Version 1.19, Quantachrome Corporation, USA.

Surface areas of $Al_2O_3$ based catalyst were measured as 85-90 $m^2$/g which were slightly lower than that of $Al_2O_3$ support (103$m^2$/g), while $TiO_2$ ($T_2$) based catalysts were obviously reduced from 204.25 to 33.34-45.91 $m^2$/g. Among four catalyst groups, alumina based catalyst has the highest surface area while those of $ZrO_2$ and $TiO_2$ ($T_1$) supported catalysts did not change when compared to their respective supports.

The morphologies of catalysts synthesized with various supports were investigated by SEM analysis, conducted after calcination at 700°C and are displayed in Fig.4.6. SEM involves the raster of a narrow electron beam over the surface and detecting the yield of either secondary or backscattered electrons as a function of the position of the primary beam (. Microstructure was characterized by scanning electron microscope (SEM; JEOL, JSM-5410). For analysis of metal dispersion of catalysts, Energy dispersive X-ray spectroscope (EDS; model Oxford Inca 300) was employed. The catalyst powders appeared as an agglomeration of particles to the size of more than 1 μm. Energy dispersive X-ray (EDX) analysis was also used to approximate the amount of several elements. Emitted X-rays are characteristic for an element and allow for a determination of the chemical composition of a selected part of the sample.

The metal loading contents on alumina (1.07-1.19%), zirconia (1.64-2.01%) rutile (0.61-0.82%) and anatase (0.77-1.32%) were found to be relatively right on target and finely distributed over the surface, the result is shown in table 4.5
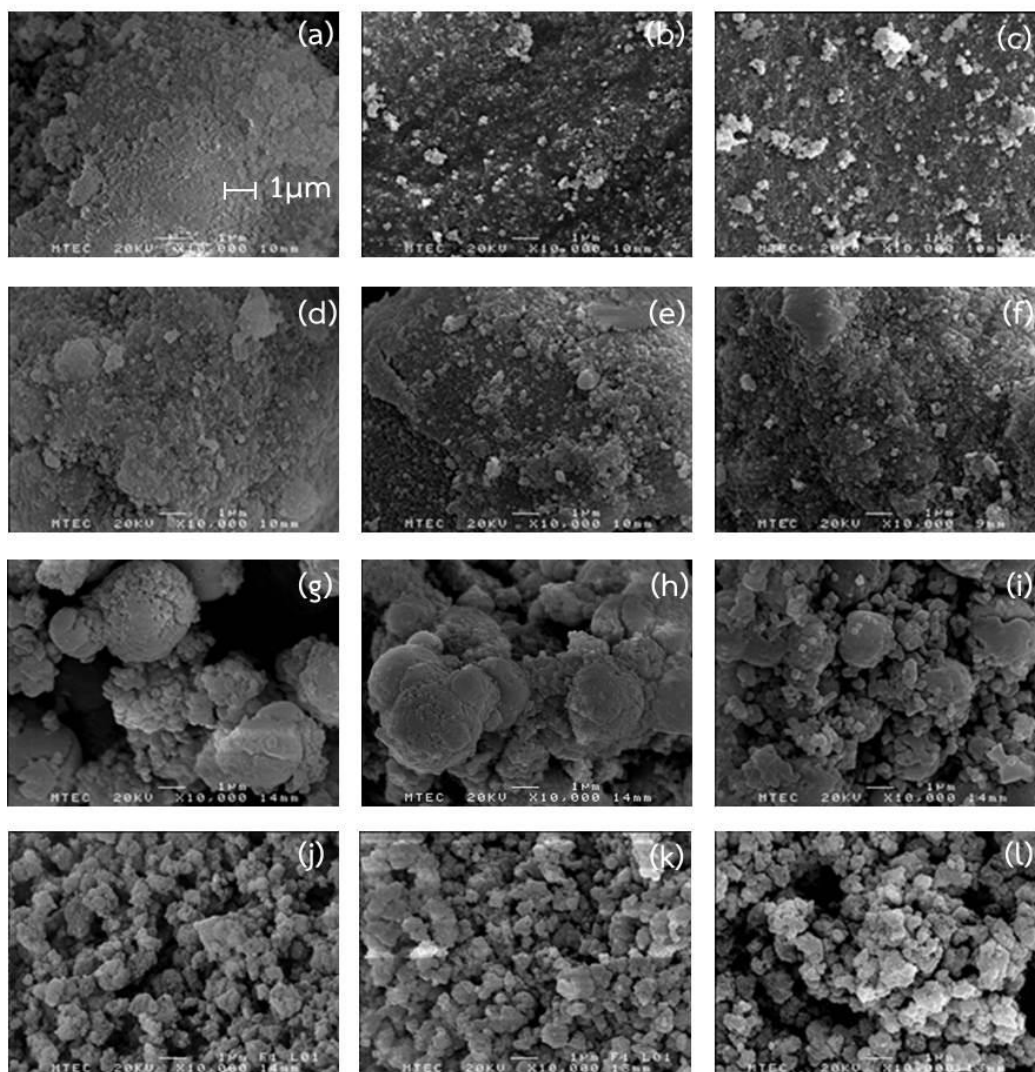
**Fig. 4.8** SEM results of various support catalysts at 10kX (a-c) $Al_2O_3$ based catalysts, (d-f) $ZrO_2$ based catalysts, (g-i) $TiO_2$ (rutile) based catalysts, (j-l) $TiO_2$ (anatase) based catalysts.

X-ray elemental analysis was also used to approximate the amount of element. The amount of metal loading content on alumina was found to be nearby purpose. X-ray diffraction is one of the oldest and most frequently applied techniques in catalyst characterization. It is used to identify crystalline phases inside catalysts by means of lattice structural parameters, and to obtain an indication of particle size. Diffraction patterns (spots from a single-crystal particle and rings from a collection of randomly oriented particles) enable one to identify crystallographic phases as in XRD

(Chorkendorff, 2006). Phase analysis of synthesized powder was performed by X-ray powder diffraction (XRD; PANalytical, X' Pert Pro) with 40 kV, 45 mA, CuKa radiation. The sample was scanned at $2\theta$ from 20 to 80° with a step size of 0.02. The X-ray diffraction patterns of metal oxide on each support catalysts are displayed in Fig.4.7.

$Al_2O_3$ crystalline phase was observed in all catalysts. The highest peak intensity at $2\theta$ of 32.79°, 45.32° and 67.32° corresponded to the tetragonal structure of $Al_2O_3$ according to JCPDS: 46-1131. After impregnating with $Ce(NO_3)_2$ promoter, the minor peaks, $2\theta$ of 28.63°and 56.44° corresponded to the $CeO_2$ cubic phase (JCPDS: 34-0394) were also observed. When further doping with various active species, $Al_2O_3$ and $CeO_2$ main phases were found accompanied by a small amount of active metal phase. Tetragonal structure of $PdO_2$ according to JCPDS: 34-1101 was detected for palladium doping case. The XRD pattern of ruthenium doped catalyst revealed the small amount of $RuO_2$ corresponding to the tetragonal phase (JCPDS: 40-1290), while small peaks of nickel doped catalyst were indexed as hexagonal NiO phase (JCPDS: 44-1159).

$ZrO_2$ crystalline phase was observed in all catalysts. The highest peak intensity at $2\theta$ of 28.19°, 31.41°, and 50.12° corresponded to the monoclinic structure of zirconia according to JCPDS: 37-1484. After impregnating with $Ce(NO_3)_2$ promoter, the minor peaks, $2\theta$ of 28.63°and 33.17° corresponded to the $CeO_2$ cubic phase (JCPDS: 34-0394) were also observed. When further doping with various active species, the presence of two major phases, $ZriO_2$ and $CeO_2$, were found accompanied by a small amount of active metal phase, $PdO_2$ (tetragonal, JCPDS: 34-1101), $RuO_2$ (tetragonal, JCPDS: 40-1290), and NiO (hexagonal, JCPDS: 44-1159) for palladium, ruthenium, and nickel doped catalysts, respectively.

$TiO_2$ crystalline phase was observed in all catalysts. The highest peak intensity at $2\theta$ of 27.44°, 36.12°, and 54.36° corresponded to the tetragonal structure of $TiO_2$ (rutile) according to JCPDS: 21-1276. After impregnating with $Ce(NO_3)_2$ promoter, the minor peaks, $2\theta$ of 28.63°and 47.56° corresponded to the $CeO_2$ cubic phase (JCPDS: 34-0394) were also observed. When further doping with various active species, $TiO_2$ and $CeO_2$ main phases were found accompanied by a small amount of active metal phase. Tetragonal structure of $PdO_2$ according to JCPDS: 34-1101 was detected for

palladium doping case. The XRD pattern of ruthenium doped catalyst revealed the small amount of $RuO_2$ corresponding to the tetragonal phase (JCPDS: 40-1290), while small peaks of nickel doped catalyst were indexed as hexagonal NiO phase (JCPDS: 44-1159).
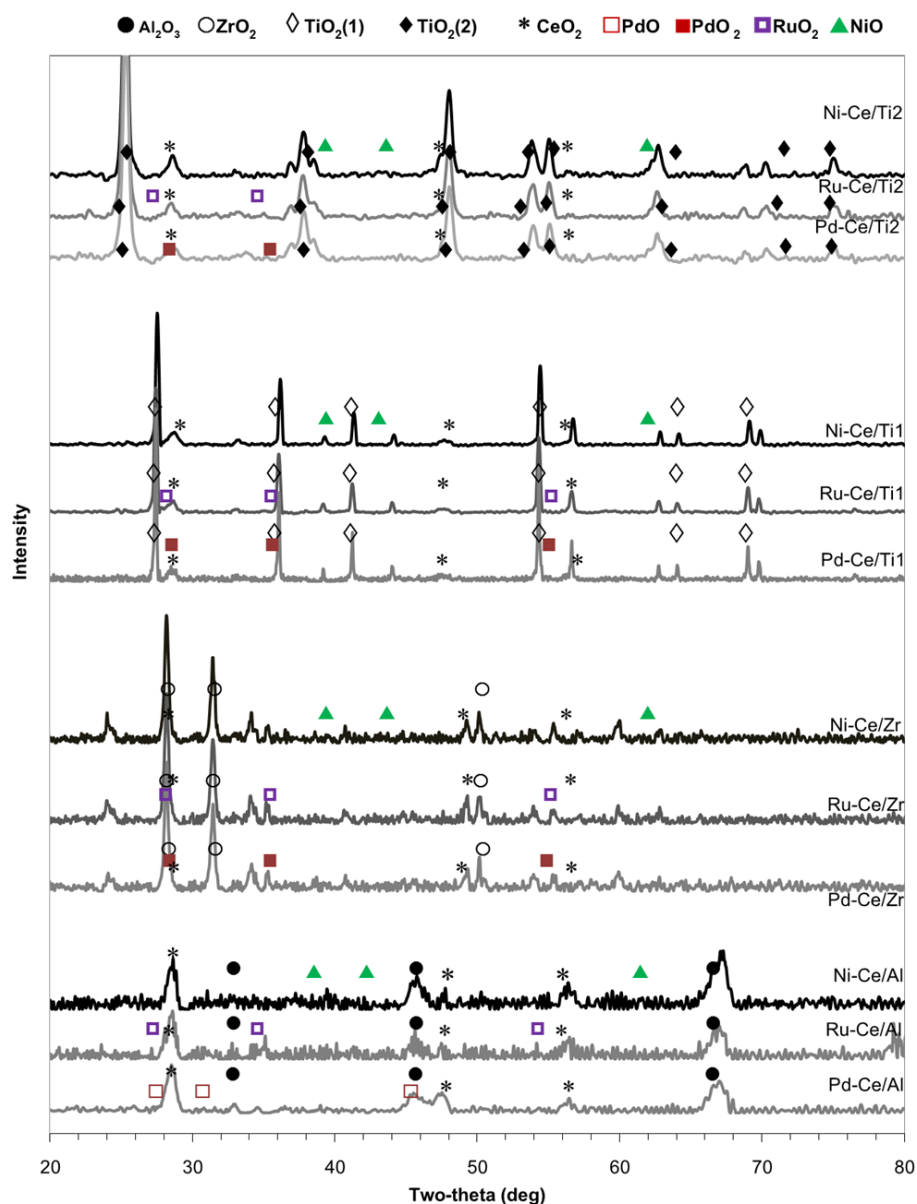


**Fig. 4.9** XRD patterns of four ceramic based catalyst

TiO$_2$ crystalline phase was observed in all catalysts. The highest peak intensity at 2$\theta$ of 25.32°, 37.88°, and 47.919° corresponded to the tetragonal structure of TiO$_2$ (anatase) according to JCPDS: 21-1272. After impregnating with Ce(NO$_3$)$_2$ promoter, the minor peaks, 2$\theta$ of 28.63°and 47.56° corresponded to the CeO$_2$ cubic phase (JCPDS: 34-0394) were also observed. When further doping with various active species, no difference in XRD pattern from that of rutile catalysts was observed. The presence of two major phases, TiO$_2$ and CeO$_2$, were found accompanied by a small amount of active metal phase, PdO$_2$ (tetragonal, JCPDS: 34-1101), RuO$_2$ (tetragonal, JCPDS: 40-1290), and NiO (hexagonal, JCPDS: 44-1159) for palladium, ruthenium, and nickel doped catalysts, respectively.

.

### 4.2.2 Characterization of Al$_2$O$_3$ based catalysts (without CeO$_2$ promoter)

From previous section, the modification of CeO$_2$/supports catalyst was performed by the impregnation of noble metals (Pd, Ru and Ni) with the aim to investigation how these metals would affect the catalytic activity. The result indicated that anatase (TiO$_2$;T$_2$) and alumina (Al$_2$O$_3$) supports catalyst displayed relatively high activity towards deoxygenation reactions which resulted in low quantity of acids and other oxygenated compounds, and produced high aromatic and hydrocarbon compounds, probably due to their high surface areas. However, the result also indicated that the promoter (CeO$_2$) had not significantly effect for distribution the metal and pyrolytic product of Jatropha residue. Thus, in this section the metal content loading onto the Al$_2$O$_3$ support by the impregnation were synthesized; the catalyst was not impregnated with CeO$_2$ as promoter and increased metal loading from 1% to 5%wt. The catalysts in this section included alumina support and active sites of 5 %wt. metal (Ce, Co, La, Mo, Ni Pd, and Ru).

The catalysts prepared included Ce/Al$_2$O$_3$, Co/Al$_2$O$_3$, La/Al$_2$O$_3$, Pd/Al$_2$O$_3$, Mo/Al$_2$O$_3$, Ni/Al$_2$O$_3$, and Ru/Al$_2$O$_3$. Table 4.5 summarizes the main characteristics of the catalyst samples. Specific surface areas were determined from adsorption isotherms using the BET equation. For the determination of surface area (BET method), pore volume and mesopore size distribution (BJH method) N$_2$ adsorption/desorption

experiments were conducted by an Automatic Volumetric Sorption Analyzer (Autosorb-1 Version 1.19, Quantachrome).

**Table 4.3** Physical properties of metal/$Al_2O_3$ catalysts

| Characteristic | Metal catalysts | | | | | | | |
|---|---|---|---|---|---|---|---|---|
| | $Al_2O_3$ | Ce | Co | La | Mo | Ni | Pd | Ru |
| Surface area ($m^2$/g) † | 103.38 | 107.9 | 115.02 | 99.3 | 74.4 | 110.3 | 103.2 | 102.9 |
| Particle size* (µm) | 11.76** | 107.9 | 129.01 | 78.65 | 45.70 | 72.55 | 78.97 | 68.93 |
| **Porosity characteristics** | | | | | | | | |
| Pore volume ($cm^3$/g) | 0.4252 | 0.78 | 0.88 | 0.86 | 0.57 | 0.816 | 0.76 | 0.69 |
| Pore size (nm) | 108.7 | 294.6 | 305.7 | 348.4 | 310.6 | 295.9 | 293.4 | 268.6 |
| Actual metal loading (EDS, %) | - | 5.77 | 4.23 | 5.72 | 4.54 | 3.97 | 4.61 | 3.15 |

\* Mastersizer-S Version 2.19, Malvern Instruments Ltd., UK, ** nm

† Autosorb-1 Version 1.19, Quantachrome Corporation, USA

The $Al_2O_3$ catalysts exhibited uniform pore-size distributions varying from 108.7 to 348.4 nm. After impregnation of active phase, the particle sizes of prepared catalysts were increased significantly to 45.70-129.01 µm. The surface areas were unabated and slightly increased than that of the support except Mo/Al and La/Al. The highest surface area was achieved by Co/Al (115.02 $m^2$/g). The morphologies of $Al_2O_3$ based catalyst calcined at 700°C for 4 h are shown in Fig. 4.8. The particles were agglomerated with size of more than 5 µm which was in good agreement with particle size determined by laser diffraction technique. In addition, the element composition of the various positions on the $Al_2O_3$ based catalysts was measured by the EDS analysis as also shown

in Table4.5. It is clearly seen that, during the catalyst preparation process, the surface becomes greatly enhanced of metal. The metal loading contents on the alumina supported were found to be nearby purposes 5 wt. % except Ni and Ru.
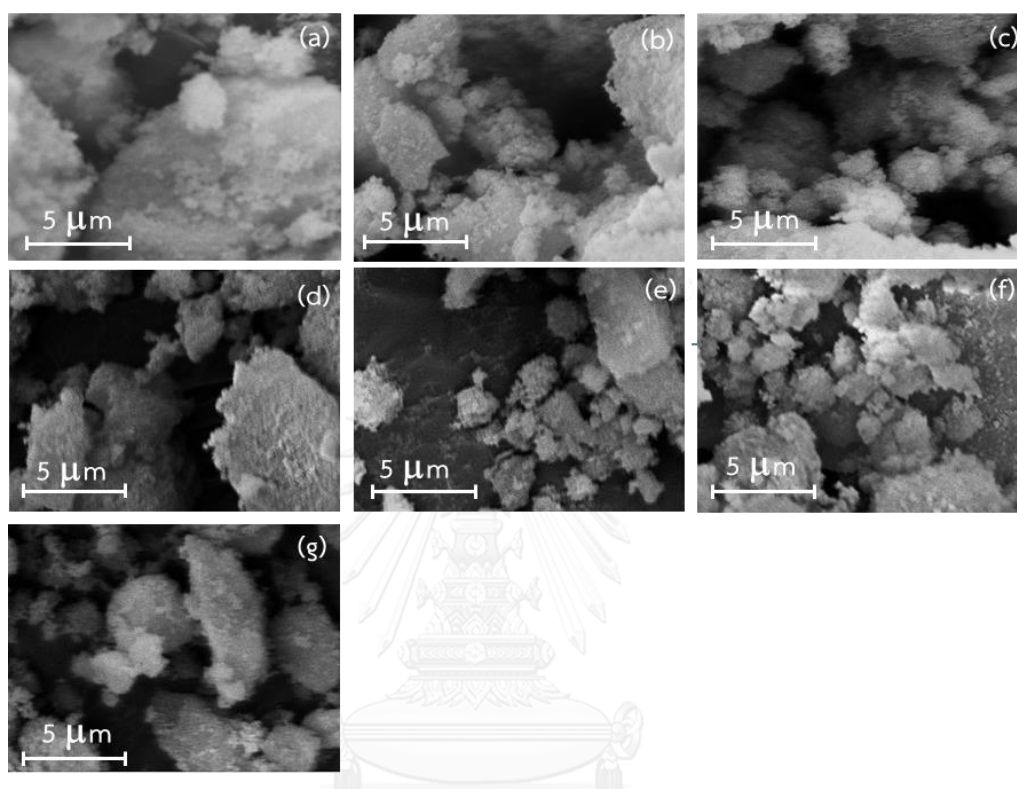


**Fig. 4.10** SEM results for $Al_2O_3$ based catalyst at 7,500X: (a) $Ce/Al_2O_3$, (b) $Co/Al_2O_3$, (c) $La/Al_2O_3$, (d) $Mo/Al_2O_3$, (e) $Ni/Al_2O_3$, (f) $Pd/Al_2O_3$ and (g) $Ru/Al_2O_3$

The crystal structures of selected catalysts were examined by powder X-ray diffraction (XRD), and step scans were taken over the range of $2\theta$ from 10 to 80. The X-ray diffraction patterns of alumina based catalysts calcined at 700°C are displayed in Fig. 4.9.
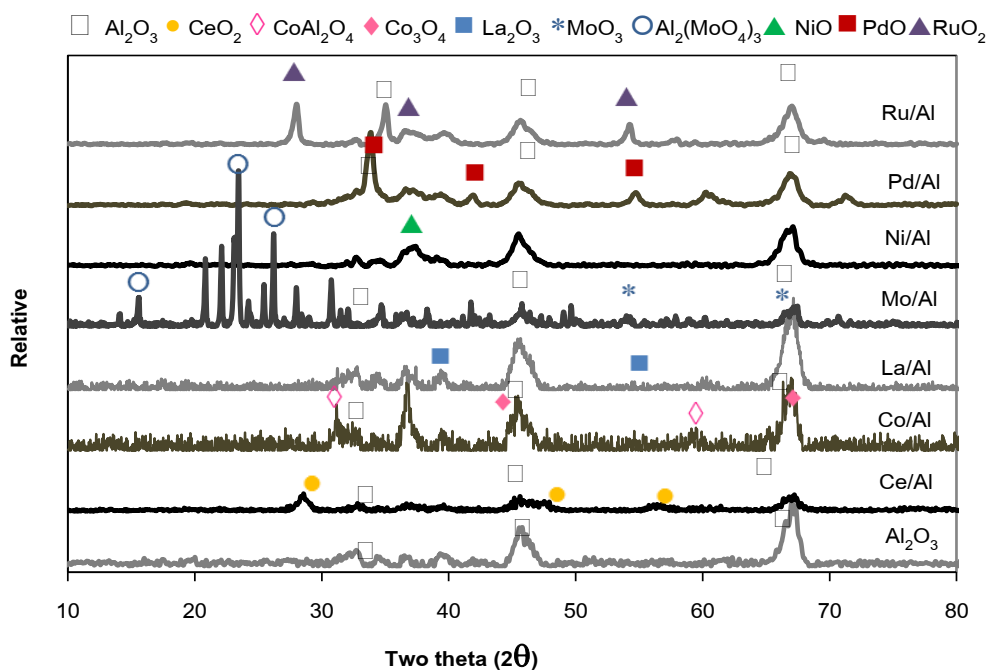
**Fig. 4.11** XRD patterns of alumina based catalysts

$Al_2O_3$ crystalline phase was observed in all catalysts. The highest peak intensity at $2\theta$ of 32.79°, 45.32° and 67.32°, corresponded to the tetragonal structure of $Al_2O_3$ according to JCPDS: 43-1131. When further doping with various active species, $Al_2O_3$ main phases were found accompanied by a small amount of active metal phase. After impregnating with metal salt solution, the peaks at $2\theta$ corresponded to the $CeO_2$ cubic phase (JCPDS: 34-0394) were observed. Tetragonal structure of PdO and $RuO_2$ were detected, according to JCPDS: 41-1107 and JCPDS: 40-1290, respectively. The XRD pattern of metal doped catalyst revealed the small amount of $Co_3O_4$, $La_2O_3$, $MoO_3$ and NiO, according to JCPDS: 78-1969, JCPDS: 89-5108, JCPDS: 050602 and JCPDS: 20-0776 respectively which corresponding to the hexagonal phase. These results suggested that the catalyst synthesized can be applied to pyrolysis of Jatropha residue, and further enhance the fast pyrolysis sequential process.

### 4.2.3 Characterization of $Al_2O_3$ based catalysts (Extruded)

The particle size, the specific surface area and pore size of the alumina and metal on alumina extruded catalysts are summarized in Table 4.6. The surface area of samples was calculated by using the Langmuir isotherm. The specific surface area, pore size and total pore volumes were detected to be 1.92-3.13 $m^2$/g, 112.9-162.9 Å and 0.0036-0.0083 $cm^3$/g. The result confirms that the extrusion process does not affect the texture of the $Al_2O_3$. This result agreed well with Tian et al., (2013) who used the extruded clay as a natural catalyst for biofuel combustion.

**Table 4.4** Physical properties of metal catalysts

| Characteristic | $Al_2O_3$ catalysts | | | |
|---|---|---|---|---|
| | $Al_2O_3$ (Raw Al47) | $Al_2O_3$ ext. | Ni/Al ext. | Pd/Al ext. |
| Surface area ($m^2$/g) † | 1.92 | 1.73 | 3.13 | N/D |
| Density (g/$cm^3$) | 2.48 | 2.40 | 2.38 | 2.34 |
| Particle size* (µm) | 10 | - | - | - |
| Porosity (%) | - | 38.74 | 39.15 | 40.37 |
| Pore size (A°) | 17.17 | 112.9 | 162.9 | N/D |
| Pore Volume ($cm^3$/g) | 0.00824 | 0.0036 | 0.0083 | N/D |
| Actual metal loading (EDS, %) | - | - | 3.97 | 1.61 |

The SEM images of the extruded catalysts are shown in Fig. 4.10. It can be seen that all samples present aggregates of variable morphology and size. The mainly particles appeared as an agglomeration of particles to the size of less than 2.5 µm. EDS was also used to investigate the elemental distributions of the synthesized catalysts and for estimating the amount of respective element.
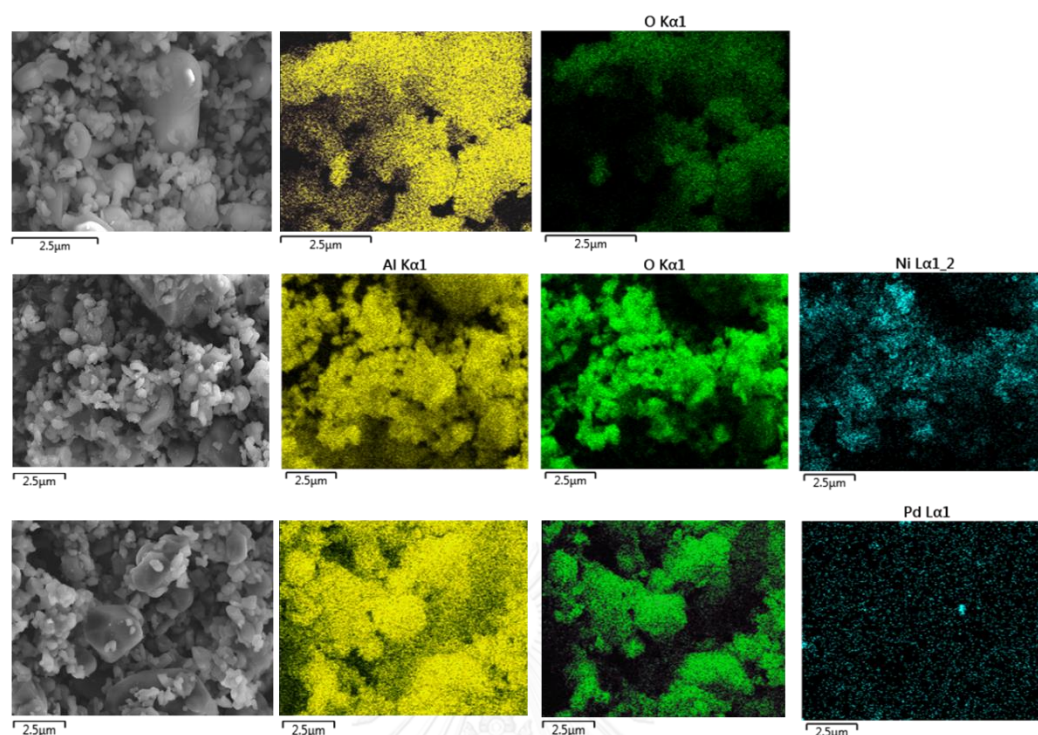
**Fig. 4.12** SEM-EDS mapping results for Al$_2$O$_3$ extruded catalysts at 10,000X: (a) Al$_2$O$_3$ extruded (c) Ni/Al$_2$O$_3$ extruded (f) Pd/Al$_2$O$_3$ extruded

The relative content of Al$_2$O$_3$ in each sample is compared by the diffraction intensity of the characteristic peaks in $2\theta$ in XRD patterns. The result shows that the relative content of Al$_2$O$_3$ increases in the following order for four samples (Fig. 4.11). Al$_2$O$_3$ crystalline phase was observed in all catalysts. The highest peak intensity at $2\theta$ of 35.16°, 43.37° and 57.22°, corresponded to the tetragonal structure of Al$_2$O$_3$ according to JCPDS: 46-1212. Especially, the Al$_2$O$_3$ extrusion is calcined at high temperature of 1200°C, the diffraction intensity of Al$_2$O$_3$ phase increases remarkably. When further doping with various active species, Al$_2$O$_3$ main phases were found accompanied by a small amount of active metal phase. After impregnating with metal salt solution, the peaks at $2\theta$ corresponded to the NiO cubic phase (JCPDS: 34-0394) were observed. Tetragonal structure of PdO was detected according to JCPDS: 41-1107.
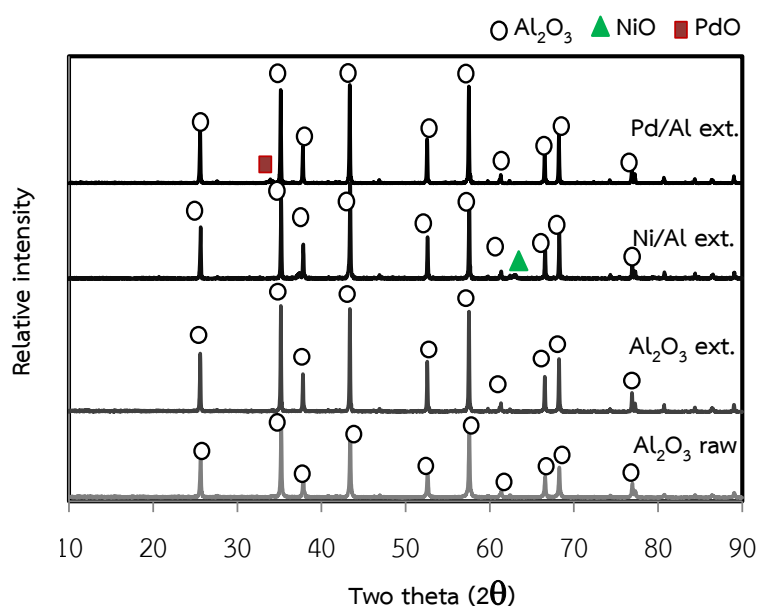
**Fig. 4.13** XRD patterns of alumina extruded catalysts

## 4.3 Activated Carbon and Bio-char catalyst synthesis

In recent years, uses of mesoporous catalysts have attracted great interest for their potential to convert large complex compounds into simpler liquid products. Particularly, the meso-pores of the activated carbon were thought to play an important role on effective conversion of heavy hydrocarbon compounds into lighter fractions. Due to their highly porous structures, activated carbons have been widely used as catalyst supports for conversions of hydrocarbons and tar cracking, not only because their mesopores would greatly improve the dispersion of metal ions, but also facilitate transport of reactant molecules (Shen et al., 2015). Recently, some transition metal based catalysts including noble metals such as Pt, Pd and Ru and carbon-based catalysts are utilized for deoxygenated reactions which were reported by several researches (ref). Therefore, in this work, these metals were selected to modify activated carbon for upgrading of bio-oil vapors.

### 4.3.1 Activated Carbon powder catalysts

The results on particle size, specific surface area and pore size are listed in Table 4.7. Activated carbon had high surface area of 1,272 $m^2/g$, particle size of 34.37 µm, pore volume of 1.30 $cm^3/g$ and an average pore diameter of 41.06 Å which was in the range of mesoporous materials. Consequently, the structure of catalyst exhibited mesoporous structure with several pore diameters less than 50 nm. After impregnation of active phase, the particle sizes of prepared catalysts were decreased significantly while surface areas were slightly lower than that of the support except Ru/Ac.

**Table 4.5** Physical properties of metal/Ac powder catalysts

| Characteristic | Metal catalysts | | | | |
|---|---|---|---|---|---|
| | Ac | Ce/Ac | Ni/Ac | Pd/Ac | Ru/Ac |
| Surface area ($m^2/g$) † | 1,272 | 1037 | 1154 | 1137 | 1469 |
| Pore volume ($cm^3/g$) | 1.30 | 1.06 | 1.13 | 1.12 | 1.03 |
| Pore size (nm) | 41.06 | 40.97 | 38.99 | 39.41 | 39.17 |
| Actual metal loading (EDS, %) | - | 4.2 | 4.5 | 5.3 | 6.3 |

The representative TEM image of the calcined 5% metal/AC catalysts is illustrated in Fig. 4.12. A close-up view (scale bar 10 nm) reveals that the supported-nanoparticles are crystalline while a large-area view with inset (scale bar 100 nm) confirms that the nanoparticles are well-dispersed on the support. In addition, the elemental composition at of the various positions on the activated carbon-based catalysts surface was measured by the EDS analysis.
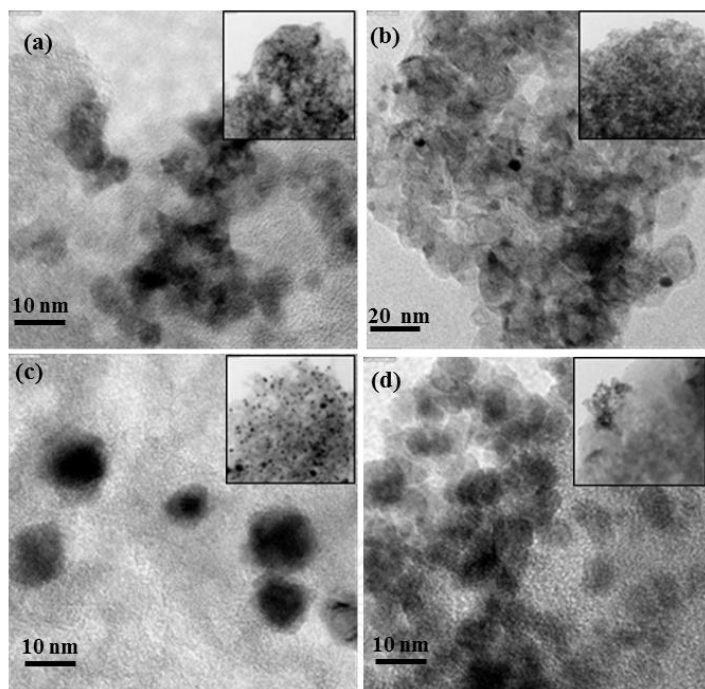
**Fig. 4.14** TEM analysis results of Activated carbon catalysts: (a) (Ce/AC) (b) Ni/AC (c) Pd/AC (d) Ru/AC

During the catalyst preparation process, the surface becomes greatly enhanced with metal in range of 4.2 – 6.3 wt. %. It is clearly seen that the metal loading contents on the activated carbon supported were found to be close to targeted nearby purposes 5 wt. %. From the mapping images displayed in Fig. 4.13, color spots represented the distribution of metal elements.
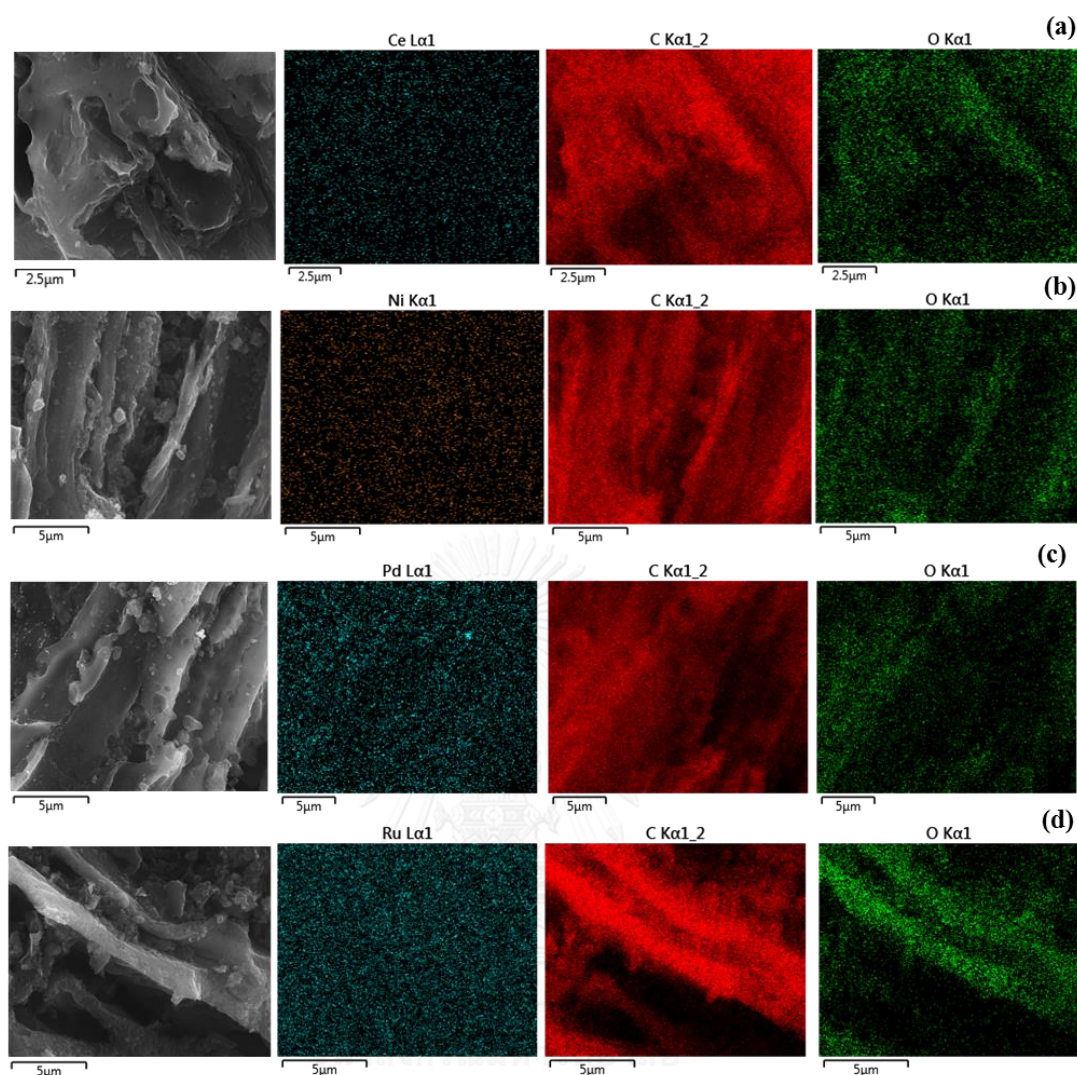
**Fig. 4.15** Representative EDS-Mapping images of the: (a) Ce/AC, (b) Ni/AC, (c) Pd/AC and (d) Ru/AC catalysts.

X-Ray diffraction (XRD) analysis were carried out on the catalysts by using X'Pert Pro MPD in the range of 10–80° with a scanning step of 0.02 using Cu Ka radiation. The XRD pattern of activated carbon-based catalysts calcined at 250°C is shown in Fig. 4.14. Carbon crystalline phase was detected in all catalysts. The highest peak intensity at $2\theta$ of 26.6° corresponded to the activated carbon (JCPDS: 26-1080). When further doping with various active species, carbon main phases were found accompanied by a small amount of active metal phase. The minor peaks at $2\theta$ of 28.4° and 47.5° matched the $CeO_2$ which corresponding to the cubic phase (JCPDS: 34-0394) were also

located. Tetragonal structure of Pd according to JCPDS: 41-1107 was noticed for palladium doping case where the peak was observed at $2\theta$ of 33.8°. Moreover, tetragonal structure of PdO according to JCPDS: 05-0681 was noted at $2\theta$ of 39.93° and 46.6°. The XRD pattern of ruthenium doped catalyst revealed the small amount of $RuO_2$ corresponding to the tetragonal phase (JCPDS: 40-1290), the peak was observed at $2\theta$ of 28.0° and 35.1°. Small peaks of nickel doped catalyst were detected at $2\theta$ of 37.2° and indexed as hexagonal NiO phase (JCPDS: 44-1159).
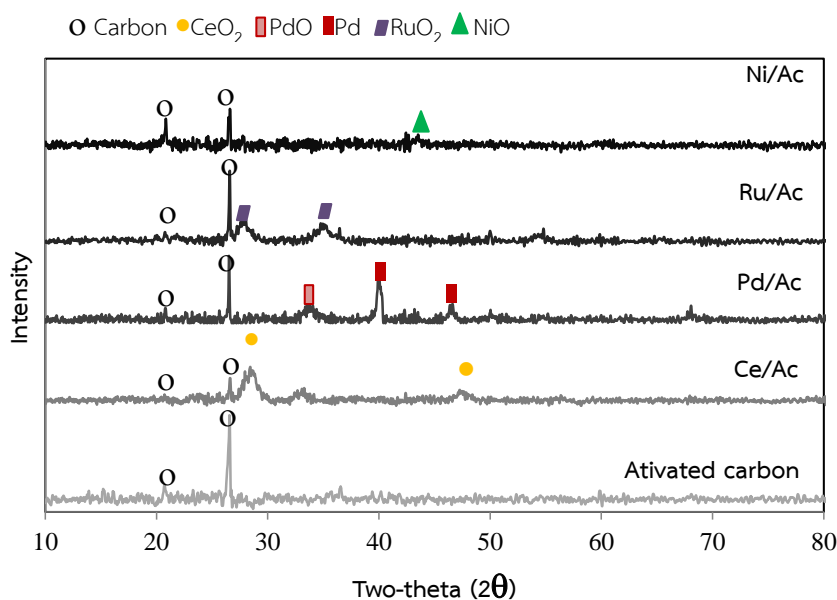


**Fig. 4.16** XRD pattern of the AC and M/AC catalysts

Thermogravimetric analysis was also carried out to estimate the weight loss of activated carbon in $N_2$ atmosphere as shown in Fig. 4.15. It was revealed that the thermal decomposition of activated carbon in range of 100-900℃. The relatively wide decomposition range followed by a rapid drop around 100℃; it could be due to the moisture content in activated carbon. The maximum weight losses of activated carbon occurred at 900℃. Activated carbon weight loss at 600℃ which was pyrolysis operation in this study has been continuously decomposed only 5 wt. %. Consequently, it was indicated that the activated carbon was not significantly oxidized during the pyrolysis process. The metal catalysts calcined in air atmosphere at 250℃ was also investigated

the oxidation by percentage weight loss of the catalysts. The result indicated that these catalysts were oxidized after calcined in range of of 7.5–25.2 wt.% especially Ce/Ac and Ru/Ac catalysts. However, the catalyst synthesized which was calcined no oxidized in the pyrolysis environment at high temperature of 600℃. Therefore, they are feasible to use the catalysts in pyrolysis of Jatropha waste at 600℃ by Py-GCMS.
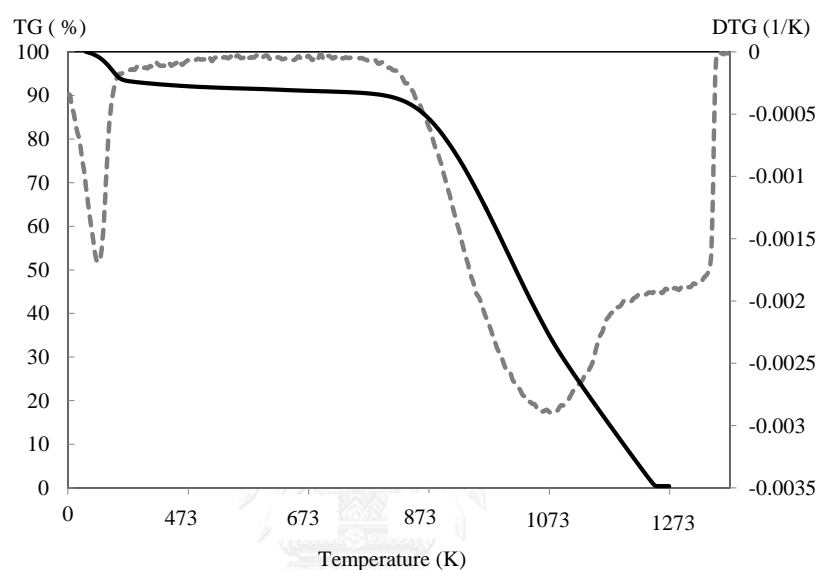


**Fig. 4.17** Representative TGA analysis of the AC

### 4.3.2 Activated Carbon granule catalyst

The catalyst supporter, activated carbon granules size of 2-5 mm (Wako Pure Chemical Industries), was impregnated with the aqueous solution of targeted metal (Ce, Ni, Pd or Ru) for 3 h at 80℃, and then dried at 110℃ for 24 h. The activated carbon-based catalysts were then calcined at 250℃ for 5 hours at atmosphere to obtain 5% metal/Ac catalysts. The prepared catalysts included $CeO_2$/Ac, NiO/Ac PdO/Ac and Ru/Ac. The morphologies of catalysts synthesized with activated carbon supports were investigated by SEM analysis, and conducted after calcination at 250℃ and are displayed in Fig. 4.16.
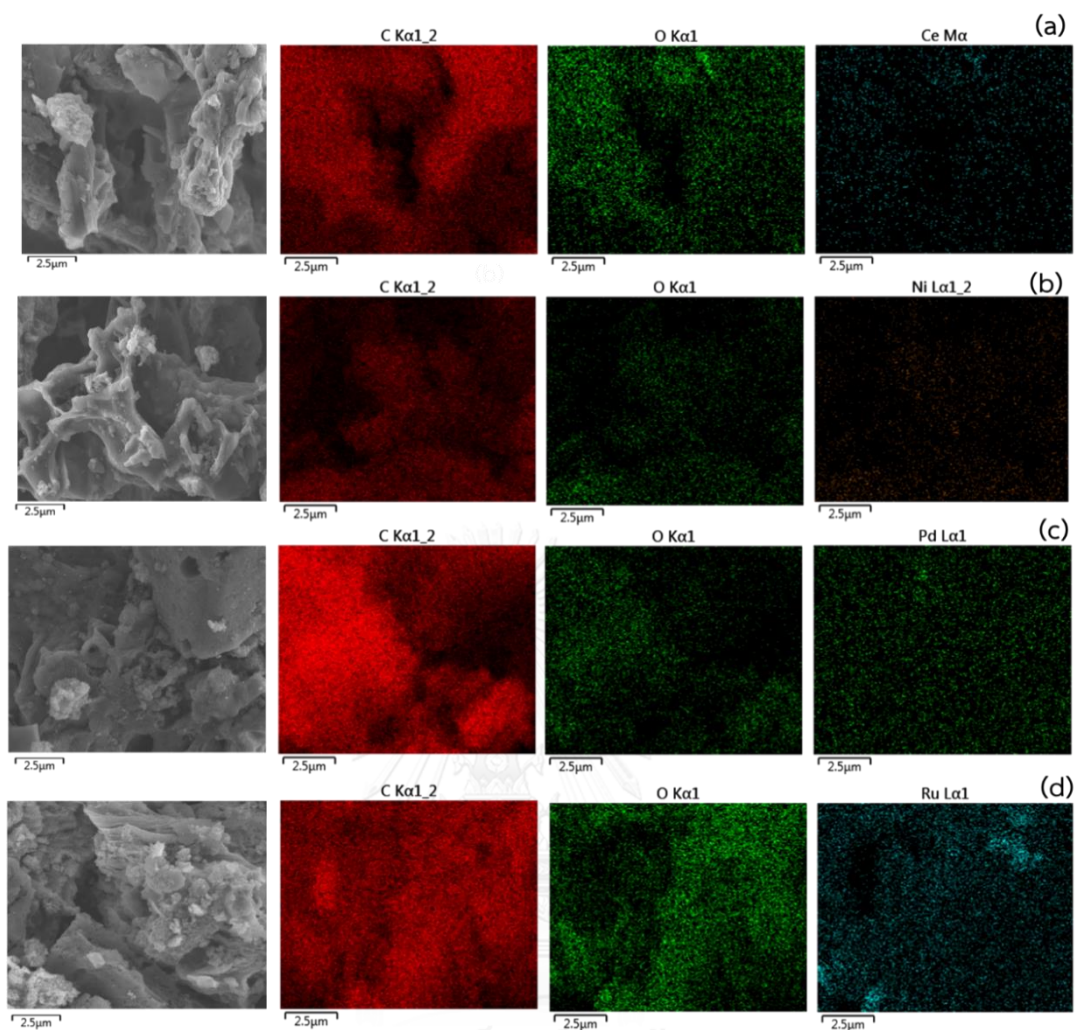
**Fig. 4.18** SEM-EDS results for Activated carbon-based catalyst at 10,000X: (a) Ce/Ac,
(b) Ni/Ac, (c) Pd/Ac and (d) Ru/Ac

In order to determine the formation of crystalline materials, phase analysis of synthesized powder was performed by X-ray powder. Crystalline phases of each sample were identified according to JCPDS. The element composition of the various positions on the synthesized catalyst was measured by the EDS analysis. In addition, specific surface area was determined by adsorption isotherms using the BET equation. The results on particle size, specific surface area and pore size are listed in Table 4.8.

The prepared catalysts included 5% active species $CeO_2$/Ac, PdO/Ac and NiO/Ac and $RuO_2$/Ac. Specific surface areas were determined from adsorption

isotherms using the BET equation. The results on particle size, specific surface area and pore size are listed in Table 4.8. Activated carbon had high surface area of 666.8 $m^2$/g, pore volume of 0.515 $cm^3$/g and an average pore diameter of 30.94 Å which was in the range of mesoporous materials. After impregnation of active phase, the pore volume and pore size of prepared catalysts were slightly decreased while surface areas were slightly lower than that of the support except Ni/Ac and Ru/Ac.

**Table 4.6** Characteristic of Activated carbon-based catalysts

| Characteristic | Metal catalysts | | | | |
|---|---|---|---|---|---|
| | Ac | Ce/Ac | Ni/Ac | Pd/Ac | Ru/Ac |
| Surface area ($m^2$/g) † | 666.8 | 548.7 | 680.3 | 610.1 | 727.6 |
| Pore volume ($cm^3$/g) | 30.94 | 25.70 | 29.45 | 29.62 | 30.65 |
| Pore size (nm) | 0.515 | 0.353 | 0.501 | 0.451 | 0.710 |
| Actual metal loading (EDS, %) | - | 5.7 | 6.1 | 4.6 | 6.4 |

The XRD pattern of activated carbon-based catalysts calcined at 250°C is shown in Fig. 4.17. Carbon crystalline phase was detected in every catalyst. The highest peak intensity at $2\theta$ of 26.58° corresponded to the activated carbon (JCPDS: 26-1076). When further doping with various active species, carbon main phases were found accompanied by a small amount of active metal phase. The minor peaks at $2\theta$ of 28.39° and 47.48° matched the $CeO_2$ (JCPDS: 34-0394) were also located.
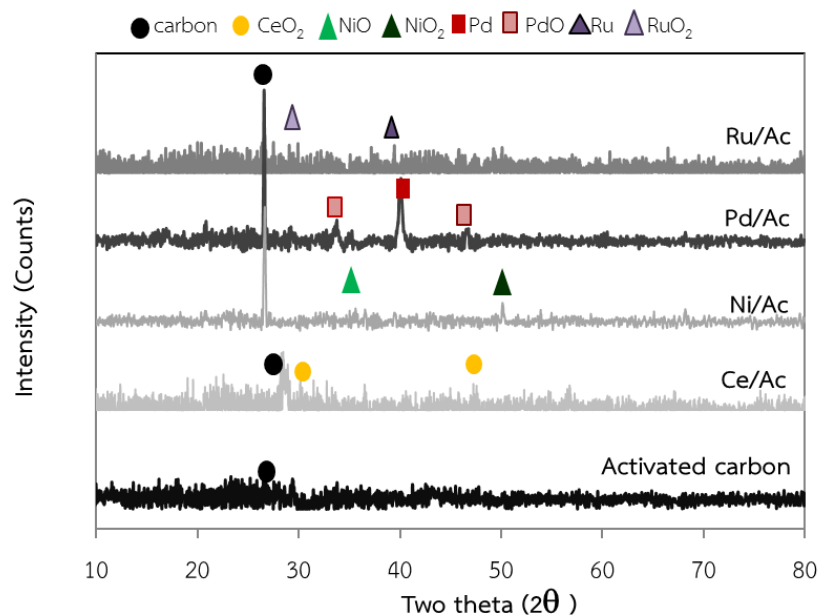
**Fig. 4.19** XRD pattern of activated carbon-based catalysts (Granule)

Tetragonal structure of Pd according to JCPDS: 88-2335 was noticed for palladium doping case where the peak was observed at $2\theta$ of 40.11°. Moreover, tetragonal structure of PdO according to the same JCPDS of activated carbon powder catalyst. Small peaks of nickel doped catalyst were detected at $2\theta$ of 37.188° and indexed as hexagonal NiO phase (JCPDS: 44-1159) while $NiO_2$ phase according to JCPDS: 89-8397 were found at $2\theta$ of 50.130°. The metal contents (Ce, Ni, Pd and Ru) on activated carbon support by EDS technique are showed in Table 4.8. The result suggested that the doped metals formed over the activated carbon support, evenly dispersed on the surface and incorporated into its pore. Therefore, these metals modified by impregnation method are suitable to be applied as potential catalysts.

### 4.3.3 Bio-Char synthesis catalyst

Bio-char is a fine-grained, highly porous charcoal substance, typically produced as a product or byproduct of pyrolysis and gasification of biomass. Bio-char has been tested and used as an energy source in combustion and co-firing processes in coal-based power stations because of its excellent fuel properties such as high energy

density and good grindability. Bio-char has also been applied as an effective adsorbent for application in environmental remediation.

In this section, synthesized catalysts were modified 5wt% metal catalysts (Ni and Pd) over char supporter which exhibited high surface area of 35.65-414.9 $m^2$/g. Specific surface areas were determined from adsorption isotherms using the Langmuir equation. The char support obtained from pyrolysis temperature of 600°C has surface area of 35.65 $m^2$/g while those of 5% Ni/char and 5% Pd/char after calcined are 414.9 $m^2$/g and 365.5 $m^2$/g, respectively. Total pore volume of 0.026-0.268 $cm^3$/g and average pore diameter of 24.75-54.03 Å are in good agreement with the result obtained by SEM (Table 4.7). The 5% Ni/char resulted in relatively high surface area of porous carbonaceous material which is suitable to be applied as catalyst. The result corresponds well with Nisamaneenate et al. (2015) who used the Ni/char as a catalyst for secondary syngas clean-up.

**Table 4.7** Characteristic of Bio-char catalysts

| Catalysts | Characteristic | | | |
|-----------|-----------------------|----------------|--------------------------|--------------|
|           | Surface area ($m^2$/g) | Pore size (Å) | Pore volume ($cm^3$/g) | EDX (wt%) |
| Char 600  | 35.65 | 54.03 | 0.026 | - |
| Char 700  | 40.78 | 35.25 | 0.153 | - |
| Ni/Char   | 414.9 | 25.91 | 0.268 | 2.8 |
| Pd/Char   | 365.5 | 24.75 | 0.145 | 3.9 |

SEM analysis of the microstructure of the bio-char was performed using a Hitachi S3400 SEM fitted with an X-ray energy dispersive spectrometry (EDS) detector. The morphologies of Bio-char catalysts are shown in Fig. 4.18. The SEM photographs indicated diverse morphology in terms of amorphous flakes (Fig. 4.18 b), lumpy granular and polygonal lamellar porous structures (Fig. 4.19) of these materials. Bio-char from Jatropha residue after slow pyrolysis at 600°C showed the microstructure

including smooth and small porous. When the bio-char was calcined at 700°C, the particles appear to be of larger porous and agglomerate as amorphous flakes and polygonal with size of less than 10 μm. These results are supported by similar observations reported by Doshi et al. (2014), for Jatropha curcus, and Pongamia pinnata samples.
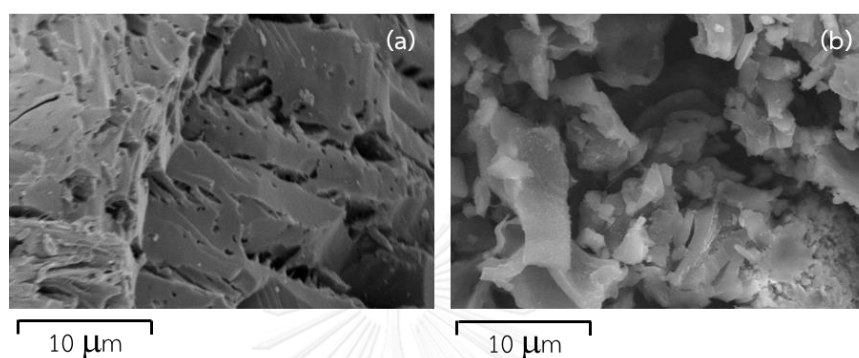


**Fig. 4.20** SEM results for synthesized catalyst at 2,000X: (a) Bio-char support and (b) Bio-char calcined at 700°C
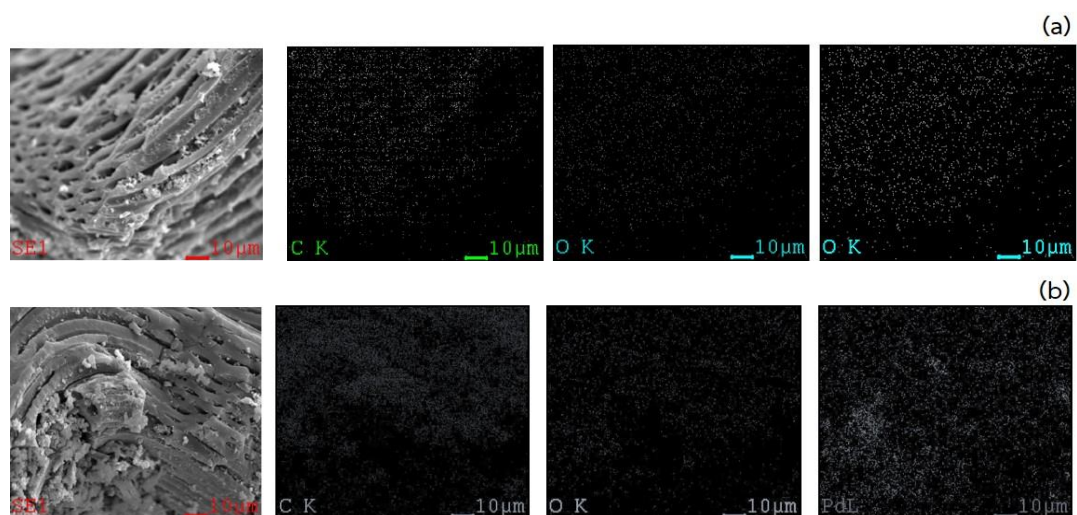


**Fig. 4.21** SEM-EDS mapping results for bio-char catalyst at 2,000X: (a) Ni/char and (b) Pd/char

The XRD pattern of bio-char catalysts are shown in Fig. 4.20. Carbon crystalline phase was detected in char support catalysts at $2\theta$ of 26.76°. The peak intensity at $2\theta$ of 21.06° and 26.68° corresponded to the $SiO_2$ (JCPDS: 46-1045). When further doping

with various active species, the main phases were found accompanied by a high amount of active metal phase. The major peaks at $2\theta$ of 37.26° and 43.30° matched the NiO which corresponding to the hexagonal phase (JCPDS: 44-1159). In addition, the peaks of nickel doped catalyst were also detected at $2\theta$ of 44.50° and 51.87° and indexed as hexagonal Ni phase (JCPDS: 87-0712). The highest peak of Pd according to JCPDS: 89-4897 was noticed for palladium doping case where the peak was observed at $2\theta$ of 40.11°, 46.66° and 68.12 and corresponded to the tetragonal structure. Moreover, tetragonal structure of PdO according to JCPDS: 43-1024 was noted at $2\theta$ of 33.87° and 42.08°.
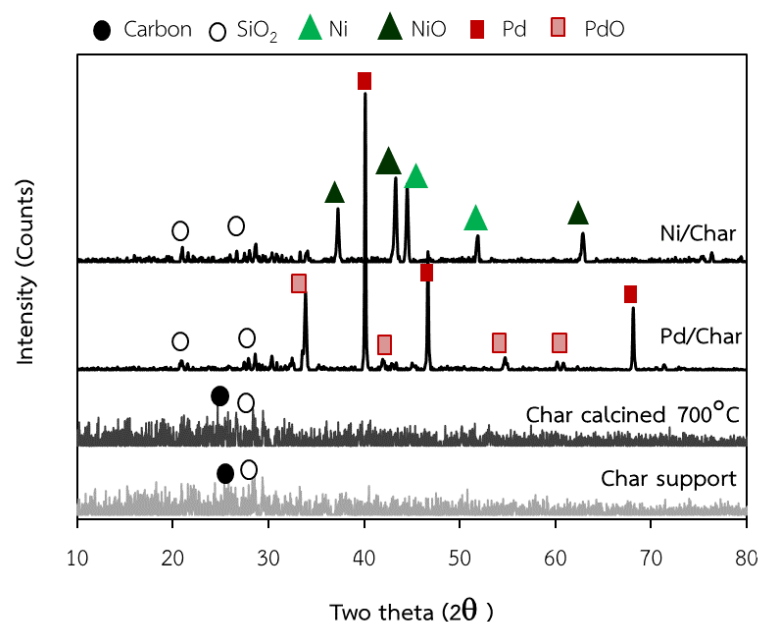


**Fig. 4.22** XRD patterns of various supports

Generally, biomass may contain a significant amount of inherent alkali and alkaline earth metallic (AAEM) species from nutrients uptake during growth of plant. After pyrolysis and/or gasification, most of the inherent AAEM species may be retained in the char (Doshi et al., 2015). It is well-known that alkali (K, Na) and alkaline earth metals (Mg, Ca) can significantly promote the catalytic activity of bio-char for bio-oil reforming by increasing the water adsorption on the surface (Ma et al., 2017). The AAEM

species in bio-char were quantified using X-ray fluorescence spectrometer (XRF-1800). The analysis results were reported in Table 4.10.

**Table 4.8** AAEM species analysis of the ash in bio-char

| AAEM species (wt%) | | | | | | | |
| --- | --- | --- | --- | --- | --- | --- | --- |
| K | Mg | P | Ca | Cl | Si | Al | |
| 2.8 | 0.942 | 0.907 | 0.846 | 0.313 | 0.242 | 0.161 | |
| AAEM species (ppm) | | | | | | | |
| Na | Fe | Si | Ni | Mn | Zn | Cr | Cu |
| 860 | 608 | 442 | 322 | 118 | 116 | 47.6 | 46.5 |

# CHAPTER 5

# RESULTS AND DISCUSSION OF CATALYTIC PYROLYSIS

# USING Py-GC/MS

## 5.1 Effect of temperature and particle size on yields of pyrolytic products

The effect of pyrolysis temperature on yields of pyrolytic products from Py-GC/MS analysis of Jatropha residue (<125 mm) is shown in Fig. 5.1. The Jatropha residue was pyrolyzed at 400-600°C. The yields of pyrolytic products were represented by percentages of peak area. Fast pyrolysis initiates decomposition of the Jatropha residue to produce a complex mixture of products. The main compounds in the vapors of the pyrolysis of Jatropha residue were classified into twelve groups, such as alcohols, aldehydes, aromatic HC, carboxylic acids, ether, esters, furans, hydrocarbons, ketones, N-compound (N-containing hydrocarbon), phenol, and sugar. Biomass pyrolysis products were generally known as a complex combination of products from pyrolysis of cellulose, hemicellulose, lignin, and extractives, each of which has its own kinetic characteristics. Firstly, the decomposition of lignin led to formation of phenolic compounds. Secondly, the depolymerization of holocellulose (cellulose and hemicellulose) generated anhydroglucose (levoglucosan), related derivatives and furan.
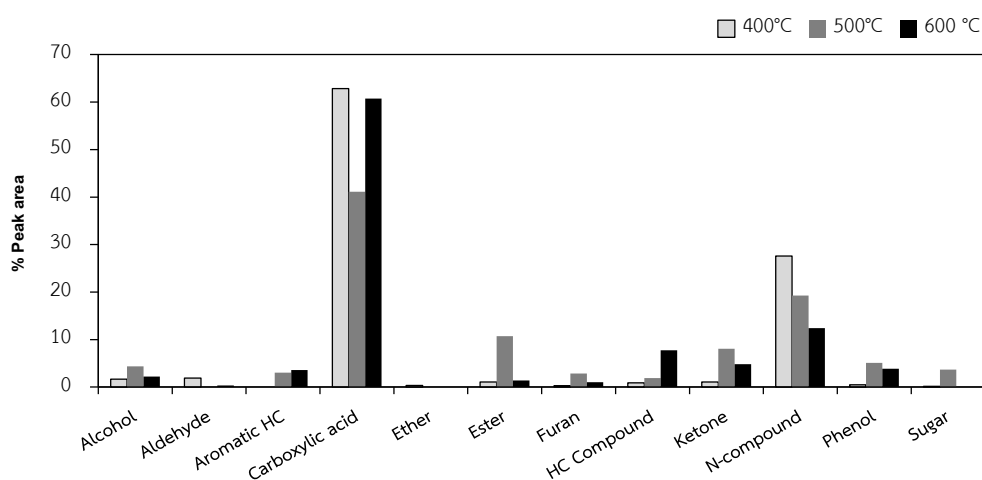


**Fig. 5.1** The effect of pyrolysis temperature on pyrolytic products

The structures of sugar (levoglucosan and a-D-glucopyranose) from pyrolysis of Jatropha residue are shown in Fig. 5.2. Whereas the pyrolytic ring scission of holocellulose produced various light products such as aldehydes, ketones, alcohols, and esters (Murata, 2012). As shown in Fig. 5.3, the yields of sugar gradually reduced with increasing temperature from 400°C to 600°C. It was inferred that high temperature showed high efficiency on cracking heavy compounds from cellulose and hemicelluloses. This result agreed with Lu et al. who studied the effects of pyrolysis temperature and time on the distribution of pyrolytic products. They found that the cellulose started decomposition to form organic volatile products at the set pyrolysis temperature of 400°C and the LG (levoglucosan) was favorable to be produced at low temperatures (Lu et al., 2011). The yield of aromatic hydrocarbon and hydrocarbon compounds (aliphatic and cyclic) tended to increase when heating temperature up to 600°C.



(a)                                (b)
levoglucosan                α-D-Glucopyranose
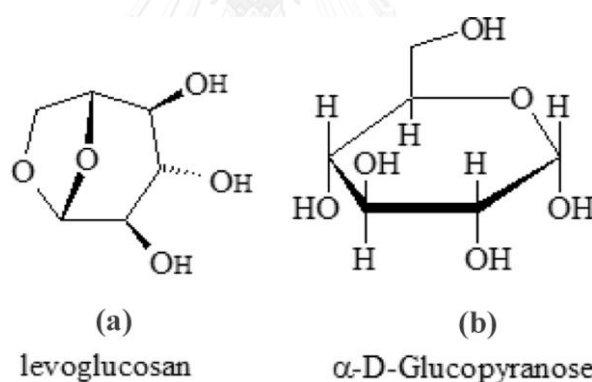
**Fig. 5.2** Structure of sugars from fast pyrolysis of Jatropha residue (Kaewpengrow et al., 2014)

Biomass liquids are known to have an acidic structure. The main products of pyrolysis vapors of Jatropha residue were fatty acid (palmitic acid, oleic acid and acetic acid) which contained carboxylic acid of 41.11-63.86%. The highest yield was obtained at 400°C. The carboxylic acids are also good indicators of the quality of bio-oils in term of pH values. Large amount of acids can cause corrosion problem in the engines (French, 2010; Mihalcik, 2011; Murata, 2012; Ying, 2012). Some of the complex pyrolytic products of Jatropha residue are shown in Fig. 5.3, which were grouped under

oxygenated compounds. Fig. 5.3 (a-c) showed structure of free fatty acids (FFA) which are usually found in Jatropha oil. These results are similar to Murata et al. who found high content of FFA from Jatropha waste in non-catalytic pyrolysis (Murata, 2012).
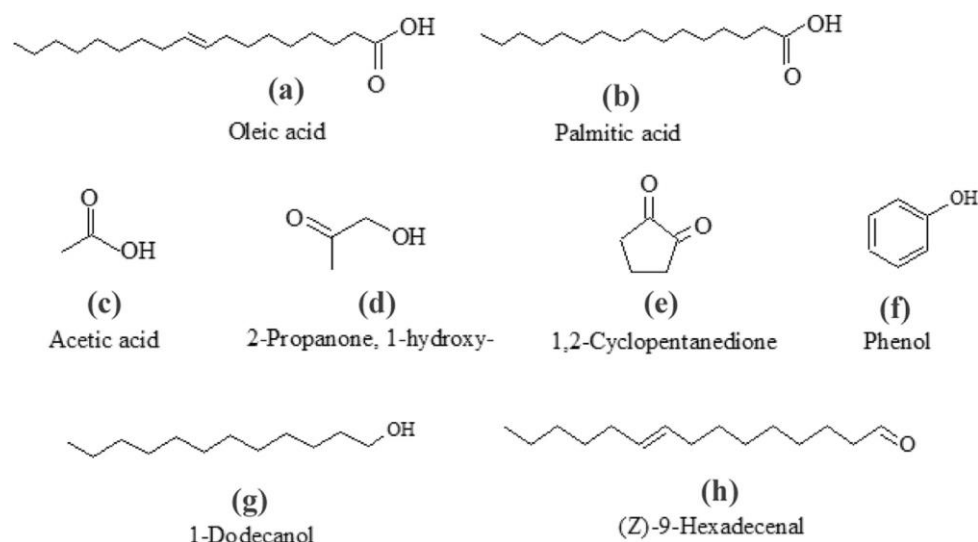


**Fig. 5.3** Typical of carboxylic acid (a-c) and oxygenated compounds of pyrolytic products (d-h)

However, their products would be completely deoxygenated to form linear hydrocarbon compounds using catalyst cracking in next experiment. Oxygenated compounds presented in slight amount were ketone, alcohol, aldehyde, and furan at lower temperature. The increase in temperature increased their presence to 18.93% and 8.44% for pyrolysis temperature of 500°C and 600°C, respectively. High yield of 10.73% ester was obtained at pyrolysis temperature of 500°C. It is possibly due to carboxylic acid conversion into ester form, the composition of biodiesel, which is advantageous for operation at this temperature. This is a significant influence of pyrolysis temperature; the oxygenated compounds from pyrolytic product are a marking for fuel quality and the abatement amount of oxygenated compounds in the liquid fuel to obtain the higher energy content (Ates, 2008). The result showed that high temperature (600°C) had positive influence on the yields of pyrolytic products. However, the yield of aromatic and hydrocarbon compounds was low compared with other pyrolytic products. This result agreed with several researches (Ates, 2008;

Bulushev, 2011; Mihalcik, 2011; Murata, 2012) who found the low yield of aromatic in non-catalytic fast pyrolysis of biomass.

Moreover, the effect of different particle sizes of Jatropha residue on yields of pyrolytic products is shown in Fig. 5.4. Three particle sizes analyzed in this part were <125μm, 125-425 μm and 425-850 μm, respectively.
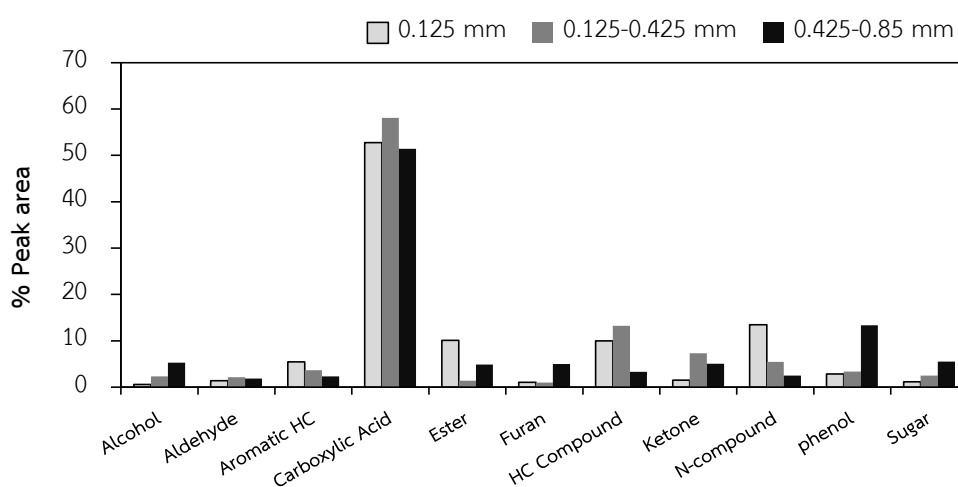


**Fig. 5.4** The effect of particle size on pyrolytic products

In case of levoglucosan and d-glucose (sugar), the resulted showed that at 600°C the larger particle sizes had higher content of sugar. It was also found that the yields of sugar with the smallest size of <125μm dropped to less than 2%. In addition, the pyrolysis of Jatropha with a medium particle size (125-425 μm) showed highest yield of hydrocarbon compounds and aromatic hydrocarbons which are considered as valuable products because of their contribution to the high heating value (pattiya et al, 2008)

Although the medium particle size exhibited high yield of hydrocarbon compounds, which is good properties for bio-oils, high ketone and carboxylic acid were also detected. These oxygenated compounds affected the instability of bio-oils. While the small particle size of <125μm showed lower yields of the ketone and alcohol, remarkably. Phenol yield is also attractive because of its value. The pyrolysis of Jatropha with the largest size showed high yield of phenol but also gave a relatively

high alcohol and furan content. From all results, it was suggested that the smaller particle size showed better results in term of low yields of oxygenated compounds and high yields of aromatic hydrocarbon. The effect of catalyst on these pyrolysis products will be further explored for comparison.

## 5.2 The effect of Jatropha to catalysts ratio on pyrolytic products

In this part, the pyrolysis of Jatropha residue with size less than 125 $\mu$m with $Al_2O_3$ based catalysts were carried out at 600℃ in a Py-GC/MS. The catalysts in this experiments included $Al_2O_3$, $6\%CeO_2$-$Al_2O_3$, $1\%Pd/6\%CeO_2$-$Al_2O_3$, $1\%Ru/6\%CeO_2$-$Al_2O_3$, and $1\%Ni/6\%CeO_2$-$Al_2O_3$. For a typical run the amount of Jatropha residue was 0.40 mg and catalyst used were 0.4, 2.0 and 4.0 mg to obtain Jatropha to catalyst ratio of 1:1, 1:5 and 1:10. The pyrolytic products were represented by quantification percentages of relative peak area of each compound with retention time obtained from the chromatogram. From this result, the compound groups found are Alcohols, Aldehydes, Aromatic HC, Carboxylic acids, Esters, Ether, Furans, HC compounds, Ketones, N-compound (N-containning hydrocarbons) and Phenol. The yield of different groups of compounds during catalytic pyrolysis over $Al_2O_3$ based catalyst with each ratio is shown in Table 5.1.

**Table 5.1** Pyrolytic products from Py-GC/MS of Jatropha waste with and w/o $Al_2O_3$ based catalysts pyrolyzed at 600°C.

| Catalyst | J : C | Hydrocarbon | | Oxygenated compounds | | | | | | | Acid | N-compound |
|---|---|---|---|---|---|---|---|---|---|---|---|---|
| | | Aliphatic | Aromatic | Phenol | Alcohol | Aldehyde | Ester | Ether | Furan | Ketone | | |
| None | 1:0 | 8.58 | 3.58 | 3.88 | 2.21 | 0.36 | 0.62 | 0.00 | 1.04 | 4.83 | 60.74 | 13.77 |
| $Al_2O_3$ | 1:1 | 23.38 | 7.31 | 2.37 | 0.00 | 14.11 | 11.39 | 0.00 | 1.17 | 0.86 | 6.48 | 31.56 |
| CA | | 12.56 | 5.82 | 2.67 | 1.05 | 22.05 | 7.85 | 0.00 | 1.70 | 0.63 | 19.50 | 26.19 |
| PdCA | | 12.99 | 7.26 | 3.18 | 2.35 | 0.00 | 1.57 | 0.00 | 1.41 | 5.04 | 30.46 | 28.13 |
| RuCA | | 22.08 | 7.20 | 4.52 | 1.68 | 16.21 | 8.86 | 0.00 | 0.00 | 4.29 | 5.71 | 29.48 |
| NiCA | | 13.17 | 4.56 | 2.37 | 2.32 | 0.00 | 10.70 | 0.00 | 1.82 | 3.84 | 31.57 | 22.35 |
| $Al_2O_3$ | 1:5 | 36.67 | 10.05 | 0.00 | 2.80 | 4.82 | 3.46 | 0.00 | 0.66 | 0.75 | 0.00 | 40.37 |
| CA | | 34.34 | 9.56 | 2.05 | 0.00 | 3.26 | 8.53 | 0.00 | 0.00 | 0.00 | 8.40 | 33.88 |
| PdCA | | 26.49 | 16.80 | 2.67 | 1.65 | 0.00 | 11.66 | 0.00 | 0.00 | 0.97 | 7.75 | 32.03 |
| RuCA | | 25.86 | 8.15 | 1.49 | 1.73 | 1.56 | 8.21 | 0.00 | 0.00 | 0.00 | 19.61 | 31.17 |
| NiCA | | 40.60 | 8.96 | 1.87 | 0.50 | 2.00 | 1.49 | 0.00 | 0.00 | 0.00 | 6.63 | 36.14 |
| $Al_2O_3$ | 1:10 | 64.06 | 1.75 | 0.00 | 0.63 | 2.50 | 0.00 | 0.00 | 0.00 | 0.83 | 0.00 | 29.64 |
| CA | | 55.92 | 11.22 | 0.00 | 5.04 | 1.84 | 0.00 | 0.00 | 0.00 | 0.00 | 0.76 | 25.24 |
| PdCA | | 42.00 | 17.16 | 0.00 | 0.00 | 0.64 | 3.27 | 5.14 | 0.00 | 2.23 | 0.00 | 29.53 |
| RuCA | | 56.62 | 5.87 | 2.67 | 0.00 | 3.20 | 7.43 | 0.00 | 0.94 | 1.26 | 0.00 | 21.99 |
| NiCA | | 48.93 | 17.27 | 0.00 | 5.28 | 2.16 | 0.00 | 0.00 | 0.00 | 2.42 | 0.00 | 23.95 |

Aromatics and hydrocarbon compounds are considered as valuable products because of their contributions to the high heating value fractions (Lu, 2010; Mihalcik, 2011 Murata, 2012). The aromatic and hydrocarbon compounds detected from Jatropha vapor included monoaromatics and aliphatic hydrocarbons with the peak area% of only 3.58 and 8.58%, respectively. The structures of aromatic and hydrocarbon are shown in Fig. 5.5. The selectivity of aromatic compounds was

maximized with content of 17.27% after catalyzed by the Ni-Ce/$Al_2O_3$. Hydrocarbon compounds were significantly increased from 8.58% to 23.38–64.06% with the highest yield obtained by $Al_2O_3$ catalyst at Jatropha to catalyst ratio of 1:10. It is apparent that hydrocarbon yields increased in all catalysts, which indicating that these catalysts were effective for deoxygenation of the pyrolysis vapors to form hydrocarbons. Among these compounds, the presence of PAH deserves more attention due to their toxicity in environmental and potential roles in the incidence of cancer (Lu, 2009). Fortunately the PAH from catalytic fast pyrolysis of Jatropha residue was not detected which is another main advantage for pyrolysis in the presence of these catalysts.
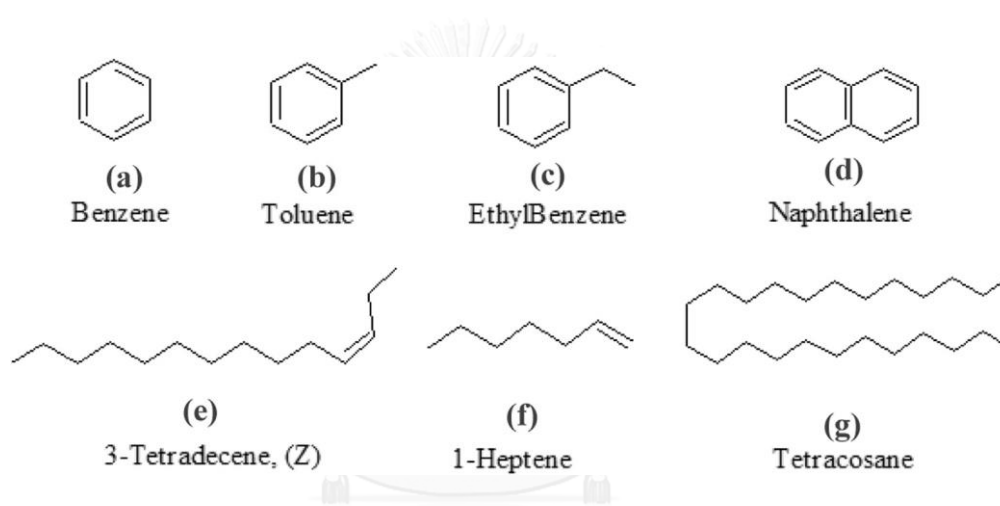


**Fig. 5.5** Products of catalytic fast pyrolysis using catalyst are typically aromatic hydrocarbons (a-d) and linear hydrocarbon (e-g).

The effect of catalysis on the product distribution with various J/C ratios by $Al_2O_3$ based catalyst is shown in Fig. 5.6. From the result, non-catalytic product contained carboxylic acid of 60.74%. The carboxylic acid fraction dropped considerably especially in the presence of $Al_2O_3$ and Ru/Ce-$Al_2O_3$ catalysts from 60.74% to 6.48% and 5.71%, respectively. The Ce/$Al_2O_3$, Pd/Ce-$Al_2O_3$, and Ni/Ce-$Al_2O_3$ were less effective such that carboxylic acid yield were still high (19.50 – 31.57%) which could cause corrosion problem.
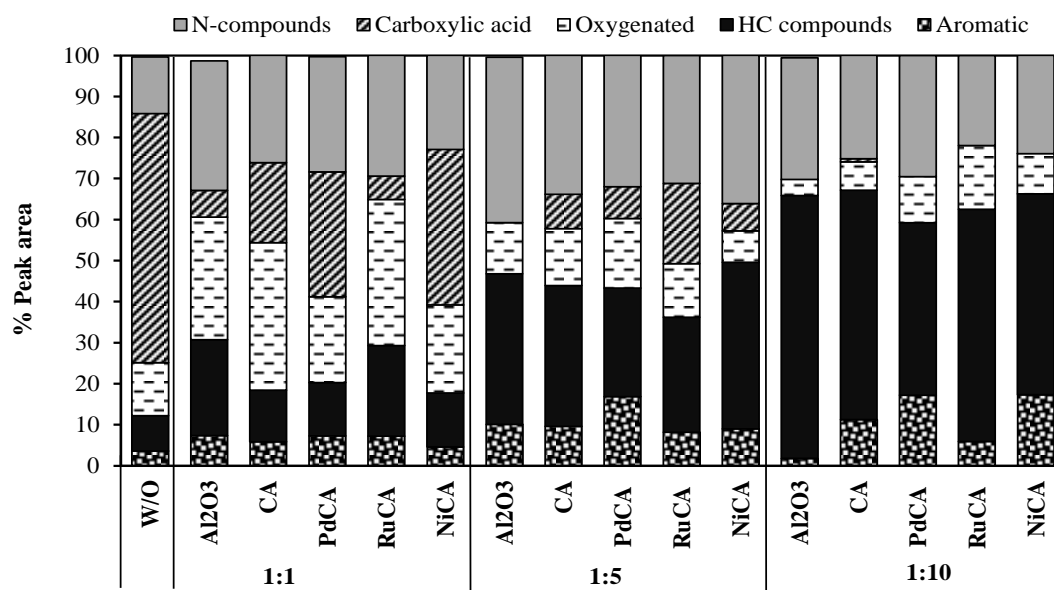
**Fig. 5.6** Average total compositional wt% of pyrolytic products from Py-GC/MS various J/C ratio of 1:1, 1:5 and 1:10 of Al$_2$O$_3$ support

With increasing Jatropha to catalyst ratio to 1:10, it was found that all catalyst led to complete reduction of carboxylic acid. While the catalytic effects on major oxygenated compounds revealed that the presence of catalyst did not significantly reduce the alcohol, aldehyde and ketones. The yield of aldehyde increased distinctly from 0.36% to 14.11 - 22.05% after catalysis with Jatropha to catalyst ratio of 1:1. It was indicated that catalysis promoted aldehydes formation which are mainly responsible for the ageing reactions and instability of bio-oils. The highest yielded was obtained after catalyzed by Ce/Al$_2$O$_3$ while Pd-Ce/Al$_2$O$_3$ and Ni-Ce/Al$_2$O$_3$ led to great reduction of aldehyde content. In addition, oxygenated compounds presented in slight amount were ketone (0.63-5.04%), alcohol (0.63-5.28%), and furan (0.94-1.70%). With increasing Jatropha to catalyst ratio to 1:5 and 1:10, aldehyde yields were almost completely reduced. The yield of furan which is toxic and may be carcinogenic was also completely reduced with the presence of all catalysts except Ru-Ce/Al$_2$O$_3$ (0.94%). The oxygenated group (included alcohol, aldehyde, ester, ether, furan, ketones and phenol) were reduced from 12.94% to 5.86-16.95% and 3.96-15.50% with Jatropha to catalyst ratio of 1:5 and 1:10, respectively.

Another important compound that is affecting the quality of the bio-oil is N-compounds. The main N-containing compounds contain the heteroatom (oleanitrile,

olelic acid amide, hexadecanamide and aniline) and their structures are show in Fig. 5.7. These products may create problems such as corrosion and poisoning of catalysts during bio-oil upgrading (Mihalcik, 2011). From the results, fast pyrolysis of Jatropha generated various N-compounds in high contents (13.77%).
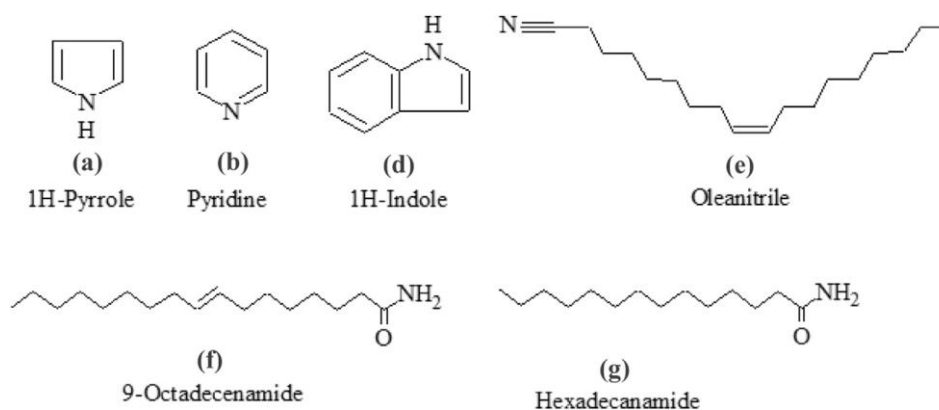


**Fig. 5.7** N-containing products from catalytic fast pyrolysis of bio-oil vapor.

After catalyzed by catalysts, the N-compounds were obviously increased to 21.99-40.37%. $Al_2O_3$ and $Ni-Ce/Al_2O_3$ favored the formation of N-compounds with Jatropha to catalyst ratio of 1:5. With increasing Jatropha to catalyst ratio to 1:10, all of catalysts reduced N-compounds yields to less than 30%. Since these catalysts are not effective on reducing N-compound, therefore it is desirable to remove the heteroatoms prior to using these renewable biofuels through denitrogenation reactions (Duan, 2011). The hydrodenitrogenation as explained by equation (1).

$$C_4H_5N + 3H_2 \rightarrow C_4H_8 + NH_3 \tag{5-1}$$

In summary increasing amount of catalysts resulted in the relatively higher activity towards deoxygentation reactions which yielded the low quantity of acids and oxygenated compounds, and high aliphatic and aromatic hydrocarbons.

## 5.3 Effect of support catalysts on pyrolytic products

In order to study how the catalyst affected the pyrolytic products, results with Alumina ($Al_2O_3$), Zirconia ($ZrO_2$), Rutile ($TiO_2$ ;$T_1$) and Anatase ($TiO_2$ ;$T_2$) based catalysts with Jatropha to catalyst ratio of 1:10 were compared as shown in Fig. 5.8. It is obviously that all the catalysts enhanced the production of aromatic hydrocarbons. The highest aromatic hydrocarbon content of 36.25% was obtained by the anatase ($T_2$), followed by Ni- Ce/$Al_2O_3$ and Pd-Ce/$Al_2O_3$. Aromatic compounds were not increased significantly by the $ZrO_2$ and rutile ($T_1$) supports catalysts. The hydrocarbon yields increased with the presence in all catalysts. $Al_2O_3$ catalyst had the highest yields of hydrocarbon compounds of 64.06%, followed by Ru-Ce/$Al_2O_3$ and Ce/$Al_2O_3$ catalysts. $Al_2O_3$ and anatase ($T_2$) based catalyst were the most effective in which carboxylic acid could be reduced completely.
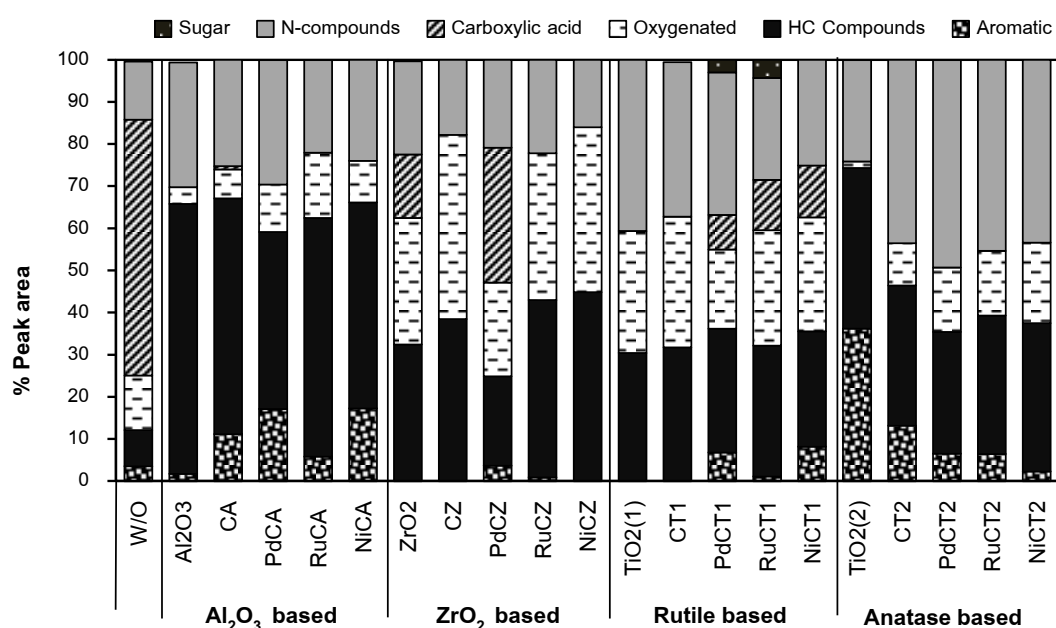


**Fig. 5.8** Average total compositional of pyrolytic products with various supported catalysts with J/C ratio of 1:10

The oxygenated compounds were detected at only 3.96% and 1.58% by Al2O3 and anatase (T2) catalysts, respectively. These results related to high surface area of both supports (103.38 and 204.25 m2/g) which probably play major role on conversion of the oxygenated compouds to hydrocarbons. ZrO2 and rutile (T1) had much lower

surface area of only 12 and 4 m2/g, respectively, which could lead to relatively high yield of oxygenated and carboxylic acid compounds.

Though $Al_2O_3$ and anatase ($T_2$) increased aromatic and hydrocarbon compounds and complete elimination of acid but it also promoted N-containing compounds. Since Jatropha contains relatively high quantity of nitrogen, the result showed relatively high percentages of N-compounds which is not preferable. Total N-containing compounds are more than 30% for $Al_2O_3$ and anatase ($T_2$) based catalysts (31.17-46.74%) which are higher than those of $ZrO_2$ and rutile ($T_1$) based catalysts (15.00-25.69%). These results are similar to several researches (Graça, 2013; Mortensena, 2011; Murata, 2012; Srinivasan, 2012) who indicated that catalyst with high surface area displayed better catalytic activity. In addition, the yield of sugar was completely eliminated by most catalysts except rutile based catalysts of Pd-Ce/$TiO_2$ and Ni-Ce/$TiO_2$. The results agree well with several researches (Lu, 2012; Pattiya, 2008; Ying, 2012) who found that sugar is easy to be converted by catalyst. $ZrO_2$ and rutile ($T_1$) based catalysts are less effective on deoxygenation (Lu, 2012). Interestingly, Pd on all supports seems to be effective on deoxygenation and production of aromatic compounds. Moreover, Ni on all supports is less effective to produce N-compounds which are advantage of this metal.

From the result, it is apparent that $Al_2O_3$ based catalyst yielded the highest hydrocarbon compounds content of 42.00-64.06% which indicating that these catalysts were effective for deoxygenation of the pyrolysis vapors to form hydrocarbon compounds. Another attention should be paid to the N-containing hydrocarbons, all catalyst promoted the yield of N-containing compounds from 13.77% to 15.97-49.27%. Apparently, total N-containing compounds are more than 30% for $TiO_2$-anatase based catalysts (24.06-49.27%) which are higher than $ZrO_2$ and $TiO_2$ (rutile) based catalysts (15.00-25.69%). However, it was noticed that $TiO_2$ (anatase) support itself did not have N-containing compounds as much as when loaded with active metal.

Among twenty catalysts tested, the yield of sugar (levoglucosan and d-glucose) was not found with any catalysts. From previous experiment, the yields of sugar gradually reduced with increasing temperature from 400 to 600°C. Therefore, it could be completely eliminated by each catalyst at the highest temperature (600°C) tested

here. The results agree well with Lu et al. that levoglucosan is easy to be converted by catalyst and it is significantly reduced or even completely eliminated (Lu, 2012). The main N-containing compounds from catalytic pyrolysis of Jatropha residues contain the N-heteroatom and N-nonheteroatom (oleanitrile, olelic acid amide, hexadecanamide and aniline). Total N-containing compounds are more than 20% for all catalysts but N-nonheteroatoms are higher for $Al_2O_3$ based catalysts while N-heteroatoms are higher for $TiO_2$ ($T_1$) and $TiO_2$ ($T_2$) based catalyst. That results similar to Kim et al., who studied pyrolysis of Jatropha seed shell cake (Kim, 2013). They found that the carbon chain lengths of the pyrolytic oils are from $C_{12}$ to $C_{18}$, similar to typical diesel fuel and nitrogen was distributed in various forms in the pyrolytic oils, owing to the fact that Jatropha seedshell cake (JSC) oil was high in amide and imide derivatives. Thus, Jatropha residues pyrolytic product has potential as a feedstock for the production of highly hydrocarbon compounds through catalytic deoxygenation. In addition, for the elimination of nitrogen impurity for fuel usage, denitrogenation catalyst could be designed or selected for efficient process because of their different main nitrogen compounds (Kaewpengkrow, 2013; Kim, 2013)

Generally, bio-oil contains some heavy aromatic compounds while gasoline and diesel include mixtures of hydrocarbons with relatively low chain lengths of 5–10 and 12–20, respectively (Choudhary, 2011). From the result, the major compounds were aliphatic hydrocarbons which were presented by the carbon range of $C_5$-$C_{11}$, $C_{12}$-$C_{20}$ and $> C_{20}$ as shown in Fig. 5.9. The main hydrocarbons are 1-Octene, 1-heptene, 1,3,5-Cycloheptatriene and 1-Heptadecene. High yield of $C_5$-$C_{11}$ was the main hydrocarbon products (30.04-48.10%) with the presence of catalyst in $Al_2O_3$ based catalysts, which are suitable as gasoline. It might be due to larger surface area of $Al_2O_3$ than other catalysts. High yields of $C_{12}$-$C_{20}$ were obtained at 35.80% by $PdCT_1$ which are suitable as diesel fuel. The result indicated that these catalysts were effective for deoxygenation of the pyrolysis vapors to form hydrocarbons for quality biofuels. However, the yield of long chain hydrocarbon ($>C_{20}$) were obtained only 0.42-2.26%.
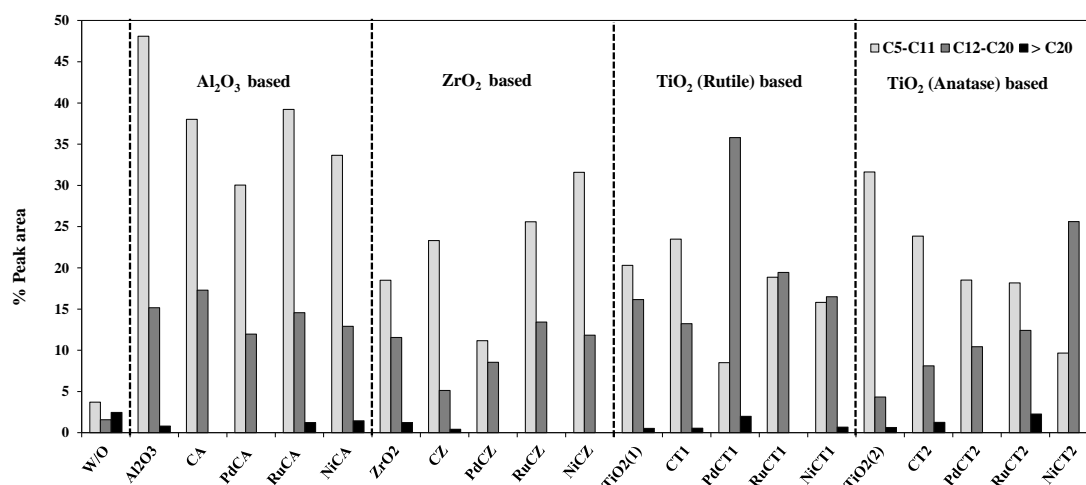
**Fig. 5.9** Hydrocarbon compounds selectivity for fast pyrolysis of Jatropha residues with various catalysts

Previous catalytic pyrolysis studies with different types and amounts of catalysts (Zeolite and metal oxide catalyst) reported the oxygenated compounds yield of around 20-60% (French, 2010; Lu, 2012; Mochizuk, 2013; Thangalazhy-Gopakumar). It can be concluded that these catalysts were more effective on cracking large molecules of hydrocarbon into light hydrocarbon than other support catalyst, although the surface area are lower than other catalysts. Other studies reported a reduction in oxygenated compounds and the presence of large amounts of polycyclic aromatic hydrocarbons (PAH) during the catalytic pyrolysis (Bridgwater, 2012; Murata, 2012; Graça, 2013). The PAH deserves more attention due to their toxicity in the environment and potential role in the incidence of cancer (Kaewpengkrow, 2013; Qiang, 2009) Because of the presence of PAHs in transportation fuel may result in possible emission by attachment to particulate matter in the exhaust from automobiles. Therefore, the proper catalyst for the catalytic pyrolysis to convert jatropha residues into bio-fuel should not only promote the monocyclic aromatic hydrocarbons (MAHs) but also inhibit the formation of coke and PAHs (Mochizuki, 2013). Among the hydrocarbon compounds, heptene, octene, and heptadecene were primary compounds. Other alkyl aromatics such as toluene, xylene, and ethylbenzene were also seen in the products. PAHs such as naphthalene were detected only 1-2% with the presence of all catalyst.

The oxygenated compound is one of the most important problems of bio-oil which led to low-quality and short shelf life fuel. Accordingly, reduction of oxygen content is one of the primary aims of this study. The result shows that all catalysts led to the decrease in oxygenated from 73.68% to less than 40% in all supporter except $Ce/ZrO_2$ catalyst. It can be suggested that the oxygenated compounds can diffuse into the pores of the catalyst, and result in hydrocarbon compound formation through decarbonylation, dehydration, and deoxygenation reactions (Vichaphund, 2013). In the presence of catalyst, high total hydrocarbon compounds were obtained by $TiO_2$ ($T_2$), $Ce/Al_2O_3$, $Ni-Ce/Al_2O_3$, and $Al_2O_3$ catalysts, respectively. The effect of various catalysts on the oxygenated compounds and total hydrocarbon is shown in Fig.5.10.
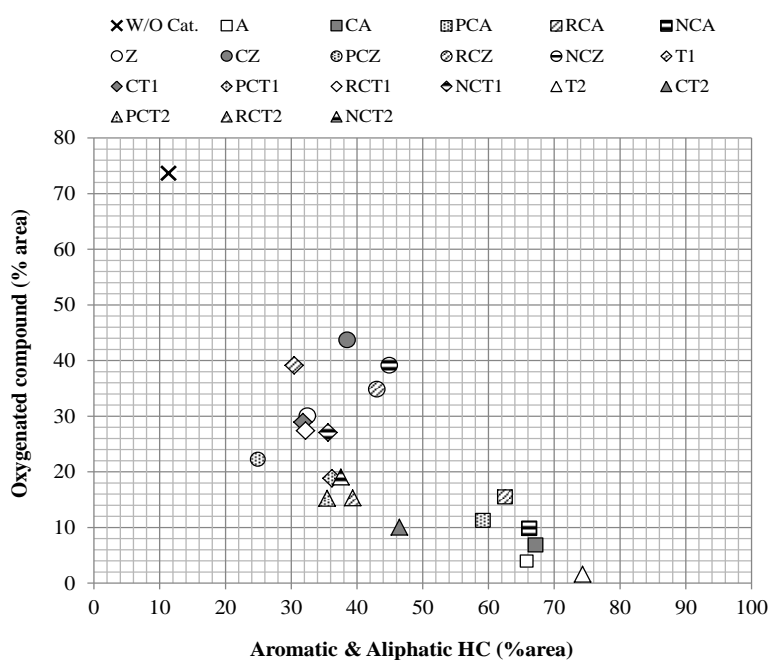


**Fig. 5. 10** Effect of the various catalysts on the oxygenated compounds and total hydrocarbon compounds of pyrolytic products using ceramic supporters.

These catalysts exhibited improved selectivity toward the aromatic and hydrocarbon production of more than 60% and decreased oxygenated compounds to less than 10%. Thus, it can be concluded that these catalysts are relatively suitable for decreasing the number of oxygenated compounds and providing bio-oil with enhanced stability. Finally, it can be noticed that these catalyst supports displayed relatively high activity towards deoxygentation reactions which resulted in low quantity

of acids and other oxygenated compounds, and produced high aromatic and hydrocarbon compounds. In addition, high J/C ratio had positive influence on low yields of oxygenated compounds and high yields of hydrocarbon compounds. Among twenty catalysts tested, the presence of the $TiO_2$ ($T_2$) catalysts displayed the highest yields of aromatic hydrocarbons (36.25%), relatively high hydrocarbon (38.07%), low oxygenated compounds (0.65%) and no carboxylic acids content. On the other hand, $Al_2O_3$, $Ce/Al_2O_3$ and $Ru$- $Ce/Al_2O_3$ presented higher yields of aliphatic hydrocarbon compounds of 64.06%, 55.92%, and 56.62%, respectively. Total hydrocarbons compounds of $TiO_2$ ($T_2$), $Ce/Al_2O_3$, $Al_2O_3$, and $Ru$- $Ce/Al_2O_3$ were 74.32%, 67.14%, 65.81%, and 62.49% while oxygenated compounds were in the range of 3.96-43.70%. The result showed that $Al_2O_3$ and $TiO_2$ ($T_2$) based catalysts reduced oxygenated yields to less than 20% while oxygenated yields of $ZrO_2$ and $TiO_2$ ($T_1$) were yet higher than 30%. However, these catalysts contained considerable amount of N-containing compounds (24.06-49.27%) implying that additional denitrogenation is further required. It was suggesting that these catalysts were effective for cracking large molecules of the pyrolysis vapors and may possibly be applied to improve the properties of pyrolytic products vapors from Jatropha residues.

## 5.4 The catalytic pyrolysis with $Al_2O_3$ based catalysts (without $CeO_2$ promoter)

From previous section, the effect of metal active sites, support type, and also jatopha-to-catalyst ratio (J/C) were discussed. Among twenty catalysts tested, the presence of the anatase based catalysts displayed the highest yields of aromatic hydrocarbons (36.25%), relatively high hydrocarbon (38.07%), low oxygenated compounds (0.65%) and no carboxylic acids content. Overall performances of $Al_2O_3$ support catalysts are acceptable and can be considered as good candidate for dexygenation process of pyrolytic vapor during fast pyrolysis of Jatropha residues. Therefore, alumina support was selected for study effect of catalytic activity on pyrolytic product further. However, the result also found that the promoter ($CeO_2$) had not significantly effect for distribution the metal and pyrolytic product of Jatropha residue. Thus, in this section the metal content loading onto the $Al_2O_3$ support by the

impregnation were synthesize; the catalyst was not impregnated with $CeO_2$ as promoter and increased metal loading from 1% to 5%wt. The catalysts in this section included alumina support and seven metal active sites of 5 %wt (Ce, Co, La, Mo, Ni Pd, and Ru).

### 5.4.1 Product distribution of Jatropha residue catalytic pyrolysis with Al2O3 based catalysts

This section mainly focused on active metal doped on alumina ($Al_2O_3$) supporter. The pyrolysis of Jatropha residue was carried out at 600°C with Jatropha to catalyst ratio as 1:1. Seven catalysts were used as the materials for catalytic fast pyrolysis of Jatropha residue. The identified compounds were classified into 11 groups as shown in Fig.5.11. Biomass fast pyrolysis vapors were composed of volatile compounds and non-volatile oligomers. Non-condensable gases were not analyzed in this study. The product distribution after catalysis was compared to study the catalytic effects of these catalysts. The main compounds groups included are acids (fatty acid), alcohols, aldehydes, aromatic, esters, ether, furans, hydrocarbon compounds, ketones, N-compound (N-containning hydrocarbons) and phenol. The identified products were similar to literature data of the chemical composition of bio-oils, and also agreed well with previous Py-GC/MS studies (French, 2010; Mihalcik, 2011; Pattiya, 2008; Vichaphund, 2013)

The liquid product from biomass pyrolysis is known to have an acidic structure. In non-catalytic, acids were detected in high yields, consisted of 9-octadecenoic acid (oleic acid), hexadecanoic acid (palmitic acid), and acetic acid which probably come from Jatropha oil in residue after extraction. In catalytic pyrolysis run, product contained acid of 60.74% and was dropped considerably to 1.65-20.56%, especially $Ce/Al_2O_3$ catalyst which completely reduced acid. The total hydrocarbon was increased from 10% to 30.05-42.33%, the maximum hydrocarbon contents were obtained by the $Co/Al_2O_3$. This result agreed with several researches (Barbaro, 2009; Mochizuki, 2013; Murata, 2012; Vichaphund; 2013) which found the low yield of hydrocarbon in non-catalytic fast pyrolysis of biomass. The selectivity of aromatics was

increased from 3.58 to 10.19% by the Pd/Al$_2$O$_3$. Furthermore, hydrocarbon compounds were significantly increased to 32.62% by the Co/Al$_2$O$_3$. Ru/Al$_2$O$_3$ was less effective such that carboxylic acid yields were still high (20.56%) which could cause corrosion problem. In addition, the yield of ester increased with the presence of catalyst. The highest ester of 11.64% was obtained by Ce/Al$_2$O$_3$; it was possibly due to carboxylic acid conversion into ester form.
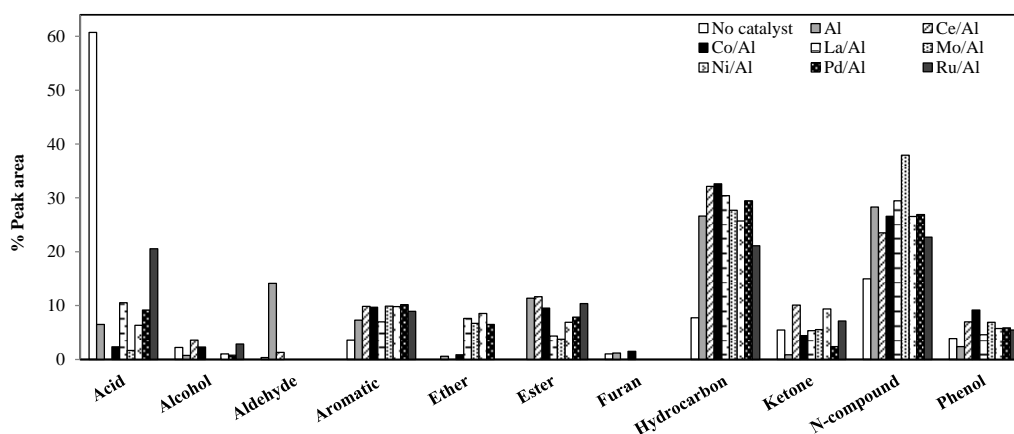


**Fig. 5.11** Compound distributions of pyrolytic vapors of Jatropha residue

The yield of aldehyde almost completely decreased except for Al$_2$O$_3$ catalyst (14.11%). It was indicated that metal active species of catalyst are effective to reduce aldehydes formation which are main responsible for the ageing reactions and instability of bio-oils. Phenols compounds from degradation of lignin- fractions were found only 2.37-9.16%. Obviously, the nitrogen element in Jatropha is higher than other woody biomass (Kaewpengkrow, 2013; Vichaphund, 2013). Accordingly, N-compounds in pyrolytic product were found in high content (22.71-37.92%). The cracking of cellulose and hemicellulose-derived components resulted in an increase of lower molecular weight aromatics (including benzene, toluene, and xylenes). The pathways for the primary decomposition of cellulose during fast pyrolysis can be explained by Fig.5.12 which corresponded to other researcher (Murata, 2012).
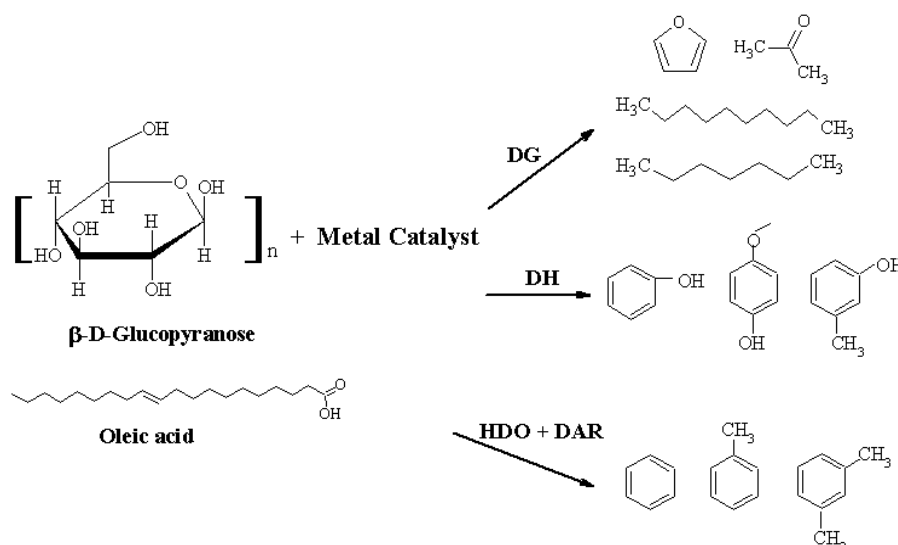
**Fig. 5.12** Proposed reaction pathway for catalytic fast pyrolysis of cellulose, DG: degradation, DH: dehydrogenation, HDO: hydrodeoxygenation, DAR: dehydroaromatization

5.4.2 The effect of Jatropha to catalysts ratio (1:1, 1:5 and 1:10) on pyrolytic products

For the catalytic experiment, the product distribution after catalysis was compared to study the catalytic effects of these catalysts. The pyrolytic vapors detected from GC/MS with various J/C ratios are displayed in Fig.5.13 (a-c). The catalytic pyrolytic products were classified into 4 groups, included aromatic, hydrocarbon, oxygenated and N-compounds. The main compound was aliphatic hydrocarbon compounds (24.72-46.01%), which was a mainly high carbon chain length of 5-11.  With increasing J/C ratio to 1:5 and 1:10, it was found that all catalyst led to complete reduction of acid. With the J/C ratio of 1:5, the yields of aromatic hydrocarbon increased rapidly up to 14.03 and 14.20% for $Ni/Al_2O_3$ and $Mo/Al_2O_3$, respectively. At the same time, the yields of other oxygenated (included acid, alcohol, aldehyde, ether, ester, furan, ketone and phenol) and N-compounds decreased significantly.

The highest yields of total hydrocarbon compound were obtained by $La/Al_2O_3$ catalysts followed by $Co/Al_2O_3$ and $Ce/Al_2O_3$ of 58.52%, 56.36% and 51.81%, respectively (J/C of 1:5). This result agrees with Mochizuki et al., who found that hydrocarbon was increased with increasing the biomass/catalyst weight ratio to 1:5

(Mochizuki, 2013). The result showed that low yield of PAHs from catalytic pyrolysis was slightly detected for only 1.48-2.27% and considered as one advantage of applying these catalysts. In addition, with J/C of 1:10, total hydrocarbon compounds obtained by Pd/Al$_2$O$_3$, Ni//Al$_2$O$_3$ and Ce/Al$_2$O$_3$ were 75.09%, 73.05, and 72.78%, respectively. The result suggested that pyrolytic products may be applied for transportation fuel. While Mo/Al$_2$O$_3$ showed the lowest total hydrocarbons production which was possibly due to lower surface area (74.46 m$^2$/g) than other catalysts.
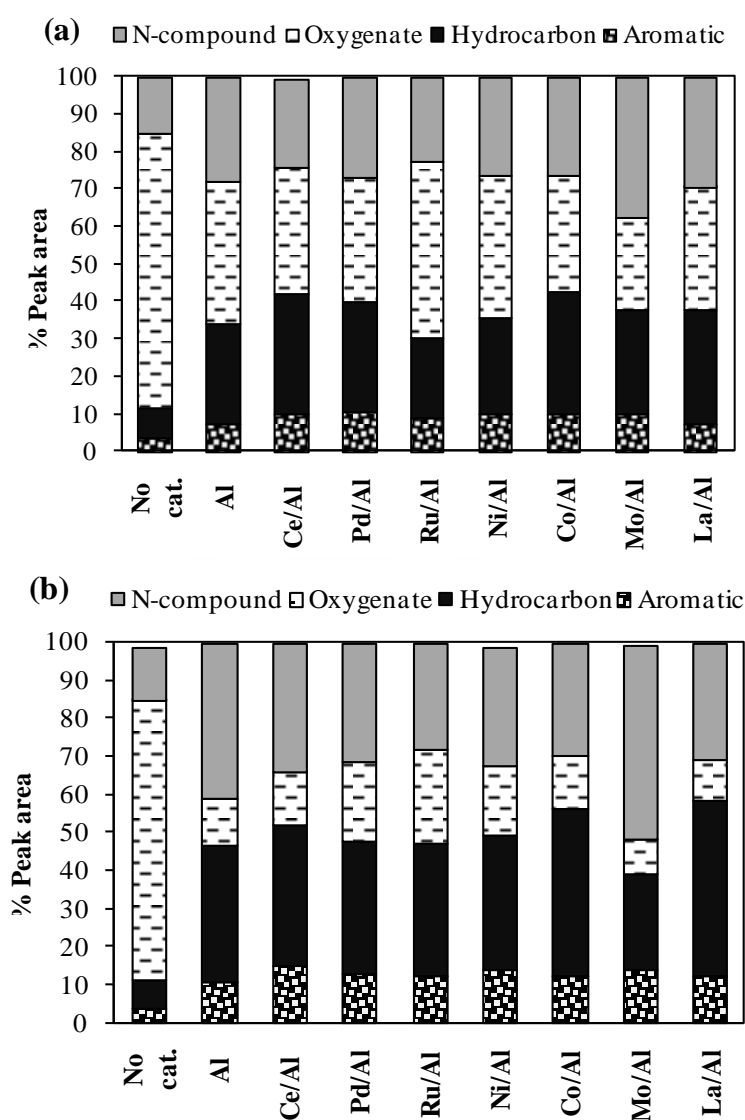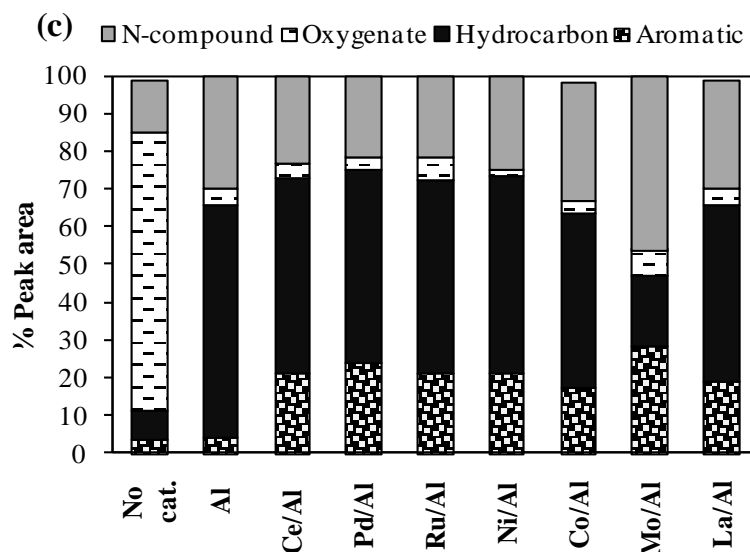
**Fig. 5.13** Average total compositional of pyrolytic products various J/C ratio (a) J/C of 1:1, (b) J/C of 1:5 (c) J/C of 1:10

From the result, the major compounds were aliphatic hydrocarbons which were presented by the carbon range of $C_5$-$C_{11}$, $C_{12}$-$C_{20}$ and > $C_{20}$ while the aromatic selectivity was represented in term of benzene, toluene and ethyl benzene (BTE) as shown in Fig. 5-14. The main hydrocarbons are alkene such as 1-heptene, 1-octene, and E-9-octadecene. $C_5$-$C_{11}$ was the main hydrocarbon products (11.14-50.33%) with the presence of catalyst in the order of $Al_2O_3$ >$Ce/Al_2O_3$ >$Pd/Al_2O_3$. It can be concluded that these catalysts were effective for cracking large molecules of hydrocarbon into light hydrocarbon which are suitable for gasoline. The high yield carbon $C_{12}$-$C_{20}$ was obtained from 7.69-19.33%, the highest yield was obtained by $Ni/Al_2O_3$ which was suitable for diesel fuel. This result similar to French et.al, which reported similar studies over 40 catalysts, and found that nickel substituted ZSM-5, gave the highest hydrocarbon yield (French, 2010). The result indicated that these catalysts were effective for deoxygenation of the pyrolysis vapors to form hydrocarbons for quality biofuels. However, the yield of long chain hydrocarbon (>$C_{20}$) were obtained only 0.42-0.8%. It may be implied that these catalysts were effective for cracking large molecules of the pyrolysis vapors and may possibly be applied to improve the properties of pyrolytic products vapors from Jatropha residues.

The aromatic selectivity noticeably increased with the presence of all catalysts except $Al_2O_3$, benzene, toluene, and ethyl benzene (BTE) are mainly produced from using of J/C ratios of 1:5 and 1:10. It is well known that BTE are major petrochemicals which are valuable and suitable as chemical feedstocks. The reaction pathway includes dehydrogenation (DH) and dehydroaromatization (DAR) of aliphatic oxygenates, and carboxylation of carboxylic acids to form phenol derivatives, which undergo hydrodeoxygenation (HDO) into toluene and xylenes (Murata, 2012). When increasing J/C ratio to 1:10, the aliphatic hydrocarbon compounds were mainly pyrolytic product. The highest yield aliphatic hydrocarbon of 62.04% was obtained by $Al_2O_3$. $Pd/Al_2O_3$ with surface area of $103.2m^2/g$ produced the highest aromatic hydrocarbon yields of 23.72%. Interestingly, $Mo/Al_2O_3$, $Pd//Al_2O_3$ and $Ru/Al_2O_3$ performs very well on enhancement of BTE production. Although $Mo/Al_2O_3$ can produce aromatic compound but it also promoted N-compounds. From the result, it is apparent that short chain hydrocarbon ($C_5$-$C_{11}$) increased with higher J/C ratio for all catalysts except $Mo/Al_2O_3$. This implied that these catalysts with J/C of 1:10 were effective for cracking large molecules (long chain of fatty acid) to form smaller hydrocarbon molecules (Thangalazhy-Gopakumar, 2011).

Moreover, all transition metal catalysts promoted formation of aromatic via dehydroaromatization reaction pathways; one candidate is $Pd/Al_2O_3$. Other candidates are $Ce/Al_2O_3$, $Ni/Al_2O_3$, $Ru/Al_2O_3$ and $La/Al_2O_3$ that could be favored for producing the BTE. This result compared with Vichaphund et al. which reported that the increase of biomass to ZSM-5 ratios from 1:1 to 1:5 and 1:10 had an effect on the increase of aromatic compounds yields catalyzed by Ni-HZSM-5 with high surface area of 625 $m^2/g$ (Vichaphund, 2013). The result of higher aromatic hydrocarbon yields by using high content of catalyst corresponded well to other works (Kaewpengkrow, 2013; Mochizuki, 2013).
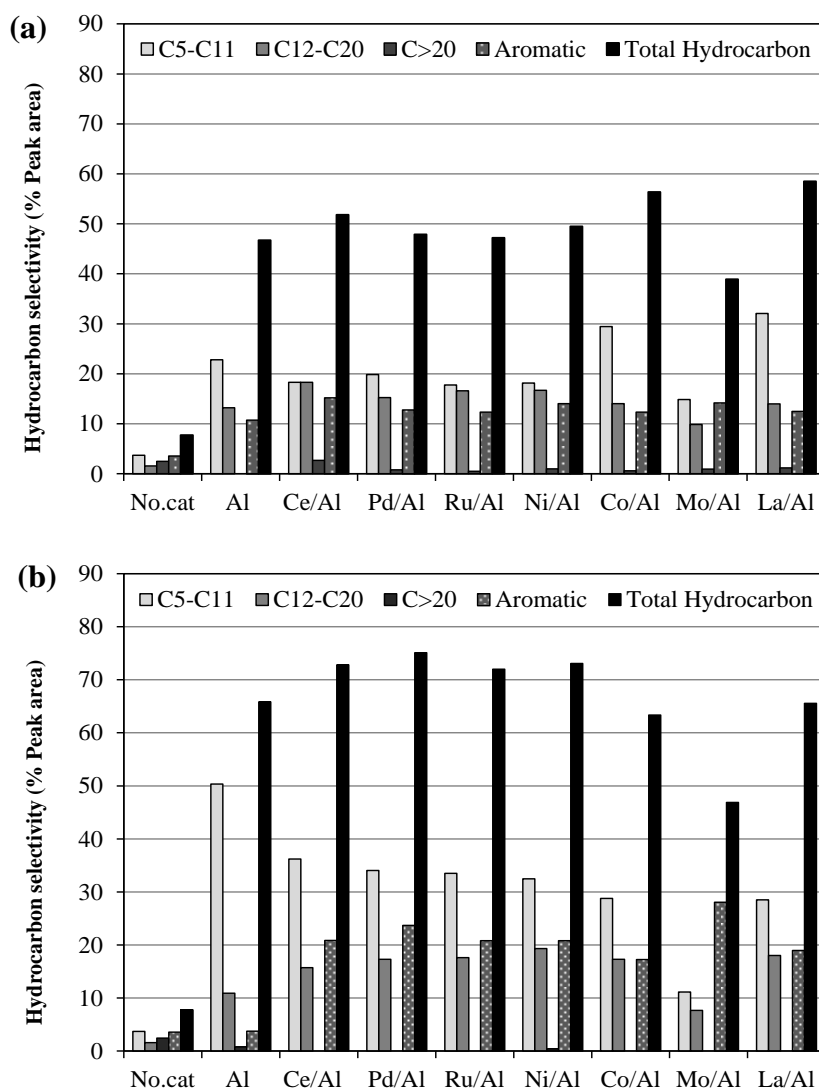
**Fig. 5.14** Hydrocarbon selectivity for fast pyrolysis of Jatropha residues with various catalysts with (a) J/C of 1:5 (b) J/C of 1:10

Another study reported a reduction in oxygenated compounds and the presence of large amounts of polycyclic aromatic hydrocarbons (PAH) during the catalytic pyrolysis (Mochizuki, 2013; Murata, 2012). The result shows that all catalysts led to the decrease in oxygenated from 73.68% to less than 50%, 20% and 10% with J/C of 1:1, 1:5 and 1:10, respectively. Oxygenated compounds are greatly reduced with increasing J/C to 1:10. The effect of various catalysts on the relativity of oxygenated compounds and total hydrocarbon compounds of pyrolytic products are shown in Fig.5.15. In the presence of catalyst, high total hydrocarbon compounds and

oxygenated compounds were obtained by $Pd/Al_2O_3$, $Ce/Al_2O_3$, $Ni/Al_2O_3$ and $Ru/Al_2O_3$ catalysts, respectively. These catalysts exhibited improved selectivity toward the aromatic and hydrocarbon production of more than 70% and decreased oxygenated compounds to less than 10%. $Pd/Al_2O_3$ is effective for deoxygenation, the oxygenated compounds were detected only 3.16%.
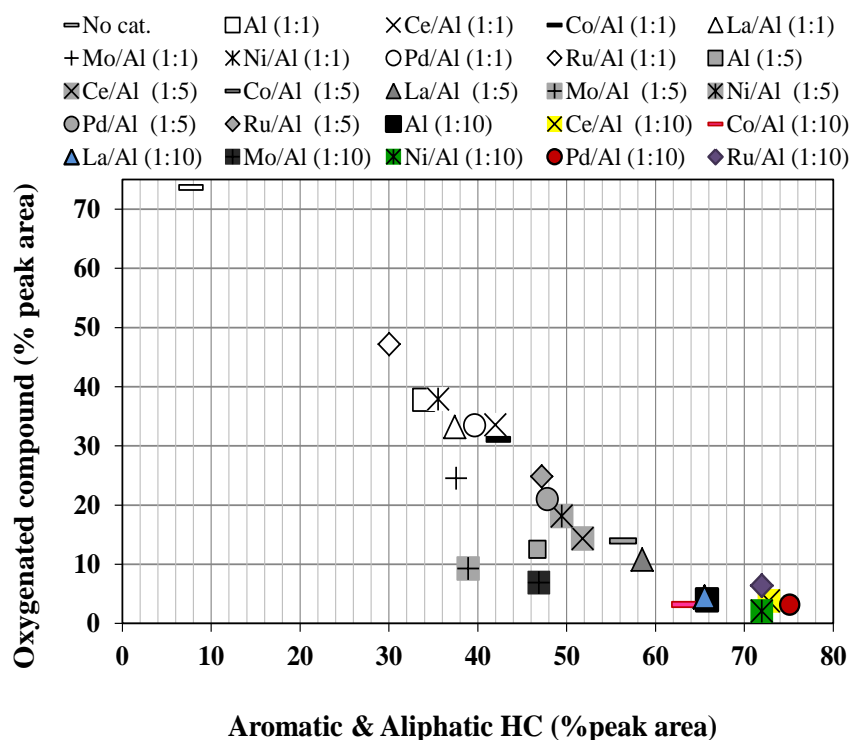


**Fig. 5.15** Effect of the various catalysts on the oxygenated and total hydrocarbon compounds of pyrolytic products

In addition, N-containing compounds, remained of 27.98-50.90% and 21.77-46.06% by J/C of 1:5 and 1:10, respectively. Total N-compounds (included N-heteroatom and N-nonheteroatom), the highest N-compounds was obtained by $Mo/Al_2O_3$ catalyst with both J/C ratio. These products may create problems such as corrosion and poisoning of catalysts during bio-oil upgrading (Mochizuki, 2013). It seems that the $Al_2O_3$ and $Mo/Al_2O_3$ catalysts favored the formation of N-compounds with J/C ratio of 1:5. Interestingly with increasing J/C ratio to 1:10, all of catalysts reduced N-compounds yields to less than 30% except $Mo/Al_2O_3$. These results corresponded to

previous section which reported metal catalysts with $Al_2O_3$ supported was effective for deoxygenation, and promoted N-compounds at the same time. However, the result suggested that high J/C ratio had positive influence on low yields of N-containing compounds.

Among the many catalysts available, Ni-based systems are universal and widely used in the laboratory and industry in several reforming processes, mainly due to the low cost of Ni. However, the main problem of Ni is the rate of C–C bond formation is high, promoting the rapid growth of a carbon deposit, which led to catalyst deactivation (Barbaro, 2009). There are several researches reported that noble metals such as Pd, Ru and Rh, are the most suitable alternative to break the C–C bonds complex in reforming processes which corresponded to this research. All transition metal catalysts caused an increase in aromatic and hydrocarbon compounds. It can be noticed that these catalysts displayed relatively high activity towards deoxygentation reactions which resulted in completely eliminated of acids, low oxygenated compounds and very high aliphatic hydrocarbons. The transition metals exert important effect on the catalytic activity of these complexes. The catalytic activity of these complexes with the following the order: Pd > Ni > Ce > La> Co> Ru> Mo. The catalytic properties of transition metal are related to the electron configuration of metal elements ((Barbaro, 2009). Pd and Ni were efficient initiating systems for the cracking of vapors products. Interestingly, Pd of all J/C ratios seems that to be effective on deoxygenation and production of aromatic compounds. Moreover Pd, Ce and Ni with all J/C ratios are less effective to produce N- compounds which are advantage of this metal catalyst. Although only $Al_2O_3$ supporter increased the hydrocarbon compounds and greatly reduced the oxygenated compounds but it also promoted N-containing compounds. Therefore, the compositions of pyrolysis products were affected by the difference in type of active metals to some extent as well as amount of catalyst. The result suggesting that these transition metal catalysts were effective for deoxygenation of the pyrolysis vapors and can be applied to improve the properties of products from Jatropha residue.

**5.5 The catalytic pyrolysis with 5% Activated carbon-based catalysts (Powder)**

In this section, the effect of the Activated carbon (AC) and Metal on Activated carbon (M/AC) catalysts on the pyrolysis product distribution was investigated at 600°C and a J/C ratio of 1:1, 1:5 and 1:10.

5.5.1 Effect of the metal catalysts on the pyrolytic product distribution

The fast pyrolysis of the Jatropha residue produced a complex mixture of products. As shown in Fig. 5.16, all the catalysts clearly reduced the proportion of oxygenated compounds and carboxylic acids, from 73.7% without a catalyst down to 21.2% for Ce/AC (at a J/C ratio of 1:1), as a likely result of their conversion to primarily hydrocarbon compounds. Typically, bio-oil is known to have acidic structures from the decomposition of biomass. In accordance, the pyrolysis without any catalyst yielded carboxylic acids as the main product (60.7%), which is similar to previous reports (French & Czernik, 2010; Kaewpengkrow et al., 2014a; Kanaujia et al., 2014; Wu et al., 2013) . Except for with Ru/AC, the carboxylic acid proportion dropped noticeably in the presence of the AC and M/AC catalysts to 3.3–21.5%, especially with the Ce/AC catalyst. However, Ru/AC was far less effective at reducing the carboxylic acid content, attaining a reduction to only ~31.5%.
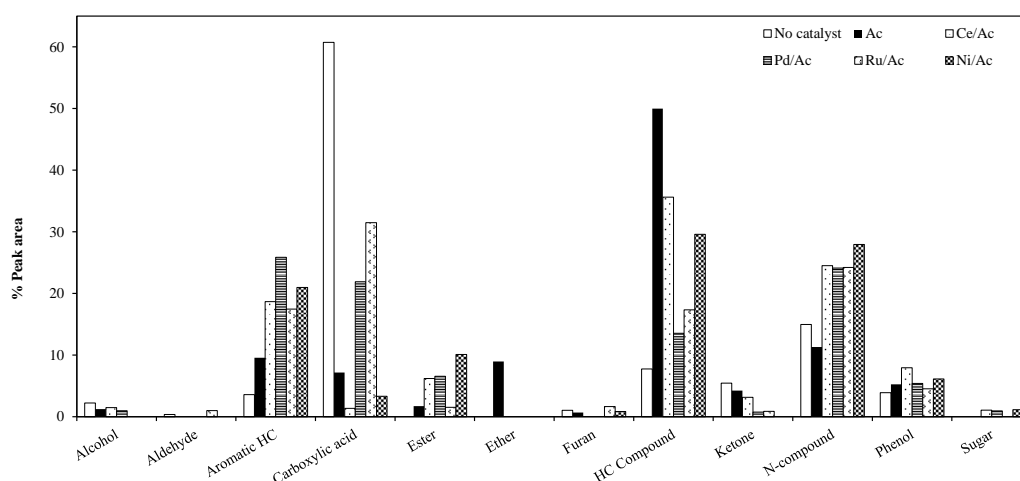


**Fig. 5.16** Effect of the catalyst type (at a J/C ratio of 1:1) on the distribution of pyrolytic products.

The aromatic and aliphatic hydrocarbon compounds obtained from the pyrolysis of Jatropha waste residue without a catalyst were only detected at 3.58% and 7.74%, respectively. The inclusion of the AC catalyst increased the aliphatic hydrocarbon yield to 59.6%, while the M/AC catalysts also promoted the formation of aromatic compounds, but to a lesser extent with a yield of 17.8% for Ru/AC up to 25.9 % for Pd/AC. This result is similar to Morgan et al. who found that 5 wt.% Pd/AC provided good yields of fuel-like aliphatic hydrocarbons in the catalytic deoxygenation of stearic and tristearin acids (Spadaro et al., 2015). Phenol compounds (lignin degradation products were detected at slightly higher levels in the presence of the AC (5.25 %) and M/AC (7.94 % with Ce/AC) catalysts than without any catalyst (3.88 %).

The pyrolytic products from the Jatropha waste biomass include various products of oxygenated compounds, such as aldehydes, ketones, alcohols, and esters, which were reduced from 73.7% in the absence of any catalyst to 9.5–22.0% in the presence of the M/AC catalysts in the order of Ru/AC < Pd/AC < Ni/AC < Ce/AC (Fig. 5.20). The yield of sugar (d-glucose) was low at only 0.94–1.12%, since it had been almost completely reduced. These results agree well with Lu et al. (Cheng et al., 2016; Lu et al., 2010; Qiang et al., 2009) who stated that sugar (levoglucosan) is easily converted by the catalyst and is mostly to completely reduced.

In addition, the ester yield increased in the presence of the M/AC catalysts (Fig. 5.), with the highest ester yield (10.1%) obtained with the Ni/AC catalyst, which was possibly from the conversion of carboxylic acids into esters. Interestingly, these catalysts did not promote the formation of undesired compounds, such as polycyclic aromatic hydrocarbons (PAHs) and furan, which are toxic and may be carcinogenic. Thus, these catalysts are effective for the deoxygenation and decarboxylation of pyrolytic vapors, reducing their contents to less than 40%, which will greatly improve the quality and stability of bio-oil. Total N-compounds were increased from 15.0% in the absence of a catalyst to between 24.1% (Ru/AC) and 28.0% (Ni/AC) in the presence of the catalyst at a J/C ratio of 1:1. However, the N-compounds were mainly N-nonheteroatom forms, in which the nitrogen can more easily be removed compared to N-heteroatom forms.

The pyrolysis of biomass involves multiple steps of parallel and competing reactions, such as dehydration, depolymerization and decomposition (Graça et al., 2013; Lu et al., 2010; Zhang et al., 2013), and usually requires high temperatures of 400-600°C for the reaction to commence. The fast pyrolysis of the Jatropha residue produced a complex mixture of products. For ease of discussion, the pyrolytic products were grouped into aromatics, aliphatic hydrocarbon compounds, carboxylic acids, oxygenated compounds (including alcohol, aldehyde, ester, furan, ketone and phenol), N-compounds (heteroatom and non-heteroatom) and sugars.

The yields of the pyrolytic products were determined from the peak area percentages of the GC-MS, and a total of 50 compounds were identified. As shown in Fig. 5.17, all the catalysts clearly reduced the proportion of oxygenated compounds and carboxylic acids, from 73.7% without a catalyst down to 21.2% for Ce/AC (at a J/C ratio of 1:1), as a likely result of their conversion to primarily hydrocarbon compounds. In accordance, the pyrolysis without any catalyst yielded carboxylic acids as the main product (60.7%), which is similar to previous reports(French & Czernik, 2010; Kaewpengkrow et al., 2014a; Kanaujia et al., 2014; Wu et al., 2013) . Except for with Ru/AC, the carboxylic acid proportion dropped noticeably in the presence of the AC and M/AC catalysts to 3.3–21.5%, especially with the Ce/AC catalyst. However, Ru/AC was far less effective at reducing the carboxylic acid content, attaining a reduction to only ~31.5%.

Total N-compounds were increased from 15.0% in the absence of a catalyst to between 24.1% (Ru/AC) and 28.0% (Ni/AC) in the presence of the catalyst at a J/C ratio of 1:1. However, the N-compounds were mainly N-nonheteroatom forms, in which the nitrogen can more easily be removed compared to N-heteroatom forms.

5.5.2 Effect of the J/C ratio on pyrolytic products

The J/C ratio was increased from 1:1 to 1:5 and 1:10 in order to investigate the effect of the amount of catalyst used on the reactions. Some 82 principals (peak area% greater than 0.5%) compounds were identified from the GC-MS

chromatograms when using the catalysts with a J/C ratio of 1:5 (Appendix A; Table 8).
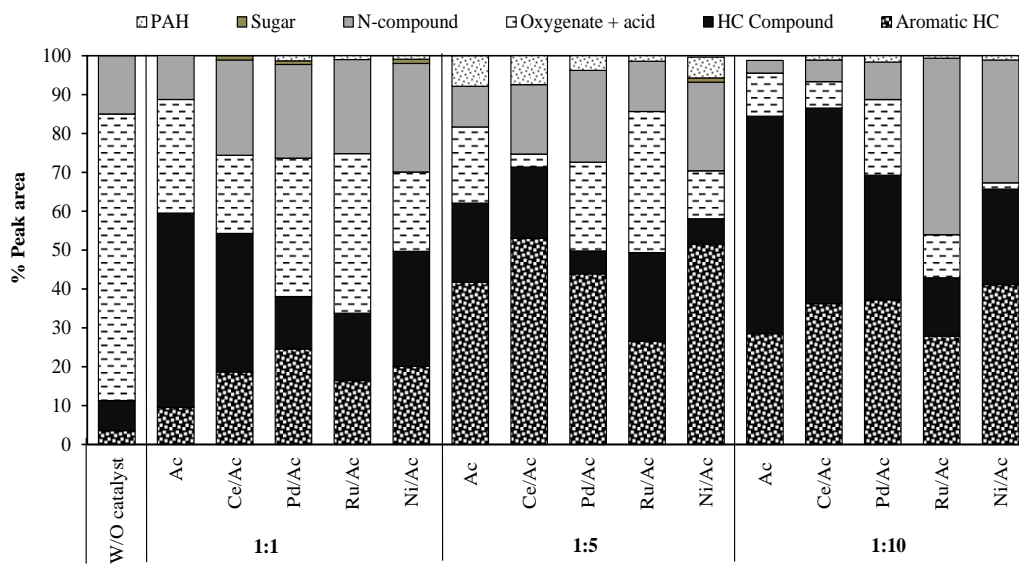


**Fig. 5.17** Average total composition of the pyrolytic products obtained with different catalysts at a J/C ratio of 1:1, 1:5 and 1:10

For all the M/AC catalysts, increasing the J/C ratio from 1:1 to 1:5 or 1:10 led to the complete reduction of carboxylic acids, through the decarboxylate reaction, and increased the aliphatic hydrocarbon and aromatic compound levels. The highest aromatic hydrocarbon content was obtained with the Ce/AC (53.0%) and Ni/AC (41.2%) catalysts, respectively, at a J/C ratio of 1:5 and 1:10, respectively. The aliphatic hydrocarbon yields increased when increasing the J/C ratio to 1:10 in the presence of the AC catalyst with the highest yield of aliphatic hydrocarbon compounds being 56.0%.

In addition, the total hydrocarbon compounds (aromatic and aliphatic) were increased in the presence of the higher levels of M/AC catalysts, reaching 42.9–86.6%. The highest yield was obtained with a J/C ratio of 1:10 for Ce/AC (86.6%), followed by AC (75.4%) and Pd/AC (69.3%), and then Ce/AC at a J/C ratio of 1:5 (71.4%). The oxygenated and acidic products were obviously decreased to 3.3–36.2% and 1.6–

19.5% at a J/C ratio of 1:5 and 1:10, respectively. The most effective deoxygenation catalysts for the acid fractions were Ce/AC and Ni/AC.

One of the most challenging problems of bio-oil production is the removal of the highly oxygenated compounds that would otherwise lead to a low-quality and short shelf-life fuel(Hu et al., 2011; Voloshin et al., 2016; Wang et al., 2016b) (Hu et al., 2011; Kanaujia et al., 2014; Srinivasan et al., 2012). Thus, the reduction of the oxygen content was one of the primary goals of this study. The level of oxygenated compounds was greatly reduced when the J/C ratio was increased to 1:10. The effect of various catalysts on the relative proportion of oxygenated and total hydrocarbon compounds of the pyrolytic products is shown in Fig. 5.18.
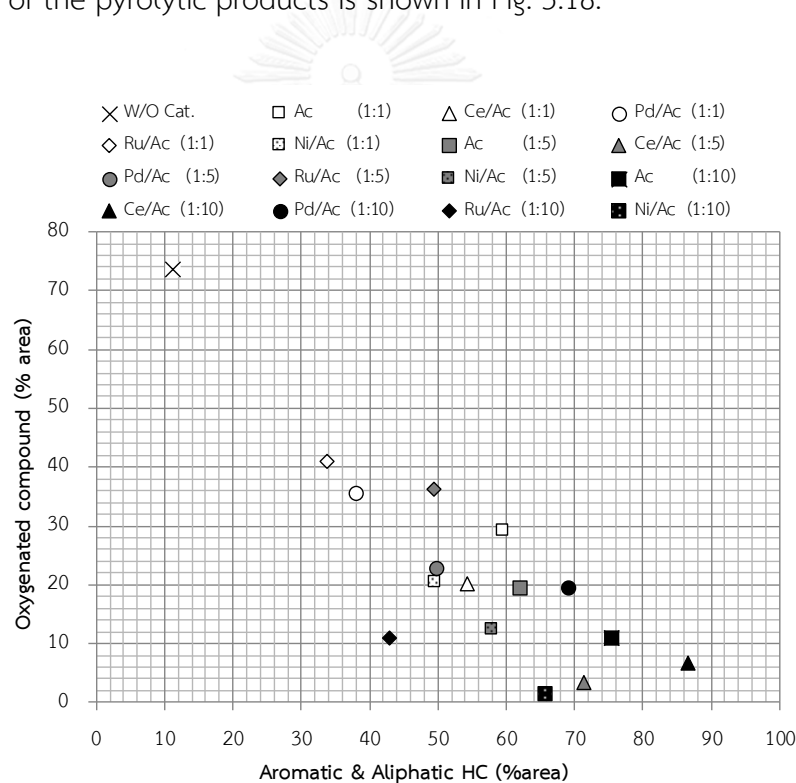


**Fig. 5.18** Effect of the various catalysts and J/C ratios on the proportion of oxygenated and total hydrocarbon compounds in the pyrolytic product.

A high proportion of total hydrocarbon compounds were obtained with the Ce/AC, Ni/AC and AC catalysts, which exhibited an improved selectivity towards the aromatic and aliphatic hydrocarbon production of more than 60% and decreased the

oxygenated compounds to less than 10%. The aliphatic hydrocarbon distribution from the catalytic fast pyrolysis of Jatropha is shown in Fig. 5.24. The aromatic selectivity noticeably increased the presence of every catalyst, where BTEX were the main aromatic products at all three tested J/C ratios for each catalyst. This is of relevance since BTEX are major petrochemicals and valuable chemical feedstocks. The highest yield of aromatic compounds and BTEX at 42.9% and 40.5%, respectively, were obtained with the Ce/AC and Pd/AC catalysts, respectively. These results are similar to the reported > 40% yield of aromatic compounds in the catalytic pyrolysis of Jatropha husk in the presence of zeolite catalysts at a J/C ratio of 1:5(Ledesma et al., 2014; Malins et al., 2015; Shim & Kim, 2010). The level of PAHs was only slightly increased by the presence of the catalysts, with a PAH yield of up to 7.83% with the AC catalyst at a J/C ratio of 1:5. However, previous studies have reported PAHs of more than 20% (such as naphthalene) in the presence of ZSM-5(Huang et al., 2016; Malins et al., 2015; Shim & Kim, 2010). (French & Czernik, 2010; Kaewpengkrow et al., 2014a; Li et al., 2014)
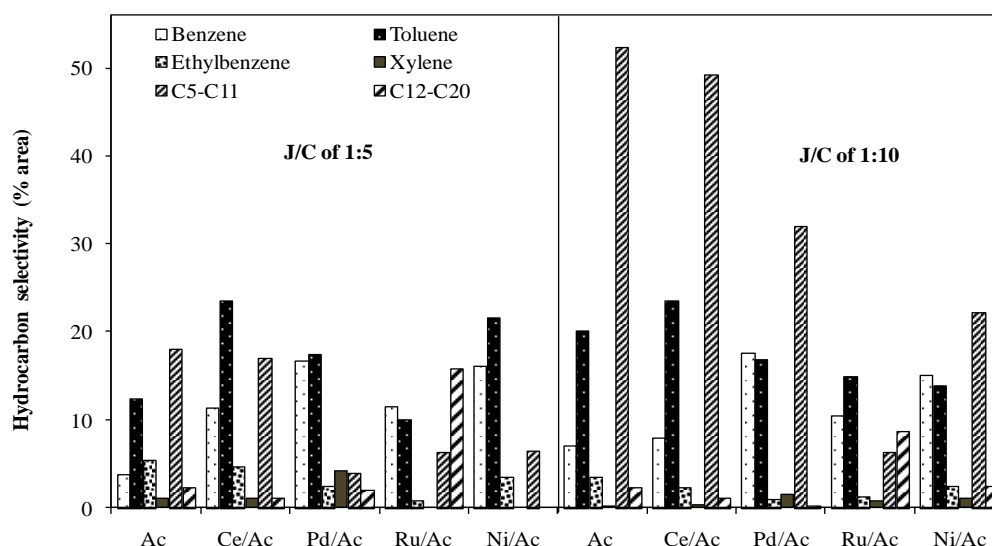


**Fig. 5.19** Hydrocarbon selectivity for the catalytic fast pyrolysis of Jatropha residue by the different catalysts at a J/C ratio of (Left) 1:5 and (Right) 1:10

Interestingly, the Ce/AC, Ni/AC and Pd/AC catalysts performed very well in enhancing BTEX production while effectively deoxygenating all of the oxygen-

containing components. At a J/C ratio of 1:10, the major compounds were aliphatic hydrocarbons (mainly heptane) in the carbon range of C5–C11 and C12–C20 as shown in Fig. 5.19.

It is apparent that the proportion of short chain hydrocarbons ($C_5$–$C_{11}$) increased at higher J/C ratios for all the catalysts except for Ru/AC, with the highest yield obtained with the AC catalyst. This implied that these catalysts at a J/C ratio of 1:10 were effective for cracking large molecules (long chain fatty acids) to form smaller hydrocarbon molecules (Kaewpengkrow et al., 2014a; Kaewpengkrow et al., 2014b; Vichaphund et al., 2015). Accordingly, one promising candidate is Ce/AC, which promoted the formation of aromatic compounds, via DAR reaction pathways, and aliphatic hydrocarbons. Other suitable catalysts are Pd/AC and Ni/AC for production of the BTEX. Overall, these suggest that these catalysts were effective for cracking large molecules in the pyrolysis vapors and could be selectively applied to improve the properties of the pyrolytic vapor products from Jatropha wastes and, potentially, other similar biomass.

## 5.6 The catalytic pyrolysis with 5% Activated carbon-based catalysts (Granule)

In this section, Ac support was modified by impregnation method in granule form and were investigated by Py-GCMS prior to use in drop tube reactor. The catalysts in this experiments included Ac, Ce/Ac, Ni/Ac, Pd/Ac and Ru/Ac. For all the M/AC catalysts, increasing the J/C ratio from 1:1 to 1:5 or 1:10 led to the complete reduction of carboxylic acids, through the decarboxylate reaction and deoxygenation which similar. The pyrolytic products from the Jatropha waste biomass were identified into five group included aromatic, hydrocarbon, oxygenated, N-compound, and sugar. In catalytic pyrolysis runs, the oxygenated compounds were reduced from 73.7% in the absence of any catalyst to 66.31–23.19% in the presence of the M/AC catalysts in the order of Ni/AC < Pd/AC < AC < Ru/Ac < Ce/AC. The total hydrocarbon was increased from 11.32% to 19.45-70.21% with the maximum total hydrocarbon contents obtained by using Pd/Ac catalyst (J: C of 1:1).
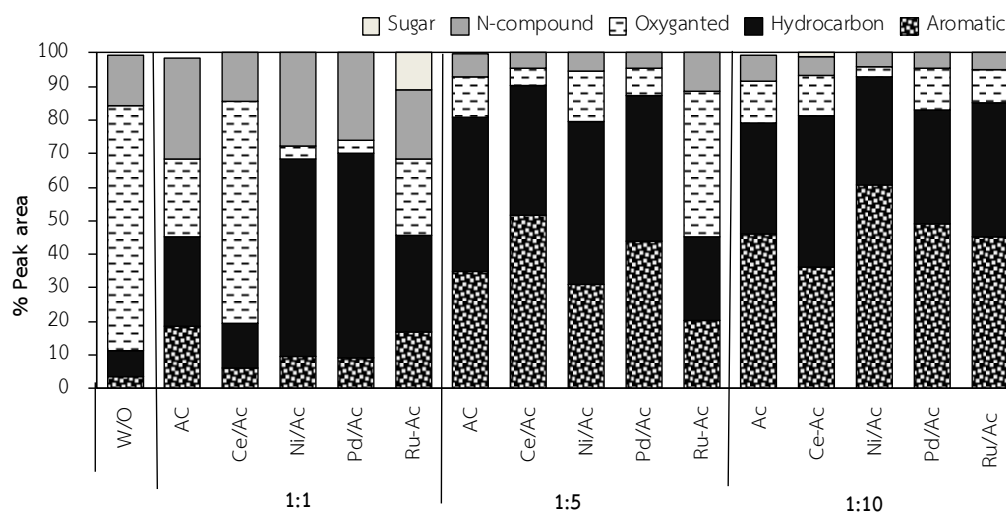
**Fig. 5. 20** Average total composition of the pyrolytic products obtained with
Activated carbon catalysts at a J/C ratio of 1:1, 1:5 and 1:10

All catalysts reduced the pyrolytic vapor acid content catalyst except for Ru/AC, while N-compounds were mainly in N-nonheteroatom forms similar to that obtained with the catalysts at a J/C ratio of 1:1 (14.25-30.10%), they were clearly decreased from 30.10% to 5.00% (J:C 1:10). It may be due to N-compound were adsorb in pore of catalyst. With increasing J:C to 1:10, the main aromatic compounds formed were BTEX, with the highest aromatic selectivity obtained in the order of Ce/AC > Ni/AC > Pd/AC > Ru/AC. Interestingly, Ni/Ac catalysts had highest hydrocarbons and aromatic content of 32.33 and 60.45, respectively. Acid compounds are a good indicator of the quality of bio-oils.  This implied that these catalysts at a J/C ratio of 1:10 were effective for cracking large molecules (long chain fatty acids) to form smaller hydrocarbon molecules. The result similar to the Ac catalyst powder in the previous section.

This result agreed well with several researches which reported low yield of hydrocarbon in non-catalytic fast pyrolysis and significant increase in hydrocarbon with catalyst addition. The aldehydes almost completely diminished by Pd/Ac catalysts (1.04%). There were several researches that studied the effect of catalyst to biomass ratio (Kaewpengkrow et al., 2014a; Mochizuki et al., 2013; Murata et al., 2012). The result indicated that high catalyst to biomass ratio (C:B of 5:1 or 10:1) noticeably increased total hydrocarbon compounds and decreased the oxygenated compounds.

Though the product distributions of pyrolysis vapors were similar to those of low catalyst to biomass ratio (Kaewpengkrow et al., 2014a; Mochizuki et al., 2013; Murata et al., 2012). Therefore, the effect of catalyst on product composition with low catalyst to biomass ratio (1:1) was studied in this work to investigate the effect of catalyst in a more realistic large-scale reactor by drop tube pyrolyzer since using large amount of catalyst would be prohibitive. Moreover, the effect of various catalysts on the relative proportion of oxygenated and total hydrocarbon compounds of the pyrolytic products is shown in Fig. 5.21.
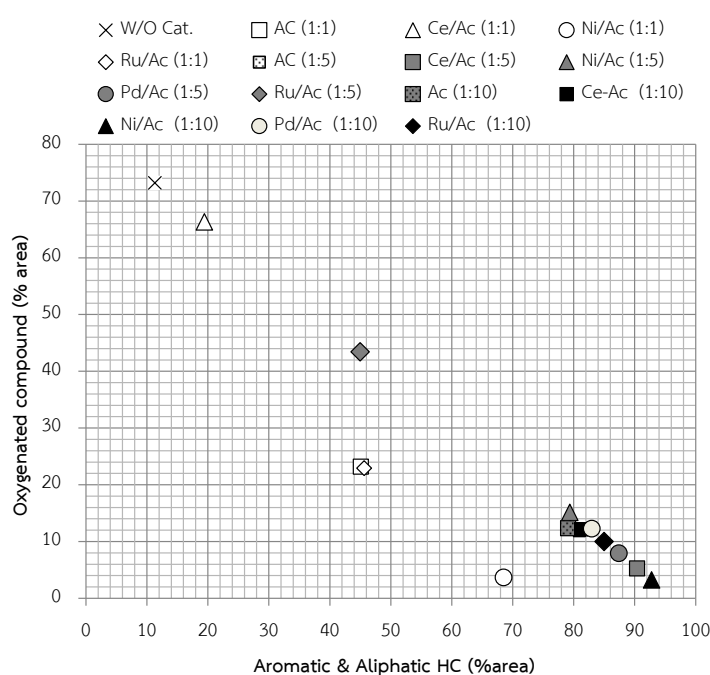


**Fig. 5.21** Effect of the metal/Ac catalysts and J/C ratios on the proportion of oxygenated and total hydrocarbon compounds in the pyrolytic product

A high proportion of total hydrocarbon compounds were obtained with the Ni/AC Ce/AC, and Pd/AC catalysts, which exhibited an improved selectivity towards the aromatic and aliphatic hydrocarbon production of more than 85% and decreased the oxygenated compounds to less than 10%. As a result, the Pd/Ac and Ni/Ac catalysts effectively increased hydrocarbon while reduced oxygenated compounds. Therefore, the metal-activated carbon catalysts included Ac, Ni/Ac and Pd/Ac were used to study the bio-oil upgrading by catalytic fast pyrolysis of Jatropha waste using in-situ drop tube pyrolyzer which were reported in the Chapter 6. These results suggest that the

M/AC catalysts were effective for the deoxygenation reaction of the pyrolysis vapors to form aromatics. The reaction pathway includes dehydrogenation and dehydroaromatization of aliphatic oxygenates, and carboxylation of carboxylic acids to form phenol derivatives, which then undergo HDO into toluene and xylenes, follow by DAR to yield naphthalenes. These results corresponded to previous section which reported M/Ac supported in powder form was effective for deoxygenation, extremely produced aromatic and less promoted N-compounds at the same time.

## 5.7 The catalytic pyrolysis with 5% metal on Bio-char catalysts

Last of all, the synthesized catalysts were modified 5 wt% metal catalysts (Ni and Pd) over char supporter from slow pyrolysis of Jatropha wastes. exhibited high surface area of 35.65-414.9 $m^2$/g. The pore size of solid char pyrolyzed at 600° and 700°C was approximately equal and less than 10 μm. Therefore, it is possible to utilize the solid char in catalyst applications. At a J/C ratio of 1:1, the yields of aliphatic hydrocarbon compounds (20.4–39.8%) were significantly increased as shown in Fig. 5.22. It is apparent that hydrocarbon yields increased in all catalysts. The char-600, and char-700 were less effective such that carboxylic acid yield were still high (>30%).
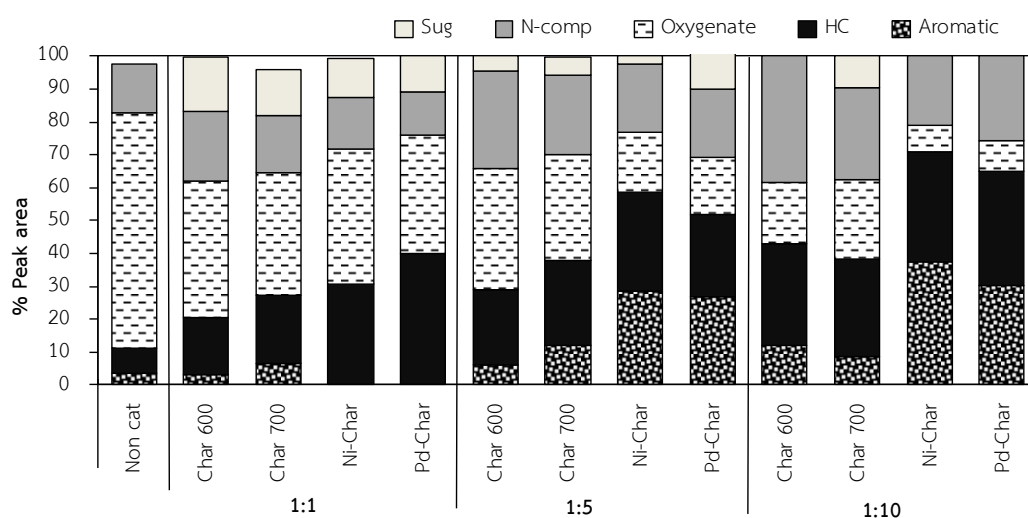


**Fig. 5. 22** Average total composition of the pyrolytic products obtained with bio-char catalysts at various of J/C ratio

With increasing J: C ratio, hydrocarbon compounds were significantly increased from 7.74% to 29.68–34.85% with the highest yield obtained by Pd/char catalyst. The selectivity of aromatic compounds was maximized with content of 37.38% after catalyzed by the Ni/char. The carboxylic acid fraction completely dropped especially in the presence of Ni/char and Pd/Char, the aliphatic hydrocarbon compounds were mainly pyrolytic product. The highest yield aliphatic hydrocarbon of 71.0% was obtained by Ni/Char which high surface area (414.9 m$^2$/g) produced the highest aromatic hydrocarbon yields of 23.72%. Interestingly, all catalysts perform very well on reduced N-compound to less than 30%. It can be inferred that the amount of catalysts affected the cracking heavy compounds because of its high surface area to react with pyrolytic vapors. The effect of bio-char catalyst on the pyrolysis products of Jatropha seem to be related to the pore size of catalyst.
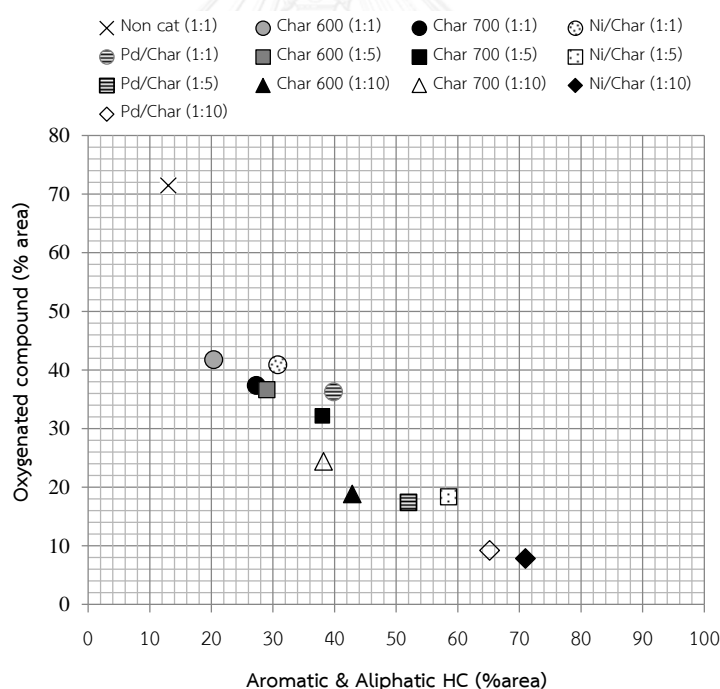


**Fig. 5.23** Effect of the metal/Ac catalysts and J/C ratios on the proportion of oxygenated and total hydrocarbon compounds in the pyrolytic product.

Among bio-char, Ni/Char showed highest decrease in oxygenated compounds with a relatively high hydrocarbon yield. The results corresponded with recent works

which have studied tar conversion using the char- supported Ni catalysts. They reported that Ni was distributed more uniformly on the surface of the coal char support, because the porous surface structures of the coal char, which enhanced adhesion of NiO particles (Shen, 2015). The effect of various catalysts on the relativity of oxygenated compounds and total hydrocarbon compounds of pyrolytic products are shown in Fig.5.23. In the presence of catalyst, high total hydrocarbon compounds and oxygenated compounds were obtained by Ni/Char (1:10), Pd/Char (1:10), Ni/Char (1:5) Pd/Al$_2$O$_3$, and Char-600 (1:10) catalysts, respectively.

# CHAPTER 6

# RESULTS AND DISCUSSION OF BIO-OIL PRODUCTION

# USING DROP TUBE REACTOR

## 6.1 Catalytic pyrolysis process of Jatropha wastes using a drop tube reactor

Catalytic fast pyrolysis of Jatropha residues was studied using ceramic catalyst in a catalytic process development unit of a drop tube reactor. One of the most interesting configurations of pyrolysis reactors is an entrained flow reactor, which is also called a free-fall reactor or a drop-tube reactor. The technical concept of this reactor is very simple compared with the other types (Pattiya et al., 2012). Biomass particles are allowed to drop or move downward under gravitational force together with some entrained flow of inert gas inside a tubular reactor.

There have been reports to investigate the effects of biomass types and pyrolysis conditions, such as reactor temperature, residence time and effective catalyst, on catalytic pyrolysis of Jatropha wastes by using a drop tube reactor. Catalytic fast pyrolysis has significant advantages over other biomass conversion processes due to its simplicity and low process cost. In this single step process, biomass is thermally decomposed into pyrolysis vapors which enter the ceramic catalysts and are converted into desired aromatics and olefins along with CO, $CO_2$, $H_2O$, and coke.

In this work, fast pyrolysis of Jatropha wastes was carried out by drop tube updraft pyrolyzer in order to produce bio-oil. Catalyst was added into the pyrolyzer to improvement the bio-oil quality. Effect of particle size, operating temperature, and type of catalysts on yield of bio-oil, quality, and product distribution were discussed. For each run, Jatropha wastes with 0.125- 0.425 mm. was fed from the top of the reactor with feed rate of 1 g/min and carried gas at 3 L/min of $N_2$. Pyrolysis temperature was carried out at $600^{\circ C}$. Gas products including $CO_2$, CO, $H_2$ and $CH_4$ were measured by online-gas analyzer. In this section, the effect of pyrolysis temperature and catalysis on product yields were investigated.

6.1.1 Effect of pyrolysis temperature on product yields

To investigate the effect of pyrolysis temperature on product yields, this experiment was carried out at pyrolysis temperature of 400, 500, 600, and 700°C with Jatropha wastes (approximate size 125-425 $\mu$m). Appearance of Bio-oil from Jatropha residue pyrolysis at 600°C was shown in Fig. 6.1. Product distributions from non-catalytic pyrolysis of Jatropha wastes were shown in Fig. 6.2 (a).



**Fig. 6.1** Appearance of Bio-oil from Jatropha residue pyrolysis at 600°C

From the results, pyrolysis temperature strongly influenced on the product yields of solid, liquid, and gas. Solid yield tended to decrease, while gas products increased at greater pyrolysis temperature. Liquid product (bio-oil) was in range of 22-36% depending on operating temperature. It was observed that the maximum liquid yield of 32.87 wt. % was achieved at 600°C.   The condensable gas products were condensed as bio-oil, and were collected in a series of condensers. They were subsequently weighed to obtain the mass of bio-oil. In addition, the bio-char was collected from the inside of the reactor and weighed. The final yields of bio-oil and bio-char were calculated using the following equation:

$$Y_{ob} = \frac{Y_1}{Y_0} \times 100 \qquad\qquad (6\text{-}1)$$

Where $Y_{Ob}$ is the product yield, $Y_1$ is the mass of the desired product (liquid product), and $Y_0$ is the initial mass of the raw material. The gas yield was determined

by difference: gas yield = 100─(bio-oil yield + bio-char yield). Bio-oil from fast pyrolysis of Jatropha waste was in range of 25.88-32.87% depending on operating temperature, and was maximized at 32.87 wt. % by pyrolysis temperature of 600°C. Solid yield (bio-char) tend to decrease with increasing the temperature, and was in range of 29.73-47.67%.

This result corresponded well to other previous works. . Pattiya and coworker suggested that the optimum pyrolysis temperature in order to obtain high liquid yield was in the range of 469-475°C for cassava rhizome and cassava stalk (Pattiya and Suttibak, 2012). It is well known that maximum liquid yield for most biomass can be obtained at pyrolysis reaction temperature of 500°C with high heating rate and short residence time to minimize the secondary reaction (Bridgwater, 2012). Kim et al. (2013) studied the pyrolysis of Jatropha seedshell cake (JSC) in a fluidized bed. The effects of bed temperature and gas flow rate on the product yields and properties of pyrolytic liquid have been determined (Kim et al., 2013). They found that the pyrolytic liquid product and fractionated oil yields of JSC were maximized at 48 wt. % and 32 wt. % with increase of bed temperature. Jourabchi et al., (2014) explored the effects of pyrolysis parameters on the yield and quality of bio-oil from Jatropha curcas pressed cake. It was pyrolysed in a fixed-bed reactor over a temperature range of 573.15 K to 1073.15 K and a nitrogen flow of 7.8 $\times 10^{-5}$ m/s to $6.7 \times 10^{-2}$ m/s. They found that at optimum pyrolysis conditions, above 50% of the waste is converted to bio-oil. At higher temperature of 600-700°C, the liquid yield decreased significantly due to enhanced cracking reaction of condensable pyrolytic vapors to non-condensable gas such as methane ($CH_4$), carbon dioxide ($CO_2$), carbon monoxide (CO) and hydrogen ($H_2$). The decomposition reaction might be described by the following reactions:

Thermal cracking:     $pC_nH_x \longrightarrow qC_mH_y + rH$     (6-2)

Carbon formation:     $C_nH_x \longrightarrow nC + x/2H_2$     (6-3)
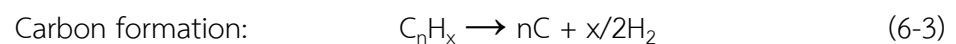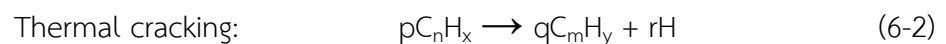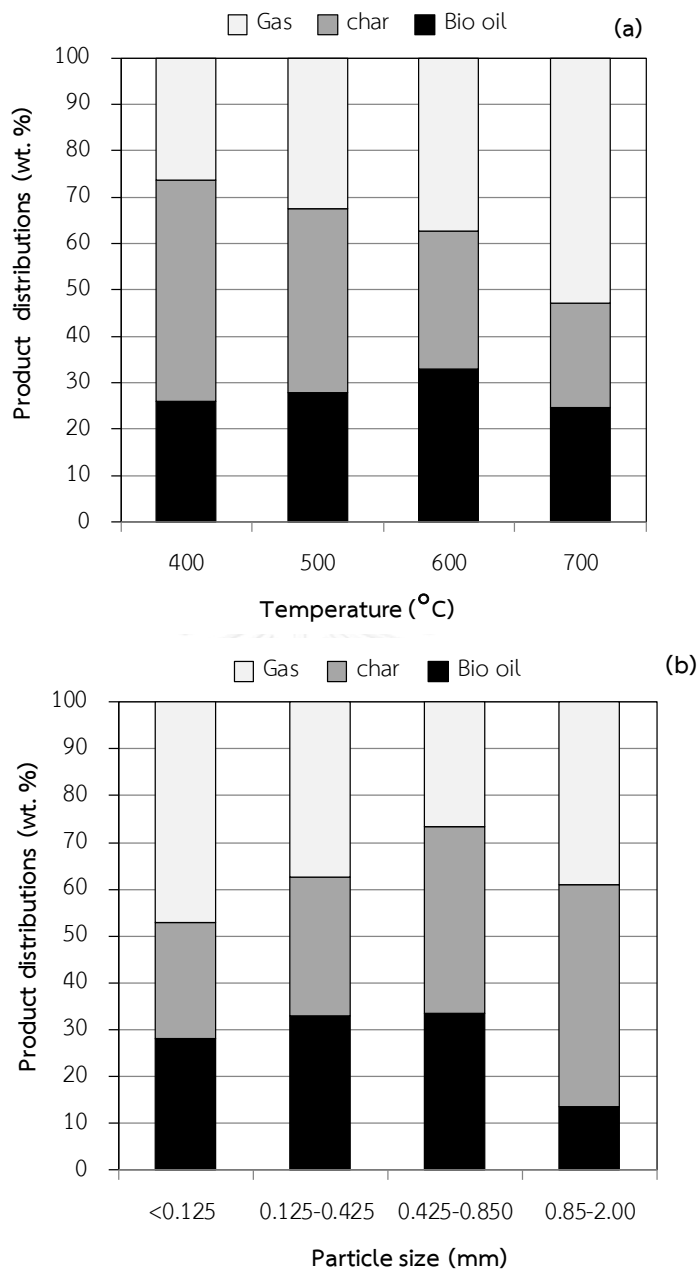
**Fig. 6.2** Product distributions (%yields) obtained from pyrolysis of Jatropha

Typically, higher temperature leads to significant positive effect on bio-oil yield (Kim et al., 2013). In many parameters, particle sizes of biomass are related with the quantitative and qualitative of bio-oil. The effect of particle size of biomass on product yields was performed at pyrolysis temperature of 600°C. Four different sizes of Jatropha waste consist of size less than 0.125, 0.125-0.425, 0.425-0.850 and 0.850-2.0 mm. Product distribution from fast pyrolysis of Jatropha waste with various temperatures

and particle size was shown in Fig 6.2 (b). The results showed that bio-oil increased with particle size of 0.125-0.425 mm and 0.425-0.850 mm. The maximum bio-oil yield of 33.54 wt.% was achieved at the particles size of 0.425-0.850 mm, while yield of only 13.55 wt.% was obtained with the largest size of 0.85-2.0 mm with the maximum char yield of 47.43 wt.% suggesting incomplete pyrolysis on the later case. The highest gas products (47.20 wt.%) obtained from <0.125 mm particle size. It can be seen that gas product increased greatly while solid and liquid yields decreased with a small particle size. Heating rate and the thermal conductivity of the biomass have significant influence on the pyrolysis products. The small particle size can be heated uniformly which is consistent with previous studies. For all pyrolysis runs, high bio-oil was achieved at reaction temperature of 600°C and particle size of 0.125-0.425 mm as well as particle size of 0.425-0.825 mm. Similar to Biradar et al., (2014) who studied pyrolytic bio-oil from Jatropha de-oiled seed cake by a fluidized bed pyrolysis, and they found that the maximum bio-oil yield was obtained from moderate particle size of 0.5-0.99 mm [14]. This result suggested that mass and heat-transfer restrictions had an influence at a larger particle size, resulting in maximum bio-oil yield.

In order to confirm this assumption, the conversion of Jatropha biomass to gas is further investigated by online gas analyzer (MRU GmbH; SWG 200-1) that coupling with Flamed Ionized Detector (FID) and Non-dispersive Infrared Detector (NDIR). During pyrolysis, gas products were analyzed by gas analyzer in the form of four non-condensable gases such as methane ($CH_4$), carbon dioxide ($CO_2$), carbon monoxide (CO) and hydrogen ($H_2$). The composition of the product gas was analyzed using an online gas analyzer capable of continuous real-time quantification of CO, $CO_2$, $C_xH_y$ (as $CH_4$) and $H_2$. These gas products are non-condensable gas which was generated from thermal cracking reaction (Bridgwater, 2012; Manurung et al., 2009). From Fig. 6.3 shows the reaction time of gaseous products during fast pyrolysis of Jatropha waste (0.125-0.425 mm) at 600°C. It can be seen that all gas product concentrations quickly reach the maximum within 20 min and remain constant for the following 30 min. At higher temperature of 600°C, the liquid yield decreased significantly due to enhanced cracking reaction of condensable pyrolytic vapors to non-condensable gas such as methane

($CH_4$), carbon dioxide ($CO_2$), carbon monoxide (CO) and hydrogen ($H_2$). Gas products from other pyrolysis conditions during fast pyrolysis are shown in the appendix C.
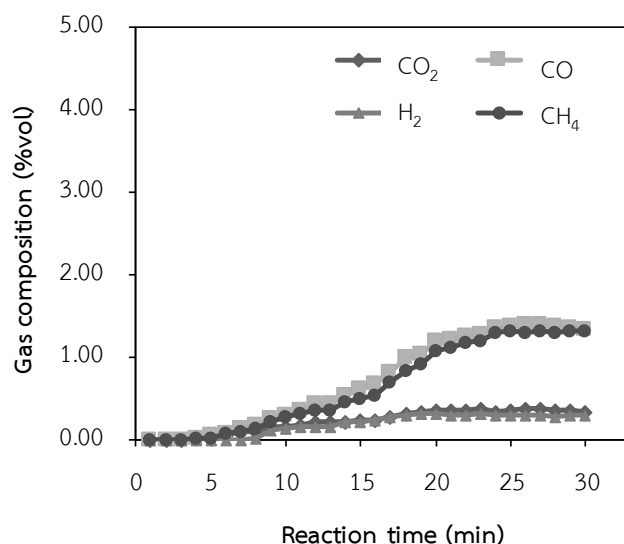


**Fig. 6.3** Gas products as a function of reaction time for fast pyrolysis of Jatropha wastes (0.125-0.425 mm) at 600°C

Gas product species from fast pyrolysis of Jatropha waste with various temperature and particle size was analyzed and reported in term of weight percentage which is shown in Fig. 6.4. The gas product contained mainly of CO and $CH_4$ in range of 1.47-15.84 wt. % and 0.81-13.89 wt. %, respectively. The relatively high $CH_4$ may result from a high carbon and hydrogen content in the raw material. The maximum yields of CO and $CH_4$ were obtained from pyrolysis temperature at 700°C. The influence of temperature on total gas product is that hydrocarbons and tar would be cracked into greater gas yields at higher temperature. As a result, it can be seen that $CH_4$ and $H_2$ greater when the temperature increasing. Results are similar to Sricharoenchaikul et al, who found that greater hydrogen and methane formation occurs at higher temperature, and methane from pyrolysis of Jatropha waste is quite common to those of other agricultural waste (Manurung et al., 2009).
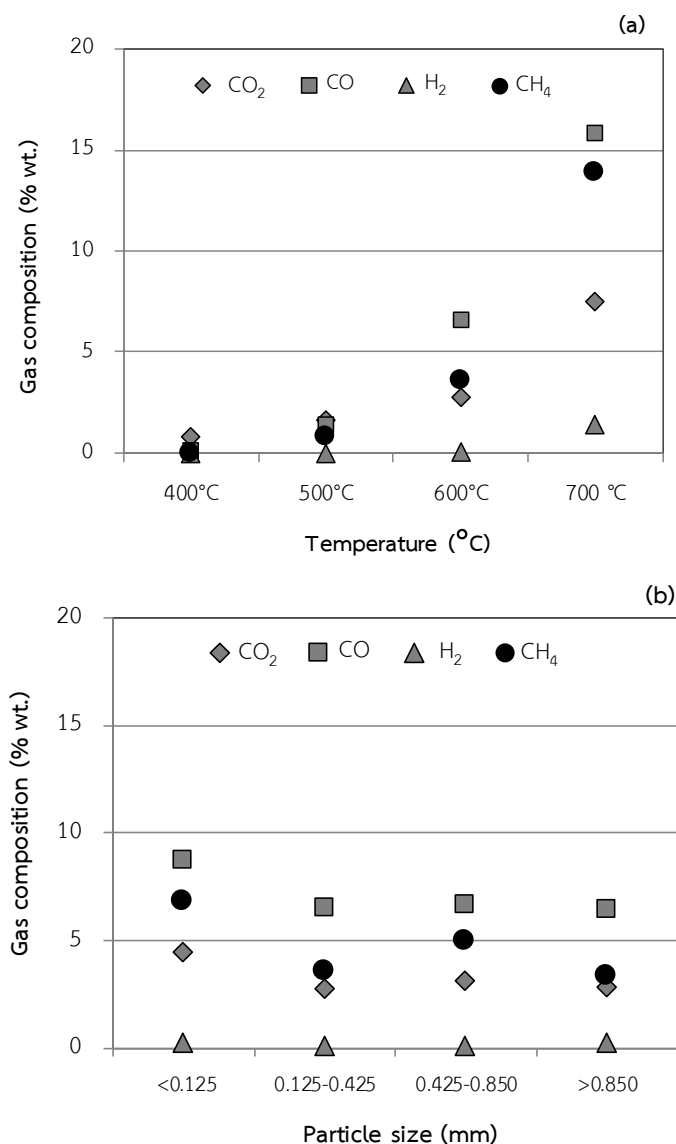
**Fig. 6.4** Gas species from fast pyrolysis of Jatropha waste at (a) different temperature with particle size of 0.125-0.425 mm and (b) different particle size at 600°C

$CO_2$ slightly increased in range of 0.8-7.5 wt.% at higher temperature; however, this process less released $CO_2$ than other researches (Biradar et al., 2014; Manurung et al., 2009). The maximum gas product of 20 wt.% obtained from the smallest particle size (<0.125 mm). Various particle size of Jatropha waste (0.125-0.425, 0.425-0.850 and >0.85 mm) have not significantly on gas products. Overall performance, at the particle size of 0.125-0.425 mm and pyrolysis temperature at 600°C seems suitable for obtaining a high yield of liquid product and low yield of $CO_2$ in fast pyrolysis of Jatropha waste.

6.1.2 The effect of gas flow rate on bio-oil products

To investigate the effect of gas flow rate on yields of pyrolysis products, the experiments were performed at three different gas flow rates of 2, 3, and 4 L/min. The pyrolysis temperature and particle size range were kept constant at 600°C and 0.125-0.425 mm, respectively. The $N_2$ flowing through the pyrolysis bed should only be enough to ensure that the absence of $O_2$ is available in the reactor for reactions with the heated biomass. Fig. 6.4 showed the product distribution with various $N_2$ gas flow rate, the maximum bio-oil was 36.20 wt%, and obtained by gas flow rate of 4 L/min. It was observed that liquid product yield increased by only 4 wt% upon increasing the nitrogen flow rate from 2 L/min to 4 L/min, the char yield decreases because uncondensed volatiles are removed from the reaction zone by the nitrogen stream (Jourabchi et al., 2014).
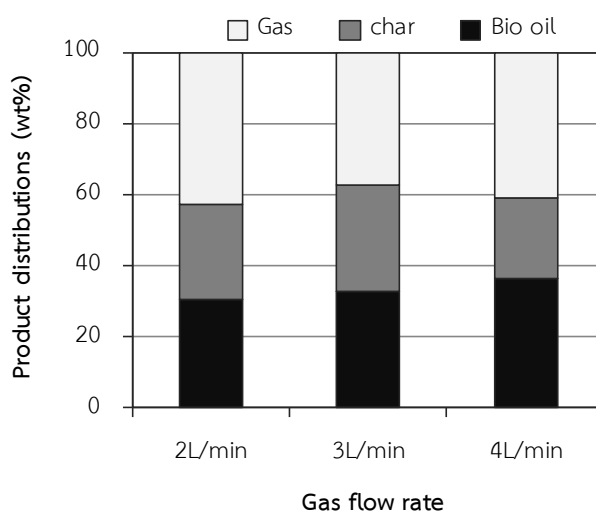


**Fig. 6.5** Product distribution from pyrolysis of Jatropha waste with various gas flow rate

The gas yield slightly decreased with increasing nitrogen flow rate from 2 L/min to 3 L/min. At lower flow rate of gas (2 L/min), there would be higher gas products because the vapor residence time is more and hence abundant amount of time is available for secondary cracking of pyrolytic vapor and bio-char (Mihalcik et al., 2011). Therefore, gaseous product was increased and decreased yield of bio-oil and bio-char. The result corresponded with Biradar et al. (2014) who studied the pyrolysis

of Jatropha de-oiled seed cake by fluidized bed pyrolysis system, and found that the moderate flow rate (8 LPM) can be produced higher bio-oil (Mihalcik et al., 2011). Whereas, Jourabchi et al., (2014) carried out a parametric study of pyrolysis of Jatropha oil cake by fixed bed reactor, the maximum oil yield of 50 wt% was obtained at 500°C, and low $N_2$ velocity positively impacted the bio-oil yield. The result suggested that higher gas flow rate less effective to increase the bio-oil yield. Therefore the optimum flow rate for higher bio-oil production in the further condition operating would be 3 L/min. Although the gas flow rate had not effect significantly on bio-oil yield, the qualitative of bio-oil were also investigated by GC-MS in the next section.

### 6.1.3 The effect of catalysts on bio-oil upgrading

As well known, the bio-oils upgrading is a complex reaction network due to the complex compositions of pyrolysis oils (Bu et al, 2012). Thus, Bio-oil would be upgraded by catalytic catalyst. From chapter 5, after the screening catalytic performance by using an analytical Py-GC/MS technique, metal catalysts with ceramic supports exhibited high catalytic performance especially $Ni/Al_2O_3$ catalyst. Based on the above results, it can be concluded that $Al_2O_3$ based catalyst behaves better ability in upgrading of Jatropha waste fast pyrolysis vapors than other support catalyst. In addition, the activated carbon catalyst exhibited improved selectivity toward the aromatic and hydrocarbon production of more than 60% and decreased oxygenated compounds to less than 10%. Consequently, these catalysts selected from Py-GC-MS experiment were tested in a semi continuous fixed bed reactor by drop tube pyrolyzer. $Al_2O_3$ support was modified by extrusion in pellet form (synthesized), while the activated carbons in granule form (commercial) were used in order to facilitate its testing in drop tube reactor. The catalytic pyrolysis was carried out at pyrolysis temperature of 600°C with Jatropha wastes (approximate size 125-425 $\mu$m). Generally, biomass fast pyrolysis vapors were composed of volatile compounds and condensable (bio-oil). Bio-oil produced was in range of 21.67-39.38%, and the maximized bio-oil obtained by activated carbon (Ac) support. In catalytic trials with $Al_2O_3$ extruded, the bio-oil was in range of 22-36wt%  The maximum liquid yield of 32.87 wt.% was

achieved with Ni/Al$_2$O$_3$. Product distributions from catalytic pyrolysis of Jatropha wastes were shown in Fig. 6.6. The result indicated that solid and liquid yields tended to decrease, while gas products increased with the presence of the activated carbon-based catalyst. Solid yields from fast pyrolysis were decrease from 29.7% to 24.87-27.23 wt.% with the presence of catalyst. In addition, gas yield increased to 34.72-53.47 wt.%, the maximum yield was obtained by Pd/Ac. With the Al$_2$O$_3$ extruded catalysts, solid yields from fast pyrolysis were not significantly decreased (24.87-31.37wt. %). In addition, gas yield increased to 37.00- 43.41%, the maximum yield was obtained by Pd/Al$_2$O$_3$ (ext.). Total non-condensable gas yields including CO$_2$, CO, CH$_4$ and H$_2$ are showed in Fig.6.6. Production of CO and CO$_2$ are an indicator of the deoxygenation capability of a catalyst in catalytic fast pyrolysis of biomass. With the presence of catalyst, more CH$_4$ and CO are produced while char and bio-oil decreased. The maximum H$_2$ was achieved by 5%Ni/Al$_2$O$_3$ (ext.), suggesting its effectiveness to deoxygenation reaction. After catalytic run, the liquid yield was reduced from 32.87 to 17.67 wt.%. It might be due to the catalyst promoted cracking reaction of the larger molecule into small molecule (Wu, et.al 2009; Iliopoulou et.al, 2012).
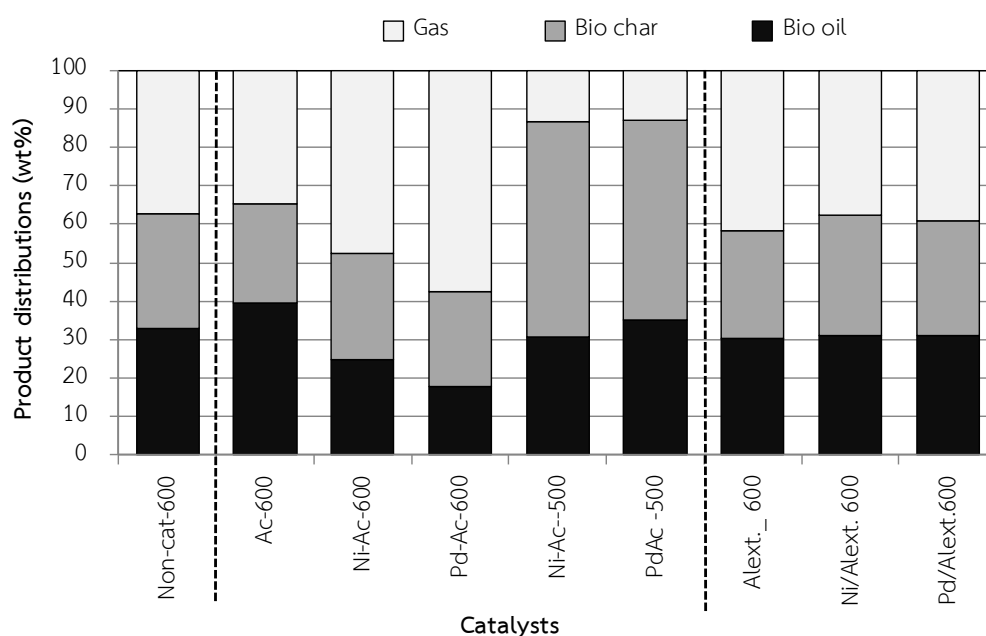


**Fig. 6.6** Product distribution from pyrolysis of Jatropha waste with various catalysts

Total non-condensable gas yields including $CO_2$, CO, $CH_4$ and $H_2$ are showed in Fig.6.7. Production of CO and $CO_2$ are an indicator of the deoxygenation capability of a catalyst in catalytic fast pyrolysis of biomass (Shen et al., 2013). With the presence of catalyst, all catalyst resulted in more $CH_4$ and CO, while char and bio-oil decreased. As a result, the oxygen can be eliminated as water, carbon monoxide, carbon dioxide, methane and short-chain acids. The maximum $CH_4$ was achieved by Pd/Ac catalyst, while Ni/Ac enhanced $H_2$ product. Of several metallic catalysts, nickel-based ones are more commonly used by researchers for hydrogen production from the thermal processing of biomass (Abnisa et al., 2013). Generally, addition of prepared catalyst resulted in greater $H_2$, CO and other light hydrocarbon yields from conversion of wastes to these gases. Pyrolysis–gasification increased the gas products of biomass achievable with the presence of catalyst have been broadly reported by several researchers (Abnisa et al., 2013; Shen et al., 2013).

Several studies have been conducted to study the effects of the addition of $Ni/Al_2O_3$ catalysts in the $CO_2$ reforming of methane. The maximum $H_2$ was achieved by $5\%Ni/Al_2O_3$ (ext.), it suggested that Ni catalyst effective to deoxygenation reaction. Of several metallic catalysts, nickel-based ones are more commonly used by researchers for hydrogen production from the thermal processing of biomass. The catalytic cracking of bio-oils removes oxygen by decarboxylation reactions, using cracking catalysts at atmospheric pressure. The oxygen can be eliminated as $H_2O$, CO, $CO_2$, and short-chain acids. The oxygenated products are converted to lighter hydrocarbons fractions. Furthermore, the results showed an increase in catalytic activity and a decrease in coke formation over the catalysts. The result corresponded well with Wu et.al, 2009 who reported that the Ni/Al catalyst significantly increased the amount of product gas ($H_2$, CO, $CO_2$ and $CH_4$), and improved the performance of the catalyst in relation to coke formation.
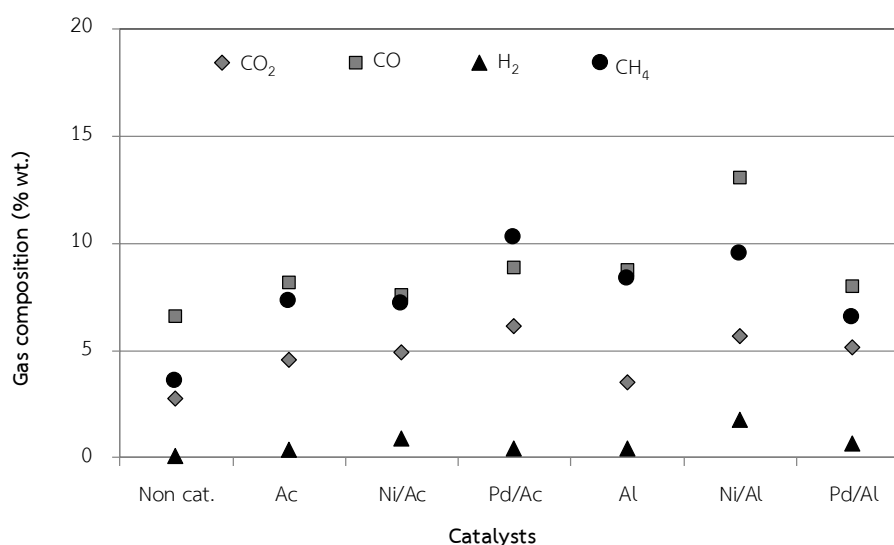
**Fig. 6.7** Product distribution from pyrolysis of Jatropha waste with various catalysts showing (a) product yield and (b) gas composition

Compared to the non-catalytic yields, water, coke and non-condensable gas increased with the presence of catalysts because oxygen was eliminated as water, carbon monoxide, carbon dioxide. The result similar to Mihalcik et al. who reported that non-condensable gas (NCG) production is increased for each catalyst run by HZSM-5 and H-Beta (Mihalcik et al., 2011). Furthermore, the qualitative of bio-oil from the fast pyrolysis of Jatropha waste would be presented in the next section. Summaries of catalytic fast pyrolysis systems for Bio-oil upgrading are shown in Table 6.1.

**Table 6.1** Summaries of catalytic fast pyrolysis systems for Bio-oil upgrading

| Reactor | Biomass types | Catalyst | Temp. (°C) | Bio-oil (%) | Reference |
|---------|---------------|----------|------------|-------------|-----------|
| Fluidized bed | palm kernel shell | zsm-5, FCC | 400 and 485 | 11.7-23.1 | (Kim et al., 2014) |
| Fluidized bed reactor | pine sawdust | ZSM-5, Ga-ZSM-5 | 600 | - | (Jae et al., 2014) |
| Fluidized bed | Jatropha curcas de-oiled seed cake | - | 450 | 48% | (Biradar et al., 2014) |
| Fixed bed | sugarcane bagasse and palm empty fruit bunch | - | 460–600 | 53.4% | (Vecino Mantilla et al., 2014) |
| Fluidized bed | Pine wood | zeolite | 500 | 50-60% | Yildiz et al., 2016 |
| Drop tube | Jatropha waste | $Al_2O_3$ and AC | 400-700 | 30-40% | This work 2017 |

## 6.2 Bio oil characterization

### 6.2.1 GC-MS analysis

The bio-oil obtained from non-catalytic pyrolysis of Jatropha wastes pyrolyzed at 400-700°C was diluted in acetone, filtered (pore size, 0.2 micron) to remove insoluble solids, and analyzed by GC/MS instrument. The organic compounds were classified into 11 groups including acids, alcohols, aliphatics, aromatics, phenols, ketones, ethers, esters, N-containing compounds, sugars, and other unidentified compounds as shown in Fig. 6.8.
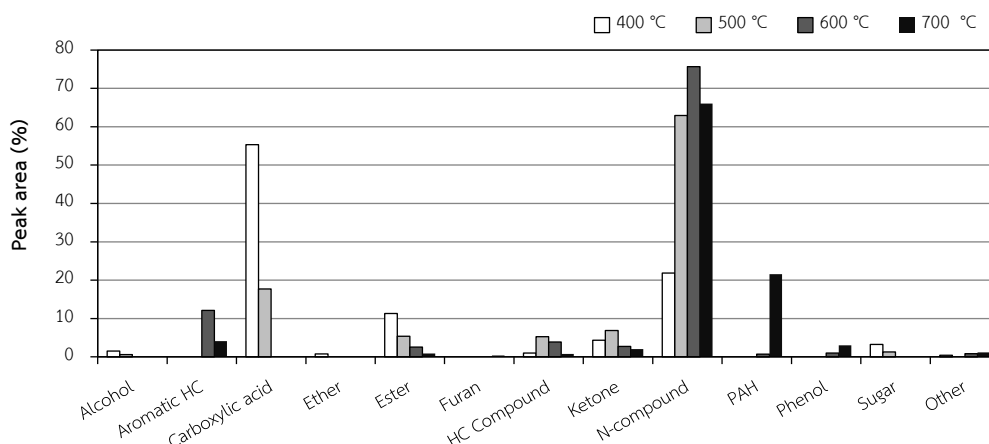
**Fig. 6.8** Chemical analysis (%area) of non-catalytic bio-oil (liquid product)

The sugar compounds were detected in low content at low temperatures (400 and 500°C), and completely eliminated at higher pyrolysis temperatures. It may be inferred that high temperature leads to high efficiency on cracking heavy compounds from cellulose and hemicelluloses. The yield of hydrocarbon compounds such as aliphatics and aromatics tended to increase when temperature was up to 700°C. Hydrocarbon compounds initially appeared after 500°C, and the highest yield was obtained with increasing temperature to 700°C. Hydrocarbons are considered as desirable compounds because it can improve heating values of bio-oil. However, the main hydrocarbon compounds found at 700°C were polycyclic aromatic hydrocarbons (PAHs) involving naphthalene, fluorene, anthracene, and phenanthrene. In addition, phenols also found in small amount at temperature of 600 and 700°C. Phenols are commonly regarded as valued-added chemicals for the production of resins and other chemical products (Qiang, et al., 2009; Lu, et al., 2010). Furthermore, oxygenated compounds (alcohols, esters, ethers, ketones) were obtained in small quantity when increasing temperature up to 700°C. Light carbonyl compounds, ketones, are responsible for ageing reactions and instability of bio-oils.

Unfortunately, the high yields of acids were obtained approximately 17.2-55.3% at lower temperature. The major acid compounds were linoleic acid (C18:2) and palmitic acid (C16:0) which are typically found in Jatropha oils (). It is well known that acids are related with high acidity leading to corrosion problem in engines (French and

Czernik, 2010; Mihalcik, et al., 2011; Murata, et al., 2012). Interestingly, the acid compounds were disappeared by thermal cracking reaction at high temperature of 600 and 700°C. In general, nitrogen element in Jatropha is higher than others woody biomass. Therefore, N-containing compounds in bio-oil were considerably high of 21.8-75.6% and including nitrile, amine, amide, piperidone, piperazine, imidazolidinedione indole, etc. It was noticed that N-containing compounds were in large quantities at high temperature (600 and 700°C) because some nitrogenates such as amides and nitriles might result from the further reaction between nitrogen compounds and fatty acids.

Biomass pyrolysis products were generally known as a complex combination of products from pyrolysis of cellulose, hemicellulose, lignin, and extractives, each of which has its own characteristics (Kim et al., 2013). Bio-oil has been thoroughly characterized by GC/MS techniques, and 50 compounds have been identified. The GC/MS technique cannot provide the direct quantitative analysis of the compounds because the complex products and the absence of commercial available standards. Nevertheless, the chromatogram peak areas are considered linear with quantity of compounds [1]. Product distributions of bio-oil from fast pyrolysis of Jatropha waste were identified into five groups included; aromatic hydrocarbon, oxygenated compound (alcohol, furans, ester, ethers, and ketones) phenols, and N-compound (amine and amide) as showed in Fig. 6.8. The major compound groups found in liquid product are carboxylic acid, included linoleic acid, pentadecanoic acid and palmitic acid which are typically found in Jatropha oils (Kaewpengkrow et al., 2014b; Kim et al., 2013; Murata et al., 2016). This result agreed well with the result of vapor fast pyrolysis in non-catalytic Py-GCMS as mention above. Unfortunately, the high yields of acids were obtained in range of 9.63-92.12%, the highest acid was obtained at 400°C. It is well known that acids are related with high acidity leading to corrosion problem in engines. Interestingly, the acid compounds were clearly reduced to 9.63% by thermal cracking reaction at high temperature of 600°C. These results agreed with Kaewpengkrow et al., (2014) and Vichapund et al., (2014) which studied fast pyrolysis of Jatropha waste was performed using (Py-GC/MS) and found that higher temperature (500-600°C) had positive influence on the yields of pyrolytic products (Vichaphund et

al., 2014). The yield of aromatic and hydrocarbon compounds (aliphatic and cyclic) tended to increase when heating temperature up to 700°C. The phenol compounds (lignin degradation products) were also detected at 600°C which is regarded as value-added chemicals for production of resins and other products.
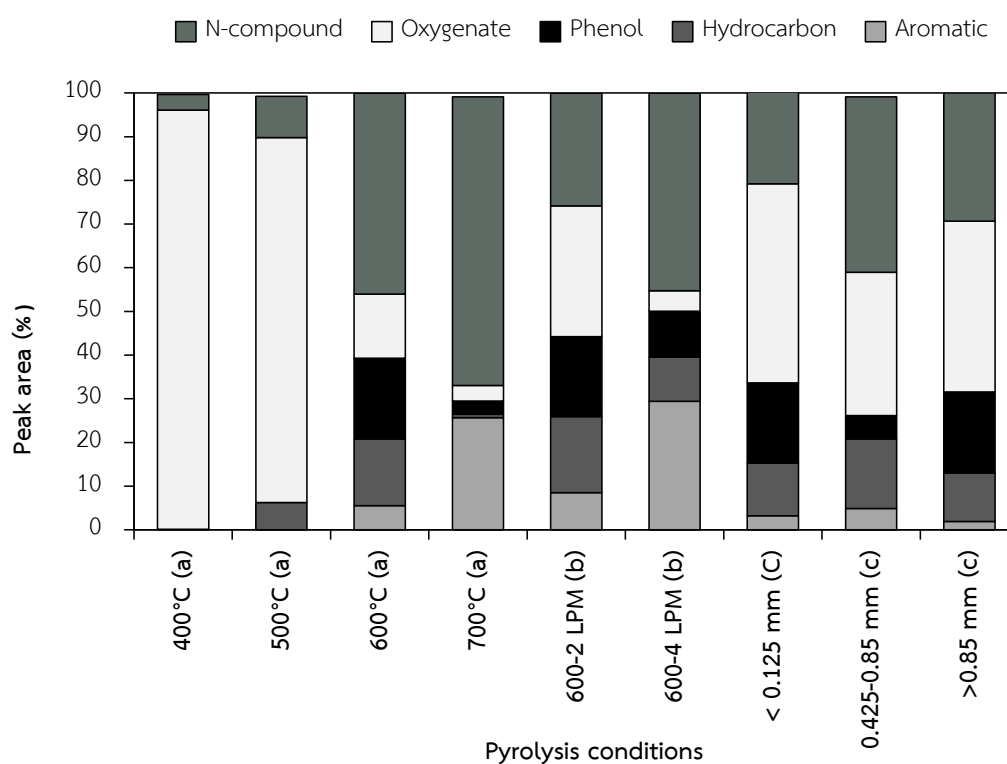


**Fig. 6.9** Product group distribution of bio-oil from different conditions (a) gas flow rate as 3L/min with size of 0.125-0.425 mm (b) 3L/min with size of 0.125-0.425 mm (C) 600°C with gas flow rate as 3L/min

Hydrocarbons are considered as desirable compounds because it can improve heating values of bio-oil. Hydrocarbon and phenol compounds initially appeared after 500°C, and the highest yield was obtained with increasing temperature to 600°C with size of 0.125-0.425 mm as 25.82% and 18.47% respectively. The higher yield of total hydrocarbon compounds (aliphatic and aromatic hydrocarbon) increased when increasing temperature to 700°C (25.58%). In term of effect of particle sizes, the results revealed that the hydrocarbon compounds with the various particle sizes less than the particle size of 0.125-0.425 mm. In addition, bio-oil from Jatropha waste pyrolysis with various particle sizes presented the high contents of phenol (5.37-18.57%) than

other studies. The acids increase the corrosion of bio-oil and cause problems in the engines during combustion as mention above. In pyrolysis trial, the oxygenated compounds presented in slight amount were ketone, alcohol, aldehyde, and furan at lower temperature. At pyrolysis temperature of 600°C, the oxygenated compounds were range of 4.70-45.58%. The highest yield was obtained at particle size of <0.125 mm. Several researches have reported the oxygen content in varying types of biomass to range from 35 to 60 wt%. Fortunately, the bio-oil produced in this work has lower oxygen content than has been previously reported. In addition, the bio-oil had a high concentration of N-containing hydrocarbon compounds, with a carbon number distribution similar to fatty acids (Kim et al., 2014).

N-compound were affected the quality of the bio-oil because they are sources of NOx when combusted as well as corrosive nature of these substances. In pyrolysis trial at high temperature, it is generated various N-containing hydrocarbon compounds in high contents of 66.05% which obtained from 700°C. N-containing compounds (such as amides and nitriles groups) in bio-oils were suggested to be due to reactions of the carboxylic group in fatty acids with nitrogen from the amino acids in Jatropha feedstock. High N-compound in bio-oil is consistent with the results obtained by several researches. The fatty nitriles could be a positive for fuel production since the carbon numbers (C11–C16) are within the diesel range. The nitrile group in the N-compounds is easily removed in the hydrotreating at a petroleum refinery and could be used as a feedstock for chemical products like surfactants. However, this compound is desirable to remove the N-containing compounds prior to using these renewable biofuels.
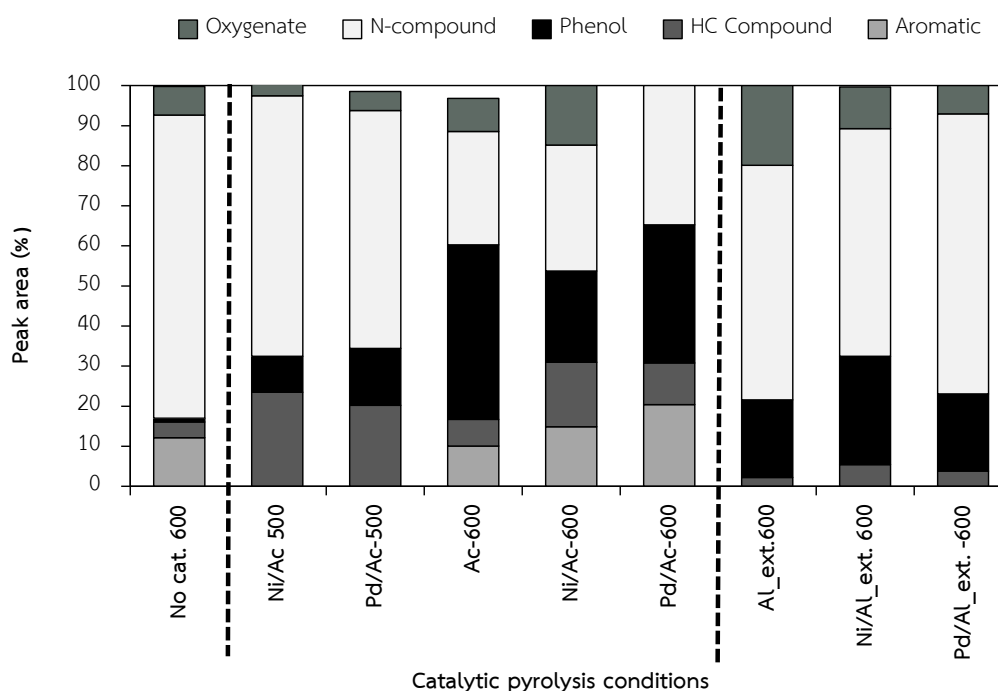
**Fig. 6.10** Product group distribution of bio-oil for (a) different conditions; (b) different catalysts

In catalytic pyrolysis, product distributions from catalytic pyrolysis of Jatropha waste with various catalysts are shown in Figure 6(b). The main products consist of aromatic, hydrocarbon and phenol which are desirable compounds. The selectivity of aromatics was increased from 5.52% to 20.37 % by Pd/Ac, and hydrocarbon compounds increased to 16% by Ni-Ac catalyst. The oxygenated compound and acid dropped considerably to 8.26%, especially with Pd/Ac catalyst which completely reduced acid. N-compounds were reduced from 46% to 31.45-34.43%. Moreover, phenol compounds were also increased to 43.52% by the applying Ac. It may be due to pore size of Ac larger than Ni/AC and Pd/Ac catalysts, so it prefers selected large molecule of phenol through their pores. Ni/Ac and Pd/Ac were the most effective for increased hydrocarbons while decreased oxygenated compounds (15%). It may be their pore and active site of catalyst promoted the deoxygenation, denitrogenation and hydrocarbon formation. This result corresponded to Murata et al., which suggested that the metal-Ac was successive reaction through $H_2$ migration effect, the reaction

could occur at 550-600°C, and $H_2$ formed over Ac surface to metal surface caused acceleration of hydrodeoxygenation (HDO) of oxygenated (acid), phenol to form aromatic Hydrocarbon. Therefore, low oxygen compounds, high aromatics hydrocarbon compounds and phenol of bio-oil are desirable for the pyrolysis of Jatropha wastes volatiles compared to non-catalytic pyrolysis.

In catalytic pyrolysis with $Al_2O_3$ extruded, the major compound groups found in bio-oil are N-compound, included 1H-Indole, 1H-Indole, 3-methyl, and 2,4-Imidazolidinedione, 5-methyl which are typically found in Jatropha oils [4-7]. This result agreed well with the result of vapor fast pyrolysis in non-catalytic from Py-GCMS. The selectivity of phenol was increased from 0.52% to 27.01 %, and N-compounds decreased to 56.81% by $Ni/Al_2O_{3\ (ext.)}$ catalyst. The oxygenated compound and acid dropped considerably to 7.04%, especially with $Pd/A_2O_{3\ (ext.)}$ catalyst which completely reduced acid. Moreover, phenol compounds were also increased to 19.25-27.01% by the applying $A_2O_3$ extruded catalyst. Comparison of $Al_2O_3$ with Ac based catalysts, Ac support were the most effective for increased hydrocarbons while decreased oxygenated compounds to less than15%. Comparison with Activated carbon-based catalysts (Ac, Ni/Ac and Pd/Ac), were the most effective for increased hydrocarbons while decreased oxygenated compounds to less than15%. It may be their pore and active site of catalyst promoted the deoxygenation, denitrogenation and hydrocarbon formation. Based on the above results, it can be concluded that $Al_2O_3$ (ext.), $Ni/Al_2O_3$ (ext.), $Pd/Al_2O_3$ (ext.) lower deoxygenation reaction than Activated carbon catalysts group.

### 6.2.2 Physical–chemical properties

Typical properties of bio-oil derived from Jatropha waste were given in Table 4. The pH values of bio-oil obtained from the pyrolysis of Jatropha waste were in the range of 3.92–7.78. Generally, the low pH is due to the high concentration of acidic compounds in bio-oil which may result from the degradation of hemicellulose and lignin during pyrolysis. From Table 6.3, it can be seen that the pH increased with higher temperature, while the particle size of Jatropha waste was not affected significantly to

the pH values. The results indicated that the chemical composition of bio-oil is dependent on reaction temperature. Furthermore, it can be seen that pH values close to 7 at temperature of 600°C. It was relative with the chemical composition (by GC/MS) as mention above which had high acid compounds in the bio-oil. Water content is an undesirable component of bio-oil because it resulted in negative for the ignition performance.

**Table 6.2** Characteristic of bio-oil from pyrolysis of Jatropha residues and other biomass; (a) pyrolysis with 0.125-0.425 mm and (b) pyrolysis at 600°C

| Pyrolysis conditions | Bio -oil properties | | | Element | | | |
|---|---|---|---|---|---|---|---|
| | Water (wt%) | pH | HHV (MJ/Kg) | C | H | N | O |
| 400°C [a] | 2.40 | 4.03 | 30.7 | 67.34 | 10.81 | 3.23 | 18.56 |
| 500°C [a] | 3.01 | 4.22 | 31.7 | 64.71 | 10.48 | 4.68 | 20.13 |
| 600°C [a] | 4.81 | 6.85 | 28.1 | 63.39 | 8.69 | 6.85 | 21.06 |
| 700°C [a] | 3.87 | 7.88 | 30.1 | 58.63 | 10.82 | 7.55 | 22.10 |
| < 0.125 mm [b] | 1.85 | 3.92 | 26.6 | 63.69 | 8.69 | 6.85 | 20.77 |
| 0.425-0.85 mm [b] | 9.41 | 4.50 | 24.2 | 63.39 | 8.65 | 7.76 | 20.82 |
| 0.85-2.00 mm [b] | 6.67 | 4.78 | 27.6 | 48.08 | 0.04 | 5.63 | 46.25 |

The measured water contents were in range of 1.85 to 9.41 wt%. The highest water content was the pyrolysis condition of the large particle size of 0.425-0.850 mm and the Ac catalytic at 600°C, and also resulted in low HHV as 24.20 MJ/kg and 26.8 MJ/kg, respectively. The result suggested that the high water and oxygen contents are mainly responsible for the low bio-oil HHV. The elemental composition, heating values and pH values of bio-oils from non-catalytic pyrolysis at different temperatures

(400-700°C) are presented in Table 6.4. The carbon of pyrolysis oil was in the range of 52.9-63.5%, which was in agreement with the results from other literatures. Czernik and Bridgwater reported that the carbon contents in bio-oil were in range of 54-58% (Czernik and Bridgwater, 2004). Hydrogen and sulfur were found in smaller amount. Oxygen content in bio-oils was lower than that obtained from its original biomass. However, the bio-oil still contained relatively high oxygen contents of 18.4-29.4%. In term of nitrogen, non-catalytic bio-oils consisted of high nitrogen contents of 3.23-7.76% at pyrolysis temperature of 600 and 700°C. This result corresponded to the selectivity of nitrogen containing compounds detected from GC/MS technique as reported above.

In catalytic trial, the highest carbon content (65.85%) of bio-oil was obtained by Pd/Ac catalyst, followed by Ni/ $Al_2O_3$ (ext.), Ni/Ac, and $Al_2O_3$ (ext.) non-catalyst. Conversely, the lowest oxygen contents of bio-oil were 17.30% by Pd/Ac. These catalysts promote the cracking of the volatile organics into non-condensable gas and water which related with water content and HHV of bio-oil. The heating values of non-catalytic bio-oil were in the range of 20.4-29.2 MJ/kg which were higher than that from other works. Czernik and Bridgwater reported that the heating values derived from woody biomass were 16-19 MJ/kg (Czernik and Bridgwater, 2004). Pattiya, 2013 pyrolyzed cassava rhizome and stalk in a fluidized bed reactor and found that the heating values of these feedstock were 12.7-15.80 MJ/kg. Moreover, the heating values of non-catalytic bio-oil from this study were closed to those of conventional liquid fuels such as 42.2 MJ/kg for diesel fuel and 40.0 MJ/kg for heavy fuel (Czernik and Bridgwater, 2004).

**Table 6.3** Characteristic of bio-oil from catalytic pyrolysis of Jatropha residues and other biomass; (a) pyrolysis with 0.125-0.425 mm and (b) pyrolysis at 600°C

| Pyrolysis conditions | Bio -oil properties | | | | Element | | |
|---|---|---|---|---|---|---|---|
| | Water (wt%) | pH | HHV (MJ/Kg) | C | H | N | O |
| $Al_2O_3$ (ext.) | 7.53 | 6.12 | 27.08 | 62.56 | 7.63 | 11.33 | 18.48 |
| $Ni/Al_2O_3$ (ext.) | 5.81 | 6.58 | 20.42 | 65.65 | 10.59 | 13.88 | 9.88 |
| $Pd/ Al_2O_3$ (ext.) | 6.12 | 6.23 | 21.56 | 59.47 | 8.16 | 11.78 | 20.59 |
| Ac [a,b] | 12.12 | 5.54 | 26.8 | 60.03 | 7.72 | 11.14 | 21.11 |
| Ni-Ac [a,b] | 5.76 | 6.62 | 28.4 | 62.94 | 9.77 | 6.82 | 20.47 |
| Pd-Ac [a,b] | 8.76 | 6.78 | 29.2 | 65.85 | 11.06 | 5.79 | 17.30 |
| Ni-Ac 500[a,b] | 4.87 | 5.86 | 23.26 | 60.08 | 11.25 | 11.33 | 17.34 |
| Pd-Ac 500[a,b] | 5.15 | 5.98 | 24.49 | 59.47 | 8.16 | 11.78 | 20.59 |
| **Source of bio-oil** | | | | | | | |
| Wood | 15-30 | 2.5 | 16-19 | 54-58 | 5.5-7.0 | 0-0.2 | 35-40 |
| Palm shell | 53 | 2.5 | 6.58 | 19.48 | 8.92 | 0.2 | 71.4 |
| Jatropha | 25 | - | 17.00 | 55.25 | 4.3 | 1.01 | 39.36 |
| Palm upgraded [22] | 15-30 | -2.5 | 23.-31 | 51.59-69.25 | 6.98-9.04 | 6.49-9.43 | 14.5-34.60 |
| Wood | - | - | 16-19 | - | 5.5-7.0 | 0-0.2 | 5-40 |
| Palm shell | 53 | 2.5 | 6.58 | 19.48 | 8.92 | 0.2 | 71.4 |
| Jatropha | 25 | - | 17.00 | 55.25 | 4.3 | 1.01 | 39.36 |
| Palm upgraded | - | - | 23.2-31.3 | 51.59-69.2 | 6.98-9.04 | 6.49-9.43 | 14.5-34.60 |

In comparison, the measured water contents were high of range from 15 to 53 wt% in bio-oil with difference materials. In order to control the water content of biomass fast-pyrolysis oil, drying the biomass feedstock is necessary to obtain very low moisture levels, and leads to a decrease in the water content (Sricharoenchaikul &

Atong, 2009). This result is consistent with the results by Abnisa et al. (2012) who reported that the amount of water content in the bio-oil has effect on the gross calorific value (HHV) and measured HHV of 16–19 MJ/kg. The HHV and water content in this work similar to Kim et al., (2013) who studied the pyrolysis of Jatropha wastes in a fluidized bed, and found that water content and HHV obtained of 1.2 wt% and 30.2 MJ/kg, respectively. Moreover, bio-oil from Jatropha waste and bio-oil upgraded revealed higher carbon and HHV than bio-oil from other biomass (Abnisa et al., 2013; Yildiz et al., 2016). The addition of the metal (Ni or Pd) on catalyst decreased the water yields but boosted NCG yields, showing that the presence of metal promotes the production of gases rather than the dehydration mechanism.

This bio-oil is seemed to be reasonable, compared with other fast pyrolysis studies (Abnisa et al., 2013; Kim et al., 2014; Pattiya et al., 2012). As a consequence, pyrolysis temperature strongly influenced on the product yields of solid, liquid, and gas, while the catalyst effected on the good quality of bio-oil. The results also corresponded with Bulushev et al. (2011) which reported that metal catalyst have studied bio-oil upgrading and concluded that the use of noble metal catalysts (Pd) gives good gas product and a superior activity with removal oxygen compound via deoxygenation. However, these catalysts are expensive. Ni catalysts are promising and not expensive catalysts for bio-oil upgrading. Since the oxygenated compounds are nonpolar, the bio-oil samples are not miscible with petroleum oil. However, bio-oil could be blended with petroleum fuel via emulsification. Therefore, these properties demonstrate that the bio-oil at the optimize condition can be applied as biofuel.

Moreover, high amount of nitrogen affected the pH value of bio-oil, particularly at temperatures of 600 and 700°C. The pH value of non-catalytic bio-oil was in range of 4.72-9.44, which was higher than that from other literatures (2.0-3.7) depending on biomass feedstock. Although, non-catalytic bio-oils have high heating value which is close to the conventional fuel, they contained high amount of oxygen and nitrogen. Therefore, bio-oil should be upgraded by catalysts in order to reduce oxygenated and nitrogen compounds.

## 6.3 Solid characterization

Solid residue collected from the experiments indicated that conversion of volatiles was not complete even at 500°C; it seemed to convert completely at 600-700°C. The residual pyrolytic content was found to be directly proportional to the final holding temperature, as shown in Fig.6.3 After pyrolysis experiment, the solid products which were mainly collected from the bottom of the reactor were characterized for elemental components (CHN) and the morphology. The elemental analysis of solid component from pyrolysis of Jatropha with 125-425 μm in size was determined as shown in Table 6.4. The carbon which was represented as the main element of solid char produced from non-catalytic pyrolysis at 400-700°C was in the range of 44.7-50.9 wt%. It can be seen that carbon, hydrogen, nitrogen and sulfur decreased with increasing temperatures. Solid char is a secondary product from pyrolysis of Jatropha wastes and can be used as an alternative solid fuel (Azargohar, et al. 2014).

The compositions of the char obtained from the experiments were also analysed for the ash content by TGA as shown in Table 6.5. The ash content of char was ranged from 4.77 to 25.33 wt%. It was indicating that volatile components in the Jatropha waste had already been converted to mostly gaseous products during the pyrolysis processes. The highest ash content of 28.53 wt% was obtained from pyrolysis at 700 °C. However, there was no significant difference in the char residue yields from the pyrolysis in the presence with these catalysts at 600°C. It was found that ash content of char residue from fast pyrolysis resulted in low oxygen content in char. The result suggested that the fast pyrolysis temperature at 600-700°C completely convert the Jatropha waste to bio-energy.

**Table 6.4** Elemental analysis of solid yields pyrolyzed

| Pyrolysis conditions | Char properties | | Element (wt%) | | | |
|---|---|---|---|---|---|---|
| | Ash Content | HHV (MJ/Kg) | C | H | N | O |
| 400°C [a] | 17.53 | 18.4 | 44.29 | 5.61 | 4.60 | 27.97 |
| 500°C [a] | 20.95 | 16.80 | 43.59 | 4.30 | 3.89 | 27.27 |
| 600°C [a] | 29.00 | 16.70 | 41.75 | 3.83 | 3.18 | 22.23 |
| 700°C [a] | 28.53 | 14.62 | 50.22 | 4.39 | 2.42 | 14.44 |
| < 0.125 mm [b] | 26.00 | 20.70 | 42.50 | 3.68 | 4.87 | 4.32 |
| 0.425-0.85 mm [b] | 9.05 | 22.51 | 51.90 | 2.89 | 2.89 | 22.24 |
| 0.85-2.00 mm [b] | 4.77 | 25.80 | 55.10 | 5.01 | 1.91 | 33.27 |
| $Al_2O_3$ (ext.) | 25.16 | 15.56 | 42.91 | 6.03 | 4.33 | 22.29 |
| Ni/ $Al_2O_3$ (ext.) | 25.83 | 15.47 | 42.15 | 5.29 | 4.13 | 22.60 |
| Pd/ $Al_2O_3$ (ext.) | 24.26 | 15.35 | 41.65 | 5.48 | 4.05 | 24.56 |
| Ac [a,b] | 20.08 | 16.32 | 54.70 | 6.27 | 2.11 | 16.84 |
| Ni-Ac [a,b] | 17.69 | 15.71 | 41.55 | 3.68 | 3.68 | 26.87 |
| Pd-Ac [a,b] | 25.64 | 16.17 | 49.64 | 6.44 | 3.29 | 14.99 |
| Ni-Ac-500 [a,b] | 21.11 | 15.69 | 40.31 | 7.37 | 5.53 | 25.86 |
| Pd-Ac-500 [a,b] | 20.36 | 15.64 | 40.17 | 7.08 | 5.75 | 26.64 |

## 6.4 Product distribution from experiment and predicted by CFD model

CFD simulations were performed at four temperatures, 400, 500, 600 and 700°C, and three differences gas flow rate (2, 3, and 4 L/min). As shown in Table 6.7, boundary conditions were set as mass flow inlet for nitrogen input and a pressure outlet for the final section of the freeboard, with a constant value equal to the atmospheric pressure. Thermal control of the reactor domain was obtained by assuming a constant temperature at the walls. The simulations were carried out using a standard k–e turbulence model.

6.4.1 Mathematical modelling of fixed bed

Several researches developed a chemically reactive fluidized bed process to predicted major species in the product gas composition using CFD model (Boateng & Mtui, 2012; Borello et al., 2014; Weber et al. 2017) This approach is able to predict all major species in the product gas composition very well. In this work, the model was developed to simulate the pyrolysis of a Jatropha residue in a fixed bed reactor using a drop tube reactor operating in steady state conditions. Transport equations for gas and solid phases are presented in term of governing transport equations.

*6.4.1.1 Continuity equation*

CFD models of the thermochemical processes include description of fluid flow, heat and mass transfer, and chemical reactions. The governing transport equations for k and $\varepsilon$ respectively is:

$$\frac{\partial(\rho Y_i)}{\partial t} + \nabla \bullet (\rho \vec{u} \, Y_i) = \nabla \bullet (\mathrm{D} \, \nabla \, (\rho \, Y_i)) + S_Y + R_f \qquad (6\text{-}4)$$

Where $\rho$ is the density, $\vec{u}$ is the velocity of the gas, m the mass exchange between phases, S is the sources terms and Y denotes the mass fraction of any specie i. For the detail of physical properties of biomass, such as radial distribution of solid phase, solid shear viscosity, ($\mu_s$), thermal dispersion coefficient ($\lambda_g$), the dispersion coefficients ($D_g$) of the species, these constants are default value base on coal properties which obtained from CFD program.

*6.4.1.2 Devolatilization*

In this work, a general method is proposed to provide the speciation of volatile products released from Jatropha residue, including the yields of all main gas species. The CFD study of combustion process requires defining reaction kinetics for the selected biomass. For this reason, experiments aiming at recreating the kinetics for different kind of biomass are required to assess the accuracy of the numerical approaches. In this process, the Jatropha residue is assumed to give rise to volatile species and char. In this process, the waste is assumed to give rise to volatile species and char.

$$R_v = -\rho\frac{dY_v}{dt} = \rho_{sb}Y_vA_v\exp(\frac{E_v}{RT}) \qquad (6\text{-}5)$$

Here $R_v$ is the reaction rate of devolatilization, $\rho_{sb}$ is the bulk density, R is the universal gas constant Av is the pre-exponent factor in devolatilization burning rate and E is the activation energy (sun et al., 2016). The chemical reaction rate is based on the Arrhenius formulation. From TGA analysis in Chapter 4, the activated energy ($E_a$) of Jatropha residue was 160.9 KJ/mol, pre-exponential factor (A) was $2.8\times10^{11}$ $s^{-1}$. These kinetic parameters were applied in CFD model. Activation energy and pre-exponential factor of the Arrhenius kinetic model were evaluated from the experimental results as being:

$$A_v = 2.8\,x10^{11}\,s^{-1}, \ \frac{E_v}{R} = 20358\,\text{K} \qquad (6\text{-}6)$$

The biomass is treated as a solid phase consisting of volatile matters, fixed carbon, ash and fixed water content. The composition of the Jatropha residue obtained from proximate analysis is given in Table 6.5.

**Table 6.5** Chemical properties of Jatropha waste (0.125-0.425mm.)

| Proximate Analysis | (wt%) |
|---|---|
| Moisture | 6.50 |
| Ash | 4.30 |
| Volatile organic content | 71.30 |
| Fixed Carbon | 17.90 |
| **Element Analysis** | **(wt%)** |
| Carbon | 48.70 |
| Hydrogen | 6.10 |
| Oxygen | 34.56 |
| Nitrogen | 5.41 |

In adding the devolatilization to the model, there are three options that can be broadly classified under the following mechanisms: (i) one step global reaction

model (Yu et al., 2015), (ii) one component with parallel reactions model (Borello et al., 2014), and (iii) multicomponent reactions model (Millin et al., 2014). In this study, a one-global reaction scheme is used for the formation of various pyrolysis products as follows:

$$BIOMASS \rightarrow \alpha_1 CHAR + \alpha_2 BIO - OIL + \alpha_3 H_2O + \alpha_4 H_2 + \alpha_5 CO + \alpha_6 CO_2 + \alpha_7 CH_4$$

(6-6)
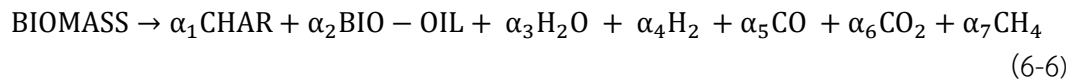
where $\alpha_i$ is the stoichiometric coefficient of reaction. As shown, the overall pyrolysis products are assumed to consist of char, condensable vapour (bio-oil), $H_2O$ and a permanent gas phase (NCG) consisting of $H_2$, CO, $CO_2$ and $CH_4$. Physical properties of Jatropha and boundary conditions of fast pyrolysis prediction are shown in Table 6.6, which used to evaluate the gas species mass fraction of each pyrolysis product at different temperatures and $N_2$ gas flow rate tested in this work.

**Table 6.6** Boundary conditions of fast pyrolysis prediction

| Boundary | Parameter (unit) | Mellin et al (2014) | Borello et al., (2016) | This work |
|---|---|---|---|---|
| Outlet | Pressure-outlet (Pa) | 101325 | 101325 | 101325 |
| Gas inlet | Mass inlet, $N_2$ (kg/s) | 4.5 E-04 | - | 4.167E-06 |
| Feeding line (25°C) | Solid feed rate (kg/h) | 2 | 0.036 | 0.06 |
| | Gas flow rate, $N_2$(Nl/min) | 6.19 | 0.4 | 3 |
| **Material parameter** | Heat conductivity (Wm$^{-1}$K$^{-1}$) | 0.105 | 0.173 | 0.105 |
| | Heat capacity (J kg$^{-1}$ K$^{-1}$) | 1500 | 2310 | 1500 |
| | Density (kg m$^{-3}$) | 600 | 400 | 330 |
| | Char density (kg m$^{-3}$) | 200 | - | 100 |
| | Biomass Particle size (um) | 850 | 1000 | 266 |

The volatile species formation mechanism has been applied by a multi-reaction one-step model to predicted different species formations. Pyrolysis products are greatly influenced by the operative conditions, especially by temperature. Char and tar yields are predominant at low temperature processes; with increased temperature, the light gases (NCG) were increased. The result agreed well with Borello et al. (2016) who developed the CFD model to predict the pyrolysis products of biomass with packed bed reactor.

The gas phase is modelled as a mixture of $H_2$, CO, $CO_2$, $CH_4$, and $N_2$, which is carrier gas in fast pyrolysis process. The condensable products are divided into water and volatile. Volatile is modelled as bio-oil since, as shown by our experimental tests, this is the main component of the pyrolysis oil. Moreover, an additional term representing the formation of water due to the evaporation of moisture within the biomass is introduced. Contour of volatile mass fraction (liquid products) at the different pyrolysis temperature and gas flow rate from CFD model at steady state are shown in Fig.6.11-Fig 6.12.
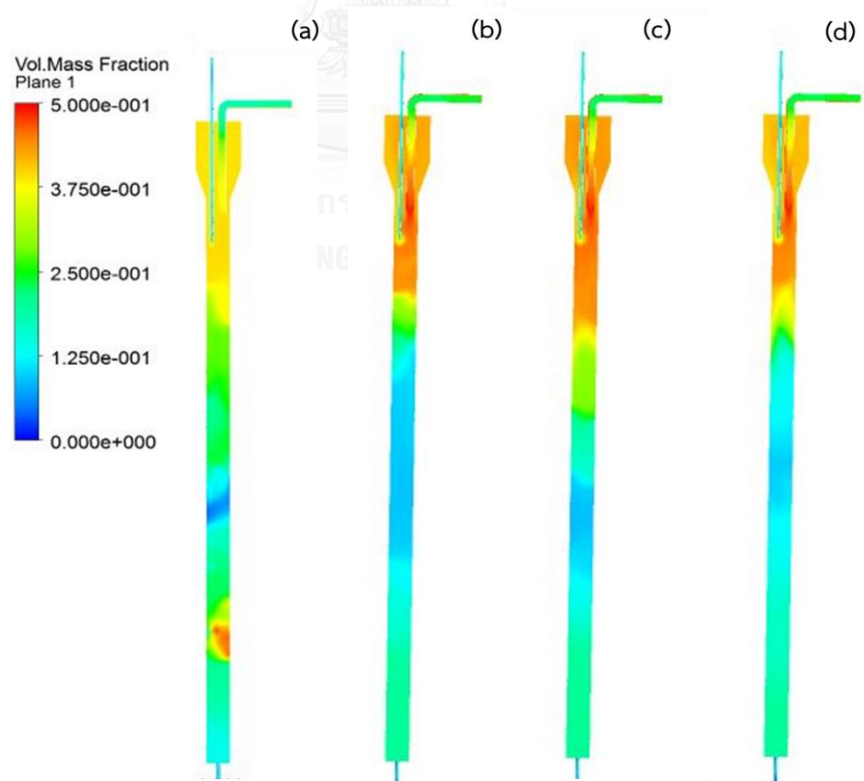


**Fig. 6.11** Contour of volatile mass fraction (liquid products) at the different pyrolysis temperature: 400°C (a), 500°C (b), 600°C (c) and 700°C (d)
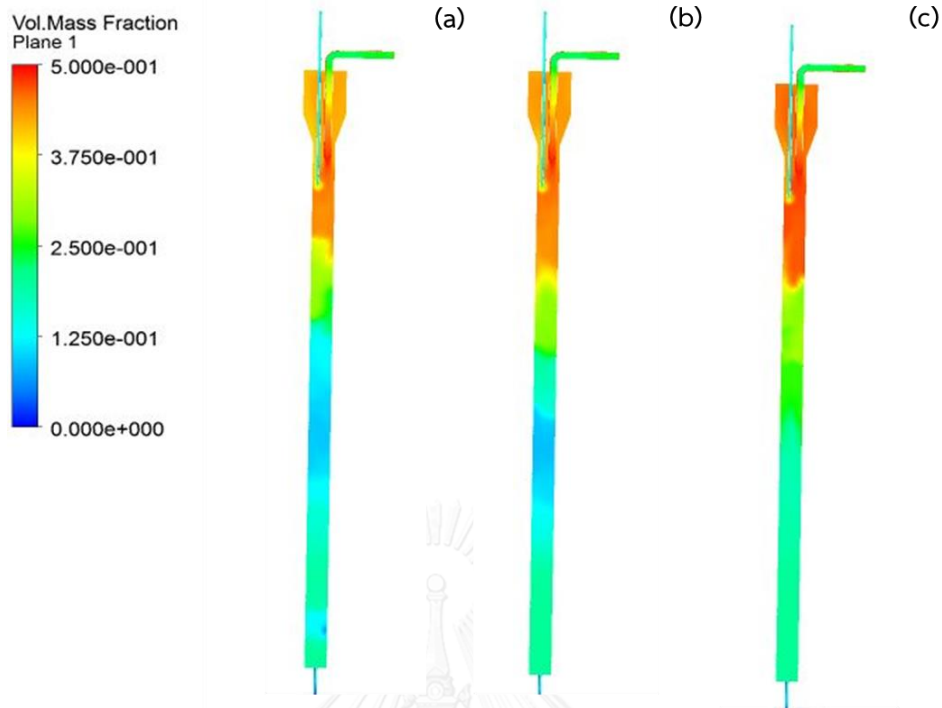
**Fig. 6.12** Contour of volatile mass fraction (liquid products) at the different gas flow rate: 2L/min (a), 3L/min (b), and 4L/min

To better understand the behaviour, volatile mass fractions for the simulation carried out with a boundary condition of $T_{wall}$ in range of 400-700°C are shown in Fig. 6.11. Interestingly, the mass fraction of the volatile occurred at the middle section of the reactor where the reaction zone of Jatropha wastes degradation. The contours of CO, $CO_2$, $CH_4$ and other products yields were shown in the appendix D. The comparisons between the final products predicted with the experimental are shown in Fig. 6.13 (a-c). Predicted bio-oil from fast pyrolysis of Jatropha waste in mass fraction was 0.319-0.386 depending on operating temperature, and was maximized at 0.386 by pyrolysis temperature of 500°C. Solid yield (char) predicted tend to decrease with increasing the temperature to 700°C in mass fraction of 0.160-0.197, while the gas products increased at higher temperature in mass fraction of 0.418-0.498. It may be due to the heterogeneous reaction of char (Wang and Yan, 2008). The simplified reactions models consider the following overall reactions:

$$C + CO_2 \rightarrow 2CO \quad -172 \ kJ/mol \tag{6-7}$$

$$C + \frac{1}{2} O_2 \rightarrow CO \quad +122.9 \ kJ/mol \tag{6-8}$$

$$C + H_2O \rightarrow CO + H \quad -131 \ kJ/mol \tag{6-9}$$
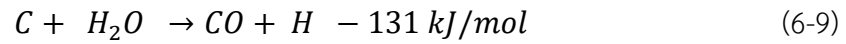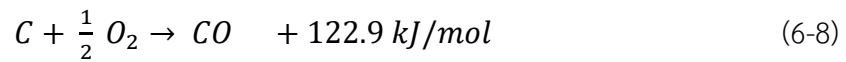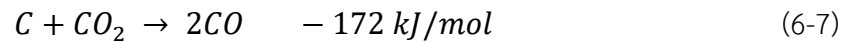
Char and tar yields are the main products at low temperature processes; on the other hand, when the temperature increases, the main products are light gases. As a matter of fact, at high temperature (greater than 600°C), the activation of tar cracking reactions leads to an increase of gas production while reducing the tar yields, whereas char amount is almost constant at temperature higher than 500°C. These results were in good agreement with Borello et al. (2015) who found that char amount was almost constant in all the tests and its value was 16.5 wt% of the initial biomass. The result was also similar to that of Xue et.al (2011) who studied fast pyrolysis of biomass in a fluidized-bed reactor. They found that the predicted yields of char from bagasse pyrolysis at steady-state were 14.42 wt% (mass fraction of 0.14).

To investigate the effect of gas flow rate on yields of pyrolysis products, the experiments were performed at three different gas flow rates. The product distribution with various $N_2$ gas flow rate was not significantly difference. The resulted suggested that at higher temperatures, bio-oil undergoes cracking reactions forming lighter gaseous species, mainly $CH_4$, $H_2$ and CO. In fact, the amount of these gaseous species increases with the increase of the pyrolysis temperature (Borello et al., 2014; Boriouchkine et al., 2015; Borello et al., 2016).
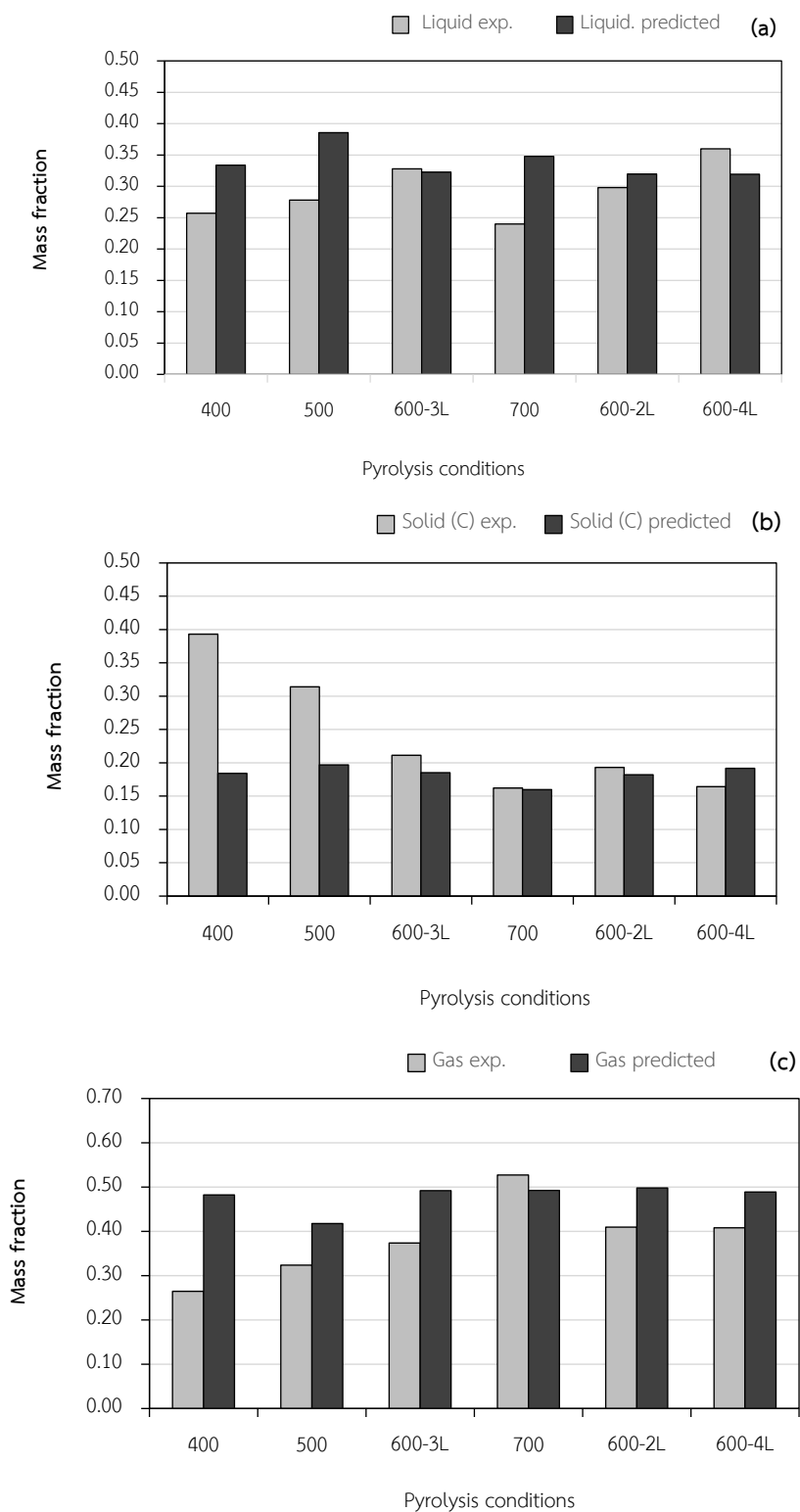
**Fig. 6.13** The mass fraction of pyrolysis product for varying temperatures and gas flow rate (a) Liquid, (b) solid, and (c) gas products

Mass fractions of gases obtained from different temperature and gas flow rate at the steady state. CO is the predominant gaseous specie due to the content of oxygen in the biomass; this oxygen is almost completely removed during the pyrolysis, leaving a solid residue (char, C) composed mainly of carbon in aromatic form. The char amount is almost constant in all the tests and its value is 0.15-0.19 by mass fraction of pyrolysis products. This value matches that measured by the proximate analysis, confirming that pyrolysis process within the reactor is complete. However, pyrolysis products predicted change slightly in each case of the increased gas flow rate. The predicted results were compared with experimental data in respect of % error, and the error of gas fraction, liquid fraction and solid fraction were in range of, 6.67-28.9%, 0.26-11.26% and 16.67-24.59%, respectively. The predicted liquid yields with the highest accuracy was achieved for pyrolysis temperature of 600°C (0.26%), and less accuracy at the lower temperature. This result agreed well with Borello et al. (2015) who studied a mathematical CFD model of pyrolysis process to predict products released in a biomass packed porous bed system. They reported the highest accuracy prediction was pyrolysis temperature at 600°C with less accuracy for tar yield predictions at the lower temperature ($T_{wall}$ = 500°C) by overestimating them of 5.44%. As a result, solid (char), liquid (bio-oil) and gas yields which were predicted by CFD agreed well with experimental data at higher temperature (Fig. 6.13-6.14).
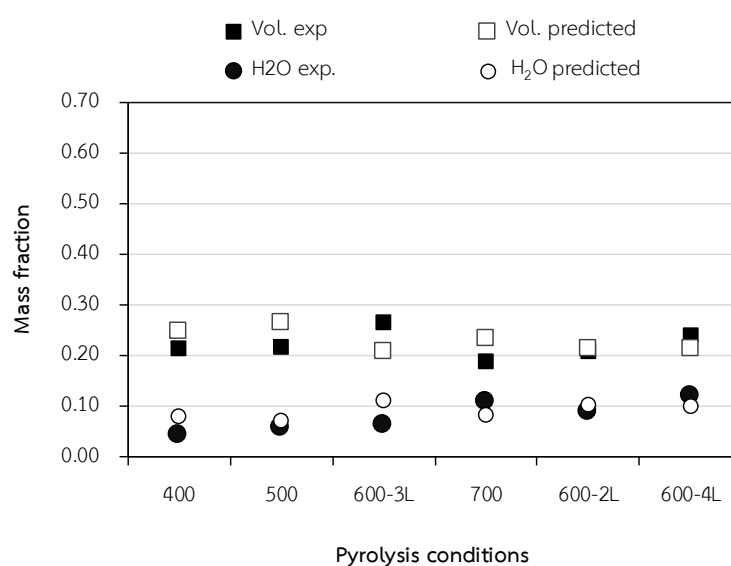


**Fig. 6.14** Mass fraction of volatile pyrolysis products (liquid products) at the different pyrolysis conditions

The formation of water evaporation is caused by the content of inherent moisture in biomass. Thus, the water fraction from volatile of Jatropha waste pyrolzed was also investigated. The water and volatile predicted in mass fraction are shown in Fig.6.14. The water predicted in mass fraction was 0.071-0.111, the highest mass fraction obtained at pyrolysis temperature was 600°C (3 L/min). The predicted results were compared with experimental data in respect of % error of volatile and water was 15.05-25.33% and 9.84-22.05%, respectively. The results were similar with Borello et al. (2015) who reported the prediction of water production in term of % error as 17%.

Furthermore, gas species mass fractions at different condition were also investigated. When temperature varies from 400 to 700 °C, the mass fraction of CO, $CO_2$ $CH_4$ and $H_2$ increase. Gas species predicted of CO, $CO_2$, $CH_4$, and $H_2$ were in range of 0.013-0.093, 0.031-0.056, 0.006-0.093, and 0.002-0.009, respectively. The predicted results were compared with experimental data in respect of % error gas species. The total gas at 600 °C with various gas flow rate agree with predicted results (22.89-38.54 %). The result was similar with Mellin et al. (2014) who developed CFD model and compared simulation data with experimental data of products generated during fast pyrolysis of biomass in fluidized bed reactor. Predicted results were compared with experimental data in respect of deviation and % deviation of gas species were in range of 0.98-16.39%. However, the highest % error was obtained at lower reaction temperature (400-500°C). It may be due to some physical properties of biomass and coefficient constant are default value base on coal properties. The result suggested that the CFD model can be applied and validated with experimental data except at low temperature (400°C). Consequently, in future work, the constant coefficients of Jatropha waste should be modified in order to improved accuracy and reliability of the developed models of gas species predicted.

# CHAPTER 7

# Conclusion

## 7.1 Effect of catalytic fast pyrolysis of Jatropha residues using Py-GCMS

Catalytic upgrading of the pyrolytic vapors after fast pyrolysis of Jatropha residue was performed using analytical pyrolysis gas chromatography/mass spectrometry (Py-GC/MS) at 400-600°C. The Py-GC/MS analyses for pyrolysis vapors show a range of aromatic hydrocarbons, hydrocarbon compounds, phenols, alcohols, aldehydes, ketones, acids and esters, furan and N-containing compounds (% area). The oxygenated compound is one of the most important problems of bio-oil which led to low-quality and short shelf life fuel. Accordingly, reduction of oxygen content is one of the primary aims of this study.

Catalytic testing included $Al_2O_3$, $ZrO_2$, $TiO_2$ (rutile, $T_1$) and $TiO_2$ (anatase, $T_2$) supporter catalysts. These supporters were impregnated with $CeO_2$ to promote metal dispersion prior to deposition of Pd, Ru, or Ni by impregnation method. Comparing among four supporters, total hydrocarbon yields increased with presence of all catalysts. Higher yields were obtained by $T_2$ > $Al_2O_3$ > CA > NiCA > RuCA catalysts. $Al_2O_3$ and $T_2$ supports were the most effective for increased hydrocarbons (42 - 64%) while favourably decreased oxygenated compounds (15%).

However, it seemed that the promoter ($CeO_2$) had no significant effect on pyrolytic product of Jatropha residue because it resulted in a low surface area of the catalysts. Thus, the metal on $Al_2O_3$ support catalysts by the impregnation were synthesized without $CeO_2$ promoter and increased metal loading from 1% to 5 wt% A significant decrease in the proportion of oxygenated compounds (including acids) from 73 % without a catalyst to less than 10 % with, and an increased conversion to hydrocarbons of more than 70% were achieved. The total hydrocarbon selectivity of the metal/$Al_2O_3$ catalysts was increased in the order of Pd > Ni > Ce > Ru > La > none > Co > Mo, with the highest proportion of total hydrocarbons obtained being 75.09 %. Another important compound that is affecting the quality of the bio-oil is N-compounds. It may create problems such as corrosion and poisoning of catalysts during

bio-oil upgrading. The result suggested that $Al_2O_3$ based catalyst adversely led to the formation of N-compounds of 27.98-40.90%. Since these catalysts are not effective on reducing N-compound, therefore it is desirable to remove the heteroatoms prior to using these renewable biofuels through denitrogenation reactions.

Recently, the use of mesoporous catalysts has attracted a lot of interest due to their potential ability to convert large complex compounds into simpler liquid products. Catalysts used in this work included AC, Ce/AC, Ni/AC, Pd/AC and Ru/AC in powder form. The inclusion of the M/AC catalysts (except for Ru/AC) increased decarboxylation reactions that involved in deoxygenation reaction. All M/Ac catalysts increased the hydrocarbon compounds in comparison to non-catalytic pyrolysis, while the Ce/AC catalysts produced the highest aromatic and hydrocarbons with the J/C ratio of 1:10 The main aromatic compounds formed were BTEX, with the highest aromatic selectivity obtained in the order of Ce/AC > Ni/AC > Pd/AC > Ru/AC. Total N-compounds were decreased to less than 10% after catalytic trials, except for with the Ru/AC and Ni/AC catalysts. These prepared catalysts are effective for deoxygenation and decarboxylation to improve the quality and stability of the bio-oil.

Moreover, added catalysts were also modified metal catalysts (Ce, Ni, Pd and Ru) over activated carbon (Ac) support in granule form. Aromatics are largely formed to 29%, and the high total hydrocarbon content of 92% and 83% was obtained by the Ni/Ac and Pd/Ac catalyst (J:C of 1:10), respectively. The highest total hydrocarbon obtained in the order of Ni/AC > Pd/AC > Ru/AC > Ac > Ce/AC. Interestingly, only a low level of PAHs production from the catalytic fast pyrolysis of Jatropha residue was detected, which is another advantage of using these catalysts. Overall, these 5 wt% M/AC catalysts are suitable for upgrading pyrolysis vapor products from Jatropha residues to improve the quality and usability of the obtained fuel products. It can conclude that the meso-pores of activated carbon are thought to play an important role in the effective conversion of heavy hydrocarbon compounds into lighter fractions due to their highly porous structures.

Lastly in synthesized catalysts, they were modified 5wt% metal catalysts (Ni and Pd) over char supporter from slow pyrolysis of Jatropha wastes which exhibited high surface area of 35.65-414.90 $m^2/g$. Therefore, it is possible to utilize the solid char

in catalyst applications. Metal/char catalysts clearly reduced the proportion of oxygenated compounds and carboxylic acids to 7.8% for Ni/char, and increased conversion to hydrocarbons of more than 70%. Overall catalysts, the product selectivity was greatly increased as the J:C ratio was increased from 1:1 to 1:10.

These catalyst supports displayed relatively high activity towards deoxygenation reactions which resulted in low quantity of acids and other oxygenated compounds, and produced high aromatic and hydrocarbon compounds. The result indicating that high surface area resulted in better catalytic activity, and also less N-compounds. Therefore, these catalysts can be applied to improve properties of pyrolytic products. Therefore, 5% $M/Al_2O_3$ and 5% M/Ac catalysts are suitable for further investigation with a scaled-up process, a drop tube reactor.

## 7.2 Effect of operating condition and catalytic fast pyrolysis of Jatropha residues using a drop tube reactor

The fast pyrolysis experiments were carried out in a drop tube reactor operating from 400 to 700°C. The pyrolysis temperature of 600°C with particle size of 0.125-0.425 mm showed the optimum yield of bio-oil of 32.54 wt. %. Solid yield (char) tended to decrease with increasing the temperature, and was in range of 29.73-47.67 wt. % while gas products was in range of 26.45-52.77 wt. %. with the highest gas product obtained at 700°C.

Bio-oil produced was in range of 17.67-39.38 wt.%, and the maximized bio-oil obtained by activated carbon (Ac) support. In catalytic with $Al_2O_3$ extruded, the bio-oil was in range of 22-36 wt. %. The maximum liquid yield of 32.87 wt. % was achieved with $Ni/Al_2O_3$. The composition of the product gas was analyzed using an online gas analyzer capable of continuous real-time quantification of CO, $CO_2$, $C_xH_y$ (as $CH_4$) and $H_2$. These gas products are non-condensable gas which was generated from thermal cracking reaction. Production of CO and $CO_2$ are an indicator of the deoxygenation capability of a catalyst in catalytic fast pyrolysis of biomass. With the presence of catalyst, all catalyst resulted in more $CH_4$ and CO. As a result, the oxygen can be eliminated as water, carbon monoxide, carbon dioxide, methane and short-chain acids.

The maximum $H_2$ and CO was achieved by 5%Ni/$Al_2O_3$ (ext.) and Ni/Ac, it suggested that Ni catalyst effective to deoxygenation reaction.

The quality of bio-oil was analyzed product distribution by GC-MS; the main compounds in bio-oil were phenol, aromatic, hydrocarbon compounds and N-compounds. The oxygenated (included acid and carbonyl group) were obviously reduced from 92.12% to 9.63% with increasing temperature. Moreover, N-containing compounds were in large quantities at high temperature because some nitrogen such as amides and nitriles might result from the further reaction between nitrogen compounds and fatty acids. The result agreed well with the analyzed the product distributions from catalytic using PY-GCMS. Product distribution reveals the main products included phenols, aromatics, and hydrocarbons with Ni/Ac and Pd/Ac catalyst. Aromatics are largely formed over 29% of GC peak area, and the highest hydrocarbon content (42%) was obtained by the Pd/Ac catalyst. The oxygenated compound and acid dropped considerably to 8.26%, especially with Pd/Ac catalyst which completely reduced acid. N-compounds were reduced from 75.65% to 31.45% by Ni/Ac. Moreover, phenol compounds were also increased to 43.52% by the applying Ac. It may be due to pore size of Ac larger than Ni/AC and Pd/Ac catalysts, so it prefers selected large molecule of phenol through their pores. With the present of $Al_2O_3$ extruded catalyst, the major compound groups found in bio-oil are N-compound (56.81-69.92%). In addtion, phenol compounds were also increased to 19.25-27.01% by the applying $A_2O_3$ extruded catalyst. Comparison of $Al_2O_3$ with Ac based catalysts, M/Ac were the most effective for increased hydrocarbons (30%) while decreased oxygenated compounds and N-compounds.

Typical properties of bio-oil derived from Jatropha waste were HHV, water content and element content. The carbon of pyrolysis oil was in the range of 52.9-63.5 wt.%, the high heating values (24.20-31.70 MJ/kg), low acidity and water content. In catalytic trial, the highest carbon content (65.85 wt.%) of bio-oil was obtained by Pd/Ac catalyst, followed by Ni/ $Al_2O_3$ (ext.), Ni/Ac, and $Al_2O_3$ (ext.) non-catalyst. Since these catalysts promote the cracking of the volatile organics into non-condensable gas, and water which related with water content and HHV of bio-oil. The result concluded that

bio-oil from this study were closed to those of conventional liquid fuels, and suggest that the liquid product at the optimize condition can potentially be applied as biofuel.

## 7.3 Predicted product distributions from fast pyrolysis of Jatropha residue using a drop tube pyrolyzer by CFD model

CFD model were performed at four temperatures, 400, 500, 600 and 700℃, and three differences gas flow rate (2, 3, and 4 L/min). The model was carried out using a standard k–e turbulence model. The main result obtained through this model is the quantification of the different species of gas released during the process taking into account their variation as a function of the temperature of the reactor. The volatile species formation mechanism has been applied by a multi-reaction one-step model to predicted different species formations. Pyrolysis products are greatly influenced by the operative conditions, especially by temperature.

Bio-oil predicted from fast pyrolysis of Jatropha waste in mass fraction was 0.319-0.386, and was maximized at 0.386 by pyrolysis temperature of 500℃. Solid yield (char) predicted tend to decrease with increasing the temperature to 700℃ in mass fraction of 0.160-0.197, while the gas products increased at higher temperature in mass fraction of 0.418-0.498. It may be due to the heterogeneous reaction of char. The predicted results were compared with experimental data in respect of % error, and the error of gas fraction, liquid fraction and solid fraction were in range of, 6.67-28.9%, 0.26-11.26% and 16.67-24.59%, respectively. The result suggested that the CFD model can be applied and validated with experimental data except at low temperature (400℃). It may be due to some physical properties of biomass and coefficient constant are default value base on coal properties. Therefore, in future work, the constant coefficients of biomass should be modified in order to improved accuracy and reliability of the developed models of gas species predicted.

In conclusion, the fast pyrolysis by Py-GC/MS at high temperature (600°C) and small particle size (<0.125 mm) had positive influence on the yields of pyrolytic products with respect to low yields of oxygenated compounds and high yields of aromatic hydrocarbon. Moreover, the synthesized catalysts displayed relatively high activity towards deoxygenation reactions which resulted in low quantity of oxygenated compounds (less than 10%, peak area) and produced high aromatic and hydrocarbon compounds (more than 60%). The findings indicated that high surface area of M/Ac based catalyst resulted in better catalytic activity, and also less N-compounds, especially Ni/Ac and Pd/Ac catalysts. By evaluation of bio-oil quantity and quality from fast pyrolysis using drop tube pyrolyzer, it was found that the pyrolysis temperature of 600°C with particle size of 0.125-0.425 mm showed the optimum yield of bio-oil. By using GC/MS analysis, it was found that quality bio-oil with the highest total hydrocarbon and phenol content (65%) and the lowest oxygenated compound (8%) was obtained by the Pd/Ac catalyst with the highest carbon content (65.85 wt%) and lowest oxygen content (17.30 wt%) as determined by CHNO analyzer. The result suggested that this catalyst can be used for reducing oxygen content of bio-oil to below 40 wt%. Moreover, the comparison of experimental measurements and model predictions by CFD model yielded satisfied accuracy in respect of % error (±25% on a quantitative basis). The predicted product yields also agreed well with experimental bio-oil data obtained at various temperature and gas flow rate.

# REFERENCES

Abnisa, F., Arami-Niya, A., Wan Daud, W.M.A., Sahu, J.N., Noor, I.M. 2013. Utilization of oil palm tree residues to produce bio-oil and bio-char via pyrolysis. *Energy Conversion and Management*, **76**, 1073-1082.

Asadieraghi, M., Wan Daud, W.M.A., Abbas, H.F. 2014. Model compound approach to design process and select catalysts for in-situ bio-oil upgrading. *Renewable and Sustainable Energy Reviews*, **36**, 286-303.

Basu, P. 2010. *Biomass gasification and pyrolysis : practical design and theory*. Academic Press, Burlington, MA.

Beste, A., Buchanan Iii, A.C. 2012. Kinetic simulation of the thermal degradation of phenethyl phenyl ether, a model compound for the β-O-4 linkage in lignin. *Chemical Physics Letters*, **550**(0), 19-24.

Biradar, C.H., Subramanian, K.A., Dastidar, M.G. 2014. Production and fuel quality upgradation of pyrolytic bio-oil from Jatropha Curcas de-oiled seed cake. *Fuel*, **119**(0), 81-89.

Boateng, A.A., Mtui, P.L. 2012. CFD modeling of space-time evolution of fast pyrolysis products in a bench-scale fluidized-bed reactor. *Applied Thermal Engineering*, **33–34**, 190-198.

Borello, D., Cedola, L., Frangioni, G.V., Meloni, R., Venturini, P., De Filippis, P., de Caprariis, B. Development of a numerical model for biomass packed bed pyrolysis based on experimental validation. *Applied Energy*.

Borello, D., Meloni, R., Venturini, P., De Filippis, P., de Caprariis, B., Di Carlo, A., Frangioni, G.V. 2014. A 3D Packed Bed Model for Biomass Pyrolysis: Mathematical Formulation and Experimental Validation. *Energy Procedia*, **61**, 958-961.

Bridgwater, A.V. 2012. Review of fast pyrolysis of biomass and product upgrading. *Biomass and Bioenergy*, **38**(0), 68-94.

Bulushev, D.A., Ross, J.R.H. 2011. Catalysis for conversion of biomass to fuels via pyrolysis and gasification: A review. *Catalysis Today*, **171**(1), 1-13.

Carels, N. 2009. Chapter 2 Jatropha curcas: A Review. in: *Advances in Botanical Research*, (Eds.) K. Jean-Claude, D. Michel, Vol. Volume 50, Academic Press, pp. 39-86.

Chen, L., Wang, X., Yang, H., Lu, Q., Li, D., Yang, Q., Chen, H. 2015. Study on pyrolysis behaviors of non-woody lignins with TG-FTIR and Py-GC/MS. *Journal of Analytical and Applied Pyrolysis*, **113**, 499-507.

Cheng, S., Wei, L., Zhao, X., Kadis, E., Cao, Y., Julson, J., Gu, Z. 2016. Hydrodeoxygenation of prairie cordgrass bio-oil over Ni based activated carbon synergistic catalysts combined with different metals. *New Biotechnology*, **33**(4), 440-448.

Choudhary, T.V., Phillips, C.B. 2011. Renewable fuels via catalytic hydrodeoxygenation. *Applied Catalysis A: General*, **397**(1–2), 1-12.

Czernik, S., Bridgwater, A.V. 2004. Overview of applications of biomass fast pyrolysis oil. *Energy and Fuels*, **18**(2), 590-598.

Duan, P., Zhang, C., Wang, F., Fu, J., Lü, X., Xu, Y., Shi, X. 2016. Activated carbons for the hydrothermal upgrading of crude duckweed bio-oil. *Catalysis Today*, **274**, 73-81.

French, R., Czernik, S. 2010. Catalytic pyrolysis of biomass for biofuels production. *Fuel Processing Technology*, **91**(1), 25-32.

Gottipati, R., Mishra, S. 2011. A kinetic study on pyrolysis and combustion characteristics of oil cakes: Effect of cellulose and lignin content. *Journal of Fuel Chemistry and Technology*, **39**(4), 265-270.

Graça, I., Lopes, J.M., Cerqueira, H.S., Ribeiro, M.F. 2013. Bio-oils Upgrading for Second Generation Biofuels. *Industrial & Engineering Chemistry Research*, **52**(1), 275-287.

Hu, C., Yang, Y., Luo, J., Pan, P., Tong, D., Li, G. 2011. Recent advances in the catalytic pyrolysis of biomass. *Frontiers of Chemical Science and Engineering*, **5**(2), 188-193.

Huang, Y., Wei, L., Zhao, X., Cheng, S., Julson, J., Cao, Y., Gu, Z. 2016. Upgrading pine sawdust pyrolysis oil to green biofuels by HDO over zinc-assisted Pd/C catalyst. *Energy Conversion and Management*, **115**, 8-16.

Jae, J., Coolman, R., Mountziaris, T.J., Huber, G.W. 2014. Catalytic fast pyrolysis of lignocellulosic biomass in a process development unit with continual catalyst addition and removal. *Chemical Engineering Science*, **108**(0), 33-46.

Jin, W., Singh, K., Zondlo, J. 2015. Co-processing of pyrolysis vapors with bio-chars for ex-situ upgrading. *Renewable Energy*, **83**, 638-645.

Jourabchi, S.A., Gan, S., Ng, H.K. 2014. Pyrolysis of Jatropha curcas pressed cake for bio-oil production in a fixed-bed system. *Energy Conversion and Management*, **78**(0), 518-526.

Kaewpengkrow, P., Atong, D., Sricharoenchaikul, V. 2014a. Catalytic upgrading of pyrolysis vapors from Jatropha wastes using alumina, zirconia and titania based catalysts. *Bioresource Technology*, **163**(0), 262-269.

Kaewpengkrow, P., Atong, D., Sricharoenchaikul, V. 2014b. Effect of Pd, Ru, Ni and ceramic supports on selective deoxygenation and hydrogenation of fast pyrolysis Jatropha residue vapors. *Renewable Energy*, **65**(0), 92-101.

Kanaujia, P.K., Sharma, Y.K., Garg, M.O., Tripathi, D., Singh, R. 2014. Review of analytical strategies in the production and upgrading of bio-oils derived from lignocellulosic biomass. *Journal of Analytical and Applied Pyrolysis*, **105**, 55-74.

Khalil, H.P.S.A., Aprilia, N.A.S., Bhat, A.H., Jawaid, M., Paridah, M.T., Rudi, D. 2013. A Jatropha biomass as renewable materials for biocomposites and its applications. *Renewable and Sustainable Energy Reviews*, **22**(0), 667-685.

Kim, S.W., Koo, B.S., Lee, D.H. 2014. Catalytic pyrolysis of palm kernel shell waste in a fluidized bed. *Bioresource Technology*, **167**, 425-432.

Kim, S.W., Koo, B.S., Ryu, J.W., Lee, J.S., Kim, C.J., Lee, D.H., Kim, G.R., Choi, S. 2013. Bio-oil from the pyrolysis of palm and Jatropha wastes in a fluidized bed. *Fuel Processing Technology*, **108**(0), 118-124.

Ledesma, B., Román, S., Álvarez-Murillo, A., Sabio, E., González, J.F. 2014. Cyclic adsorption/thermal regeneration of activated carbons. *Journal of Analytical and Applied Pyrolysis*, **106**, 112-117.

Li, X., Gunawan, R., Wang, Y., Chaiwat, W., Hu, X., Gholizadeh, M., Mourant, D., Bromly, J., Li, C.-Z. 2014. Upgrading of bio-oil into advanced biofuels and chemicals.

Part III. Changes in aromatic structure and coke forming propensity during the catalytic hydrotreatment of a fast pyrolysis bio-oil with Pd/C catalyst. *Fuel*, **116**, 642-649.

Liu, H., Cattolica, R.J., Seiser, R. 2016. CFD studies on biomass gasification in a pilot-scale dual fluidized-bed system. *International Journal of Hydrogen Energy*, **41**(28), 11974-11989.

Lorenzetti, C., Conti, R., Fabbri, D., Yanik, J. 2016. A comparative study on the catalytic effect of H-ZSM5 on upgrading of pyrolysis vapors derived from lignocellulosic and proteinaceous biomass. *Fuel*, **166**, 446-452.

Lu, Q., Zhang, Y., Tang, Z., Li, W.-z., Zhu, X.-f. 2010. Catalytic upgrading of biomass fast pyrolysis vapors with titania and zirconia/titania based catalysts. *Fuel*, **89**(8), 2096-2103.

Luo, J., Li, J., Shen, D., He, L., Tong, D., Hy, C. 2010. Catalytic pyrolysis of Pubescens to phenols over Ni/C catalyst. *Science China Chemistry*, **53**(7), 1487-1491.

Malins, K., Kampars, V., Brinks, J., Neibolte, I., Murnieks, R. 2015. Synthesis of activated carbon based heterogenous acid catalyst for biodiesel preparation. *Applied Catalysis B: Environmental*, **176–177**, 553-558.

Manurung, R., Wever, D.A.Z., Wildschut, J., Venderbosch, R.H., Hidayat, H., van Dam, J.E.G., Leijenhorst, E.J., Broekhuis, A.A., Heeres, H.J. 2009. Valorisation of Jatropha curcas L. plant parts: Nut shell conversion to fast pyrolysis oil. *Food and Bioproducts Processing*, **87**(3), 187-196.

Masnadi, M.S., Habibi, R., Kopyscinski, J., Hill, J.M., Bi, X., Lim, C.J., Ellis, N., Grace, J.R. 2014. Fuel characterization and co-pyrolysis kinetics of biomass and fossil fuels. *Fuel*, **117, Part B**(0), 1204-1214.

Mellin, P., Kantarelis, E., Yang, W. 2014. Computational fluid dynamics modeling of biomass fast pyrolysis in a fluidized bed reactor, using a comprehensive chemistry scheme. *Fuel*, **117, Part A**, 704-715.

Mellin, P., Zhang, Q., Kantarelis, E., Yang, W. 2013. An Euler–Euler approach to modeling biomass fast pyrolysis in fluidized-bed reactors – Focusing on the gas phase. *Applied Thermal Engineering*, **58**(1–2), 344-353.

Mihalcik, D.J., Mullen, C.A., Boateng, A.A. 2011. Screening acidic zeolites for catalytic fast pyrolysis of biomass and its components. *Journal of Analytical and Applied Pyrolysis*, **92**(1), 224-232.

Mochizuki, T., Atong, D., Chen, S.-Y., Toba, M., Yoshimura, Y. 2013. Effect of SiO2 pore size on catalytic fast pyrolysis of Jatropha residues by using pyrolyzer-GC/MS. *Catalysis Communications*, **36**(0), 1-4.

Mortensen, P.M., Grunwaldt, J.D., Jensen, P.A., Knudsen, K.G., Jensen, A.D. 2011. A review of catalytic upgrading of bio-oil to engine fuels. *Applied Catalysis A: General*, **407**(1–2), 1-19.

Murata, K., Kreethawate, L., Larpkiattaworn, S., Inaba, M. 2016. Evaluation of Ni-based catalysts for the catalytic fast pyrolysis of jatropha residues. *Journal of Analytical and Applied Pyrolysis*, **118**, 308-316.

Murata, K., Liu, Y., Inaba, M., Takahara, I. 2012. Catalytic fast pyrolysis of jatropha wastes. *Journal of Analytical and Applied Pyrolysis*, **94**(0), 75-82.

Murata, K., Sricharoenchaikul, V., Liu, Y., Inaba, M., Takahara, I. 2013. Effect of Metal-modified Carbon Catalysts on Fast Pyrolysis of Jatropha Waste. *Journal of the Japan Petroleum Institute*, **56**(6), 371-380.

Pande, M., Bhaskarwar, A. 2012. Biomass Conversion to Energy. in: *Biomass Conversion*, (Eds.) C. Baskar, S. Baskar, R.S. Dhillon, Springer Berlin Heidelberg, pp. 1-90.

Pattiya, A., Sukkasi, S., Goodwin, V. 2012. Fast pyrolysis of sugarcane and cassava residues in a free-fall reactor. *Energy*, **44**(1), 1067-1077.

Pattiya, A., Titiloye, J.O., Bridgwater, A.V. 2008. Fast pyrolysis of cassava rhizome in the presence of catalysts. *Journal of Analytical and Applied Pyrolysis*, **81**(1), 72-79.

Peters, B. 2011. Prediction of pyrolysis of pistachio shells based on its components hemicellulose, cellulose and lignin. *Fuel Processing Technology*, **92**(10), 1993-1998.

Qiang, L., Wen-zhi, L., Dong, Z., Xi-feng, Z. 2009. Analytical pyrolysis–gas chromatography/mass spectrometry (Py–GC/MS) of sawdust with Al/SBA-15 catalysts. *Journal of Analytical and Applied Pyrolysis*, **84**(2), 131-138.

Regalbuto, J.R., ENGnetBASE Supplement. 2007. Catalyst preparation science and engineering, Taylor & Francis. Boca Raton.

Sharma, R., Sheth, P.N., Gujrathi, A.M. 2016. Kinetic modeling and simulation: Pyrolysis of Jatropha residue de-oiled cake. *Renewable Energy*, **86**, 554-562.

Shen, Y. 2015. Chars as carbonaceous adsorbents/catalysts for tar elimination during biomass pyrolysis or gasification. *Renewable and Sustainable Energy Reviews*, **43**, 281-295.

Shen, Y., Yoshikawa, K. 2013. Recent progresses in catalytic tar elimination during biomass gasification or pyrolysis—A review. *Renewable and Sustainable Energy Reviews*, **21**, 371-392.

Shim, W.G., Kim, S.C. 2010. Heterogeneous adsorption and catalytic oxidation of benzene, toluene and xylene over spent and chemically regenerated platinum catalyst supported on activated carbon. *Applied Surface Science*, **256**(17), 5566-5571.

Shimizu, K.-i., Imaiida, N., Kon, K., Hakim Siddiki, S.M.A., Satsuma, A. 2013. Heterogeneous Ni Catalysts for N-Alkylation of Amines with Alcohols. *ACS Catalysis*, **3**(5), 998-1005.

Spadaro, L., Palella, A., Frusteri, F., Arena, F. 2015. Valorization of crude bio-oil to sustainable energy vector for applications in cars powering and on-board reformers via catalytic hydrogenation. *International Journal of Hydrogen Energy*, **40**(42), 14507-14518.

Sricharoenchaikul, V., Atong, D. 2009. Thermal decomposition study on Jatropha curcas L. waste using TGA and fixed bed reactor. *Journal of Analytical and Applied Pyrolysis*, **85**(1–2), 155-162.

Srinivasan, V., Adhikari, S., Chattanathan, S.A., Park, S. 2012. Catalytic Pyrolysis of Torrefied Biomass for Hydrocarbons Production. *Energy & Fuels*, **26**(12), 7347-7353.

Sun, S., Tian, H., Zhao, Y., Sun, R., Zhou, H. 2010. Experimental and numerical study of biomass flash pyrolysis in an entrained flow reactor. *Bioresource Technology*, **101**(10), 3678-3684.

Tabet, F., Gökalp, I. 2015. Review on CFD based models for co-firing coal and biomass. *Renewable and Sustainable Energy Reviews*, **51**, 1101-1114.

Thangalazhy-Gopakumar, S., Adhikari, S., Gupta, R.B., Tu, M., Taylor, S. 2011. Production of hydrocarbon fuels from biomass using catalytic pyrolysis under helium and hydrogen environments. *Bioresource Technology*, **102**(12), 6742-6749.

Vecino Mantilla, S., Gauthier-Maradei, P., Álvarez Gil, P., Tarazona Cárdenas, S. 2014. Comparative study of bio-oil production from sugarcane bagasse and palm empty fruit bunch: Yield optimization and bio-oil characterization. *Journal of Analytical and Applied Pyrolysis*, **108**(0), 284-294.

Vichaphund, S., Aht-ong, D., Sricharoenchaikul, V., Atong, D. 2015. Production of aromatic compounds from catalytic fast pyrolysis of Jatropha residues using metal/HZSM-5 prepared by ion-exchange and impregnation methods. *Renewable Energy*, **79**, 28-37.

Voloshin, R.A., Rodionova, M.V., Zharmukhamedov, S.K., Nejat Veziroglu, T., Allakhverdiev, S.I. 2016. Review: Biofuel production from plant and algal biomass. *International Journal of Hydrogen Energy*, **41**(39), 17257-17273.

Wang, G., Peng, H., Qiao, X., Du, L., Li, X., Shu, T., Liao, S. 2016a. Biomass-derived porous heteroatom-doped carbon spheres as a high-performance catalyst for the oxygen reduction reaction. *International Journal of Hydrogen Energy*, **41**(32), 14101-14110.

Wang, S., Chen, J., Cai, Q., Zhang, F., Wang, Y., Ru, B., Wang, Q. 2016b. The effect of mild hydrogenation on the catalytic cracking of bio-oil for aromatic hydrocarbon production. *International Journal of Hydrogen Energy*, **41**(37), 16385-16393.

Wang, Y., Yan, L. 2008. CFD Studies on Biomass Thermochemical Conversion. *International Journal of Molecular Sciences*, **9**(6), 1108-1130.

Weber, K., Li, T., Løvås, T., Perlman, C., Seidel, L., Mauss, F. 2017. Stochastic reactor modeling of biomass pyrolysis and gasification. *Journal of Analytical and Applied Pyrolysis*, **124**, 592-601.

Wu, C., Wang, Z., Huang, J., Williams, P.T. 2013. Pyrolysis/gasification of cellulose, hemicellulose and lignin for hydrogen production in the presence of various nickel-based catalysts. *Fuel*, **106**, 697-706.

Xue, Q., Heindel, T.J., Fox, R.O. 2011. A CFD model for biomass fast pyrolysis in fluidized-bed reactors. *Chemical Engineering Science*, **66**(11), 2440-2452.

Yang, Y., Chiang, K., Burke, N. 2011. Porous carbon-supported catalysts for energy and environmental applications: A short review. *Catalysis Today*, **178**(1), 197-205.

Yildiz, G., Ronsse, F., Vercruysse, J., Daels, J., Toraman, H.E., van Geem, K.M., Marin, G.B., van Duren, R., Prins, W. 2016. In situ performance of various metal doped catalysts in micro-pyrolysis and continuous fast pyrolysis. *Fuel Processing Technology*, **144**, 312-322.

Ying, X., Tiejun, W., Longlong, M., Guanyi, C. 2012. Upgrading of fast pyrolysis liquid fuel from biomass over Ru/$\gamma$-Al2O3 catalyst. *Energy Conversion and Management*, **55**(0), 172-177.

Zellagui, S., Schönnenbeck, C., Zouaoui-Mahzoul, N., Leyssens, G., Authier, O., Thunin, E., Porcheron, L., Brilhac, J.F. 2016. Pyrolysis of coal and woody biomass under N2 and CO2 atmospheres using a drop tube furnace - experimental study and kinetic modeling. *Fuel Processing Technology*, **148**, 99-109.

Zhang, B., Zhong, Z.-P., Wang, X.-B., Ding, K., Song, Z.-W. 2015. Catalytic upgrading of fast pyrolysis biomass vapors over fresh, spent and regenerated ZSM-5 zeolites. *Fuel Processing Technology*, **138**, 430-434.

Zhang, H., Xiao, R., Jin, B., Xiao, G., Chen, R. 2013. Biomass catalytic pyrolysis to produce olefins and aromatics with a physically mixed catalyst. *Bioresource Technology*, **140**(0), 256-262.

Zhang, X., Sun, L., Chen, L., Xie, X., Zhao, B., Si, H., Meng, G. 2014. Comparison of catalytic upgrading of biomass fast pyrolysis vapors over CaO and Fe(III)/CaO catalysts. *Journal of Analytical and Applied Pyrolysis*, **108**(0), 35-40.

Zhong, W., Yu, A., Zhou, G., Xie, J., Zhang, H. 2016. CFD simulation of dense particulate reaction system: Approaches, recent advances and applications. *Chemical Engineering Science*, **140**, 16-43.

APPENDIX

**Appendix A**

**Pyrolytic product by Py-GC-MS**

**Table A-1** Pyrolytic products of Jatropha residue with $Al_2O_3$ catalysts using Jatropha to catalyst ratio of 1:10

| Compound Name | RT | % Peak area | | | | | |
|---|---|---|---|---|---|---|---|
| | | No cat. | $Al_2O_3$ | Ce/ Al | Pd-Ce/ Al | Ru-Ce/ Al | Ni-Ce/ Al |
| *Alcohol* | | | | | | | |
| 1-Pentanol, 4-methyl- | 2.125 | - | - | 5.04 | - | - | 4.57 |
| 2,6 NONADIEN-1-OL | 10.761 | - | 0.63 | - | - | - | - |
| 1-Dodecanol | 24.79 | 1.27 | - | - | - | - | - |
| 1-Tetradecanol | 29.796 | 0.55 | - | - | - | - | - |
| Stigmast-5-en-3-ol, (3.beta.)- | 46.876 | 0.39 | - | - | - | - | 0.71 |
| *Aldehyde* | | | | | | | |
| Butanal, 2-methyl- | 2.506 | - | 2.5 | 1.84 | - | 3.2 | 2.16 |
| Hexanal | 4.563 | 0.36 | - | - | - | - | - |
| Benzenepentanal | 18.736 | - | - | - | 0.64 | - | - |
| *Aromatic* | | | | | | | |
| Benzene | 2.539 | - | - | - | 9.67 | - | - |
| Methylbenzene | 3.941 | 2.75 | - | 9.59 | - | - | 8.41 |
| Benzene, ethyl- | 6.216 | 0.42 | 0.98 | 1.63 | 1.93 | 1.28 | 2.19 |
| Benzene, 1,4-dimethyl- | 6.334 | - | - | - | - | - | 1.23 |
| Styrene | 7.066 | 0.41 | - | - | - | 2.27 | - |
| Benzene, 1-ethenyl-2-methyl- | 10.35 | - | - | - | 0.57 | - | - |
| Benzene, 1-propynyl- | 11.897 | - | - | - | 1.18 | 1.17 | 1.22 |
| Benzene, butyl- | 12.342 | - | - | - | 0.47 | 0.53 | - |
| Benzene, (1-methyl-2-cyclopropen-1-yl)- | 15.266 | - | - | - | - | - | 1.42 |
| 1,4-Dihydronaphthalene | 15.455 | - | - | - | - | - | 2 |

**Table A-1 (cont.)** Pyrolytic products of Jatropha residue with $Al_2O_3$ catalysts using Jatropha to catalyst ratio of 1:10

| Compound Name | RT | % Peak area | | | | | |
|---|---|---|---|---|---|---|---|
| | | No cat. | $Al_2O_3$ | Ce/ Al | Pd-Ce/ Al | Ru-Ce/ Al | Ni-Ce/ Al |
| *Aromatic* | | | | | | | |
| Naphthalene, 1,2-dihydro- | 15.5 | - | - | - | 1.2 | - | - |
| Naphthalene | 16.38 | - | 0.77 | - | 2.14 | 0.62 | 0.8 |
| *Carboxylic acid* | | | | | | | |
| Acetic oxide | 2.06 | 3.01 | - | - | - | - | - |
| Oleic acid | 35.47 | 0.83 | - | - | - | - | - |
| Palmitic acid | 35.87 | 10.85 | - | 0.76 | - | - | - |
| Oleic acid | 38.47 | 39.69 | - | - | - | - | - |
| Oleic acid | 38.68 | 6.36 | - | - | - | - | - |
| *Ester* | | | | | | | |
| Methoxyacetic acid, hexyl ester | 2.11 | - | - | - | - | 6.66 | - |
| 2-Propenoic acid, 1,4-butanediyl ester | 4.24 | 0.75 | - | - | - | - | - |
| Acetol | 6.33 | 0.62 | - | - | - | - | - |
| Carbonic acid, ethyl nonyl ester | 7.04 | - | - | - | 3.27 | - | - |
| Stigmast-5-en-3-ol, oleate | 47.02 | - | - | - | - | 0.77 | - |
| *Ether* | | | | | | | |
| Hydroperoxide, hexyl | 2.118 | - | - | - | 5.14 | - | - |
| *Furan* | | | | | | | |
| Furan, 2,5-dimethyl- | 5.217 | - | - | - | - | 0.94 | - |

**Table A-1 (cont.)** Pyrolytic products of Jatropha residue with $Al_2O_3$ catalysts using Jatropha to catalyst ratio of 1:10

| Compound Name | RT | % Peak area | | | | | |
|---|---|---|---|---|---|---|---|
| | | No cat. | $Al_2O_3$ | Ce/ Al | Pd-Ce/ Al | Ru-Ce/ Al | Ni-Ce/ Al |
| *Furan* | | | | | | | |
| 2-Furancarboxaldehyde | 5.356 | 0.67 | - | - | - | - | - |
| 2-Furanmethanol | 5.989 | 0.37 | - | - | - | - | - |
| *HC Compound* | | | | | | | |
| 1-Hexene | 2.119 | - | 5.66 | - | - | - | - |
| hexatriene isomer | 2.42 | - | - | - | - | 3.37 | - |
| 1-Hexen-3-yne | 2.426 | - | - | - | 1.61 | - | - |
| 1,4-Cyclohexadiene | 2.432 | - | 3.05 | 3.7 | - | - | 2.86 |
| 3-Cyclopentyl-1-propyne | 2.605 | - | - | - | - | 4.09 | 2.99 |
| 3-Cyclopentyl-1-propyne | 2.625 | - | 3.22 | 3.29 | - | - | - |
| Cyclopentane, 1-methyl-2-(2-propenyl)-, trans- | 2.801 | - | 5.16 | - | - | - | - |
| Cyclopentane, 1,2-dimethyl- | 2.805 | - | - | 4.7 | - | 4.5 | 4.08 |
| 1-Heptene | 2.814 | 1.78 | 2.81 | - | 4.33 | - | - |
| Heptane | 2.9 | - | - | 2.16 | - | 2.37 | - |
| CYCLOPENTENE, 3-ETHENYL- | 3.427 | - | - | - | - | - | 2.74 |
| 3-Hepten-1-yne, (Z)- | 3.449 | - | 2.14 | - | - | - | - |
| 2-METHYL-CYCLOHEXA-1,3-DIENE | 3.451 | - | - | 2.65 | - | - | - |
| Cyclopentene,3-(2-propenyl)- | 3.625 | - | 4.26 | 4.39 | - | 4.27 | 4.33 |

**Table A-1 (cont.)** Pyrolytic products of Jatropha residue with $Al_2O_3$ catalysts using Jatropha to catalyst ratio of 1:10

| Compound Name | RT | % Peak area | | | | | |
|---|---|---|---|---|---|---|---|
| | | No cat. | $Al_2O_3$ | Ce/ Al | Pd- Ce/ Al | Ru- Ce/ Al | Ni-Ce/ Al |
| *HC Compound* | | | | | | | |
| 1,3,5-Cycloheptatriene | 3.881 | - | 8.73 | - | 10.97 | 9.78 | - |
| 1-Octene | 4.452 | 1.01 | 2.51 | 2.23 | 2.77 | 2.08 | 2.57 |
| 1-Undecene, 4-methyl- | 4.566 | - | 0.98 | - | - | 1.49 | 1.75 |
| Octane | 4.567 | - | - | - | 1.32 | - | - |
| Hexane, 2,3,4-trimethyl- | 4.575 | - | - | 1.74 | - | - | - |
| 1-Pentene, 4,4-dimethyl- | 5.4 | - | 0.5 | - | 0.46 | - | - |
| Bicyclo[4.2.0]octa-1,3,5-triene | 6.963 | - | 1.79 | 1.76 | 2.1 | - | 1.98 |
| 1-Nonene /Nonene | 7.133 | 0.29 | 3.4 | 3.03 | - | - | 2.81 |
| Decane | 7.322 | - | - | - | 1.58 | 1.05 | 1.8 |
| Nonane | 7.331 | - | - | 1.24 | - | - | - |
| 2-Nonene | 7.477 | - | - | - | - | 0.71 | 0.6 |
| 2-Nonene | 7.506 | - | - | - | 0.5 | 2.95 | - |
| 1,5-Hexadiene, 2,5-dimethyl | 7.639 | 0.62 | - | - | - | - | - |
| Cyclopropane, 1-heptyl-2-methyl- | 10.268 | - | - | - | 1.64 | 1.6 | 2.08 |
| Cyclopropane, 1-ethyl-2-heptyl- | 10.276 | - | 2.02 | 2.02 | 1.65 | 2.14 | 1.74 |
| Cyclopropane, 1-butyl-2-pentyl-, trans- | 10.278 | - | - | 1.84 | - | - | - |
| Decane | 10.565 | - | - | - | 0.52 | - | - |
| Octane, 2,4,6-trimethyl- | 10.572 | - | - | 0.73 | - | 10.53 | |

**Table A-1 (cont.)** Pyrolytic products of Jatropha residue with $Al_2O_3$ catalysts using Jatropha to catalyst ratio of 1:10

| Compound Name | RT | % Peak area | | | | | |
|---|---|---|---|---|---|---|---|
| | | No cat. | $Al_2O_3$ | Ce/ Al | Pd-Ce/ Al | Ru-Ce/ Al | Ni-Ce/ Al |
| *HC Compound* | | | | | | | |
| trans-4-Decene | 10.717 | - | - | - | - | 1.01 | - |
| 2-Decene, (Z)- | 10.759 | - | - | 0.82 | 0.58 | - | 0.99 |
| 1H-Indene | 11.913 | - | 0.9 | - | - | - | - |
| 1H-Indene | 11.913 | - | - | 1.17 | - | - | - |
| 3-Tetradecene, (Z) | 13.673 | 0.42 | - | - | - | - | - |
| Undecane | 13.848 | - | - | - | 1.05 | - | 1.1 |
| Octane, 2,4,6-trimethyl- | 13.857 | - | - | 1.33 | - | - | - |
| 2-Undecene, (E)- | 14.016 | - | 0.4 | 0.99 | 0.61 | 0.55 | 0.88 |
| 2-Undecene, (E)- | 14.297 | - | - | 0.61 | - | - | - |
| 5-Undecene, (E)- | 14.638 | - | 0.78 | - | - | - | - |
| 5,6-Undecadiene | 14.639 | - | - | 0.94 | - | - | 0.94 |
| 1H-Indene, 1-methyl- | 15.323 | - | 1.12 | 1.14 | | 0.89 | |
| Cycloprop[a]indene, 1,1a,6,6a-tetrahydro- | 15.512 | - | 1.67 | - | - | - | - |
| 2-Dodecene, (Z)- | 16.737 | - | 2.01 | 1.83 | 1.49 | 1.59 | 1.76 |
| 5-Dodecene, (E)- | 16.997 | - | - | - | 0.71 | - | - |
| Tetradecane | 17.005 | - | - | 0.86 | - | 2.14 | 0.81 |
| 5-Dodecyne | 17.744 | - | 0.57 | - | - | - | - |
| 1-Heptadecene | 19.722 | - | - | 2.49 | 2.46 | 2.75 | 2.42 |
| Tetradecane | 19.925 | - | - | - | - | 0.78 | - |
| 1-Tetradecene | 19.967 | - | - | 0.98 | 0.72 | - | - |
| 1-Tetradecene | 22.527 | - | - | - | 2.48 | - | - |
| 7-Hexadecene, (Z)- | 22.538 | - | - | 3.13 | - | 2.69 | - |
| 3-Hexadecene, (Z)- | 22.539 | - | 3.47 | - | - | - | - |
| (3Z)-3-Hexadecene | 22.639 | 0.5 | - | - | - | - | - |

**Table A-1 (cont.)** Pyrolytic products of Jatropha residue with $Al_2O_3$ catalysts using Jatropha to catalyst ratio of 1:10

| Compound Name | RT | % Peak area | | | | | |
|---|---|---|---|---|---|---|---|
| | | No cat. | $Al_2O_3$ | Ce/ Al | Pd- Ce/ Al | Ru- Ce/ Al | Ni-Ce/ Al |
| *HC Compound* | | | | | | | |
| 5-Tetradecene, (E)- | 22.883 | - | - | 0.6 | - | - | - |
| 9-Octadecene, (E)- | 25.15 | - | - | - | - | 0.88 | - |
| 1-Tridecene | 25.183 | - | - | - | 0.67 | - | - |
| Hexadecane | 25.399 | - | 0.8 | 1.33 | 1.14 | - | - |
| (3Z)-3-Hexadecene | 25.507 | 0.34 | - | - | - | - | - |
| 1,13-Tetradecadiene | 27.34 | - | 0.43 | - | - | - | - |
| 5-Octadecene, (E)- | 27.711 | - | - | 1.02 | 0.64 | - | 2.73 |
| 5-Eicosene, (E)- | 27.711 | - | 1.36 | - | - | 0.89 | 1 |
| 5-Eicosene, (E)- | 29.7 | - | - | - | - | 0.82 | 0.92 |
| 5-Octadecene, (E)- | 29.867 | 0.32 | 0.73 | 0.61 | - | - | 0.7 |
| Hexadecane | 30.267 | - | - | 0.59 | - | - | - |
| Heptacosane | 30.267 | - | 0.44 | - | - | 1.23 | 1.45 |
| 1,E-8,Z-10-Pentadecatriene | 38.527 | - | 0.56 | - | - | - | - |
| Tetracosane | 44.02 | 0.29 | - | - | - | - | - |
| Pentacosane | 45.235 | - | 0.36 | - | - | - | - |
| Tetratetracontane | 45.294 | 0.39 | - | - | - | - | - |
| Cholesta-3,5-diene | 47.135 | 1.78 | - | - | - | - | - |
| *Ketone* | | | | | | | |
| Acetol | 2.507 | 2.65 | - | - | - | - | - |
| 3-Penten-2-one, (E) | 2.617 | 0.4 | - | - | - | - | - |
| 3-Hexanone | 2.9 | - | - | - | 2.23 | - | 1.67 |
| Cyclohexanone | 3.1 | - | - | - | - | 1.26 | 0.75 |
| 2-Propanone, 1-(acetyloxy) | 4.249 | 0.75 | - | - | - | - | - |

**Table A-1 (cont.)** Pyrolytic products of Jatropha residue with $Al_2O_3$ catalysts using Jatropha to catalyst ratio of 1:10

| Compound Name | RT | % Peak area | | | | | |
|---|---|---|---|---|---|---|---|
| | | No cat. | $Al_2O_3$ | Ce/ Al | Pd- Ce/ Al | Ru- Ce/ Al | Ni-Ce/ Al |
| *Ketone* | | | | | | | |
| 2-Cyclopenten-1-one, 2-methyl- | 7.351 | - | 0.83 | - | - | - | - |
| 6-Oxa-bicyclo[3.1.0]hexan-3-one | 8.023 | 0.59 | - | - | - | - | - |
| 2-Cyclopenten-1-one, 2-hydroxy-3-methyl- | 11.451 | 0.44 | - | - | - | - | - |
| *N-compound* | | | | | | | |
| Butanenitrile,2-methyl | 3.117 | - | 0.66 | - | 0.82 | - | - |
| Butanenitrile, 3-methyl | 3.183 | 0.36 | 1.44 | 1.57 | 1.49 | 1.67 | 1.47 |
| Benzenamine, 3-methyl- | 3.251 | 0.52 | - | - | - | - | - |
| Azine | 3.419 | - | - | - | - | 2.59 | - |
| 2,4-Pentadienenitrile | 3.435 | - | - | - | 2.45 | - | - |
| 1H-Pyrrole | 3.621 | - | - | - | 5.29 | - | - |
| Cyclopentane, nitro- | 3.686 | 0.97 | - | - | - | - | - |
| Formamide, N,N-dimethyl- | 4.005 | - | - | - | - | - | 2.15 |
| Pyridine, 2-ethyl- | 4.867 | - | - | - | 1.51 | - | - |
| 1H-Pyrrole, 2-methyl- | 5.588 | 0.6 | 3.33 | - | - | 0.99 | - |
| 1H-Pyrrole, 3-methyl- | 5.753 | - | 1.8 | 3.03 | 2.46 | 2.04 | 2.76 |
| Pyridine, 3-methyl- | 6.05 | - | 0.6 | - | - | - | - |
| Hexanenitrile | 6.556 | - | 0.83 | 0.77 | 0.68 | - | - |
| 1H-Pyrrole, 2,5-dimethyl- | 8.058 | - | - | 1.23 | - | - | 1.93 |
| 1H-Pyrrole, 1-ethyl- | 8.068 | - | 2.44 | - | - | - | - |

**Table A-1 (cont.)** Pyrolytic products of Jatropha residue with $Al_2O_3$ catalysts using Jatropha to catalyst ratio of 1:10

| Compound Name | RT | % Peak area | | | | | |
|---|---|---|---|---|---|---|---|
| | | No cat. | $Al_2O_3$ | Ce/ Al | Pd-Ce/ Al | Ru-Ce/ Al | Ni-Ce/ Al |
| *N-compound* | | | | | | | |
| 1H-Pyrrole, 2,5-dimethyl- | 8.15 | - | - | 0.91 | - | - | - |
| 1H-Pyrrole, 2,5-dimethyl- | 8.427 | - | - | 0.7 | - | - | - |
| 1H-Pyrrole, 2,5-dimethyl- | 8.428 | - | 0.83 | 1.5 | 1.04 | - | 1.56 |
| Aniline | 9.685 | - | 1.65 | 1.85 | 2.12 | 2.32 | 1.84 |
| Benzenamine | 9.798 | 0.7 | - | - | - | - | - |
| Benzonitrile, 2-methyl- | 9.883 | - | - | - | 1.47 | - | - |
| Succinimide | 14.754 | 0.49 | - | - | - | - | - |
| Benzyl cyanide | 15.034 | 0.49 | - | - | 0.43 | 0.51 | - |
| Indolizine | 19.802 | 0.85 | - | - | - | - | - |
| 1H-Indole, 3-methyl- | 22.313 | - | 1.02 | 1.03 | 0.8 | 1.07 | 1.05 |
| 1-Dodecanamine, N,N-dimethyl- | 25.44 | - | - | - | - | - | 0.93 |
| Heptadecanenitrile | 34.514 | - | - | - | - | 2.88 | - |
| Heptadecanenitrile | 34.568 | - | 5.66 | 4.59 | 4 | 1.13 | - |
| Oleanitrile | 37.453 | - | 4.53 | 1.84 | 1.3 | - | - |
| Pyrazine, methyl- | 37.517 | - | 2.37 | - | - | - | - |
| Oleanitrile | 37.529 | 0.59 | 0.41 | 3.69 | 1.44 | 3.29 | 3.89 |
| Nonadecanenitrile | 37.776 | - | 2.67 | 1.92 | 2.23 | - | 1.8 |
| Hexadecanamide | 38.692 | - | - | - | - | 0.7 | 3.3 |
| Hexadecanamide | 38.879 | 3.67 | - | - | - | 0.41 | - |
| 2,5-Pyrrolidinedione | 39.762 | 0.29 | - | - | - | - | - |
| 9-Octadecenamide, (Z)- | 41.032 | 0.49 | - | 0.61 | - | 1.5 | 1.27 |

**Table A-1 (cont.)** Pyrolytic products of Jatropha residue with $Al_2O_3$ catalysts using Jatropha to catalyst ratio of 1:10

| Compound Name | RT | % Peak area | | | | | |
|---|---|---|---|---|---|---|---|
| | | No cat. | $Al_2O_3$ | Ce/ Al | Pd-Ce/ Al | Ru-Ce/ Al | Ni-Ce/ Al |
| *N-compound* | | | | | | | |
| 9-Octadecenamide, (Z)- | 44.354 | - | - | - | - | 0.89 | - |
| *Phenol* | | | | | | | |
| Phenol | 10.062 | 1.5 | - | - | - | 2.67 | - |
| p-Cresol | 13.147 | 1.37 | - | - | - | - | - |
| 2-methoxy- Phenol | 13.495 | 1.01 | - | - | - | - | - |

**Table A-2** Pyrolytic products of Jatropha residue with $ZrO_2$ catalysts using Jatropha to catalyst ratio of 1:10

| Compound Name | RT | % Peak area | | | | | |
|---|---|---|---|---|---|---|---|
| | | No cat. | $ZrO_2$ | Ce/ $ZrO_2$ | Pd-Ce/ $ZrO_2$ | Ru-Ce/ $ZrO_2$ | Ni-Ce/ $ZrO_2$ |
| *Alcohol* | | | | | | | |
| 1-Dodecanol | 24.79 | 1.27 | - | 0.72 | - | - | - |
| Tetradecanol | 29.796 | 0.55 | - | - | - | - | - |
| Stigmast-5-en-3-ol, (3.beta.)- | 46.876 | 0.39 | - | - | - | - | - |
| *Aldehyde* | | | | | | | |
| Hexanal | 4.563 | 0.36 | - | - | - | - | - |
| cis-9-Hexadecenal/9-Hexadecenal, (Z) | 37.424 | - | 8.97 | 8.63 | 5.08 | 2.16 | 4.01 |
| 7-Hexadecenal, (Z)- | 37.432 | - | - | - | 2.54 | 1.63 | |
| 13-Octadecenal, (Z)- | 37.433 | - | - | - | - | - | 2.09 |
| *Aromatic* | | | | | | | |
| Benzene | 2.517 | - | - | - | 3.68 | - | - |
| Methylbenzene | 3.941 | 2.75 | - | - | - | - | - |
| Benzene, 1,2-dimethyl- | 6.054 | - | - | - | - | 0.96 | - |
| Benzene, ethyl- | 6.216 | 0.42 | - | - | - | - | - |
| Styrene | 7.066 | 0.41 | - | - | - | - | - |
| *Carboxylic acid* | | | | | | | |
| Acetic oxide | 2.063 | 3.01 | - | - | - | - | - |
| Acetic acid | 2.129 | - | - | - | 3.8 | - | - |
| Propanoic acid | 2.934 | - | - | - | 1.03 | - | - |
| Oleic acid | 35.477 | 0.83 | - | - | - | - | - |
| Pentadecanoic acid | 35.72 | - | 6.62 | - | - | - | - |
| Palmitic acid | 35.871 | 10.85 | - | - | 12.03 | - | - |
| OCTADEC-9-ENOIC ACID | 38.279 | - | 8.41 | - | - | - | - |
| Oleic acid | 38.477 | 39.69 | - | - | - | - | - |
| Octadecanoic acid | 38.55 | - | - | - | 3.5 | - | - |
| Oleic acid | 38.689 | 6.36 | - | - | 11.67 | - | - |

**Table A-2 (cont.)** Pyrolytic products of Jatropha residue with $ZrO_2$ catalysts using Jatropha to catalyst ratio of 1:10

| Compound Name | RT | % Peak area | | | | | |
|---|---|---|---|---|---|---|---|
| | | No cat. | $ZrO_2$ | Ce/ $ZrO_2$ | Pd-Ce/ $ZrO_2$ | Ru-Ce/ $ZrO_2$ | Ni-Ce/ $ZrO_2$ |
| *Ester* | | | | | | | |
| Methoxyacetic acid, hexyl ester | 2.109 | - | 2.183 | 8.82 | - | 9.51 | - |
| 2-HEXENYL ACETATE | 2.467 | - | - | 4.89 | - | - | - |
| Acetic acid, hexyl ester | 2.47 | - | 4.29 | - | - | - | 7.58 |
| Propanoic acid, 2-oxo-, methyl ester | 4.125 | - | - | - | - | 0.91 | 1.11 |
| 2-Propenoic acid, 1,4-butanediyl ester | 4.249 | 0.75 | 1.03 | - | 0.6 | - | - |
| Acetol | 6.331 | 0.62 | - | - | - | - | - |
| Carbonic acid, ethyl nonyl ester | 6.891 | - | - | 2.08 | - | - | - |
| Hexanoic acid, heptadecyl ester | 19.674 | - | 1.69 | 1.84 | - | - | 2.06 |
| 1,2-Benzenedicarboxylic acid, butyl 2-methylpropyl ester | 35.579 | - | - | 1.1 | - | - | - |
| Stigmast-5-en-3-ol, oleate | 47.029 | - | 1.2 | 1.12 | 1.36 | 1.08 | 1.53 |
| *Furan* | | | | | | | |
| 2-Furancarboxaldehyde | 5.356 | 0.67 | - | - | - | - | - |
| 2-Furanmethanol | 5.989 | 0.37 | - | - | - | - | - |
| *HC Compound* | | | | | | | |
| 1,6-Heptadiene, 2-methyl- | 2.603 | - | 2.54 | - | - | - | - |
| 1-Butene, 2,3-dimethyl- | 2.603 | - | - | 3.4 | - | - | - |

**Table A-2 (cont.)** Pyrolytic products of Jatropha residue with ZrO$_2$ catalysts using Jatropha to catalyst ratio of 1:10

| Compound Name | RT | % Peak area | | | | | |
|---|---|---|---|---|---|---|---|
| | | No cat. | ZrO$_2$ | Ce/ ZrO$_2$ | Pd-Ce/ ZrO$_2$ | Ru-Ce/ ZrO$_2$ | Ni-Ce/ ZrO$_2$ |
| *HC Compound* | | | | | | | |
| 3-Cyclopentyl-1-propyne | 2.619 | - | - | - | - | 3.22 | 6.01 |
| 1-Hexene, 5-methyl- | 2.767 | - | - | - | - | 3.83 | - |
| Cyclopentane, 1,2-dimethyl- | 2.773 | - | 3.42 | - | - | - | - |
| n-Hept-1-ene | 2.814 | 1.78 | - | 4.03 | 1.57 | - | 4.68 |
| Heptane | 2.869 | - | 1.64 | - | - | - | - |
| 2,3-Hexadiene, 2-methyl- | 2.933 | - | - | - | - | 2.04 | 2.15 |
| 1-Pentene, 4,4-dimethyl- | 3.173 | - | - | - | - | - | 4.15 |
| 1-Butyne, 3,3-dimethyl- | 3.6 | - | 2.25 | - | - | - | - |
| 1,3,5-Cycloheptatriene | 3.847 | - | 5.42 | 7.78 | 3.4 | 6.62 | 7.27 |
| 2-Nonene | 4.325 | - | - | - | - | 1.76 | 1.41 |
| 1-Octene | 4.452 | 1.01 | 1.5 | 1.87 | 0.95 | - | 2.18 |
| Octane | 4.533 | - | - | 1.43 | - | - | - |
| Hexane, 2,4-dimethyl- | 4.535 | - | 0.63 | - | - | - | - |
| 2,4-Dimethyl-1-heptene | 5.564 | - | - | - | - | 3.19 | - |
| 1,3,7-Octatrien-5-yne | 6.919 | - | 1.43 | - | 1.18 | 1.92 | 1.96 |
| Nonene | 7.133 | 0.29 | 1.09 | 1.45 | 0.86 | 1.21 | - |
| Decane | 7.273 | - | - | 1.29 | - | - | 0.7 |
| Cyclopropane, (2,2-dimethylpropylidene)- | 7.442 | - | - | - | - | 1.13 | - |
| Cyclopropane, 2-(1,1-dimethyl-2-pentenyl)-1,1-dimethyl- | 7.45 | - | - | 0.78 | - | - | - |

**Table A-2 (cont.)** Pyrolytic products of Jatropha residue with $ZrO_2$ catalysts using Jatropha to catalyst ratio of 1:10

| Compound Name | RT | % Peak area | | | | | |
|---|---|---|---|---|---|---|---|
| | | No cat. | $ZrO_2$ | Ce/ $ZrO_2$ | Pd-Ce/ $ZrO_2$ | Ru-Ce/ $ZrO_2$ | Ni-Ce/ $ZrO_2$ |
| *HC Compound* | | | | | | | |
| 1,5-Hexadiene, 2,5-dimethyl | 7.639 | 0.62 | - | - | - | - | - |
| Cyclopropane, 1-heptyl-2-methyl- | 10.194 | - | - | 0.79 | 0.56 | 0.66 | - |
| 1-Decene | 10.235 | - | 0.83 | - | - | - | 1.07 |
| Cyclopropane, 1-butyl-2-pentyl-, trans- | 13.476 | - | - | - | - | 0.57 | - |
| Cyclopropane, octyl | 13.48 | - | - | 1.58 | - | - | - |
| 4-DODECENE, (Z)- | 13.531 | - | 1.32 | - | - | - | 1.5 |
| 3-Tetradecene, (Z) | 13.673 | 0.42 | - | - | - | - | - |
| 1-Undecene, 4-methyl- | 14.535 | - | - | - | - | - | 0.93 |
| Cyclohexene, 4,4-dimethyl- | 14.54 | - | - | 1.27 | - | - | - |
| 1-Dodecene | 16.639 | - | - | 1.05 | 0.51 | 0.8 | 1.13 |
| 2-Dodecene, (Z)- | 16.697 | - | 0.9 | - | 0.68 | - | - |
| 1-Pentadecene | 22.44 | - | - | 1.1 | 0.54 | - | 1.04 |
| 3-Hexadecene, (Z)- | 22.446 | - | - | - | 1.06 | - | - |
| 7-Hexadecene, (Z)- | 22.496 | - | 1.54 | - | - | - | - |
| (3Z)-3-Hexadecene | 22.639 | 0.5 | - | - | - | - | - |
| 7-Tetradecene, (E)- | 23.679 | - | - | - | 0.81 | 0.87 | - |
| Eicosane | 24.565 | - | - | - | 1.27 | - | 1.76 |
| Cyclododecene | 24.582 | - | - | - | - | 0.69 | - |
| Cyclopropane, nonyl- | 24.585 | - | - | 0.57 | - | - | 0.7 |
| 5-Eicosene, (E)- | 25.153 | - | 0.52 | - | 1.34 | 3.08 | - |
| Heptadecane | 25.304 | - | - | 1.06 | - | - | - |
| Pentadecane | 25.309 | - | - | - | 0.74 | - | - |
| Hexadecane | 25.36 | - | 1.25 | - | - | 1.04 | 1.06 |

**Table A-2 (cont.)** Pyrolytic products of Jatropha residue with ZrO$_2$ catalysts using Jatropha to catalyst ratio of 1:10

| Compound Name | RT | % Peak area | | | | | |
|---|---|---|---|---|---|---|---|
| | | No cat. | ZrO$_2$ | Ce/ ZrO$_2$ | Pd-Ce/ ZrO$_2$ | Ru-Ce/ ZrO$_2$ | Ni-Ce/ ZrO$_2$ |
| *HC Compound* | | | | | | | |
| (3Z)-3-Hexadecene | 25.507 | 0.34 | - | - | - | - | - |
| 9-Octadecene, (E)- | 27.606 | - | - | - | - | - | 0.56 |
| 9-Octadecene, (E)- | 27.613 | - | - | 0.5 | 0.71 | - | 0.74 |
| 5-Eicosene, (E)- | 27.667 | - | 0.62 | - | - | - | - |
| 3-Hepten-1-yne, (Z)- | 29.409 | - | - | - | 1.07 | - | - |
| 9-Octadecyne | 29.467 | - | - | - | - | - | 0.79 |
| 1,13-Tetradecadiene | 29.481 | - | - | - | - | 2.6 | - |
| 1,19-Eicosadiene | 29.628 | - | - | - | - | 3.46 | - |
| 9-Octadecene, (E)- | 29.643 | - | - | - | - | - | 2.42 |
| 5-Octadecene, (E)- | 29.705 | - | 0.98 | 0.76 | - | - | - |
| 5-Octadecene, (E)- | 29.867 | 0.32 | - | - | - | - | - |
| 1-Nonadecene | 29.996 | - | - | - | - | 2.55 | - |
| Heptacosane | 30.222 | - | 0.79 | 0.42 | - | - | - |
| 2-Pentadecanone | 34.511 | - | - | 6.53 | - | - | - |
| 1,E-8,Z-10-Hexadecatriene | 38.454 | - | - | - | - | - | 0.71 |
| 1,E-8,Z-10-Pentadecatriene | 38.462 | - | - | 0.86 | 2.47 | 0.85 | - |
| 1,E-8,Z-10-Tridecatriene | 38.514 | - | 3.37 | - | - | - | - |
| Tetracosane | 44.02 | 0.29 | - | - | - | - | - |
| Pentacosane | 45.215 | - | 0.45 | - | 0.54 | - | - |
| Tetratetracontane | 45.294 | 0.39 | - | - | 0.96 | - | - |
| Cholesta-3,5-diene | 47.135 | 1.78 | - | - | - | - | - |
| *Ketone* | | | | | | | |
| 2-Propanone, 1-hydroxy- | 2.46 | - | - | - | - | 6.88 | 4.5 |

**Table A-2 (cont.)** Pyrolytic products of Jatropha residue with ZrO$_2$ catalysts using Jatropha to catalyst ratio of 1:10

| Compound Name | RT | % Peak area | | | | | |
|---|---|---|---|---|---|---|---|
| | | No cat. | ZrO$_2$ | Ce/ ZrO$_2$ | Pd-Ce/ ZrO$_2$ | Ru-Ce/ ZrO$_2$ | Ni-Ce/ ZrO$_2$ |
| *Ketone* | | | | | | | |
| Acetol | 2.507 | 2.65 | - | - | - | - | - |
| 3-Penten-2-one, (E) | 2.617 | 0.4 | - | - | - | - | - |
| 1-Hydroxy-3-methyl-2-butanone | 2.871 | - | - | 1.94 | - | - | - |
| 1-Heptyn-6-one | 3.175 | - | - | 1.9 | - | - | - |
| Cyclopentanone | 4.229 | - | 0.46 | 1.21 | 0.65 | 0.74 | 0.95 |
| 2-Propanone, 1-(acetyloxy) | 4.249 | 0.75 | - | - | - | - | - |
| 2-Cyclopenten-1-one | 5.213 | - | 1.1 | 1.19 | 0.59 | 1.35 | 1.32 |
| 6-Oxa-bicyclo[3.1.0]hexan-3-one | 8.023 | 0.59 | - | - | - | - | - |
| 2-Cyclopenten-1-one, 2-methyl- | 9.104 | - | - | - | - | - | 0.63 |
| 2-Cyclopenten-1-one, 3-methyl- | 9.105 | - | - | - | - | 0.67 | - |
| 2-Cyclopenten-1-one, 3-methyl- | 9.105 | - | - | 0.71 | - | - | - |
| Cycloheptanone | 10.716 | - | 0.71 | 0.96 | - | 0.81 | 0.76 |
| 2-Cyclopenten-1-one, 2-hydroxy-3-methyl- | 11.451 | 0.44 | 0.55 | - | - | - | - |
| 2-Nonadecanone | 34.48 | - | - | - | 7.38 | - | 5.09 |
| 3-Hexanone | 34.492 | | - | - | - | 3.61 | - |
| 2-Pentadecanone, 6,10,14-trimethyl- | 37.697 | - | - | 2.77 | - | - | 2.44 |
| Cyclopentadecanone | 39.913 | - | 0.58 | - | 0.73 | - | - |

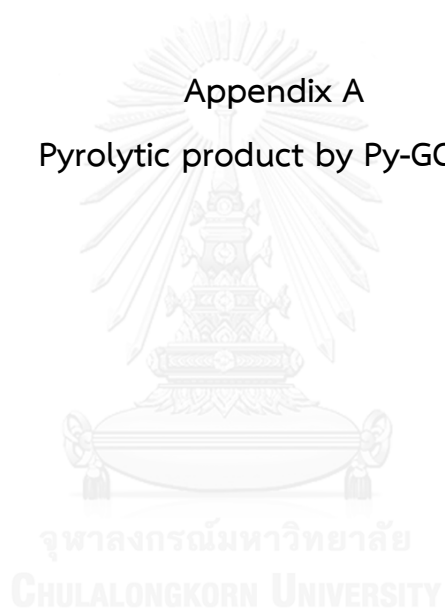**Table A-2 (cont.)** Pyrolytic products of Jatropha residue with $ZrO_2$ catalysts using Jatropha to catalyst ratio of 1:10

| Compound Name | RT | % Peak area | | | | | |
|---|---|---|---|---|---|---|---|
| | | No cat. | $ZrO_2$ | Ce/ $ZrO_2$ | Pd-Ce/ $ZrO_2$ | Ru-Ce/ $ZrO_2$ | Ni-Ce/ $ZrO_2$ |
| *N-compound* | | | | | | | |
| 2H-Pyran-2,6(3H)-dione, dihydro- | 2.23 | - | 0.3 | - | - | - | - |
| Propanenitrile, 2-methyl- | 2.231 | - | - | - | - | - | 0.8 |
| Aziridine, 1-vinyl | 2.6 | - | - | - | 1.33 | - | - |
| Butanenitrile,2-methyl | 3.179 | - | 1.17 | 1.25 | - | 1.44 | - |
| Butanenitrile, 3-methyl | 3.183 | 0.36 | - | - | 0.71 | 2.03 | - |
| Benzenamine, 3-methyl- | 3.251 | 0.52 | - | - | - | - | - |
| 2,4-Pentadienenitrile | 3.402 | - | - | - | 1.04 | - | - |
| Azine | 3.408 | - | 0.87 | 2.23 | - | 2.53 | 2.99 |
| 1H-Pyrrole | 3.599 | - | - | 3.61 | 1.76 | 2.9 | 3.63 |
| Cyclopentane, nitro- | 3.686 | 0.97 | - | - | - | - | - |
| Formamide, N,N-dimethyl- | 4.017 | - | - | - | - | 0.99 | 1.26 |
| 2-Acetyl-2-methyl-succinonitrile | 4.134 | - | 0.5 | 1 | - | - | - |
| 1H-Pyrrole, 1-methyl- | 5.439 | - | - | 1.54 | 0.62 | 1.17 | 0.98 |
| 1H-Pyrrole, 2-methyl- | 5.588 | 0.6 | 1.37 | 0.9 | - | 0.7 | - |
| Hexanenitrile | 6.514 | - | 0.6 | - | - | - | - |
| 1H-Pyrrole, 3-methyl- | 9.6 | - | - | - | - | 0.63 | 0.76 |
| Aniline | 9.646 | - | 1.05 | 0.74 | - | - | - |
| Benzonitrile | 9.792 | - | - | - | - | - | 0.97 |
| Benzenamine | 9.798 | 0.7 | - | - | 0.84 | - | - |
| Cyclopentanone, oxime | 14.6 | - | 1.31 | - | - | - | - |
| Succinimide | 14.754 | 0.49 | - | - | - | - | - |
| Benzonitrile, 2-methyl- | 14.814 | - | - | - | 0.66 | - | 1.04 |

**Table A-2 (cont.)** Pyrolytic products of Jatropha residue with $ZrO_2$ catalysts using Jatropha to catalyst ratio of 1:10

| Compound Name | RT | % Peak area | | | | | |
|---|---|---|---|---|---|---|---|
| | | No cat. | $ZrO_2$ | Ce/ $ZrO_2$ | Pd-Ce/ $ZrO_2$ | Ru-Ce/ $ZrO_2$ | Ni-Ce/ $ZrO_2$ |
| *N-compound* | | | | | | | |
| Benzeneacetonitrile | 15.034 | 0.49 | 0.78 | 0.92 | - | 0.84 | - |
| 1H-Indole | 19.611 | - | - | - | 1.2 | - | - |
| Indolizine | 19.802 | 0.85 | - | - | - | 1.54 | - |
| 1H-Indole, 3-methyl- | 22.268 | - | 0.58 | - | 0.74 | - | - |
| Hexadecanenitrile | 34.53 | - | 6.02 | - | - | - | - |
| Oleanitrile | 37.529 | 0.59 | - | - | - | - | - |
| Nonadecanenitrile | 37.701 | - | - | - | 3.35 | - | - |
| Heptadecanenitrile | 37.747 | - | 3.21 | - | - | 1.64 | - |
| Hexadecanamide | 38.879 | 3.67 | 2.45 | 0.47 | - | - | 0.53 |
| Pyridine, 2-ethyl- | 39.017 | - | - | - | 2.4 | - | - |
| 2,5-Pyrrolidinedione | 39.762 | 0.29 | - | - | - | - | - |
| Octadecanamide | 40.901 | - | - | - | 0.77 | 0.65 | - |
| Hexadecanamide | 40.927 | - | 0.48 | 1.47 | 2.93 | 1.85 | 1.17 |
| 9-Octadecenamide, (Z)- | 41.032 | 0.49 | 1.75 | 1.73 | 2.48 | 2.08 | 1.84 |
| 9-Octadecenamide, (Z)- | 44.322 | - | - | 1.92 | - | 1.15 | - |
| *Phenol* | | | | | | | |
| Phenol | 10.062 | 1.5 | 1.44 | 1.26 | 0.97 | 1.35 | 1.44 |
| Phenol, 3-methyl- | 13.045 | - | 1.41 | 1.63 | 1.4 | 2.08 | - |
| Phenol, 4-methyl/ p-Cresol | 13.147 | 1.37 | - | - | - | - | 1.92 |
| Phenol, 2-methyl- | 13.284 | - | - | 0.93 | - | - | 1.1 |
| 2-methoxy- Phenol | 13.495 | 1.01 | - | - | 0.95 | 2.03 | - |
| Phenol, 2-octyl- | 35.006 | - | - | - | - | - | 0.59 |

**Table A-3** Pyrolytic products of Jatropha residue with Rutile catalysts using Jatropha to catalyst ratio of 1:10

| Compound Name | RT | % Peak area | | | | | |
|---|---|---|---|---|---|---|---|
| | | No cat. | $TiO_2$ (Rutile) | Ce/ $TiO_2$ | Pd-Ce/ $TiO_2$ | Ru-Ce/ $TiO_2$ | Ni-Ce/ $TiO_2$ |
| *Alcohol* | | | | | | | |
| 1-Hexanol | 2.07 | - | - | - | - | - | 4.18 |
| Propan-2-ol, 1-(2-isopropyl-5-methylcyclohexyloxy)-3-(4-morpholyl)- | 24.038 | - | - | - | - | 1.28 | - |
| 1-Dodecanol | 24.79 | 1.27 | - | - | - | - | - |
| Tetradecanol | 29.796 | 0.55 | - | - | - | - | - |
| Stigmast-5-en-3-ol, (3.beta.)- | 46.876 | 0.39 | - | - | - | - | - |
| *Aldehyde* | | | | | | | |
| Hexanal | 4.563 | 0.36 | - | - | - | - | - |
| 2,4-Hexadienal | 5.196 | - | 1.34 | 1.61 | - | - | 1.68 |
| *Aromatic* | | | | | | | |
| Toluene | 3.941 | 2.75 | - | - | 5.97 | - | 7.23 |
| Benzene, ethyl- | 6.216 | 0.42 | - | - | - | 1.12 | - |
| Styrol | 7.066 | 0.41 | - | - | 0.89 | - | 1.02 |
| *Carboxylic acid* | | | | | | | |
| Acetic oxide | 2.063 | 3.01 | - | - | - | - | - |
| Acetic acid | 2.111 | - | - | - | 8.2 | 11.95 | - |
| Oleic acid | 35.477 | 0.83 | - | - | - | - | - |
| Pentadecanoic acid | 35.636 | - | - | - | - | - | 4.38 |
| Palmitic acid | 35.871 | 10.85 | - | - | - | - | - |
| Oleic acid | 38.477 | 39.69 | - | - | - | - | - |
| Oleic acid | 38.689 | 6.36 | - | - | - | - | 7.92 |

**Table A-3 (cont.)** Pyrolytic products of Jatropha residue with Rutile catalysts using Jatropha to catalyst ratio of 1:10

| Compound Name | RT | % Peak area | | | | | |
|---|---|---|---|---|---|---|---|
| | | No cat. | $TiO_2$ (Rutile) | Ce/ $TiO_2$ | Pd-Ce/ $TiO_2$ | Ru-Ce/ $TiO_2$ | Ni-Ce/ $TiO_2$ |
| *Ester* | | | | | | | |
| Methoxyacetic acid, hexyl ester | 2.11 | - | 9.05 | 10.88 | - | - | - |
| tert-Butyl perbenzoate | 2.483 | - | - | - | 5.67 | - | - |
| 2-Ethylhexyl pentenoate | 3.083 | - | - | - | - | 1.66 | - |
| Propanoic acid, 2-oxo-, methyl ester | 4.128 | - | 0.98 | 1.29 | 1.05 | 1.52 | 1.38 |
| 2-Propenoic acid, 1,4-butanediyl ester | 4.249 | 0.75 | - | - | 0.98 | 1.42 | - |
| Acetol | 6.331 | 0.62 | - | - | - | - | - |
| Dibutyl phthalate | 35.507 | - | - | - | 1.14 | - | - |
| Stigmast-5-en-3-ol, oleate | 46.982 | - | 1.55 | 1.72 | 1.51 | - | 1.16 |
| *Ether* | | | | | | | |
| 1,3-Dioxolane, 2-methyl- | 2.883 | - | - | 2.08 | - | - | - |
| *Furan* | | | | | | | |
| 2-Furancarboxaldehyde | 5.356 | 0.67 | - | - | - | 1.47 | - |
| 2-Furanmethanol | 5.989 | 0.37 | - | - | - | - | - |
| 2,3-DIHYDRO-BENZOFURAN | 17.451 | - | - | - | - | 0.93 | - |
| *HC Compound* | | | | | | | |
| Cyclopropane, 1,1,2-trimethyl- | 2.586 | - | - | - | - | - | 2.87 |
| 1-Butene, 2,3-dimethyl- | 2.606 | - | 3.13 | 3.2 | - | - | - |
| 1,4-Pentadiene, 2-methyl- | 2.667 | - | - | - | - | - | 1 |
| 1-Heptene | 2.814 | 1.78 | 3.39 | 3.65 | 2.55 | 2.15 | 2.67 |

**Table A-3 (cont.)** Pyrolytic products of Jatropha residue with Rutile catalysts using Jatropha to catalyst ratio of 1:10

| Compound Name | RT | % Peak area | | | | | |
| --- | --- | --- | --- | --- | --- | --- | --- |
| | | No cat. | TiO$_2$ (Rutile) | Ce/ TiO$_2$ | Pd-Ce/ TiO$_2$ | Ru-Ce/ TiO$_2$ | Ni-Ce/ TiO$_2$ |
| 1-Pentene, 4-methyl- | 3.171 | - | - | 2.66 | - | - | 2.75 |
| 1-Pentene, 4-methyl- | 3.172 | - | 2.54 | - | - | - | - |
| 1,3,5-Cycloheptatriene | 3.841 | - | 5.8 | 5.57 | - | 8.02 | - |
| 2-Nonene | 4.326 | - | 1.42 | - | - | - | 1.89 |
| 1-Octene | 4.452 | 1.01 | - | 2.31 | 1.51 | 2.2 | - |
| Hexane, 2,4-dimethyl- | 4.483 | - | - | - | - | - | 0.87 |
| Octane | 4.49 | - | - | - | - | 0.78 | - |
| Bicyclo[4.2.0]octa-1,3,5-triene | 6.841 | - | - | - | 1.35 | - | - |
| 1,3,7-Octatrien-5-yne | 6.889 | - | 1.26 | 1.54 | - | 1.56 | 1.68 |
| 1-Nonene | 7.133 | 0.29 | 0.84 | 0.9 | 0.92 | 1.02 | 1 |
| Cyclopropane, (2,2-dimethylpropylidene)- | 7.399 | - | - | - | - | 1.36 | 1.15 |
| 2,4-Hexadiene, 2,5-dimethyl- | 7.447 | - | 0.65 | 0.7 | - | - | - |
| 1,5-Hexadiene, 2,5-dimethyl | 7.639 | 0.62 | - | - | - | - | - |
| Cyclopentanone, 2-methyl- | 7.83 | - | - | - | - | 0.93 | - |
| 3-Octyne, 7-methyl- | 9.103 | - | 0.59 | 0.64 | - | 0.72 | 0.9 |
| 1-Decene | 10.186 | - | 1.27 | 1.3 | 2.18 | 1.78 | 2.09 |
| 1-Undecene | 13.405 | - | - | - | - | - | 0.71 |
| 5-Dodecene, (E)- | 13.424 | - | - | - | 1.49 | 1.83 | - |
| 4-DODECENE, (Z)- | 13.466 | - | - | 0.56 | - | - | - |
| Cyclopropane, 1-ethyl-2-heptyl- | 13.473 | - | 0.72 | - | - | - | - |

**Table A-3 (cont.)** Pyrolytic products of Jatropha residue with Rutile catalysts using Jatropha to catalyst ratio of 1:10

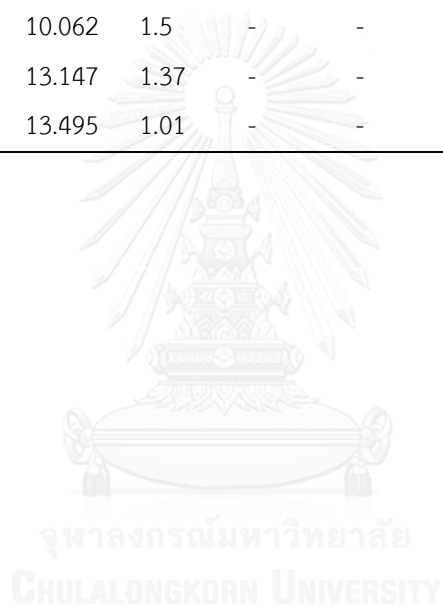| Compound Name | RT | % Peak area | | | | | |
|---|---|---|---|---|---|---|---|
| | | No cat. | TiO$_2$ (Rutile) | Ce/ TiO$_2$ | Pd-Ce/ TiO$_2$ | Ru-Ce/ TiO$_2$ | Ni-Ce/ TiO$_2$ |
| *HC Compound* | | | | | | | |
| 3-Tetradecene, (Z) | 13.673 | 0.42 | 0.94 | - | - | - | - |
| 1-Octene, 2-methyl- | 14.533 | - | - | 1.66 | - | - | - |
| 2-Dodecene, (Z)- | 16.581 | - | - | - | 1.4 | - | - |
| 1-Dodecene | 16.633 | - | 0.63 | 0.65 | - | 1.59 | 0.74 |
| 3-Hexadecene, (Z)- | 22.349 | - | - | - | - | - | 1.22 |
| 7-Tetradecene, (E)- | 22.368 | - | - | - | 1.58 | - | - |
| 9-Octadecene, (E)- | 22.371 | - | - | - | - | 1.94 | - |
| 1-Tetradecene | 22.418 | - | - | 0.91 | - | - | - |
| (3Z)-3-Hexadecene | 22.639 | 0.5 | - | - | - | - | - |
| 5-Tetradecene, (E)- | 24.513 | - | - | - | 1.46 | - | - |
| Cyclododecene | 24.567 | - | - | 1.01 | - | - | - |
| Cyclopropane, nonyl- | 24.576 | - | 0.94 | - | - | 1.99 | 1.07 |
| Heptadecane | 25.233 | - | - | - | - | 2.03 | - |
| Hexadecane | 25.284 | - | - | 1.27 | 1.92 | - | 1.29 |
| Eicosane | 25.29 | - | 1.45 | - | - | - | - |
| (3Z)-3-Hexadecene | 25.507 | 0.34 | - | - | - | - | - |
| 9-Octadecyne | 29.403 | - | - | - | 0.89 | - | - |
| 1-Nonadecene | 29.567 | - | - | 0.82 | - | - | - |
| 5-Octadecene, (E)- | 29.571 | - | - | - | 3.16 | - | - |
| 5-Eicosene, (E)- | 29.638 | - | 1.74 | - | 0.9 | 1.17 | 1.95 |
| 5-Octadecene, (E)- | 29.867 | 0.32 | - | 0.99 | 1.64 | - | - |
| Heptacosane | 30.092 | - | - | - | 1.33 | - | 0.68 |
| 3,9-Dodecadiyne | 37.919 | - | - | - | 1.67 | - | - |
| 1,E-8,Z-10-Hexadecatriene | 38.402 | - | - | - | 1.54 | - | - |
| 1,E-8,Z-10-Hexadecatriene | 38.453 | - | 1.54 | 0.9 | - | - | - |

**Table A-3 (cont.)** Pyrolytic products of Jatropha residue with Rutile catalysts using Jatropha to catalyst ratio of 1:10

| Compound Name | RT | % Peak area | | | | | |
|---|---|---|---|---|---|---|---|
| | | No cat. | TiO$_2$ (Rutile) | Ce/ TiO$_2$ | Pd-Ce/ TiO$_2$ | Ru-Ce/ TiO$_2$ | Ni-Ce/ TiO$_2$ |
| *HC Compound* | | | | | | | |
| 1-Octadecene | 38.733 | - | - | - | - | - | 0.82 |
| 5-Eicosene, (E)- | 41.892 | - | 1.08 | - | 1.21 | - | - |
| Tetracosane | 44.02 | 0.29 | - | - | - | - | - |
| TETRACONTANE | 45.12 | - | - | - | 0.65 | - | - |
| Pentacosane | 45.166 | - | - | 0.54 | - | - | - |
| TETRACONTANE | 45.168 | - | 0.52 | - | - | - | - |
| Tetratetracontane | 45.294 | 0.39 | - | - | - | - | - |
| Cholesta-3,5-diene | 47.135 | 1.78 | - | - | - | - | - |
| *Ketone* | | | | | | | |
| 2-Propanone, 1-hydroxy- | 2.448 | - | - | - | - | 7.04 | 5.59 |
| Acetol | 2.507 | 2.65 | 5.47 | 5.54 | - | - | - |
| 3-Penten-2-one, (E) | 2.617 | 0.4 | - | - | - | - | - |
| 3-Hexanone | 2.85 | - | - | - | - | - | 2.13 |
| 2-Hydroxy-3-hexanone Cyclopentanone | 4.184 | - | - | - | - | 0.56 | 0.54 |
| 2-Propanone, 1-(acetyloxy) | 4.249 | 0.75 | - | - | - | 0.78 | - |
| Cyclopentanone, 2-methyl- | 7.873 | - | 0.57 | 0.73 | - | - | 1.16 |
| 6-Oxa-bicyclo[3.1.0]hexan-3-one | 8.023 | 0.59 | - | - | - | - | - |
| Cycloheptanone | 10.603 | - | - | - | - | - | 1.58 |

**Table A-3 (cont.)** Pyrolytic products of Jatropha residue with Rutile catalysts using Jatropha to catalyst ratio of 1:10

| Compound Name | RT | % Peak area | | | | | |
|---|---|---|---|---|---|---|---|
| | | No cat. | TiO$_2$ (Rutile) | Ce/ TiO$_2$ | Pd-Ce/ TiO$_2$ | Ru-Ce/ TiO$_2$ | Ni-Ce/ TiO$_2$ |
| *Ketone* | | | | | | | |
| Cycloheptanone | 10.613 | - | - | - | - | 1.03 | - |
| 2-Cyclopenten-1-one, 2-hydroxy-3-methyl- | 11.233 | - | - | 0.9 | - | 0.88 | 0.86 |
| 2-Cyclopenten-1-one, 2-hydroxy-3-methyl- | 11.451 | 0.44 | 0.8 | - | - | - | - |
| CYCLOEICOSANE | 27.601 | - | 0.47 | - | - | - | - |
| Cyclotridecanone | 39.81 | - | - | - | 0.75 | - | - |
| Cyclopentadecanone | 39.863 | - | 1.07 | - | - | - | - |
| *N-compound* | | | | | | | |
| N-VINYLAZIRIDINE | 2.584 | - | - | - | - | 2.03 | - |
| Aziridine, 1-vinyl | 2.585 | - | - | - | 1.91 | - | - |
| Butanenitrile, 3-methyl | 3.183 | 0.36 | - | - | 1.25 | 1.99 | - |
| Benzenamine, 3-methyl- | 3.251 | 0.52 | 0.42 | 0.72 | - | - | - |
| Pyridine / Azine | 3.403 | - | - | 1.43 | - | 1.88 | 1.49 |
| 2,4-Pentadienenitrile | 3.406 | - | 1.37 | - | 1.26 | - | - |
| 1H-Pyrrole | 3.596 | - | 2.57 | 2.65 | 2.42 | 2.87 | 2.67 |
| Cyclopentane, nitro- | 3.686 | 0.97 | - | - | - | - | - |
| Formamide, N,N-dimethyl- | 3.996 | - | 1.41 | 1.26 | - | 0.85 | - |
| 1H-Pyrazole, 3,5-dimethyl- | 5.156 | - | - | - | 0.86 | - | - |
| 1H-Pyrrole, 1-methyl- | 5.391 | - | - | - | 0.95 | 1.34 | - |
| 1H-Pyrrole, 3-methyl- | 5.434 | - | 1.08 | 1.08 | - | - | 1.41 |
| 1H-Pyrrole, 2-methyl- Pyridine, 3-methyl- | 5.588 | 0.6 | - | - | - | - | - |
| Pyridine, 3-methyl- | 9.597 | - | 1.23 | 1.34 | - | 1.34 | 0.98 |
| Benzenamine | 9.798 | 0.7 | - | - | 1.32 | - | - |

**Table A-3 (cont.)** Pyrolytic products of Jatropha residue with Rutile catalysts using Jatropha to catalyst ratio of 1:10

| Compound Name | RT | % Peak area | | | | | |
| --- | --- | --- | --- | --- | --- | --- | --- |
| | | No cat. | TiO$_2$ (Rutile) | Ce/ TiO$_2$ | Pd-Ce/ TiO$_2$ | Ru-Ce/ TiO$_2$ | Ni-Ce/ TiO$_2$ |
| *N-compound* | | | | | | | |
| 1H-Pyrrole-2,5-dione | 10.03 | - | - | - | - | 0.94 | - |
| 2(1H)-Pyridinone | 14.317 | - | - | - | - | 1.86 | - |
| Propanenitrile, 2-methyl- | 14.75 | - | - | - | - | 1.14 | - |
| Succinimide | 14.754 | 0.49 | 1.45 | - | 1.69 | 2.42 | - |
| Benzonitrile, 2-methyl- | 14.8 | - | 0.72 | 0.73 | - | - | 0.81 |
| Benzeneacetonitrile | 15.034 | 0.49 | - | - | 0.82 | - | - |
| 2H-Pyran-2,6(3H)-dione, dihydro- | 16.093 | - | - | - | - | 0.98 | - |
| Indole | 19.577 | - | - | 1.57 | - | 2.23 | - |
| 1H-Indole | 19.585 | - | 1.39 | - | - | - | 1.49 |
| Indolizine | 19.802 | 0.85 | - | - | 1.89 | - | - |
| 1H-Indole, 3-methyl- | 22.183 | - | - | 1.25 | - | 0.78 | - |
| N,N-DIMETHYL-UNDECYLAMINE | 25.387 | - | 1.39 | 1.09 | - | - | - |
| Hexadecanenitrile | 34.452 | - | - | 2.29 | 3.1 | - | - |
| Heptadecanenitrile | 34.465 | - | 4.74 | 1.35 | 2.89 | - | - |
| 9-Octadecynenitrile | 37.283 | - | 0.8 | - | - | - | - |
| Oleanitrile | 37.529 | 0.59 | 9.27 | 3.9 | 4.29 | - | 1.91 |
| Heptadecanenitrile | 37.694 | - | 3.07 | - | - | - | 0.89 |
| 6-Octadecynenitrile | 38.386 | - | - | - | - | - | 4.92 |
| Hexadecanamide | 38.69 | - | 1.8 | 1.1 | 2.94 | - | 1.02 |
| Hexadecanamide | 38.879 | 3.67 | 0.93 | 1.96 | 0.87 | - | 2.73 |
| 2,5-Pyrrolidinedione | 39.762 | 0.29 | - | - | - | - | - |
| Hexadecanamide | 40.818 | - | - | - | - | - | 0.68 |
| 9-Octadecenamide, (Z)- | 41.032 | 0.49 | 3.45 | 5.96 | 3.15 | - | 2.33 |
| Oleanitrile | 41.888 | - | - | 0.98 | - | - | - |

**Table A-3 (cont.)** Pyrolytic products of Jatropha residue with Rutile catalysts using Jatropha to catalyst ratio of 1:10

| Compound Name | RT | % Peak area | | | | | |
|---|---|---|---|---|---|---|---|
| | | No cat. | $TiO_2$ (Rutile) | Ce/ $TiO_2$ | Pd-Ce/ $TiO_2$ | Ru-Ce/ $TiO_2$ | Ni-Ce/ $TiO_2$ |
| *N-compound* | | | | | | | |
| 9-Octadecenamide, (Z)- | 44.318 | - | 3.55 | 6.02 | 2.18 | - | - |
| *Phenol* | | | | | | | |
| Phenol | 10.062 | 1.5 | 2.73 | 2.75 | 2.03 | 2.06 | 3.76 |
| Phenol, 3-methyl- | 13.004 | - | 2.17 | 2.27 | 2.45 | 3.09 | - |
| Phenol, 4-methyl/ p-Cresol | 13.147 | 1.37 | - | 1.23 | - | | 2.12 |
| Phenol, 2-methyl- | 13.228 | - | - | - | 1.59 | - | 0.91 |
| 2-methoxy- Phenol | 13.495 | 1.01 | 0.92 | - | - | 2.01 | - |
| *Sugar* | | | | | | | |
| Isosorbide | 19.265 | - | - | - | - | 1.09 | - |
| levoglucosan | 24.875 | - | - | - | 2.99 | 3.19 | - |

**Table A-4** Pyrolytic products of Jatropha residue with Anatase catalysts (Jatropha to catalyst ratio of 1:10)

| Compound Name | RT | % Peak area | | | | | |
|---|---|---|---|---|---|---|---|
| | | No cat. | TiO$_2$ (Anatase | Ce/ TiO$_2$ | Pd- Ce/ TiO$_2$ | Ru- Ce/ TiO$_2$ | Ni-Ce/ TiO$_2$ |
| *Alcohol* | | | | | | | |
| 2-Pentadecyn-1-ol | 10.614 | - | 0.93 | - | - | - | - |
| 1-Dodecanol | 24.79 | 1.27 | - | - | - | - | - |
| Tetradecanol | 29.796 | 0.55 | - | - | - | - | - |
| Stigmast-5-en-3-ol, (3.beta.)- | 46.876 | 0.39 | - | - | - | - | - |
| *Aldehyde* | | | | | | | |
| Butanal, 3-methyl- | 2.403 | - | - | - | 2.5 | 2.53 | 1.04 |
| Hexanal | 4.563 | 0.36 | - | - | - | - | - |
| Benzenepentanal | 18.56 | - | 0.65 | - | - | - | - |
| *Aromatic* | | | | | | | |
| Benzene | 2.562 | - | 6.63 | 5.33 | 4.53 | 5.06 | 0.74 |
| Methylbenzene | 3.941 | 2.75 | 12.34 | 6.89 | - | - | - |
| Benzene, ethyl- | 6.216 | 0.42 | 4.07 | - | - | 0.69 | 1.56 |
| Benzene, 1,4-dimethyl- | 6.274 | - | 3.32 | - | - | - | - |
| Benzene, 1,2-dimethyl- | 6.936 | - | 2.03 | - | - | - | - |
| Styrol | 7.066 | 0.41 | - | 1.02 | 0.64 | - | - |
| Benzene, propyl- | 8.84 | - | 0.71 | - | - | - | - |
| Benzene, 1,3,5-trimethyl- | 10.137 | - | 1.21 | - | - | - | - |
| Benzene, 1-propynyl- | 11.748 | - | 1.11 | - | - | - | - |
| Benzene, butyl- | 12.189 | - | 0.67 | - | - | - | - |
| Benzene, pentyl- | 15.45 | - | 0.68 | - | - | - | - |
| Naphthalene | 16.201 | - | 1.15 | - | 0.65 | - | - |
| Naphthalene, 2-methyl- | 19.531 | - | 1.6 | - | - | - | - |
| Naphthalene, 2-methyl- | 20.015 | - | 0.73 | - | - | - | - |
| Benzene, decyl- | 29.483 | - | - | - | - | 0.75 | - |

**Table A-4 (cont.)** Pyrolytic products of Jatropha residue with Anatase catalysts (J:C catalyst ratio of 1:10)

| Compound Name | RT | % Peak area | | | | | |
|---|---|---|---|---|---|---|---|
| | | No cat. | TiO$_2$ (Anatase | Ce/ TiO$_2$ | Pd-Ce/ TiO$_2$ | Ru-Ce/ TiO$_2$ | Ni-Ce/ TiO$_2$ |
| *Aromatic* | | | | | | | |
| Benzene, (1-methyl-1-propylpentyl)- | 37.901 | - | - | - | 0.71 | - | - |
| *Carboxylic acid* | | | | | | | |
| Acetic oxide | 2.063 | 3.01 | - | - | - | - | - |
| Oleic acid | 35.477 | 0.83 | - | - | - | - | - |
| Palmitic acid | 35.871 | 10.85 | - | - | - | - | - |
| Oleic acid | 38.477 | 39.69 | - | - | - | - | - |
| Oleic acid | 38.689 | 6.36 | - | - | - | - | - |
| *Ester* | | | | | | | |
| Acetic acid, hexyl ester | 2.6 | - | - | - | - | - | 2.09 |
| 2-Propenoic acid, 1,4-butanediyl ester | 4.249 | 0.75 | - | - | - | - | - |
| Acetol | 6.331 | 0.62 | - | - | - | - | - |
| Hexanoic acid, heptadecyl ester | 19.541 | - | - | 1.8 | - | - | - |
| Hexanoic acid, octadecyl ester | 29.384 | - | - | - | - | - | 1.08 |
| Hydroperoxide, 1-methylpentyl | 2.096 | - | - | - | 5.78 | 5.49 | - |
| Hexane, 1-(hexyloxy)-5-methyl- | 5.936 | - | - | - | - | - | 1.68 |
| *Furan* | | | | | | | |
| Furan, 2,5-dimethyl- | 2.917 | - | - | - | - | 0.55 | 3.59 |
| 2,4-Dimethylfuran | 2.917 | - | - | - | 0.5 | - | - |
| 2-Furancarboxaldehyde | 5.356 | 0.67 | - | - | - | - | - |
| 2-Furanmethanol | 5.989 | 0.37 | - | - | - | - | - |

**Table A-4 (cont.)** Pyrolytic products of Jatropha residue with Anatase catalysts (Jatropha to catalyst ratio of 1:10)

| Compound Name | RT | % Peak area | | | | | |
| --- | --- | --- | --- | --- | --- | --- | --- |
| | | No cat. | TiO$_2$ (Anatase | Ce/ TiO$_2$ | Pd-Ce/ TiO$_2$ | Ru-Ce/ TiO$_2$ | Ni-Ce/ TiO$_2$ |
| *HC Compound* | | | | | | | |
| 1-Pentene, 4-methyl- | 2.102 | - | - | 4.89 | - | - | - |
| 1,3-Cyclopentadiene, methyl- | 2.406 | - | - | 2.52 | - | - | - |
| Cyclopentane, 1,2-dimethyl- | 2.75 | - | 0.99 | 3.76 | - | 3.26 | 1.68 |
| 1-Heptene | 2.814 | 1.78 | - | - | 3.22 | - | - |
| Heptane | 2.85 | - | - | - | 1.12 | 0.93 | 1.52 |
| Pentane, 2,3,4-trimethyl- | 2.853 | - | - | 1.62 | - | - | - |
| Hexane, 3-methyl- | 2.864 | - | 2.18 | - | - | - | - |
| CYCLOPENTENE, 3-ETHENYL- | 3.422 | - | 3.25 | - | - | - | - |
| Cyclopentene,3-(2-propenyl)- | 3.571 | - | 6.02 | - | - | 3.27 | - |
| 1,3,5-Cycloheptatriene | 3.808 | - | - | - | 5.42 | 4.96 | - |
| 1-Octene | 4.452 | 1.01 | - | 1.5 | 1.51 | 1.42 | 1.06 |
| Octane | 4.483 | - | - | - | 0.83 | - | - |
| Hexane, 2,4-dimethyl- | 4.499 | - | - | 0.94 | - | 0.77 | - |
| 1-Decene, 2,4-dimethyl | 4.501 | - | 1.89 | - | - | - | - |
| 1-Pentene, 4,4-dimethyl- | 5.333 | - | 1.72 | 0.59 | - | 0.62 | - |
| 1,5-Hexadiene, 3-methyl- | 5.411 | - | 3.14 | - | - | - | - |
| 2,4-Dimethyl-1-heptene | 5.516 | - | 1.59 | - | - | - | - |
| Bicyclo[4.2.0]octa-1,3,5-triene | 6.847 | - | 1.96 | 1.72 | 1.86 | 1.64 | 1.92 |
| 2-Decene, (Z)- | 6.924 | - | - | - | - | 1.31 | - |

**Table A-4 (cont.)** Pyrolytic products of Jatropha residue with Anatase catalysts (Jatropha to catalyst ratio of 1:10)

| Compound Name | RT | % Peak area | | | | | |
| --- | --- | --- | --- | --- | --- | --- | --- |
| | | No cat. | $TiO_2$ (Anatase | Ce/ $TiO_2$ | Pd-Ce/ $TiO_2$ | Ru-Ce/ $TiO_2$ | Ni-Ce/ $TiO_2$ |
| *HC Compound* | | | | | | | |
| 1-Nonene | 7.133 | 0.29 | - | 1.57 | 1.41 | - | 1.99 |
| Decane | 7.218 | - | 2.24 | 1.18 | - | - | - |
| 1,5-Hexadiene, 2,5-dimethyl | 7.639 | 0.62 | - | - | - | - | - |
| 3-Oxabicyclo[3.3.0]octan-2-one, 6-methylene-7-methyl- | 8.033 | - | 1.49 | - | - | - | - |
| Cyclopropane, 1-hexyl-2-propyl-, cis- | 10.127 | - | - | - | - | 0.97 | - |
| 1-Decene | 10.129 | - | - | - | 2.11 | - | - |
| Cyclopropane, 1-ethyl-2-heptyl- | 10.144 | - | - | 1.72 | 1.09 | - | 1.07 |
| Octane, 3,5-dimethyl- | 10.43 | - | - | - | 1.04 | - | - |
| Octane, 2,4,6-trimethyl- | 10.431 | - | 1.1 | - | - | - | - |
| Cyclopropane, 1-hexyl-2-propyl-, cis- | 13.402 | - | - | - | - | 1.27 | - |
| 2-Dodecene, (Z)- | 13.415 | - | - | 1.5 | 1.14 | 1.1 | 1.49 |
| 3-Tetradecene, (Z) | 13.673 | 0.42 | - | - | - | - | - |
| Octane, 2,4,6-trimethyl- | 13.693 | - | 0.71 | - | - | - | - |
| Undecane | 13.697 | - | - | 1.03 | - | - | - |
| 1,6-Heptadiene, 2-methyl- | 14.469 | - | - | 1.21 | - | - | - |
| 1H-Indene, 1-methyl- | 15.135 | - | 1.65 | - | - | - | - |
| 2-Methylindene | 15.318 | - | 1.43 | - | - | - | - |
| 1-Dodecene | 16.566 | - | - | 1.18 | - | - | - |
| 1-Heptadecene | 19.533 | - | - | - | 1.71 | 1.62 | - |

**Table A-4 (cont.)** Pyrolytic products of Jatropha residue with Anatase catalysts (Jatropha to catalyst ratio of 1:10)

| Compound Name | RT | % Peak area | | | | | |
|---|---|---|---|---|---|---|---|
| | | No cat. | $TiO_2$ (Anatase | Ce/ $TiO_2$ | Pd-Ce/ $TiO_2$ | Ru-Ce/ $TiO_2$ | Ni-Ce/ $TiO_2$ |
| *HC Compound* | | | | | | | |
| Cyclopropane, 1-ethyl-2-heptyl- | 19.534 | - | - | - | - | - | 1.71 |
| Tridecane, 6-methyl- | 19.79 | - | 0.67 | - | - | - | - |
| 1,6-Heptadiene, 2-methyl- | 22.352 | - | - | - | - | - | 1.49 |
| 9-Octadecene, (E)- | 22.358 | - | - | 1.59 | 1.3 | - | 2.39 |
| (3Z)-3-Hexadecene | 22.639 | 0.5 | - | - | - | - | - |
| 9-Octadecene, (E)- | 25.011 | - | - | 0.53 | 0.88 | - | 0.74 |
| Pentadecane | 25.208 | - | - | - | 1.43 | - | - |
| Tridecane, 6-methyl- | 25.218 | - | 1.76 | - | - | - | - |
| (3Z)-3-Hexadecene | 25.507 | 0.34 | - | - | - | - | - |
| 5-Eicosene, (E)- | 27.516 | - | - | - | - | 0.54 | 6.95 |
| 1,13-Tetradecadiene | 29.382 | - | - | - | - | 0.63 | - |
| 5-Eicosene, (E)- | 29.548 | - | - | - | 0.85 | 0.94 | 5.08 |
| 5-Eicosene, (E)- | 29.55 | - | - | - | - | 0.96 | - |
| 9-Octadecene, (E)- | 29.559 | - | - | 0.66 | 0.55 | - | - |
| 5-Octadecene, (E)- | 29.867 | 0.32 | - | - | - | 1.24 | - |
| Hexadecane | 29.901 | - | - | - | - | - | 0.83 |
| 9-Octadecyne | 30.076 | - | - | - | - | - | 0.79 |
| Heptacosane | 30.077 | - | 0.63 | 1.25 | - | 1.41 | - |
| 1-Nonadecene | 37.625 | - | - | - | - | - | 3.09 |
| 3,9-Dodecadiyne | 37.901 | - | - | - | - | 1.64 | - |
| Hexadecane | 38.381 | - | - | - | - | - | 0.91 |
| 1,E-8,Z-10-Hexadecatriene | 38.384 | - | - | 0.94 | 1.48 | 1.51 | 0.56 |
| 17-Pentatriacontene | 39.787 | - | - | - | - | 0.85 | - |
| Tetracosane | 44.02 | 0.29 | - | - | - | - | - |

**Table A-4 (cont.)** Pyrolytic products of Jatropha residue with Anatase catalysts (Jatropha to catalyst ratio of 1:10)

| Compound Name | RT | % Peak area | | | | | |
|---|---|---|---|---|---|---|---|
| | | No cat. | TiO$_2$ (Anatase | Ce/ TiO$_2$ | Pd-Ce/ TiO$_2$ | Ru-Ce/ TiO$_2$ | Ni-Ce/ TiO$_2$ |
| *HC Compound* | | | | | | | |
| Tetratetracontane | 45.294 | 0.39 | - | - | - | - | - |
| Cholesta-3,5-diene | 47.135 | 1.78 | - | - | - | - | - |
| *Ketone* | | | | | | | |
| Acetol | 2.507 | 2.65 | - | - | - | - | - |
| 3-Penten-2-one, (E) | 2.617 | 0.4 | - | - | - | - | - |
| Cyclopentanone | 4.197 | - | - | 1.34 | - | 1.07 | - |
| 2-Propanone, 1-(acetyloxy) | 4.249 | 0.75 | - | - | - | - | - |
| 2-Cyclopenten-1-one | 5.165 | - | - | 1.17 | 1.12 | 1.14 | 1.81 |
| Cycloheptanone | 5.398 | - | - | - | - | - | 1.74 |
| 2-Cyclopenten-1-one, 2-methyl- | 7.214 | - | - | - | 1.29 | 0.85 | 1.66 |
| 6-Oxa-bicyclo[3.1.0]hexan-3-one | 8.023 | 0.59 | - | - | - | - | - |
| 2-Cyclopenten-1-one, 3-methyl- | 9.068 | - | - | 0.79 | - | - | - |
| Ethanone, 1-(2-furanyl)- | 10.621 | - | - | 0.6 | 0.58 | 0.59 | - |
| 2-Cyclopenten-1-one, 2-hydroxy-3-methyl- | 11.451 | 0.44 | - | - | - | - | - |
| 2-Cyclopenten-1-one, 2-methyl- | 12.962 | - | - | - | - | - | 1.62 |
| Cyclopentadecanone | 39.785 | - | - | - | 0.82 | - | - |
| *N-compound* | | | | | | | |
| Butanenitrile, 4-oxo- | 2.102 | - | - | - | - | - | 6.47 |
| Propanenitrile, 2-methyl- | 2.216 | - | - | - | 0.53 | 0.43 | 3.86 |

**Table A-4 (cont.)** Pyrolytic products of Jatropha residue with Anatase catalysts (Jatropha to catalyst ratio of 1:10)

| Compound Name | RT | % Peak area | | | | | |
| --- | --- | --- | --- | --- | --- | --- | --- |
| | | No cat. | TiO$_2$ (Anatase | Ce/ TiO$_2$ | Pd-Ce/ TiO$_2$ | Ru-Ce/ TiO$_2$ | Ni-Ce/ TiO$_2$ |
| *N-compound* | | | | | | | |
| Butanenitrile, 4-oxo- | 2.218 | - | - | - | - | - | 0.56 |
| Propanenitrile, 2-methyl- | 2.22 | - | - | 0.41 | - | - | - |
| Isobutyronitrile | 2.235 | - | 0.89 | - | - | - | - |
| Butanenitrile, 4-oxo- | 2.403 | - | - | - | - | - | 2.75 |
| Butanenitrile, 4-oxo- | 2.533 | - | - | - | - | - | 4.21 |
| N-VINYLAZIRIDINE | 2.583 | - | - | - | 1.81 | - | 1.28 |
| Butanenitrile,2-methyl | 3.083 | - | - | 0.94 | 0.9 | 0.81 | 6.06 |
| Butanenitrile, 3-methyl | 3.17 | - | 1.98 | - | - | - | 4.85 |
| Butanenitrile, 3-methyl | 3.183 | 0.36 | 1.36 | 1.54 | 1.76 | 1.62 | - |
| Benzenamine, 3-methyl- | 3.251 | 0.52 | - | - | - | - | - |
| 2,4-Pentadienenitrile | 3.375 | - | - | - | - | 1.75 | - |
| Azine | 3.383 | - | - | 2.63 | 1.77 | - | 0.98 |
| 1H-Pyrrole | 3.576 | - | - | 4.36 | 3.79 | - | 1.87 |
| Cyclopentane, nitro- | 3.686 | 0.97 | - | - | - | - | - |
| Formamide, N,N-dimethyl- | 3.976 | - | - | 3.18 | - | 2.93 | 1.48 |
| Pyridine, 4-methyl- | 4.822 | - | 1.79 | - | - | - | - |
| Diazene, bis(1,1-dimethylethyl)- | 5.3 | - | - | - | 0.63 | - | - |
| 1H-Pyrrole, 1-methyl- | 5.39 | - | - | - | 1.69 | 1.47 | - |
| 1H-Pyrrole, 2-methyl- | 5.588 | 0.6 | - | 2.08 | - | - | 1.57 |
| 1H-Pyrrole, 3-methyl- | 5.658 | - | 1.23 | 1.35 | 1.16 | 1 | 1.15 |
| Pyridine, 3-methyl- | 5.946 | - | - | 1.08 | 1.1 | 1.36 | 0.8 |
| Hexanenitrile | 6.443 | - | 1.16 | 0.84 | 0.77 | - | - |
| 1H-Pyrrole, 2,3-dimethyl- | 7.922 | - | 1.19 | - | - | - | - |

**Table A-4 (cont.)** Pyrolytic products of Jatropha residue with Anatase catalysts (Jatropha to catalyst ratio of 1:10)

| Compound Name | RT | % Peak area | | | | | |
|---|---|---|---|---|---|---|---|
| | | No cat. | TiO$_2$ (Anatase | Ce/ TiO$_2$ | Pd-Ce/ TiO$_2$ | Ru-Ce/ TiO$_2$ | Ni-Ce/ TiO$_2$ |
| *N-compound* | | | | | | | |
| 1H-Pyrrole, 2,5-dimethyl- | 8.298 | - | 0.76 | - | - | - | - |
| Aniline | 9.552 | - | 2.5 | 2.01 | 2.09 | 2.12 | 1.5 |
| Heptanenitrile | 9.618 | - | - | - | - | 0.67 | - |
| Heptanenitrile | 9.633 | - | - | - | 0.77 | 0.8 | - |
| Benzonitrile | 9.73 | - | 2.74 | - | 1.2 | 0.81 | - |
| Benzenamine | 9.798 | 0.7 | - | - | - | - | - |
| Benzonitrile, 2-methyl- | 14.738 | - | - | 0.89 | - | - | 1.43 |
| Succinimide | 14.754 | 0.49 | - | - | - | - | - |
| Benzeneacetonitrile | 15.034 | 0.49 | - | - | 0.99 | 0.95 | - |
| Quinoline | 17.818 | - | 1.57 | - | - | - | - |
| Indolizine | 19.802 | 0.85 | - | - | - | - | - |
| 1H-Indole, 3-methyl- | 22.123 | - | 0.78 | - | - | - | - |
| Heptadecanenitrile | 34.38 | - | 2.63 | - | 5.64 | 5.43 | 0.89 |
| Tetradecanenitrile | 34.397 | - | - | - | 10.38 | 9.06 | 0.82 |
| Oleanitrile | 37.529 | 0.59 | 1.5 | 10.06 | 7.28 | 14.11 | 0.82 |
| Nonadecanenitrile | 37.621 | - | 1.31 | - | - | - | - |
| Heptadecanenitrile | 37.633 | - | - | 3.66 | - | - | - |
| Hexadecanamide | 38.879 | 3.67 | - | 6.71 | - | - | - |
| 2,5-Pyrrolidinedione | 39.762 | 0.29 | - | - | - | - | - |
| 9-Octadecenamide, (Z)- | 41.032 | 0.49 | 0.67 | 0.64 | - | - | - |
| Oleanitrile | 41.825 | - | - | 0.65 | 5.01 | - | - |
| 9-Octadecenamide, (Z)- | 44.244 | - | - | 0.45 | - | - | - |
| *Phenol* | | | | | | | |
| Phenol | 10.062 | 1.5 | - | 1.74 | 1.51 | 1.73 | 1.53 |
| Phenol, 3-methyl- | 12.977 | - | - | 1.28 | 1.13 | 1.37 | 1.23 |

**Table A-5** Pyrolytic products with $Al_2O_3$ catalysts without Ce promoter (J: C of 1:10)

| Compound Name | RT | % Peak area | | | | | | |
|---|---|---|---|---|---|---|---|---|
| | | Ce/Al | Co/Al | La/Al | Mo/Al | Ni/Al | Pd/Al | Ru-Al |
| *Aldehyde* | | | | | | | | |
| E,E-2,4-hexadien-1-ol | 2.33 | - | - | - | 2.27 | - | - | |
| 2-Penten-1-ol, 2-methyl-, (Z)- | 2.07 | - | - | - | 2.34 | - | - | |
| Butanal, 2-methyl- | 2.51 | - | 1.58 | 2.15 | - | 1.31 | - | 1.93 |
| cis-9-Hexadecenal | 37.01 | 2.53 | - | - | - | - | - | - |
| *Aromatic* | | | | | | | | |
| Benzene, methyl- | 3.65 | 12.72 | 11.75 | 13.77 | 13.41 | 13.44 | 11.37 | 11.86 |
| Styrene | 7.07 | 1.92 | - | - | - | - | - | - |
| Benzene, ethyl- | 6.22 | 1.12 | 1.95 | 1.50 | 1.44 | 1.40 | 1.60 | 1.35 |
| Benzene | 2.43 | - | - | - | 7.24 | - | 4.58 | 2.28 |
| Benzene, 1,2-dimethyl- | 6.60 | - | - | - | 1.60 | - | - | - |
| Benzene, 1,4-dimethyl- | 5.96 | - | - | - | 0.62 | - | 0.97 | - |
| Benzene, 1,3,5-trimethyl- | 9.33 | 0.97 | - | 1.05 | - | 1.04 | - | - |
| Benzene, (1-methyl-2-cyclopropen-1-yl)- | 14.75 | 1.40 | - | 1.31 | - | 0.66 | 1.04 | 1.08 |
| Benzene, 1-propynyl- | 11.38 | 1.24 | 0.79 | 1.37 | 0.68 | 0.94 | 0.96 | - |
| Benzene, butyl- | 11.84 | - | - | - | - | 0.61 | - | - |
| Benzene, pentyl- | 15.07 | - | 0.80 | - | - | 0.61 | 0.90 | 0.99 |
| 1H-Indene | 11.91 | - | - | - | - | - | - | 1.02 |
| 1H-Indene, 1-methyl- | 15.32 | - | 1.00 | - | - | - | - | - |
| 1,4-Dihydronaphthalene | 14.96 | - | 0.99 | - | 1.37 | - | 1.11 | 1.23 |
| Naphthalene | 16.38 | - | - | - | 1.69 | 1.36 | 1.19 | 1.02 |
| 2-Methylindene | 14.94 | 1.48 | - | - | - | 0.75 | - | - |
| *Carboxylic acid* | | | | | | | | |
| 2-Propenoic acid, 2-methyl-, 2-propenyl ester | 38.69 | | 1.62 | - | - | - | - | - |

**Table A-5 (cont.)** Pyrolytic products with Al$_2$O$_3$ catalysts W/O promoter (J:C of 1:10)

| Compound Name | RT | % Peak area | | | | | | |
|---|---|---|---|---|---|---|---|---|
| | | Ce/Al | Co/Al | La/Al | Mo/Al | Ni/Al | Pd/Al | Ru-Al |
| *Carboxylic acid* | | | | | | | | |
| OCTADEC-9-ENOIC ACID | 41.55 | 1.26 | - | - | - | - | - | - |
| 1,6-Hexanediol dibenzoate $$ | 9.33 | - | - | - | - | - | 1.06 | - |
| 3-Cyclopentylpropionic acid, 2-phenylethyl ester | 6.57 | - | - | - | - | - | - | 1.84 |
| 1,2-Benzenedicarboxylic acid, mono(2-ethylhexyl) ester | 41.98 | - | - | - | 0.46 | - | - | - |
| 2-Hexen-2-yl acetate | 2.77 | - | - | 1.37 | - | - | 2.10 | - |
| 4,8-Dioxaspiro[2.5]oct-1-ene, 6,6-dimethyl- | 2.97 | - | - | - | - | 0.77 | - | - |
| *Hydrocarbon* | | | | | | | | |
| 1-Pentene, 4-methyl- | 2.07 | 5.67 | 1.84 | - | - | - | - | 1.97 |
| 1,3-Cyclohexadiene | 2.34 | 4.19 | - | - | - | - | - | - |
| 1-Butene, 3,3-dimethyl- | 2.51 | 1.84 | - | - | - | - | - | - |
| 1-Hexene | 2.12 | | 3.65 | - | - | - | 7.07 | 7.78 |
| 1,3-Cyclohexadiene | 2.34 | - | - | 2.54 | - | 2.06 | 1.38 | - |
| 1,5-Hexadien-3-yne | 2.52 | - | - | - | - | 2.99 | - | - |
| 1,4-Cyclohexadiene | 2.43 | - | - | - | 0.60 | - | - | - |
| 1-Heptene / n-Hept-1-ene | 2.81 | - | - | 2.37 | 2.64 | - | 3.44 | - |
| 1-Heptene | 19.72 | 4.46 | 4.41 | - | 1.40 | 4.74 | - | 3.30 |

**Table A-5 (cont.)** Pyrolytic product with Al$_2$O$_3$ catalysts W/O promoter (J/C of 1:10)

| Compound Name | RT | % Peak area | | | | | | |
|---|---|---|---|---|---|---|---|---|
| | | Ce/Al | Co/Al | La/Al | Mo/Al | Ni/Al | Pd/Al | Ru-Al |
| *Hydrocarbon* | | | | | | | | |
| 3-Methylenecyclohexene | 3.26 | 2.60 | 1.97 | 2.80 | - | - | 1.45 | 0.97 |
| 1-Pentene, 4,4-dimethyl- | 5.40 | - | - | - | 0.99 | - | - | - |
| 1-Octene | 4.45 | 2.24 | 2.04 | 1.86 | 0.46 | 2.19 | 2.63 | 2.34 |
| 1,3,7-Octatrien-5-yne 3-Cyclopentyl-1-propyne | 2.63 | - | - | - | - | - | - | - |
| Cyclopentene,3-(2-propenyl)- | 3.63 | - | - | - | - | - | - | - |
| Bicyclo[4.2.0]octa-1,3,5-triene | 6.96 | - | 1.96 | 2.22 | 1.84 | 2.26 | 1.98 | - |
| Octane | 4.30 | 1.71 | 2.07 | 1.78 | - | 1.80 | 2.20 | 2.57 |
| Hexane, 2,4-dimethyl- | 4.27 | - | - | - | 2.37 | - | - | - |
| 1-Nonene /Nonene | 7.13 | 3.39 | 3.31 | - | - | - | 4.04 | - |
| 2-Nonene | 6.66 | | | 3.27 | | 3.79 | | 4.15 |
| Nonane | 6.92 | 1.84 | 1.86 | 2.13 | 0.84 | 2.00 | 1.93 | 2.25 |
| 5-methyloctene-1 $$ | 2.08 | - | - | 5.48 | - | 5.88 | - | - |
| 1-Decene | 9.80 | 2.17 | - | 1.84 | - | 2.39 | - | - |
| Decane | 10.10 | 0.67 | - | - | - | - | 0.64 | - |
| 1-Decene | 9.75 | - | 2.32 | - | - | - | - | - |
| Cycloprop[a]indene, 1,1a,6,6a-tetrahydro- | 15.51 | - | - | - | - | - | - | - |
| 2-Decene, (E)- | 10.28 | 0.77 | 0.66 | - | - | 0.65 | 0.50 | 0.56 |
| 1-Undecene | 13.06 | 1.93 | - | - | - | - | 2.06 | 2.14 |
| 2-Undecene, (E)- | 14.02 | 1.00 | 0.90 | - | - | - | 0.75 | 0.81 |
| 2-Undecene, (E)- | 13.78 | 0.47 | - | 1.01 | - | 0.80 | - | - |

**Table A-5 (cont.)**  Pyrolytic product with Al$_2$O$_3$ catalysts W/O promoter (J/C of 1:10)

| Compound Name | RT | % Peak area | | | | | | |
|---|---|---|---|---|---|---|---|---|
| | | Ce/Al | Co/Al | La/Al | Mo/Al | Ni/Al | Pd/Al | Ru-Al |
| *Hydrocarbon* | | | | | | | | |
| Undecane | 13.35 | 1.24 | 0.62 | 1.22 | - | 0.94 | 1.13 | 0.73 |
| | 13.36 | - | 1.16 | - | - | - | 2.85 | 1.02 |
| 5-Undecene, (E)- | 14.64 | - | - | - | - | - | - | 2.91 |
| | - | 36.19 | 28.77 | 28.52 | 11.14 | 32.49 | 34.05 | 33.50 |
| 1-Dodecene | 16.20 | 1.77 | 2.15 | 1.51 | 0.90 | 1.97 | 2.31 | 2.61 |
| 2-Dodecene, (Z)- | 16.74 | - | 1.84 | 1.72 | - | 0.55 | - | - |
| Cyclopropane, 1-methyl-2-octyl- | - | - | - | - | - | 1.84 | - | - |
| 5-Dodecyne | 17.74 | - | - | - | - | - | - | - |
| Tetradecane | 22.20 | 1.13 | 0.93 | 0.73 | 0.48 | 1.00 | - | - |
| 1-Tridecene | 21.97 | 2.98 | - | 2.43 | - | 2.43 | 3.43 | - |
| Dodecane | - | - | - | - | 0.59 | - | - | - |
| Tridecane | 16.47 | 0.89 | - | - | - | 1.00 | 1.11 | 1.30 |
| 4-Dodecene, (Z)- | 16.62 | - | - | 0.53 | - | - | 0.51 | - |
| 1-Undecene, 4-methyl- | 4.57 | - | - | - | - | - | - | - |
| 1-Tetradecene | 24.62 | - | - | - | 0.89 | 1.07 | 0.76 | |
| 3-Tetradecene, (Z) | 13.67 | 0.52 | - | - | - | - | 0.63 | 0.51 |
| Pentadecane | 24.82 | 1.65 | 0.57 | 0.59 | 3.36 | 1.63 | 1.23 | 1.48 |
| Pentadecane | 29.67 | 0.58 | - | - | 1.48 | 0.82 | 0.55 | 0.71 |
| 1-Hexadecene | 24.61 | 0.74 | - | 0.67 | - | - | - | 1.06 |
| (3Z)-3-Hexadecene | 22.64 | - | - | - | 0.58 | - | - | - |
| 1-Hexadecene | 27.12 | 1.15 | 0.59 | 0.83 | - | 0.90 | 1.16 | - |
| 6-Tetradecene | 29.49 | - | 1.08 | 0.72 | - | 0.54 | - | - |
| 3-Hexadecene, (Z)- | 21.98 | - | 2.84 | - | - | - | - | 3.14 |
| 3-Hexadecene, (Z)- | 24.62 | - | - | - | - | - | - | 1.14 |
| Hexadecane | 25.40 | 1.31 | 1.26 | 1.53 | - | 0.67 | 1.39 | 0.86 |
| Hexadecane | 19.42 | - | 1.43 | 1.21 | - | - | - | 1.63 |

Table A-5 (cont.) Pyrolytic product with $Al_2O_3$ catalysts W/O promoter (J/C of 1:10)

| Compound Name | RT | % Peak area | | | | | | |
|---|---|---|---|---|---|---|---|---|
| | | Ce/Al | Co/Al | La/Al | Mo/Al | Ni/Al | Pd/Al | Ru-Al |
| *Hydrocarbon* | | | | | | | | |
| 7-Hexadecene, (Z) | 22.32 | 0.78 | 0.81 | 0.71 | - | 0.58 | 0.78 | 0.71 |
| 7-Hexadecene, (Z) | 24.95 | - | 0.59 | - | - | 0.65 | - | - |
| 1-Heptadecene | 19.16 | 2.24 | 2.17 | 2.45 | - | 2.40 | 2.42 | 2.49 |
| Heptadecane | 22.20 | - | 1.03 | 1.23 | - | - | 1.04 | - |
| *N-heterocyclic* | | | | | | | | |
| 1H-Pyrrole | 8.07 | 5.31 | 4.23 | 5.56 | 4.61 | 5.16 | 4.19 | 2.91 |
| 1H-Pyrrole, 2,5-dimethyl- | 8.43 | 2.09 | 1.62 | - | - | - | - | - |
| 1H-Pyrrole, 2-methyl- | 5.59 | 2.31 | 2.89 | 3.18 | 0.55 | 2.91 | 2.20 | 1.45 |
| 1H-Pyrrole, 2-methyl- | 5.40 | 0.54 | 1.20 | 1.64 | - | - | 1.02 | - |
| 3-Methylpyrrole | 5.75 | - | - | - | - | 1.07 | - | - |
| Pyridine / Azine | 3.28 | - | - | - | 2.79 | 2.04 | - | - |
| Pyridine, 3-methyl- | 6.05 | - | - | - | 0.88 | - | - | - |
| Pyridine, 4-methyl- | 9.17 | - | - | - | 0.85 | - | - | - |
| 2,5-Pyrrolidinedione | 14.75 | 1.17 | - | - | - | - | - | - |
| 9-Octadecenamide, (Z)- | 41.03 | 2.84 | 1.51 | - | 1.20 | - | 0.83 | 1.23 |
| 9-Octadecynenitrile | 38.00 | - | - | - | 0.44 | - | - | - |
| Octadecanamide | 38.18 | - | - | - | 0.54 | - | - | - |
| Octanenitrile | 12.55 | - | - | - | 1.10 | - | - | - |
| Aniline | 9.69 | 1.82 | 1.66 | 1.91 | - | 1.95 | 1.70 | - |
| Benzenamine | 9.80 | - | - | - | - | - | - | 1.06 |
| Benzenamine, 3-methyl- | 3.25 | - | - | - | 2.14 | 1.95 | - | - |
| Benzeneacetonitrile | 15.03 | - | - | - | 1.46 | - | - | - |
| Benzonitrile, 2-methyl- | - | - | - | - | 1.69 | - | - | - |
| Butanenitrile, 2-methyl | 3.18 | - | 0.61 | - | - | - | - | 0.83 |

**Table A-5 (cont.)** Pyrolytic product with $Al_2O_3$ catalysts W/O promoter (J/C of 1:10)

| Compound Name | RT | % Peak area | | | | | | |
|---|---|---|---|---|---|---|---|---|
| | | Ce/Al | Co/Al | La/Al | Mo/Al | Ni/Al | Pd/Al | Ru-Al |
| *Hydrocarbon* | | | | | | | | |
| Butanenitrile, 3-methyl- | | 0.89 | 1.51 | 2.00 | 4.51 | - | 1.32 | 2.06 |
| Propanenitrile, 2-methyl- | 2.16 | - | - | - | 0.59 | - | - | - |
| Pentanenitrile, 4-methyl- | 5.11 | - | - | - | 2.23 | - | - | - |
| Hexadecanenitrile | 33.97 | - | 3.69 | - | 7.35 | 4.27 | 4.37 | - |
| Heptadecanenitrile | 34.57 | 4.8 | 2.22 | | 4.09 | 2.34 | 2.16 | 6.87 |
| Hexadecanamide | 33.87 | - | - | 3.68 | - | - | - | - |
| Hexanenitrile | 6.56 | - | - | - | 1.11 | - | 0.75 | - |
| Heptanenitrile | 9.32 | - | 0.89 | 1.81 | 1.25 | - | - | 1.04 |
| 1-Tridecanamine, N,N-dimethyl | 24.84 | - | - | - | 2.02 | - | - | - |
| Octadecanamide | 38.25 | 0.48 | - | - | - | - | - | - |
| Oleanitrile | 37.53 | - | 1.63 | 1.78 | 1.61 | 3.17 | 2.52 | 1.01 |
| Oleanitrile | 37.45 | - | 1.50 | 1.41 | 2.12 | - | - | 1.88 |
| Oleanitrile | 37.03 | - | 6.36 | 1.76 | 1.12 | - | - | 1.35 |
| 3-TERT-BUTYL-7A-DIMETHYLAMINOMETHYL-TETRAHYDRO-PYRROLO[1,2-C]OXAZOL-1-ONE | 24.93 | - | - | - | - | - | 0.71 | - |
| 1-Dodecanamine, N,N-dimethyl- | 24.90 | 1.16 | - | 1.08 | - | - | - | - |
| Propanenitrile, 2,2'-azobis[2-methyl- | 2.50 | - | - | 2.87 | - | - | - | - |
| *phenol* | | | | | | | | |
| Phenol | 10.06 | - | - | - | 1.27 | - | - | - |

**Table A-6** Pyrolytic products of Activated carbon powder catalysts (J:C of 1:10)

| Compound Name | RT | % Peak area | | | | | |
|---|---|---|---|---|---|---|---|
| | | W/O | Ac | Ce/Ac | Pd/Ac | Ru/Ac | NiAc |
| *Alcohol* | | | | | | | |
| 1-Dodecanol | 24.79 | 1.27 | - | - | - | - | - |
| 1-Tetradecanol | 29.80 | 0.55 | - | - | - | - | - |
| 1-Hexanol, 2-ethyl- | 10.92 | - | - | - | - | - | 0.41 |
| Stigmast-5-en-3-ol, (3.beta.) | 46.88 | 0.39 | - | - | - | - | - |
| Hexanal | 4.56 | 0.36 | - | - | - | - | - |
| Benzaldehyde | - | - | - | - | - | 0.48 | - |
| *Aromatic* | | | | | | | |
| Benzene, methyl- | 3.55 | - | - | 23.58 | 16.87 | 14.92 | 13.83 |
| Benzene | 2.41 | - | - | 7.96 | 17.65 | 10.49 | 15.12 |
| Styrene | 7.07 | 0.41 | - | 1.09 | | 0.54 | 0.91 |
| Benzene, ethyl- | 6.22 | 0.42 | - | 1.13 | 0.87 | 0.66 | 1.16 |
| Toluene /Methylbenzene | 3.94 | 2.75 | - | - | - | - | - |
| Benzene, 1,2-dimethyl- (O-Xylene) | 5.87 | - | - | 0.35 | 1.48 | 0.70 | 1.09 |
| Benzene, 1,3-dimethyl- (M-Xylene) | 5.88 | - | - | - | 0.28 | - | - |
| Benzene, 1-ethenyl-3-methyl- | 9.72 | - | - | 0.63 | - | - | - |
| Benzene, 1-methyl-3-propyl- | | | | | | | |
| Benzene, 1-propynyl- | 11.28 | - | - | - | 0.08 | - | - |
| Benzene, 1,2,4-trimethyl- | - | - | - | - | - | - | 0.23 |
| Benzene, 1,3,5-trimethyl- | 9.20 | - | - | 0.41 | - | - | 7.57 |

**Table A-6 (cont.)** Pyrolytic products of Activated carbon powder catalysts (J:C of 1:10)

| Compound Name | RT | % Peak area | | | | | |
|---|---|---|---|---|---|---|---|
| | | W/O | Ac | Ce/Ac | Pd/Ac | Ru/Ac | NiAc |
| *PAH* | | | | | | | |
| Naphthalene | 15.67 | - | - | 0.61 | 1.12 | 0.45 | 0.68 |
| 1,1'-Biphenyl | 21.40 | - | - | 0.50 | 0.49 | 0.17 | 0.39 |
| Acetic acid | 2.14 | - | - | - | 1.42 | 5.10 | |
| ACETIC ACID, ANHYDRIDE WITH FORMIC ACID | 2.06 | 3.01 | - | - | - | - | - |
| Butanoic acid | 4.50 | - | - | - | - | 4.73 | - |
| Pentanoic acid | 7.10 | - | - | - | - | 0.52 | - |
| (Z)-9-Octadecenoic acid/ Oleic acid | 38.48 | 39.69 | - | - | - | - | - |
| *Carbox acid* | | | | | | | |
| (Z)-9-Octadecenoic acid/ Oleic acid | 35.48 | 0.83 | - | - | - | - | - |
| | 38.69 | 6.36 | - | - | - | - | - |
| Hexadecanoic acid | 35.87 | 10.85 | - | - | - | - | - |
| Eicosanoic acid | 38.02 | - | - | - | 0.14 | - | - |
| Tetradecanoic acid | 35.08 | - | - | - | 0.17 | - | - |
| *Ester* | | | | | | | |
| 1,7-Octadien-3-ol, acetate | | | | | | | |
| Dibutyl phthalate | 35.00 | - | - | 0.92 | 0.31 | 0.23 | - |
| Hexadecanoic acid, methyl ester | 34.37 | - | - | 1.62 | 0.56 | - | 0.10 |
| Hexanedioic acid, dioctyl ester | 40.57 | - | - | - | 0.04 | - | - |
| 9-Octadecenoic acid (Z)-, methyl ester | 37.17 | - | - | 0.32 | 0.06 | - | - |

**Table A-6 (cont.)** Pyrolytic products of Activated carbon powder catalysts (J:C of 1:10)

| Compound Name | RT | % Peak area | | | | | |
|---|---|---|---|---|---|---|---|
| | | W/O | Ac | Ce/Ac | Pd/Ac | Ru/Ac | NiAc |
| *Ester* | | | | | | | |
| Propanoic acid, 2-oxo-, methyl ester | | | | | | | |
| Propanoic acid, 2-methyl-, 3-hydroxy-2,4,4-trimethylpentyl ester | 21.32 | - | - | 0.20 | - | - | - |
| Propanoic acid, 2-methyl-, 1-(1,1-dimethylethyl)-2-methyl-1,3-propanediyl ester | 27.13 | - | - | 0.70 | - | - | - |
| Benzeneacetic acid, heptyl ester | 8.42 | - | - | - | - | - | 0.42 |
| PENTAN-1,3-DIOLDIISOBUTYRATE, 2,2,4-TRIMETHYL- | - | - | - | - | 0.23 | - | - |
| 1,2-Benzenedicarboxylic acid, butyl octyl ester | 41.99 | - | - | 0.18 | 0.11 | - | - |
| 1,2-Benzenedicarboxylic acid, bis(2-methylpropyl) este | 33.19 | - | - | 0.33 | 0.12 | - | - |
| Carbonic acid, ethyl nonyl ester | 13.23 | - | - | - | - | - | 0.66 |
| Benzenepropanoic acid, 3,5-bis(1,1-dimethylethyl)-4-hydroxy-, octadecyl ester | 49.61 | - | - | 0.96 | - | - | - |

**Table A-6 (cont.)** Pyrolytic products of Activated carbon powder catalysts (J:C of 1:10)

| Compound Name | RT | % Peak area | | | | | |
|---|---|---|---|---|---|---|---|
| | | W/O | Ac | Ce/Ac | Pd/Ac | Ru/Ac | NiAc |
| *Ester* | | | | | | | |
| Cholest-5-en-3-ol (3.beta.)-, tetradecanoate | 46.53 | - | - | - | 0.06 | - | - |
| Stigmast-5-en-3-ol, oleate | - | - | - | - | - | - | - |
| benzyl 2-O-methylbaeomycesate | 49.17 | - | - | - | 9.16 | - | - |
| Benzenepropanoic acid, 3,5-bis(1,1-dimethylethyl)-4-hydroxy-, octadecyl ester | 49.60 | - | - | - | 4.83 | - | - |
| Oxalic acid, cyclohexylmethyl octyl ester | 17.31 | - | - | - | 0.04 | - | - |
| *Furan* | | | | | | | |
| Furan, 2,5-dimethyl- | | | | | | | |
| 2-Furancarboxaldehyde | 5.36 | 0.67 | - | - | - | - | - |
| 2-Furanmethanol | 5.99 | 0.37 | - | - | - | - | - |
| Furan, 2-methyl- | | | | | | | |
| Benzofuran | 9.73 | - | - | - | 0.99 | - | - |
| *Ketone* | | | | | | | |
| 1,2-Cyclopentanedione | | | | | | | |
| 1-hydroxy- 2-Propanone | 2.51 | 2.65 | - | - | - | - | - |
| 1-hydroxy- 2-Propanone | 4.25 | 0.75 | - | - | - | - | - |
| 2-Cyclopenten-1-one | | | | | | | |
| 2-Cyclopenten-1-one, 2-hydroxy-3-methyl- | 11.45 | 0.44 | - | - | - | - | - |

**Table A-6 (cont.)** Pyrolytic products of Activated carbon powder catalysts (J:C of 1:10)

| Compound Name | RT | % Peak area | | | | | |
|---|---|---|---|---|---|---|---|
| | | W/O | Ac | Ce/Ac | Pd/Ac | Ru/Ac | NiAc |
| *Ketone* | | | | | | | |
| 2-Pentanone, 4,4-dimethyl- | | | | | | | |
| 2-Propanone, 1-(acetyloxy)- | 6.33 | 0.62 | - | - | - | - | - |
| 3-Penten-2-one, (E) | 2.62 | 0.40 | - | - | - | - | - |
| 4-Hexen-2-one, 3-methyl- | 2.96 | - | - | 0.93 | - | - | - |
| 6-Oxa-bicyclo[3.1.0]hexan-3-one | 8.02 | 0.59 | - | - | - | - | - |
| *Hydrocarbo* | | | | | | | |
| 2-Hexyne | - | - | - | - | - | - | 0.45 |
| 1-Heptene / n-Hept-1-ene | 2.81 | 1.78 | - | - | - | - | - |
| Heptane | 2.68 | - | - | 45.15 | 30.04 | 0.93 | 4.59 |
| Butane, 2,2,3-trimethyl | 2.05 | - | - | 0.83 | - | - | - |
| 1-Butene, 2,3,3-trimethyl | 4.99 | - | - | - | - | - | 0.69 |
| 1-Pentene, 4,4-dimethyl- | 4.99 | - | - | - | 0.20 | - | - |
| 2-Heptene | 2.84 | - | - | 1.36 | - | - | - |
| 1,5-Heptadiene, (E)- | | | | | | | |
| 3-Heptyne | 3.37 | - | - | 1.26 | - | - | - |
| 1,2-Pentadiene, 4,4-dimethyl- | 2.06 | - | - | - | 1.16 | - | - |
| 1,5-Hexadiene, 2,5-dimethyl | 7.64 | 0.62 | - | - | - | - | - |

**Table A-6 (cont.)** Pyrolytic products of Activated carbon powder catalysts (J:C of 1:10)

| Compound Name | RT | % Peak area | | | | | |
|---|---|---|---|---|---|---|---|
| | | W/O | Ac | Ce/Ac | Pd/Ac | Ru/Ac | NiAc |
| *Hydrocarbo* | | | | | | | |
| 1,6-Heptadiene, 2-methyl- | | | | | | | |
| 1-Octene | 4.45 | 1.01 | - | - | - | - | - |
| Octane | 4.20 | - | - | 0.48 | 0.30 | - | 3.28 |
| 1,3,7-Octatrien-5-yne | | | | | | | |
| 3-Cyclopentyl-1-propyne | | | | | | | |
| Butane, 2,2,3,3-tetramethyl- | 2.58 | - | - | - | - | 0.17 | 1.99 |
| Cyclohexane, 1,2-dimethyl-, cis- | 4.30 | - | - | - | - | - | 1.12 |
| Cyclopentane, (1-methylethyl)- | 4.43 | - | - | - | - | - | 0.94 |
| 4-Octen-3-one | - | - | - | - | - | 2.91 | - |
| Nonane | 6.82 | - | - | - | 0.07 | - | 0.22 |
| 1-Nonene /Nonene | 7.13 | 0.29 | - | - | - | - | - |
| Heptane, 2,4-dimethyl- | 4.69 | - | - | - | - | 0.40 | 2.55 |
| | 5.77 | - | - | - | - | - | 0.58 |
| 2,4-Dimethyl-1-heptene | 5.15 | - | - | - | - | - | 0.72 |
| Nonane | 6.81 | - | - | 0.18 | - | 0.21 | - |
| Nonane, 4-methyl- | 8.74 | - | - | - | - | - | 0.43 |
| Hexane, 2,3,4-trimethyl- | 4.53 | - | - | - | - | - | 1.26 |
| BICYCLO[4.2.0]OCTA-1,3,5-TRIENE, 7-METHYL-$$ | | | | | | | |
| l-Limonene | 10.84 | - | - | - | 0.13 | - | - |
| Octane, 2,7-dimethyl- | 10.02 | - | - | - | 0.07 | - | - |

**Table A-6 (cont.)** Pyrolytic products of Activated carbon powder catalysts (J:C of 1:10)

| Compound Name | RT | % Peak area | | | | | |
|---|---|---|---|---|---|---|---|
| | | W/O | Ac | Ce/Ac | Pd/Ac | Ru/Ac | NiAc |
| *Hydrocarbo* | | | | | | | |
| Octane, 5-ethyl-2-methyl | 11.88 | - | - | - | - | - | 0.35 |
| | 13.32 | - | - | - | - | - | 0.26 |
| 3-Ethyl-3-methylheptane | 11.87 | - | - | - | - | 0.34 | - |
| Undecane | 9.97 | - | - | - | - | 0.57 | - |
| Undecane | 13.22 | - | - | - | - | 0.13 | - |
| Nonane, 2,6-dimethyl- | 10.28 | - | - | - | - | 0.31 | 2.19 |
| | 10.42 | - | - | - | - | 0.34 | 0.56 |
| Undecane | | - | - | - | - | - | - |
| 1-Decene, 2,4-dimethyl | 12.57 | - | - | - | - | - | 0.15 |
| 1-Dodecene | | - | - | - | - | - | - |
| 2-Dodecene, (Z)- | | - | - | - | - | - | - |
| Dodecane | 9.67 | - | - | - | - | 0.35 | 1.31 |
| Heptane, 2,2,4,6,6-pentamethyl- | | - | - | - | - | 1.03 | - |
| 1,1'-Biphenyl | | - | - | - | - | - | - |
| 4-UNDECENE, 6-METHYL-, CIS/TRANS $$ | | - | - | - | - | 1.87 | - |
| Tridecane | 19.31 | - | - | - | - | - | 0.12 |
| Undecane, 2,4-dimethyl- | | - | - | - | - | 4.58 | - |
| 1-Tetradecene | | - | - | - | - | - | |
| Dodecane, 4,6-dimethyl- (CAS) | 18.76 | - | - | - | - | - | 0.09 |
| Tetradecane | 16.36 | - | - | - | - | 0.18 | 0.33 |
| 2-Tetradecene, (E)- | | | | | | | |
| 3-Tetradecene, (Z) | 13.67 | 0.42 | - | - | - | - | - |

**Table A-6 (cont.)** Pyrolytic products of Activated carbon powder catalysts (J:C of 1:10)

| Compound Name | RT | % Peak area | | | | | |
|---|---|---|---|---|---|---|---|
| | | W/O | Ac | Ce/Ac | Pd/Ac | Ru/Ac | NiAc |
| *Hydrocarbo* | | | | | | | |
| 1-Pentadecene | 22.09 | - | - | - | - | - | 0.21 |
| Pentadecane | - | - | - | - | - | 0.33 | - |
| Pentadecane | - | - | - | - | - | | - |
| 1-Hexadecene | - | - | - | - | - | 0.14 | - |
| (3Z)-3-Hexadecene | 22.64 | 0.50 | - | - | - | - | - |
| (3Z)-3-Hexadecene | 25.51 | 0.34 | - | - | - | - | - |
| Cyclobuta[1,2:3,4]dicyclooctene, hexadecahydro- | 50.46 | - | - | 1.09 | - | - | - |
| 3-Hexadecene, (Z)- | - | - | - | - | - | 0.23 | - |
| Nonane, 2,2,4,4,6,8,8-heptamethyl | 19.97 | - | - | - | - | - | 0.16 |
| 5-Octadecene, (E)- | 29.87 | 0.32 | - | - | - | - | - |
| 9-Eicosene, (E)- | 36.93 | - | - | - | 0.03 | - | - |
| Tetracosane | 44.02 | 0.29 | - | - | - | - | - |
| Cholesta-3,5-diene | 47.14 | 1.78 | - | - | - | - | - |
| Heptacosane | - | - | - | - | 0.02 | - | - |
| Tetratetracontane | 45.29 | 0.39 | - | - | - | - | - |
| Summary total CH | - | 7.74 | 0.00 | 50.34 | 32.03 | 15.01 | 24.56 |
| Formamide, N,N-dimethyl- | - | - | - | - | - | 19.97 | 24.69 |
| 1H-Pyrrole | - | - | - | - | 1.26 | - | - |
| *homocyclic* | | | | | | | |
| 2,5-Pyrrolidinedione | 39.76 | 0.29 | - | - | - | - | - |
| Propanenitrile, 2-methyl- | 2.15 | | - | - | - | - | 0.45 |
| 1H-Pyrrole, 2-methyl- | 5.59 | 0.60 | - | - | - | - | - |
| 3-Methylpyrrole | - | - | - | - | 0.12 | - | - |
| Pyridine / Azine | 3.21 | - | - | 1.15 | 1.92 | - | 1.50 |
| Pyridine, 2-methyl- | - | - | - | - | 0.12 | - | - |

**Table A-6 (cont.)** Pyrolytic products of Activated carbon powder catalysts (J:C of 1:10)

| Compound Name | RT | % Peak area | | | | | |
|---|---|---|---|---|---|---|---|
| | | W/O | Ac | Ce/Ac | Pd/Ac | Ru/Ac | NiAc |
| *homocyclic* | | | | | | | |
| Pyridine, 3-methyl- | | | | | | | |
| Pyridine, 3-methyl- | | | | | | | |
| 2-Furancarbonitrile | 4.16 | - | - | - | - | 4.85 | - |
| *N-hetero+ O* | | | | | | | |
| 2-methyl-Benzonitrile/ o-Tolunitrile | 3.51 | 0.40 | - | - | - | - | - |
| 3-methyl-Butanenitrile/ Isovaleronitrile/ 3-methyl-Butyronitrile | 39.18 | 1.18 | - | - | - | - | - |
| 2-Butenenitrile | 2.30 | - | - | - | 0.07 | - | - |
| Aniline | 9.13 | - | - | 0.26 | - | - | - |
| Benzenamine | 9.80 | 0.70 | - | - | - | - | - |
| Benzonitrile | 9.28 | - | - | 1.98 | 3.47 | 9.23 | - |
| Benzeneacetonitrile | 15.03 | 0.49 | - | - | 0.31 | 0.55 | 0.53 |
| Benzonitrile, 2-methyl- | 12.74 | - | - | - | - | 0.23 | 0.84 |
| Butanenitrile, 2-methyl | 3.18 | 0.36 | - | - | - | 1.75 | - |
| Butanenitrile, 3-methyl- | 1.57 | - | - | 0.25 | 1.17 | 1.18 | - |
| | | - | - | - | 0.32 | 0.80 | - |
| Benzene, 1-isocyano-2-methyl- | 12.05 | - | - | - | - | - | 0.75 |
| Hexadecanamide | | | | | | | |
| Indolizine | 19.80 | 0.85 | - | - | - | - | - |
| Nonadecanenitrile | | | | | | | |
| 1H-Indole, 3-methyl- | | | | | | | |
| Oleanitrile | 37.53 | 0.59 | - | 0.64 | 0.14 | 0.40 | 0.68 |
| Benzenamine, 3-methyl- | 3.25 | 0.52 | - | - | - | - | - |
| Hexanenitrile | - | - | - | - | 0.08 | 0.23 | - |
| Indole, 3-methyl | | | | | | | |

**Table A-6 (cont.)** Pyrolytic products of Activated carbon powder catalysts (J:C of 1:10)

| Compound Name | RT | % Peak area | | | | | |
|---|---|---|---|---|---|---|---|
| | | W/O | Ac | Ce/Ac | Pd/Ac | Ru/Ac | NiAc |
| *N-hetero+ O* | | | | | | | |
| 4,4-Dimethyl-3-oxopentanenitrile | 4.97 | - | - | 0.19 | - | 1.49 | - |
| Diazene, bis(1,1-dimethylethyl)- | | | | | | | |
| 2,4,6-Trimethyl-1,5-diazabicyclo[3.1.0]hexane | 4.92 | - | - | - | - | - | 0.64 |
| Hydrazinecarboxylic acid, phenylmethyl este | - | - | - | - | - | 0.48 | - |
| *N-compound* | | | | | | | |
| OELIC ACID AMIDE | - | - | - | - | - | 0.50 | - |
| OELIC ACID AMIDE | - | - | - | - | - | 3.79 | - |
| 2,5-Pyrrolidinedione | 14.75 | 0.49 | - | - | - | - | - |
| 2-Cyanato Methyl Cyclohexane | 13.03 | 0.80 | - | - | - | - | - |
| 9-Octadecenamide, (Z)- | 41.03 | 0.49 | - | - | - | - | - |
| 9-Octadecenamide, (Z)- | 40.80 | 2.55 | - | - | - | - | - |
| Cyclopentane, nitro- | 3.69 | 0.97 | - | - | - | - | - |
| Hexadecanamide | | | - | | - | - | - |
| Hexadecanamide | 38.88 | 3.67 | - | - | - | - | - |
| cis-11-Eicosenamide | 43.93 | - | - | 1.11 | 0.71 | - | - |
| *phenol* | | | | | | | |
| Phenol | 10.06 | 1.50 | - | - | 0.98 | - | - |
| Phenol, o-methoxy | | | | | | | |
| Phenol, 4-methyl/ p-Cresol | 13.15 | 1.37 | - | - | - | - | - |
| Phenol, 4-methoxy- | | | | | | | |
| 2-methoxy- Phenol | 13.50 | 1.01 | - | - | - | - | - |
| Phenol, 3-pentadecyl- | 41.34 | - | - | 0.59 | - | - | - |
| Phenol, 3-undecyl- | 41.35 | - | - | - | 0.23 | - | - |

**Appendix B**

**Bio-oil composition by GC-MS**

**Table B-1** Chemical compounds detected in bio-oil from pyrolysis at different temperatures

| Compound Names | RT | Peak area (%) | | | |
|---|---|---|---|---|---|
| | (min) | 400°C | 500°C | 600°C | 700°C |
| *Acid* | | | | | |
| Undec-10-ynoic acid | 39.52 | - | 0.23 | - | - |
| OCTADEC-9-ENOIC ACID | 55.06 | 27.72 | 4.61 | - | - |
| 9,12-Octadecadienoic acid (Z,Z)- | 55.21 | 19.45 | - | - | - |
| Octadecanoic acid | 55.23 | - | - | - | - |
| Hexadecanoic acid /Palmitic acid | 50.86 | 8.14 | 7.28 | - | - |
| *Alcohol* | | | | | |
| 1-Undecanol | 30.81 | 0.25 | - | - | - |
| 8-Dodecen-1-ol, (Z)- | 36.74 | - | 0.58 | - | - |
| Bicyclo[2.2.2]octan-1-ol, 2-methyl- | 50.15 | 0.47 | | - | - |
| 1-Tetradecanol / Tetradecanol | 59.39 | 0.57 | - | - | - |
| 2-(4-HYDROXY-BUTYL)- CYCLOHEXANOL | 60.26 | 0.21 | - | - | - |
| *Aliphatics* | | | | | |
| 1,3-Cyclopentadiene, 5-(1-methylethylidene) | 12.74 | - | - | - | 0.75 |
| 3-Dodecene, (E)- | 15.98 | - | - | 0.71 | - |
| Cyclobuta[1,2:3,4]dicyclopentene, 1,3a,3b,4,6a,6b-hexahydro- | 18.46 | - | - | 0.22 | - |
| Butane, 2,2-dimethyl- | 25.04 | - | 0.32 | - | - |
| Bicyclo[2.2.1]hept-2-ene, 1-methyl- | 25.78 | - | - | 0.28 | - |
| Bicyclo[2.2.1]hept-2-ene, 1-methyl- | 27.06 | - | - | 0.10 | - |
| Azulene | 27.15 | - | - | 0.86 | - |
| Bicyclo[2.2.1]hept-2-ene, 1-methyl- | 27.29 | - | - | 0.51 | - |
| 3-Tetradecene, (Z) | 27.39 | - | 0.39 | - | - |
| Bicyclo[2.2.1]hept-2-ene, 1-methyl- | 28.08 | - | - | 0.53 | - |
| 1-Tridecene | 30.77 | - | 1.38 | - | - |

**Table B-1 (cont.)** Chemical compounds detected in bio-oil from pyrolysis at different temperatures

| Compound Names | RT (min) | Peak area (%) | | | |
|---|---|---|---|---|---|
| | | 400°C | 500°C | 600°C | 700°C |
| *Aliphatics* | | | | | |
| Cyclopentene, 1-octyl | 33.02 | - | 0.23 | - | - |
| Heptadecane | 33.86 | - | 0.18 | 0.29 | - |
| Pentadecane | 33.87 | - | - | 0.39 | - |
| Heptadec-8-ene | 33.96 | - | 0.59 | - | - |
| Cyclopentene, 1-octyl | 36.66 | - | 0.50 | - | - |
| Heptadecane, 2,6,10,14-tetramethyl- | 36.87 | - | 0.29 | - | - |
| 9-Octadecene, (E)- | 36.97 | 0.17 | - | - | - |
| 9-Octadecene, (E)- | 36.97 | - | 1.03 | - | - |
| 10-Heneicosene (c,t) | 39.82 | - | 0.33 | - | - |
| Fluoranthene | 55.76 | 0.46 | - | - | - |
| 1,3,12-Nonadecatriene | 59.55 | 0.36 | - | - | - |
| *Aromatics* | | | | | |
| MAH | | | | | |
| Benzene, methyl- | 8.90 | - | - | 4.57 | 1.32 |
| Benzene | 6.00 | - | - | 3.72 | 0.68 |
| Benzene, 1,2-dimethyl- | 12.74 | - | - | 1.25 | - |
| Benzene, 1,2-dimethyl- | 13.90 | - | - | 0.26 | - |
| Styrene | 14.26 | - | - | 1.15 | 1.01 |
| 1H-Indene | 21.02 | - | - | 0.47 | 1.10 |
| 1H-Indene, 1-ethylidene- | 31.04 | - | - | 0.35 | - |
| | 31.66 | - | - | 0.37 | - |
| *PAH* | | | | | |
| Naphthalene | 27.12 | - | - | - | 2.77 |
| Naphthalene | 31.00 | - | - | - | 1.06 |
| Naphthalene, 1-methyl- | 31.63 | - | - | - | 1.02 |

**Table B-1 (cont.)** Chemical compounds detected in bio-oil from pyrolysis at different temperatures

| Compound Names | RT | Peak area (%) | | | |
|---|---|---|---|---|---|
| | (min) | 400°C | 500°C | 600°C | 700°C |
| *PAH* | | | | | |
| Biphenylene | 33.80 | - | - | - | 1.13 |
| Naphthalene, 2-ethenyl- | 35.10 | - | - | - | 0.61 |
| Naphthalene, 2-ethenyl- | 35.85 | - | - | - | 1.32 |
| Naphthalene, 2-ethenyl- | 37.00 | - | - | 0.42 | 3.43 |
| Acenaphthene | 37.51 | - | - | - | 0.41 |
| 9H-Fluorene | 40.80 | - | - | - | 1.07 |
| 9H-Fluorene | 41.14 | - | - | - | 0.45 |
| 9H-Fluorene | 42.27 | - | - | - | 0.45 |
| 9H-Fluorene, 1-methyl- | 43.87 | - | - | - | 0.35 |
| Phenanthrene | 46.98 | - | - | - | 3.08 |
| Benz[a]azulene | 47.02 | - | - | 0.27 | - |
| Anthracene | 47.23 | - | - | - | 1.21 |
| Phenanthrene, 4-methyl- | 49.83 | - | - | - | 0.49 |
| Anthracene, 1-methyl- | 49.98 | - | - | - | 0.24 |
| 4H-Cyclopenta[def]phenanthrene | 50.42 | - | - | - | 0.31 |
| Naphtho[2,3-b]norbornadiene | 50.49 | - | - | - | 0.28 |
| 2-Phenylnaphthalene | 51.54 | - | - | - | 0.30 |
| Pyrene | 54.49 | - | - | - | 0.49 |
| Pyrene | 55.10 | - | - | - | 0.35 |
| Pyrene | 55.73 | - | - | - | 0.75 |
| *Ester* | | | | | |
| 2-Propenoic acid, cyclohexyl ester | 35.05 | - | 0.20 | - | - |
| 2,2,4-Trimethyl-1,3-pentanediol diisobutyrate | 40.03 | 0.46 | 0.25 | 0.16 | - |

**Table B-1 (cont.)** Chemical compounds detected in bio-oil from pyrolysis at different temperatures

| Compound Names | RT (min) | Peak area (%) | | | |
|---|---|---|---|---|---|
| | | 400°C | 500°C | 600°C | 700°C |
| *Ester* | | | | | |
| 1,2-Benzenedicarboxylic acid, diethyl ester | 42.36 | 1.71 | 1.56 | 0.83 | 0.43 |
| Z-2-Octadecen-1-ol acetate | 47.47 | 0.28 | - | - | - |
| Hexanoic acid, tridecyl ester | 47.53 | 0.49 | - | - | - |
| Hexadecanoic acid, methyl ester | 47.53 | - | 0.31 | - | - |
| Octadecanoic acid, methyl ester | 47.54 | - | - | 0.13 | - |
| Octadecanoic acid, 2-propenyl ester | 51.13 | - | 0.69 | - | - |
| Dibutyl phthalate | 51.37 | 0.36 | - | 0.16 | - |
| 1,2-Benzenedicarboxylic acid, bis(2-methoxyethyl) ester | 51.37 | - | 0.45 | - | - |
| 9-Octadecenoic acid (Z)-, methyl ester | 51.88 | 0.36 | - | - | - |
| Cyclopentanetridecanoic acid, methyl ester | 52.19 | 0.23 | - | - | - |
| ETHYL 9-HEXADECENOATE | 53.27 | 1.76 | - | - | - |
| ETHYL 9-HEXADECENOATE | 53.59 | 0.59 | - | - | - |
| 1-Propene-1,2,3-tricarboxylic acid, tributyl ester | 55.21 | - | - | 0.30 | - |
| Hexadecanoic acid, propyl ester | 55.48 | 1.70 | - | - | - |
| Tributyl acetylcitrate | 57.68 | 1.45 | 1.38 | 0.73 | 0.47 |
| Hexanedioic acid, mono(2-ethylhexyl)ester | 59.25 | 1.00 | - | - | - |

**Table B-1 (cont.)** Chemical compounds detected in bio-oil from pyrolysis
at different temperatures

| Compound Names | RT (min) | Peak area (%) | | | |
|---|---|---|---|---|---|
| | | 400°C | 500°C | 600°C | 700°C |
| *Ester* | | | | | |
| Hexanedioic acid, bis(2-ethylhexyl) ester | 59.26 | - | 0.55 | 0.23 | - |
| 9-Octadecenoic acid (Z)-, 2,3-dihydroxypropyl ester | 63.21 | 0.41 | - | - | - |
| 9-Octadecenoic acid (Z)-, tetradecyl ester | 65.65 | 0.51 | - | - | - |
| *Ether* | | | | | |
| Benzofuran, 2,3-dihydro- | 33.71 | - | - | - | 0.37 |
| (Z,Z)-6,9-cis-3,4-epoxy-nonadecadiene | 53.41 | 0.75 | - | - | - |
| Ketone | | | | | |
| 2-Pentanone, 4-hydroxy-4-methyl- | 15.39 | - | 5.09 | 2.73 | - |
| 2-Pentanone, 4-hydroxy-4-methyl- | 15.44 | 4.05 | - | - | 2.05 |
| 3-Ethyl-2-hydroxy-2-cyclopenten-1-one | 32.78 | - | 0.22 | - | - |
| Cyclohexanone, 2,2-dimethyl- | 37.54 | - | 0.26 | - | - |
| 2H-Pyran-2-one, tetrahydro-6-tridecyl- | 56.40 | 0.31 | - | - | - |
| *N-containing compounds* | | | | | |
| Acetonitrile | 4.66 | - | 0.17 | 2.36 | 0.81 |
| Propanenitrile | 5.96 | - | - | 0.20 | - |
| Propanenitrile, 2-methyl- | 6.80 | - | - | 0.12 | - |
| 1H-1,2,4-Triazole | 12.51 | - | 0.41 | - | - |
| 1H-Pyrrole | 12.69 | - | - | 0.55 | - |
| 1H-1,2,4-Triazole | 12.45 | - | - | 3.90 | 1.36 |

**Table B-1 (cont.)** Chemical compounds detected in bio-oil from pyrolysis
at different temperatures

| Compound Names | RT | Peak area (%) | | | |
| --- | --- | --- | --- | --- | --- |
| | (min) | 400°C | 500°C | 600°C | 700°C |
| *N-containing compounds* | | | | | |
| 2-Pentanone, 4-amino-4-methyl- | 15.83 | - | 19.03 | 1.43 | - |
| Acetone cyanohydrin | 18.29 | - | 0.72 | 1.16 | 2.57 |
| 2H-Imidazole, 2,2,4,5-tetramethyl- | 18.59 | - | 0.18 | - | - |
| Piperazine, 2,5-dimethyl-, trans | 19.30 | - | 8.25 | 46.51 | 36.08 |
| 3,6-Dimethylpiperazine-2,5-dione | 19.62 | - | 1.29 | - | - |
| N-Cyano-2-methylpyrrolidine | 20.30 | - | - | 1.29 | - |
| Bicyclo[2.2.1]hept-5-ene-2-carbonitrile, exo- | 24.24 | - | - | 0.83 | - |
| 1-Methyl-5-piperidin-1-yl-imidazolidin-2,4-dione | 24.68 | - | 8.24 | - | - |
| Piperidine, 2-methyl- | 24.74 | 1.85 | - | - | - |
| 2,2,6,6-Tetramethyl-4-piperidone | 26.09 | 2.01 | 14.98 | 2.82 | 10.41 |
| Aziridine, 1,2-diisopropyl-3-methyl-, trans- | 28.08 | - | 0.92 | - | - |
| Diazene, bis(1,1-dimethylethyl)- | 28.67 | - | 0.41 | - | - |
| N-Nitro-N',N'-pentamethyleneguanidine | 30.23 | - | 0.23 | - | - |
| Quinoline | 30.27 | - | - | - | 1.62 |
| Quinoline | 31.31 | - | - | - | 0.45 |
| Acetamide, N-2-propynyl- | 32.04 | - | 0.77 | - | - |
| 2,6-Piperidinedione | 32.88 | 0.38 | - | - | - |
| Guanosine | 33.41 | 2.17 | - | - | - |
| Acetamide, N-2-propynyl- | 34.21 | - | 0.98 | - | - |
| 1H-Indole | 35.54 | - | - | - | 3.74 |

**Table B-1 (cont.)** Chemical compounds detected in bio-oil from pyrolysis at different temperatures

| Compound Names | RT | Peak area (%) | | | |
|---|---|---|---|---|---|
| | (min) | 400°C | 500°C | 600°C | 700°C |
| *N-containing compounds* | | | | | |
| 5H-1-Pyrindine | 35.63 | - | - | 0.45 | - |
| 4-Aminoresorcinol | 39.14 | - | - | - | 3.10 |
| 2,4-Imidazolidinedione, 1-(hydroxymethyl)-5,5-dimethyl- | 39.51 | - | - | - | 1.65 |
| 1-Naphthalenecarbonitrile | 40.17 | - | - | - | 1.70 |
| 2,4-Imidazolidinedione, 5-(2-methylpropyl)-, (S)- | 41.06 | - | - | 4.46 | - |
| 5-Ethyl-5-methylhydantoin | 41.99 | - | - | 0.86 | - |
| 5-Isopropyl-2,4-imidazolidinedione | 44.16 | 0.37 | - | - | - |
| 2,4-Imidazolidinedione, 5-(2-methylpropyl)-, (S)- | 46.86 | 0.77 | - | 5.25 | - |
| 1-Naphthalenecarbonitrile | 41.39 | - | - | - | 0.83 |
| Tridecanenitrile | 49.14 | - | 0.20 | - | - |
| dl-Alanyl-l-leucine | 51.19 | 0.43 | - | - | - |
| Cycloalanylleucine | 51.22 | - | 0.51 | - | - |
| 3-Pyrrolidin-2-yl-propionic acid | 51.44 | 0.21 | - | - | - |
| 5H-Indeno[1,2-b]pyridine | 51.75 | - | - | - | 0.28 |
| Pyrrolo[1,2-a]pyrazine-1,4-dione, hexahydro- | 52.47 | 0.48 | - | - | - |
| N,N-Diethyl-1-oxaspiro[4.4]nonan-2-one-4-carboxamide | 52.53 | 0.46 | - | - | - |
| Cyclopentanamine, N-ethyl | 53.22 | 1.71 | - | - | - |
| Oleanitrile | 53.61 | - | 0.32 | - | 0.39 |
| Pyrrolo[1,2-a]pyrazine-1,4-dione, hexahydro-3-(2-methylpropyl)- | 54.56 | 0.40 | - | - | - |

**Table B-1 (cont.)** Chemical compounds detected in bio-oil from pyrolysis at different temperatures

| Compound Names | RT (min) | Peak area (%) | | | |
|---|---|---|---|---|---|
| | | 400°C | 500°C | 600°C | 700°C |
| *N-containing compounds* | | | | | |
| 5,10-Diethoxy-2,3,7,8-tetrahydro-1H,6H-dipyrrolo[1,2-a;1',2'-d]pyrazine | 54.73 | 0.59 | - | - | - |
| 1,4-diaza-2,5-dioxo-3-isobutyl bicyclo[4.3.0]nonane | 55.44 | - | 0.74 | - | - |
| Pyrrolo[1,2-a]pyrazine-1,4-dione, hexahydro- | 55.45 | 1.77 | - | - | - |
| Pyrrolo[1,2-a]pyrazine-1,4-dione, hexahydro-3-(2-methylpropyl)- | 55.57 | 3.27 | 0.71 | - | - |
| Hexadecanamide | 57.37 | 1.30 | 1.75 | - | - |
| Dodecanal, O-methyloxime | 57.53 | - | 0.23 | - | - |
| 9-Octadecenamide, (Z)- | 61.27 | 2.79 | - | 0.63 | 0.71 |
| 9-Octadecenamide, (Z)- | 61.29 | - | 2.23 | - | - |
| Octadecanamide | 61.48 | 0.88 | 0.94 | 0.73 | 0.35 |
| *Phenol* | | | | | |
| Phenol | 24.66 | - | - | 0.98 | 2.77 |
| Phenol, 4-methyl/ p-Cresol | 27.68 | - | - | - | 0.27 |
| *Sugar* | | | | | |
| 1,4:3,6-Dianhydro-.alpha.-d-glucopyranose | 36.44 | 2.55 | 1.30 | - | - |
| D-Allose | 45.39 | 0.72 | - | - | - |
| *Other S/P* | | | | | |
| Propanenitrile, 3,3'-thiobis- | 45.85 | - | - | 0.84 | 1.17 |
| Phosphine oxide, triphenyl- | 68.32 | 0.42 | - | - | - |

**Table B-2 (cont.)** Chemical compounds detected in bio-oil from pyrolysis at different particle sizes

| Compound Names | RT | Peak area (%) | | | | |
|---|---|---|---|---|---|---|
| | (min) | 125-425 2L/min | 0.425-0.85, 4L/min | 0.125, 3L/min | 0.425-0.85, 3L/min | >0.85, 3L/min |
| *Alcohol* | | | | | | |
| 1-Pentadecanol | - | - | - | 1.19 | - | - |
| 2-Methyl-1-phenyl-1-butanol | 28.97 | 0.79 | - | - | - | - |
| 1,2,2,3-TETRAMETHYL-CYCLOPENT-3-ENOL $$ | 30.68 | - | - | - | 5.00 | - |
| INDENOL $$ | 36.96 | - | - | - | - | 2.14 |
| INDENOL $$ | 36.99 | - | - | - | 0.51 | 1.64 |
| *Aromatic* | | | | | | |
| Benzene, methyl- | 8.85 | 0.58 | - | 1.08 | 4.20 | 0.87 |
| Benzene | 5.99 | - | - | - | 0.70 | - |
| Benzene, (2-methyl-1-methylenebutyl)- | 37.63 | 0.50 | - | - | - | - |
| Benz[a]azulene $$ | 46.88 | 0.48 | 1.92 | - | - | 1.03 |
| Naphthalene | 27.04 | 0.81 | 4.28 | 0.61 | | |
| Naphthalene, 1-ethyl- | 34.09 | 0.80 | 0.52 | - | - | - |
| Naphthalene, 1-ethyl- | 34.22 | 0.59 | 0.39 | - | - | - |
| Naphthalene, 1-methyl- | 35.76 | | 1.62 | - | - | - |
| Naphthalene, 2-ethenyl- | 31.53 | 1.11 | 2.13 | - | - | - |
| Naphthalene, 2-methyl- | 30.90 | 1.20 | 2.10 | 0.85 | | - |
| Naphthalene, 1,8-dimethyl- | 35.00 | 0.84 | 0.27 | 0.67 | | - |
| Acenaphthene | 36.92 | - | 3.28 | - | - | - |
| Acenaphthene | 37.42 | - | 0.81 | - | - | - |
| Naphthalene, 1-(2-propenyl)- | 39.13 | - | 0.45 | - | - | - |
| Acenaphthylene, 1,2-dihydro- | 35.75 | 0.36 | - | - | - | - |
| Acenaphthylene, 1,2-dihydro | 37.40 | 0.76 | - | - | - | - |
| 9H-Fluorene | 40.69 | 0.46 | 0.53 | - | - | - |
| Naphthalene, 1,8-dimethyl- | 35.00 | 0.84 | 0.27 | 0.67 | - | - |

**Table B-2 (cont.)** Chemical compounds detected in bio-oil from pyrolysis at different particle sizes

| Compound Names | RT | Peak area (%) | | | | |
|---|---|---|---|---|---|---|
| | (min) | 125-425 2L/min | 0.425-0.85, 4L/min | 0.125, 3L/min | 0.425-0.85, 3L/min | >0.85, 3L/min |
| *Aromatic* | | | | | | |
| 9H-Fluorene | 40.71 | - | 0.87 | - | - | - |
| 9H-Fluorene | 40.84 | - | 0.32 | - | - | - |
| 9H-Fluorene, 1-methyl- | 42.18 | - | 0.60 | - | - | - |
| 9H-Fluorene, 9-methyl- | 43.77 | - | 0.75 | - | - | - |
| Phenanthrene | 47.14 | - | 0.64 | - | - | - |
| 1H-Phenalene | 41.05 | - | 1.09 | - | - | - |
| 2-Methylindene | 24.85 | - | 0.70 | - | - | - |
| 2-Methyl-1H-indene | 24.92 | - | 0.58 | - | - | - |
| Pyrene | 55.63 | - | 0.37 | - | - | - |
| *Carboxylic* | | | | | | |
| Pentadecanoic acid | 50.80 | 11.10 | - | - | - | - |
| OCTADEC-9-ENOIC ACID | 54.96 | 5.71 | - | - | 1.57 | - |
| Pentadecanoic acid | 50.75 | | - | 8.58 | 5.63 | 11.63 |
| Octadecanoic acid | 55.16 | 5.19 | - | - | - | - |
| Octanoic Acid | 44.66 | - | - | 0.47 | - | - |
| HEPTADECENE-(8)-CARBONIC ACID-(1) $$ | 54.89 | - | - | 2.06 | - | - |
| Decanoic acid | 35.37 | - | - | - | 0.81 | - |
| 3-Heptenoic acid | 26.24 | - | - | - | - | 0.84 |
| 9-Octadecenoic acid (Z)- | 55.09 | - | - | 1.16 | - | - |
| *Ester* | | | | | | |
| 1,2,3-Propanetriol, monoacetate | 33.44 | - | - | - | - | 0.74 |
| Dibutyl phthalate | 42.21 | - | - | - | 0.34 | 0.56 |
| Diethyl Phthalate | 41.79 | - | - | 1.12 | 1.36 | - |
| Tetratriacontane | 41.95 | - | - | 1.26 | - | - |
| Hexanoic acid, tridecyl ester | 47.30 | - | - | 7.87 | - | - |

**Table B-2 (cont.)** Chemical compounds detected in bio-oil from pyrolysis at different particle sizes

| Compound Names | RT | Peak area (%) | | | | |
| --- | --- | --- | --- | --- | --- | --- |
| | (min) | 125-425 2L/min | 0.425-0.85, 4L/min | 0.125, 3L/min | 0.425-0.85, 3L/min | >0.85, 3L/min |
| *Ester* | | | | | | |
| Hexadecanoic acid, methyl ester ( | 47.39 | - | - | 4.12 | - | - |
| Dibutyl phthalate | 51.22 | - | - | 0.73 | - | - |
| Hexadecanoic acid, methyl ester | 47.41 | 2.03 | 0.25 | - | 4.98 | 5.41 |
| Hexadecanoic acid, 1-methylethyl ester | 49.51 | 0.68 | - | - | - | - |
| Isopropyl Palmitate | 49.49 | - | - | - | - | 2.33 |
| Octadecanoic acid, methyl ester | 52.04 | - | - | 1.87 | - | 1.23 |
| Tributyl acetylcitrate | 57.52 | - | - | 0.91 | 1.20 | - |
| Triacontanoic acid, methyl ester | 52.05 | - | - | - | 1.24 | - |
| Tetracosanoic acid, methyl ester | 52.06 | 0.59 | - | - | - | 0.96 |
| Propanoic acid, 2-methyl-, 1-(1,1-dimethylethyl)-2-methyl-1,3-propanediyl ester | 39.17 | - | - | 1.29 | - | - |
| 9-Octadecenoic acid (Z)-, methyl ester | 51.76 | 0.66 | - | 8.27 | - | - |
| 9,12-Octadecadienoic acid (Z,Z)-, methyl ester | 51.86 | - | - | 2.40 | - | - |
| 9H-Fluoren-9-ol, acetate | 42.01 | - | 0.36 | - | - | - |
| 11-Octadecenoic acid, methyl ester, (Z)- | 51.75 | - | - | - | 2.29 | 1.70 |

**Table B-2 (cont.)** Chemical compounds detected in bio-oil from pyrolysis at different particle sizes

| Compound Names | RT | Peak area (%) | | | | |
|---|---|---|---|---|---|---|
| | (min) | 125-425 2L/min | 0.425-0.85, 4L/min | 0.125, 3L/min | 0.425-0.85, 3L/min | >0.85, 3L/min |
| *furan* | | | | | | |
| Benzofuran, 2,3-dihydro- | 33.61 | 2.12 | 1.17 | 2.28 | 1.48 | 1.56 |
| Benzofuran, 2,3-dihydro- | 33.59 | - | - | - | - | 4.10 |
| *Hydrocarbon* | | | | | | |
| 1-Tetradecene | 30.66 | - | - | 3.66 | - | - |
| 1-Hexadecene | 39.71 | 1.11 | - | - | - | - |
| 3-Tetradecene, (Z) | 27.29 | 0.42 | - | - | - | - |
| 5-Eicosene, (E)- | 39.70 | - | - | 1.04 | 2.02 | |
| 9-Octadecene, (E)- | 33.85 | 1.81 | 0.59 | 1.82 | 0.69 | 1.33 |
| 9-Octadecene, (E)- | 36.86 | 3.16 | - | 2.31 | 2.03 | 1.97 |
| 9-Octadecene, (E)- | 39.28 | 0.44 | - | - | 3.22 | - |
| Bicyclo[2.2.1]hept-2-ene, 1-methyl- | 27.99 | - | 1.55 | - | - | - |
| Bicyclo[2.2.1]hept-2-ene, 1-methyl- | 27.21 | - | 1.38 | - | - | - |
| Bicyclo[2.2.1]hept-2-ene, 1-methyl- | 24.16 | - | 1.78 | - | 0.58 | |
| Cyclobuta[1,2:3,4]dicyclopentene, 1,3a,3b,4,6a,6b-hexahydro- | 18.40 | - | 0.28 | - | - | - |
| Cyclopropane, nonyl- $$ Nonylcyclopropane # $$ | 23.72 | - | 0.29 | - | 0.57 | |
| | 27.30 | - | 0.35 | - | - | - |
| Eicosane (CAS) n-Eicosane $$ | 39.61 | - | 1.02 | - | - | - |
| | 39.60 | 1.97 | | | - | - |
| Hexadecane | 33.75 | 3.45 | 0.96 | 2.26 | 2.92 | 2.05 |
| | 39.61 | - | - | - | 3.53 | 3.26 |
| 1H-Indene, octahydro- | 39.59 | - | - | 1.00 | - | - |

**Table B-2 (cont.)** Chemical compounds detected in bio-oil from pyrolysis at different particle sizes

| Compound Names | RT | Peak area (%) | | | | |
|---|---|---|---|---|---|---|
| | (min) | 125-425 2L/min | 0.425-0.85, 4L/min | 0.125, 3L/min | 0.425-0.85, 3L/min | >0.85, 3L/min |
| *Hydrocarbon* | | | | | | |
| 9-Eicosene, (E)- | 39.72 | - | 0.48 | - | 0.32 | 2.51 |
| 9-Eicosene, (E)- | 39.35 | 0.48 | - | - | - | - |
| trans-7-tetradecene $$ | 30.66 | 4.58 | 1.37 | - | - | - |
| *Ketone* | | | | | | |
| 2-Pentanone, 4-hydroxy-4-methyl- | 15.39 | 1.08 | 2.92 | - | 2.04 | - |
| 2-Pentadecanone | 47.66 | - | - | - | 0.48 | 0.82 |
| 2-n-Heptylcyclopentanone | 47.33 | - | - | - | 0.95 | - |
| 2-n-Hexylcyclopentanone | 47.31 | - | - | - | - | 0.92 |
| 9-Octadecanone | 46.70 | - | - | - | 0.68 | - |
| *N-compound* | | | | | | |
| Acetonitrile | 4.65 | - | - | 0.23 | - | - |
| Propanenitrile | 45.68 | - | 2.75 | - | - | - |
| Acetamide, N-2-propynyl- | 34.11 | - | | - | 0.78 | - |
| Bicyclo[2.2.1]hept-5-ene-2-carbonitrile, exo- | 24.31 | - | 0.81 | - | - | - |
| Bicyclo[2.2.2]oct-5-ene-2,3-dicarbonitrile | 25.70 | - | 0.73 | - | - | - |
| | 26.04 | - | 4.28 | - | - | - |
| 1H-Indole | 35.43 | 3.56 | 3.17 | 0.81 | 0.89 | - |
| 1H-Indole, 3-methyl- | 37.75 | 2.82 | 1.13 | 2.61 | 1.90 | 1.71 |
| 1H-Indazole, 3-methyl- | 37.64 | - | - | - | 0.78 | - |
| Quinoline | 32.13 | - | 0.54 | - | - | - |
| 1-Acetyl-3,3-pentamethylenediaziridine | 48.25 | - | 0.52 | - | - | - |
| 1-Naphthalenecarbonitrile | 40.09 | - | 0.75 | - | - | - |

**Table B-2 (cont.)** Chemical compounds detected in bio-oil from pyrolysis at different particle sizes

| Compound Names | RT (min) | Peak area (%) | | | | |
|---|---|---|---|---|---|---|
| | | 125-425 2L/min | 0.425-0.85, 4L/min | 0.125, 3L/min | 0.425-0.85, 3L/min | >0.85, 3L/min |
| *N-compound* | | | | | | |
| Acetonitrile | 4.65 | - | - | 0.23 | - | - |
| Propanenitrile | 45.68 | - | 2.75 | - | - | - |
| Acetamide, N-2-propynyl- | 34.11 | - | | - | 0.78 | |
| Bicyclo[2.2.1]hept-5-ene-2-carbonitrile, exo- | 24.31 | - | 0.81 | - | - | - |
| Bicyclo[2.2.2]oct-5-ene-2,3-dicarbonitrile | 25.70 | - | 0.73 | - | - | - |
| | 26.04 | - | 4.28 | - | - | - |
| 1H-Indole | 35.43 | 3.56 | 3.17 | 0.81 | 0.89 | |
| 1H-Indole, 3-methyl- | 37.75 | 2.82 | 1.13 | 2.61 | 1.90 | 1.71 |
| 1H-Indazole, 3-methyl- | 37.64 | - | - | - | 0.78 | - |
| Quinoline | 32.13 | - | 0.54 | - | - | - |
| 1-Acetyl-3,3-pentamethylenediaziridine | 48.25 | - | 0.52 | - | - | - |
| 1-Naphthalenecarbonitrile | 40.09 | - | 0.75 | - | - | - |
| 1-Naphthalenecarbonitrile | 41.31 | - | 0.57 | - | - | - |
| 2-Propen-1-amine, N,N-bis(1-methylethyl)- | 24.65 | 1.53 | 2.77 | - | - | 2.21 |
| 1-Phenyl-5-(methylamino)-1H-tetrazole $$ 1-Phenyl-5-(methylamino)(1H)tetrazole $$ N-Methyl-1-phenyl-1H-tetraazol-5-amine # $$ | 40.03 | 1.18 | - | - | - | - |
| 1H-Indole, 2,3-dimethyl- | 41.03 | 1.07 | - | - | - | - |

**Table B-2 (cont.)** Chemical compounds detected in bio-oil from pyrolysis at different particle sizes

| Compound Names | RT (min) | Peak area (%) | | | | |
|---|---|---|---|---|---|---|
| | | 0.125-0.425 2L/min | 0.425-0.85, 4L/min | 0.125, 3L/min | 0.425-0.85, 3L/min | >0.85, 3L/min |
| *N-compound* | | | | | | |
| 2H-Tetrazole-2-acetic acid, 5-phenyl-, (phenylmethylene)hydrazide | 40.02 | - | - | 1.22 | - | - |
| 2,4-Imidazolidinedione, 5-(2-methylpropyl)-, (S)- | 39.47 | - | 6.26 | - | 0.53 | - |
| 2,4-Imidazolidinedione, 5-(2-methylpropyl)-, (S)- | 40.96 | - | 3.22 | - | - | - |
| 2,5-Dimethylbenzonitrile | 28.97 | - | - | 0.66 | - | - |
| 2,2,6,6-Tetramethyl-4-piperidone | 26.01 | - | - | - | 3.53 | 3.06 |
| 4-Piperidinone, 2,2,6,6-tetramethyl- | 25.98 | - | 1.74 | - | - | - |
| 4-Hydroxybenzimidazole $$ | 33.52 | - | - | - | - | 2.05 |
| 5H-Indeno[1,2-b]pyridine | 51.64 | - | 0.46 | - | - | - |
| 5-Norbornene-2,3-diacetonitrile | 24.71 | - | 1.32 | - | - | - |
| 9-Octadecenamide, (Z)- | 61.15 | 3.59 | 3.40 | 3.16 | - | - |
| 9-Octadecenamide, (Z)- | 61.11 | - | - | - | 5.02 | 4.74 |
| Aziridine, 1,2-diisopropyl-3-methyl-, trans- | 28.01 | - | - | - | 2.65 | 1.14 |
| Benzyl nitrile | 28.50 | - | - | 2.24 | - | - |
| Benzonitrile, 2-methyl- | 28.50 | 1.58 | 1.04 | - | - | - |
| Piperidine, 2-methyl- | 24.65 | - | - | - | 5.96 | - |
| Dodecanal, O-methyloxime | 57.41 | 0.76 | - | 0.97 | 1.28 | 1.57 |
| Dodecanamide | 42.83 | 0.86 | 0.41 | 0.73 | 1.23 | - |
| *N-compound* | | | | | | |
| Glycyl-l-glutamine | | | | | | |

**Table B-2 (cont.)** Chemical compounds detected in bio-oil from pyrolysis at different particle sizes

| Compound Names | RT | Peak area (%) | | | | |
|---|---|---|---|---|---|---|
| | (min) | 125-425 2L/min | 0.425-0.85, 4L/min | 0.125, 3L/min | 0.425-0.85, 3L/min | >0.85, 3L/min |
| *N-compound* | | | | | | |
| Isoquinoline (CAS) | 30.19 | 0.90 | 1.63 | - | - | - |
| | 31.25 | - | 0.48 | - | - | - |
| N-[2-(Quinolin-8-yloxy)-ethyl]-acetamide | 41.04 | - | - | - | 1.95 | - |
| Hexadecanamide | 57.23 | - | - | 5.55 | - | 8.42 |
| Oleanitrile | 53.47 | - | 0.86 | - | - | - |
| Octadecanamide | 61.36 | 2.13 | 1.33 | 2.26 | 0.62 | 3.32 |
| | 57.23 | - | - | - | 8.60 | - |
| | 61.32 | - | - | - | 3.38 | - |
| Hexadecanamide | 57.24 | - | 2.79 | - | - | - |
| Hexadecanamide | 57.26 | 4.69 | - | - | - | - |
| Hexadecanenitrile | 49.01 | 0.69 | 0.26 | 0.58 | 1.05 | - |
| Heptadecanenitrile | 53.71 | 0.42 | - | - | - | 1.11 |
| Tetradecanal, O-methyloxime | 57.39 | - | 0.33 | - | - | - |
| Pentamethylenehydantoin | 50.41 | - | 0.53 | - | - | - |
| dl-Alanyl-l-leucine | 41.89 | - | 1.18 | - | - | - |
| *Phenol* | | | | | | |
| Phenol | 24.53 | 4.75 | 2.39 | 3.98 | - | 1.16 |
| Phenol, 2-methyl- | 26.26 | 4.59 | 2.15 | 4.31 | 3.89 | 2.04 |
| Phenol, 2,5-dimethyl- | 29.17 | 0.86 | 0.64 | 0.48 | - | 4.86 |
| Phenol, 3-ethyl- | 30.61 | - | - | 1.50 | - | 0.77 |
| Phenol, 4-methyl/ p-Cresol | 27.55 | 7.68 | 5.34 | 7.37 | 1.48 | 2.65 |
| Phenol, 4-(1-methylethyl)- | 32.04 | - | - | - | - | 1.22 |
| Phenol, 3-ethyl- | 30.62 | - | - | - | - | 5.09 |
| Phenol, 4-propyl- | 33.50 | 0.45 | - | 0.67 | - | - |
| 2-Allylphenol | 34.98 | - | - | - | - | 1.67 |

Appendix C

Gas composition of fast pyrolysis by drop tube reactor

**Fig.C-1** Gas species from fast pyrolysis of Jatropha waste at 400°C
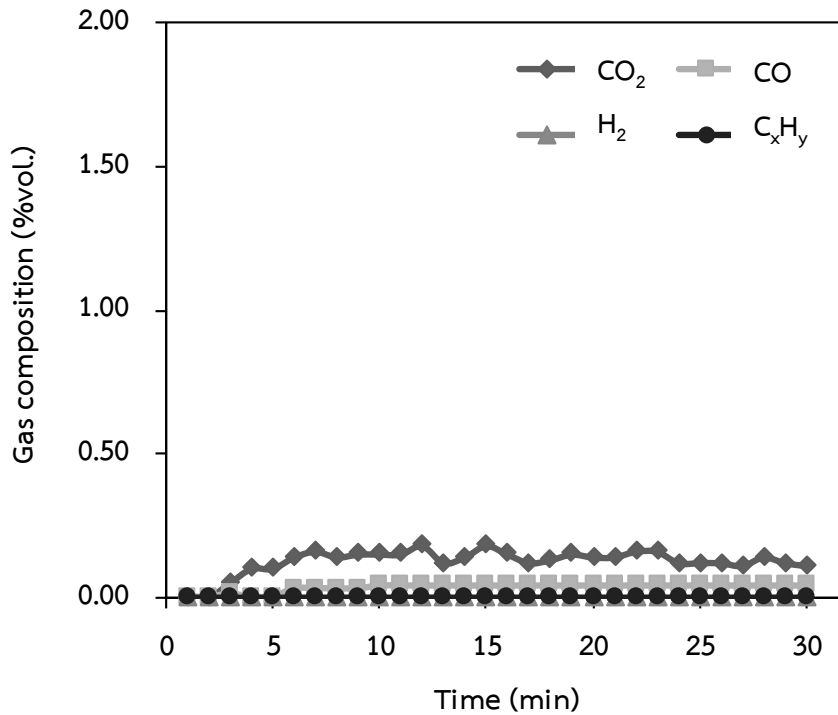


**Fig.C-2** Gas species from fast pyrolysis of Jatropha waste at 500°C
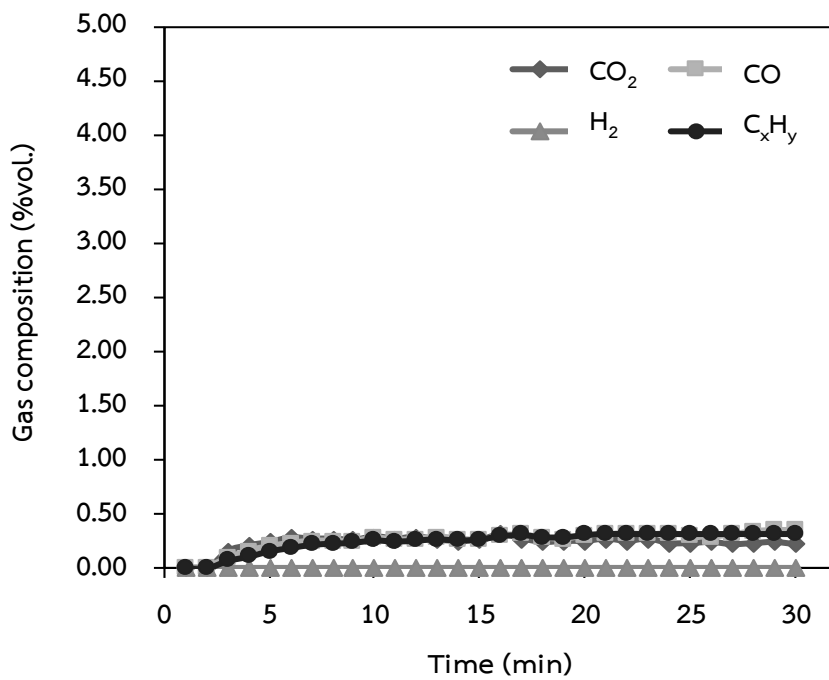
**Fig.C-3** Gas species from fast pyrolysis of Jatropha waste at 600°C
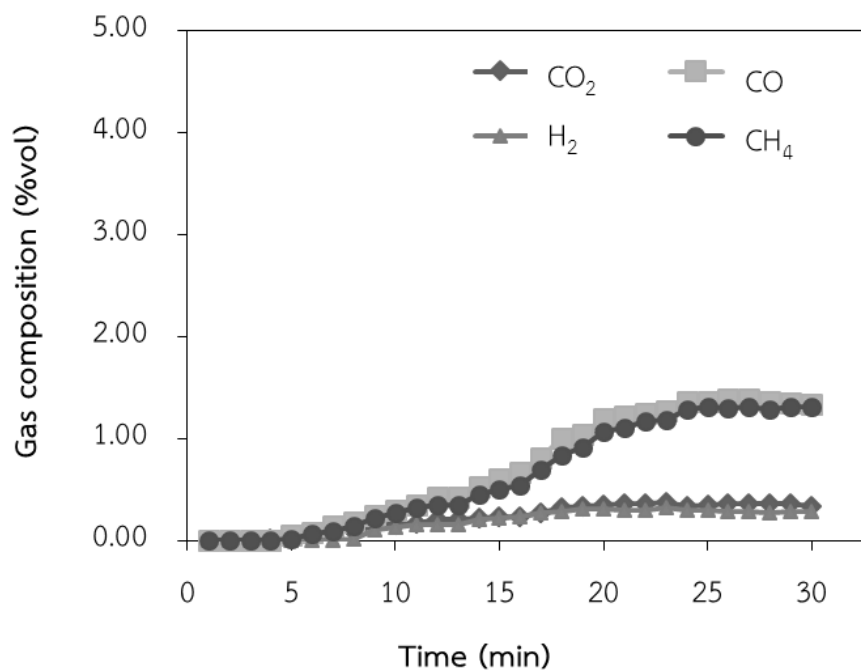


**Fig.C-4** Gas species from fast pyrolysis of Jatropha waste at 700°C
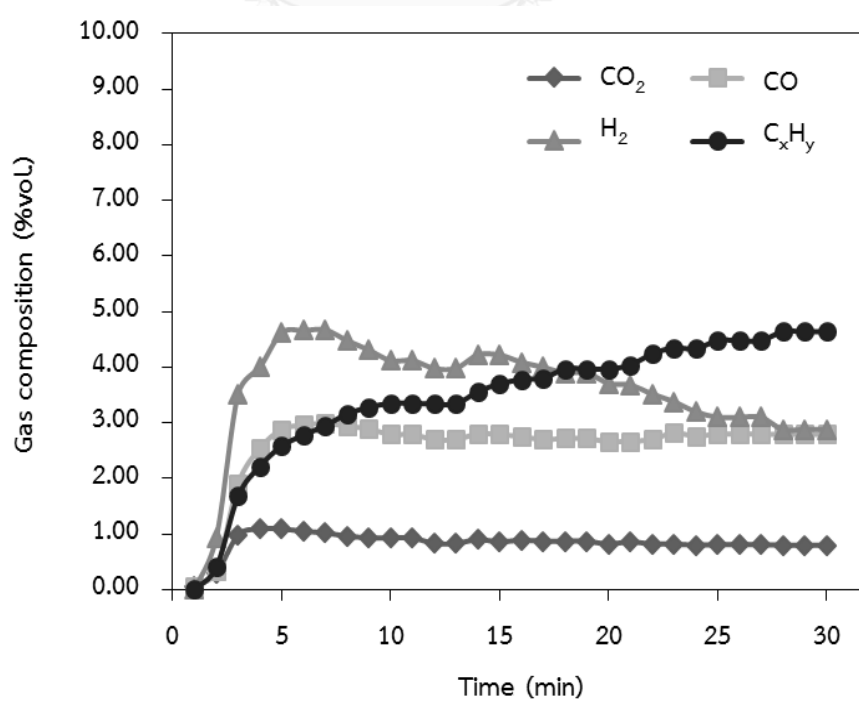
**Fig.C-5** Gas species from fast pyrolysis of Jatropha waste with size of 0.125 mm
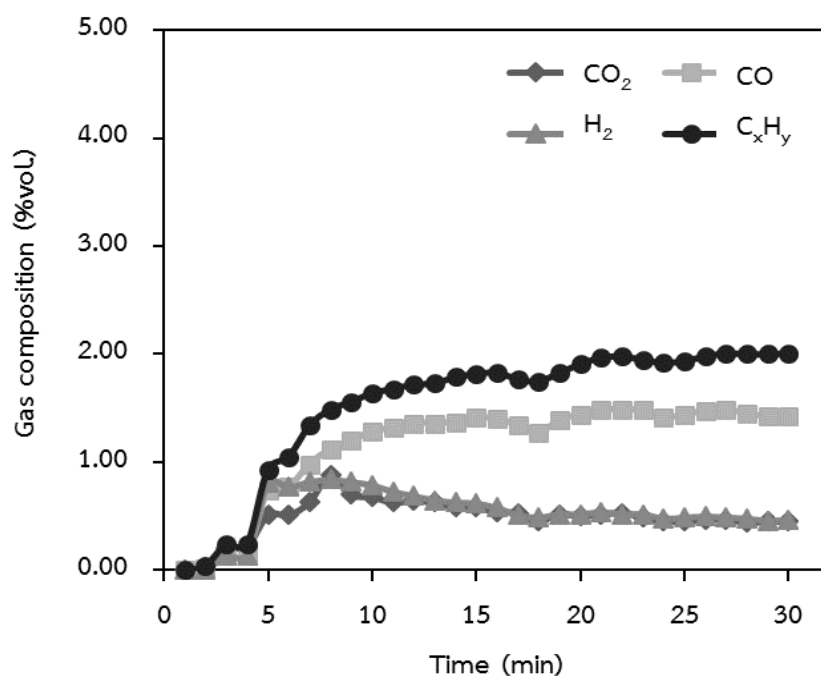


**Fig.C-6** Gas species from fast pyrolysis with size of 0.125-0.425 mm
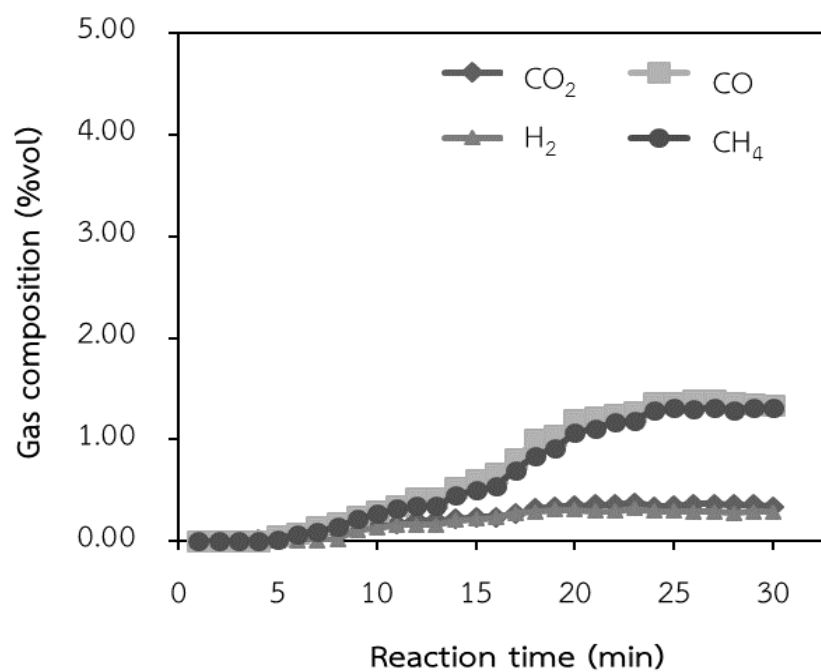
**Fig.C-7** Gas species from fast pyrolysis with size of -0.425-0.85 mm
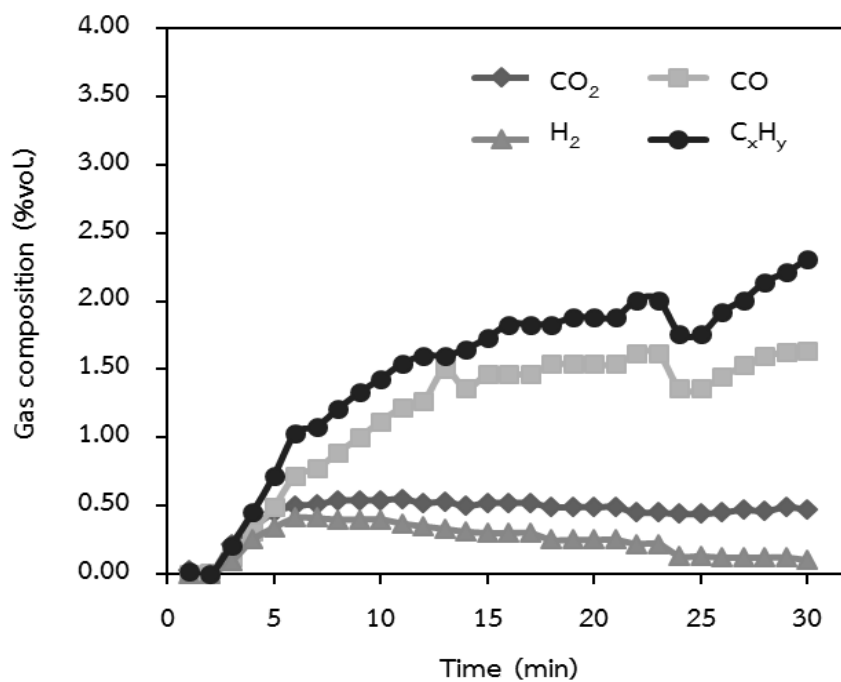


**Fig.C-8** Gas species from fast pyrolysis of Jatropha waste at 2L/min
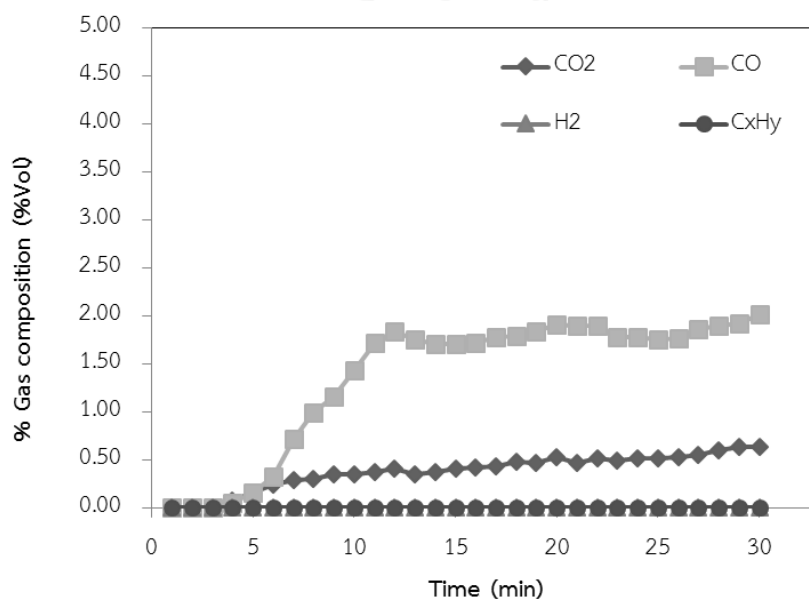
**Fig.C-9** Gas species from fast pyrolysis of Jatropha waste at 4L/min
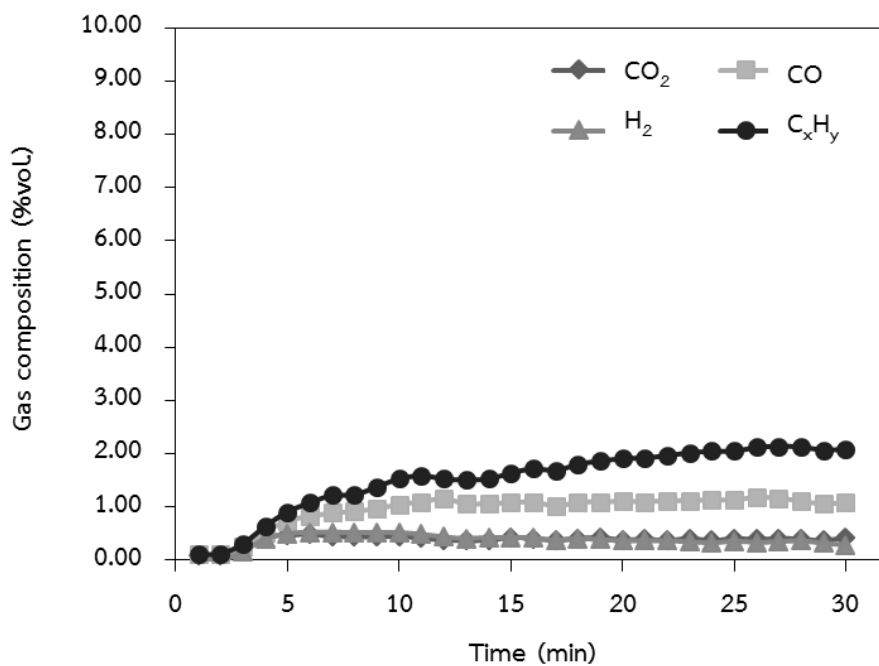


**Fig.C-10** Gas species from fast pyrolysis at 600°C with Ac (7.5g)
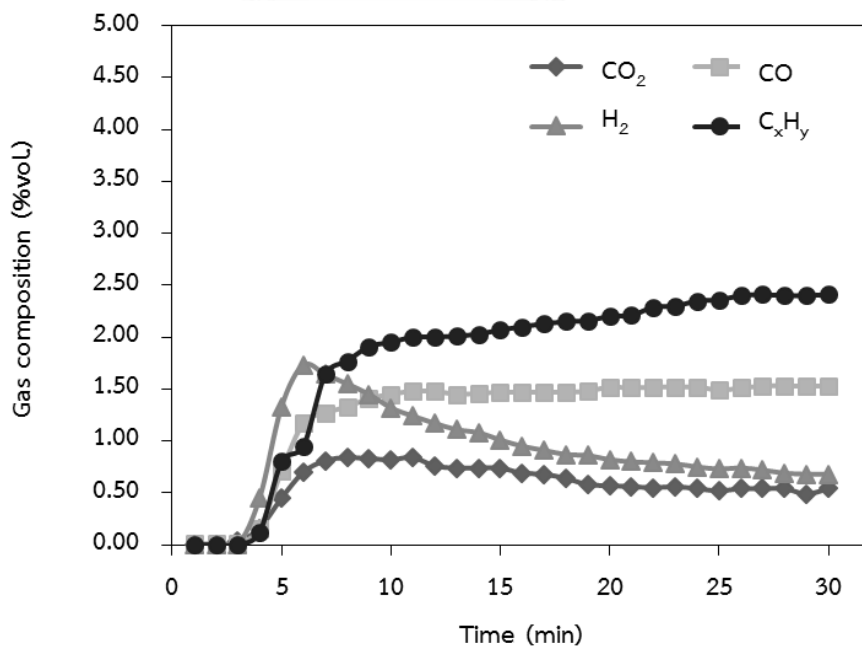
**Fig.C-11** Gas species from fast pyrolysis at 600°C with Ac (15g)
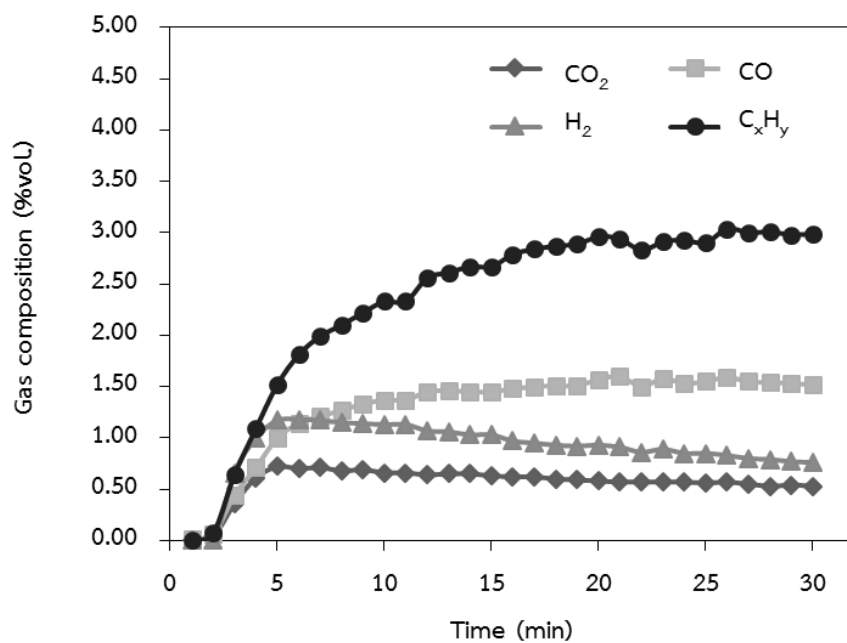


**Fig.C-12** Gas species from fast pyrolysis at 400°C with Ni/Ac (15g)
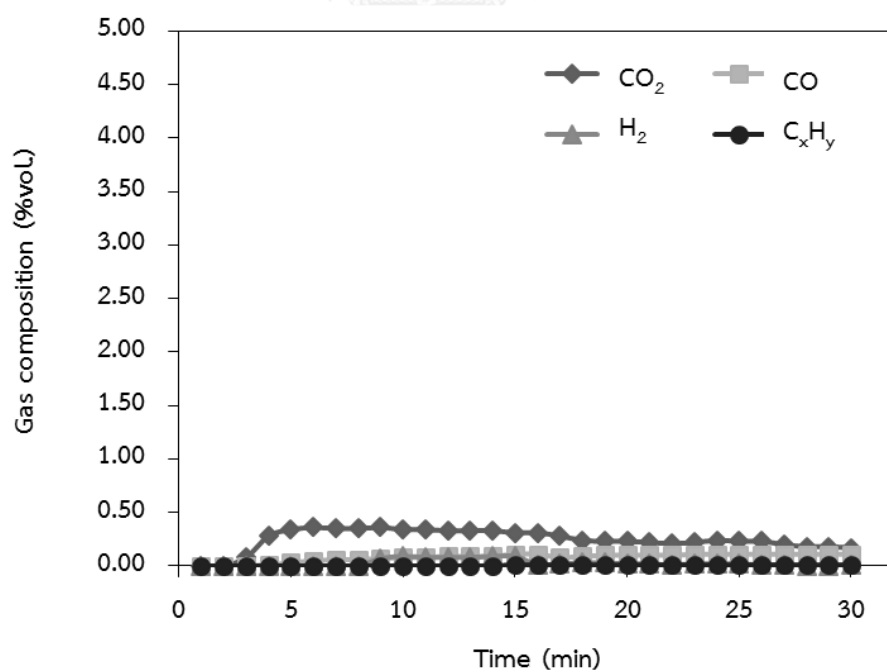
**Fig.C-13** Gas species from fast pyrolysis at 500°C with Ni/Ac (15g)
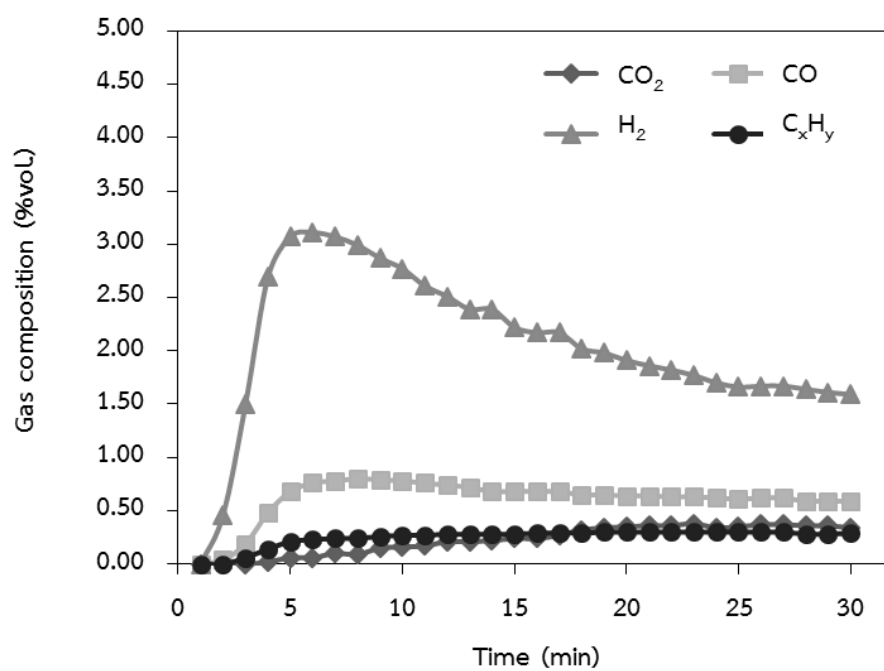


**Fig.C-14** Gas species from fast pyrolysis at 600°C with Ni/Ac (15g)
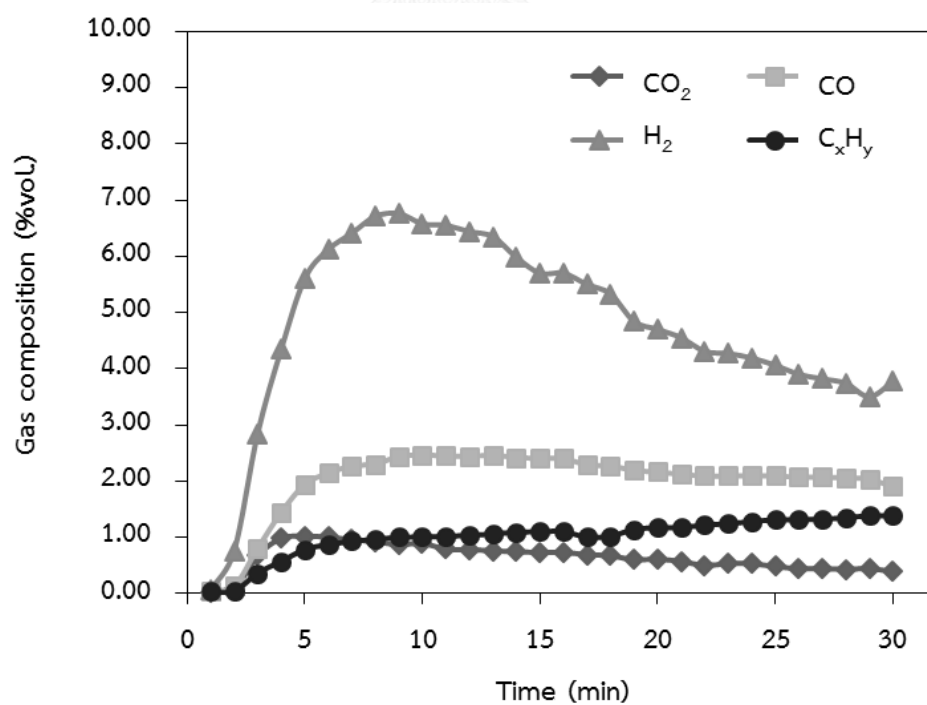
**Fig.C-15** Gas species from fast pyrolysis at 500°C with Ni/Ac (7.5g)
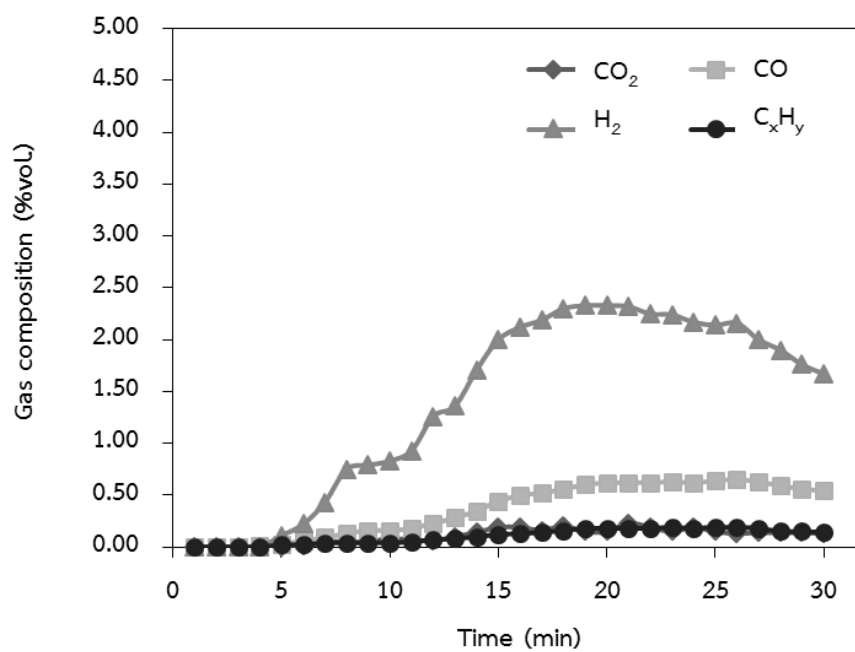


**Fig.C-16** Gas species from fast pyrolysis at 600°C with Ni/Ac (7.5g)
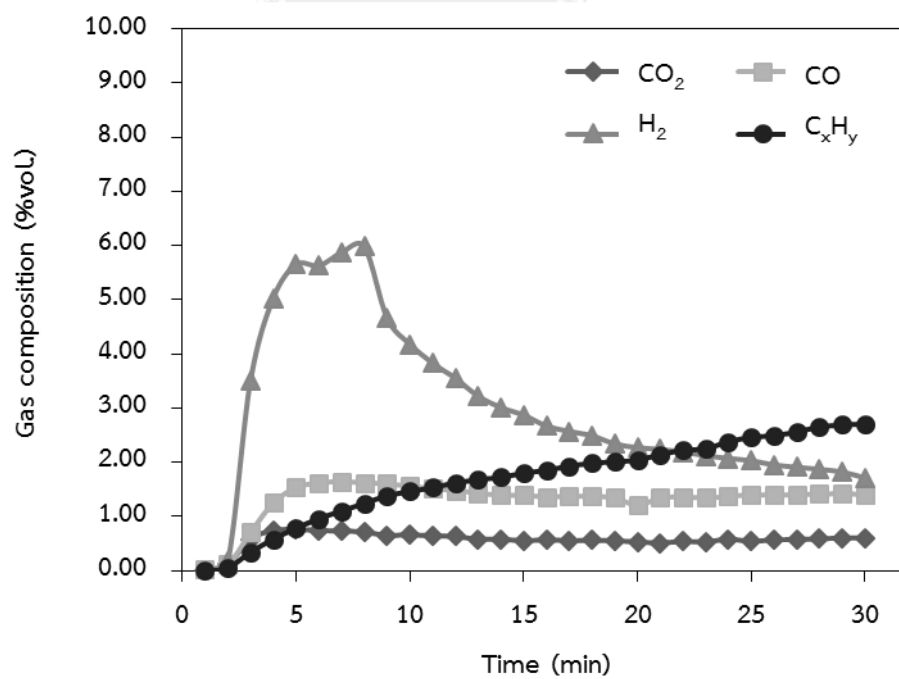
**Fig.C-17** Gas species from fast pyrolysis at 500°C with Pd/Ac (7.5g)
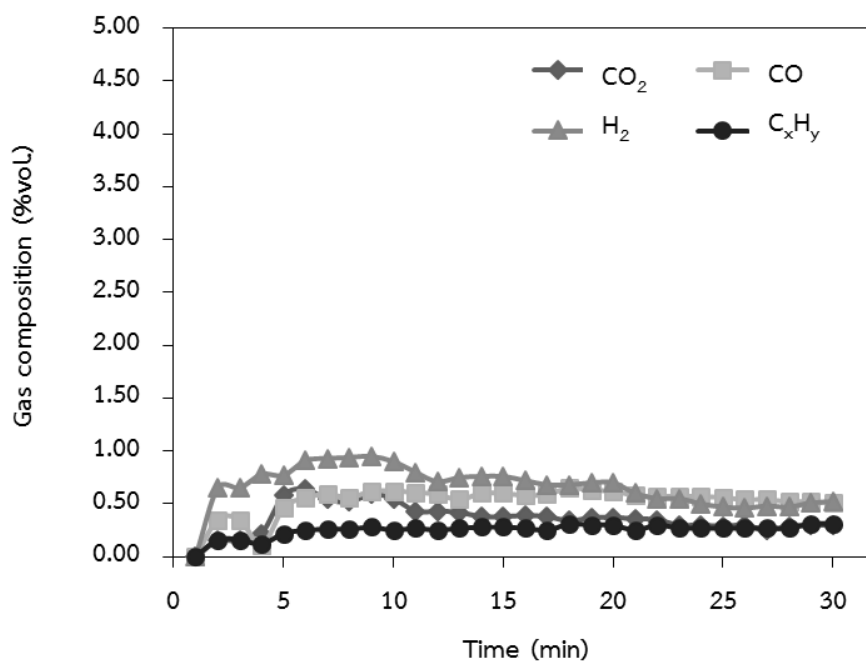


**Fig.C-18** Gas species from fast pyrolysis at 600°C with Pd/Ac (7.5g)
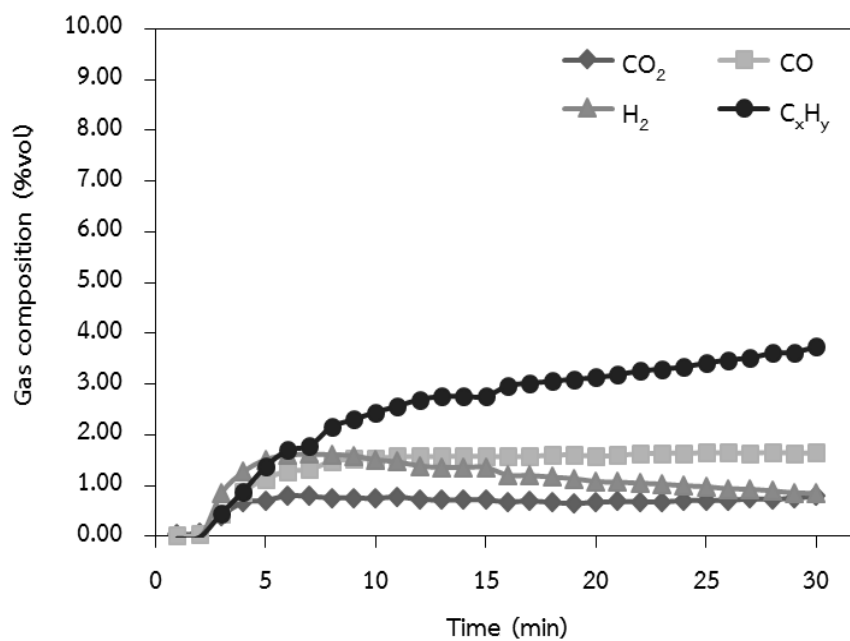
**Fig.C-19** Gas species from fast pyrolysis at 600°C with $Al_2O_3$
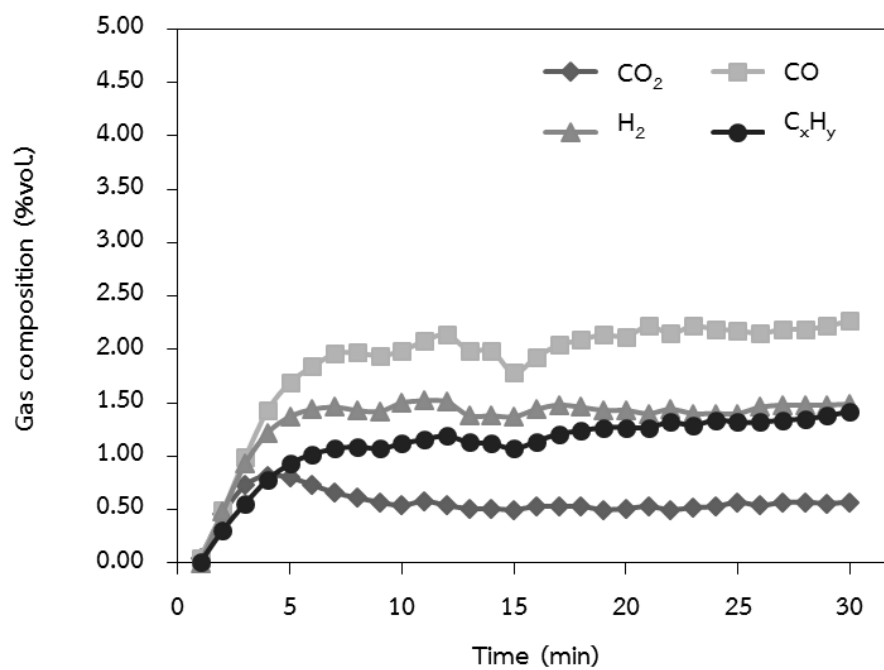


**Fig.C-20** Gas species from fast pyrolysis at 600°C with $Ni/Al_2O_3$
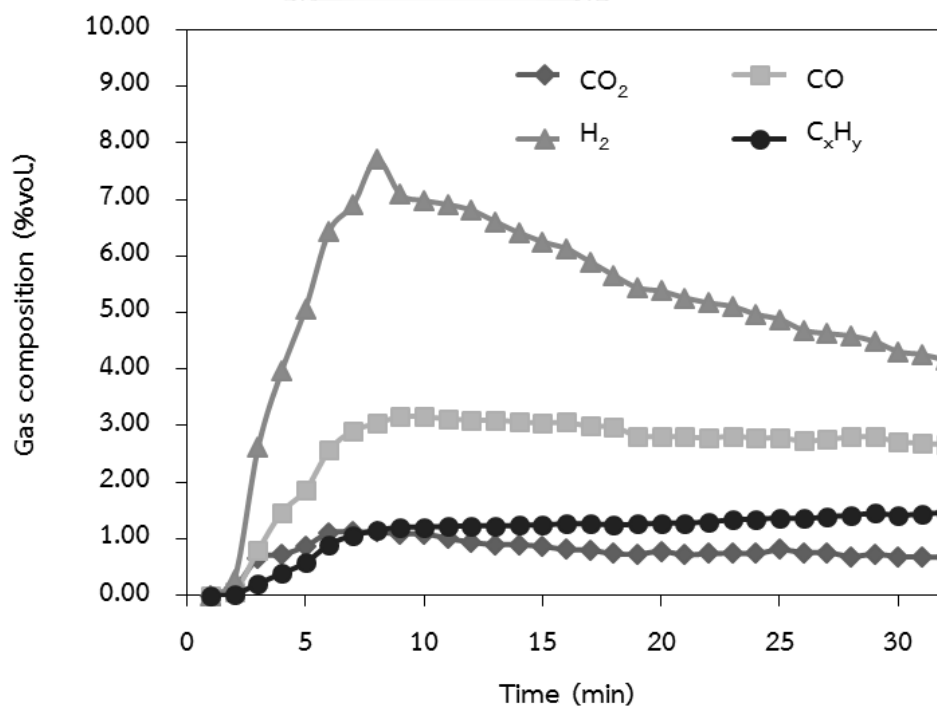
**Fig.C-21** Gas species from fast pyrolysis at 600°C with Pd/Al$_2$O$_3$
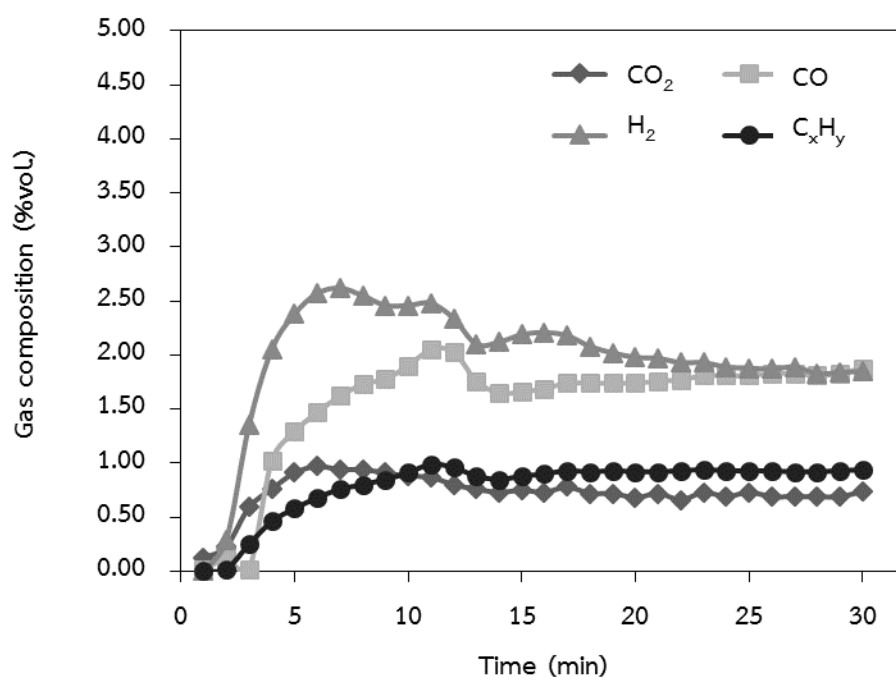
**Appendix D**

**Product distribution of fast pyrolysis by CFD model**
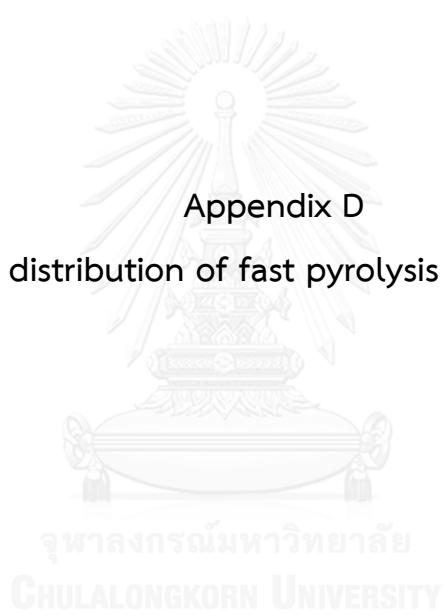
**Fig.D-1 Contour of product distributions at pyrolysis temperature of 400℃**
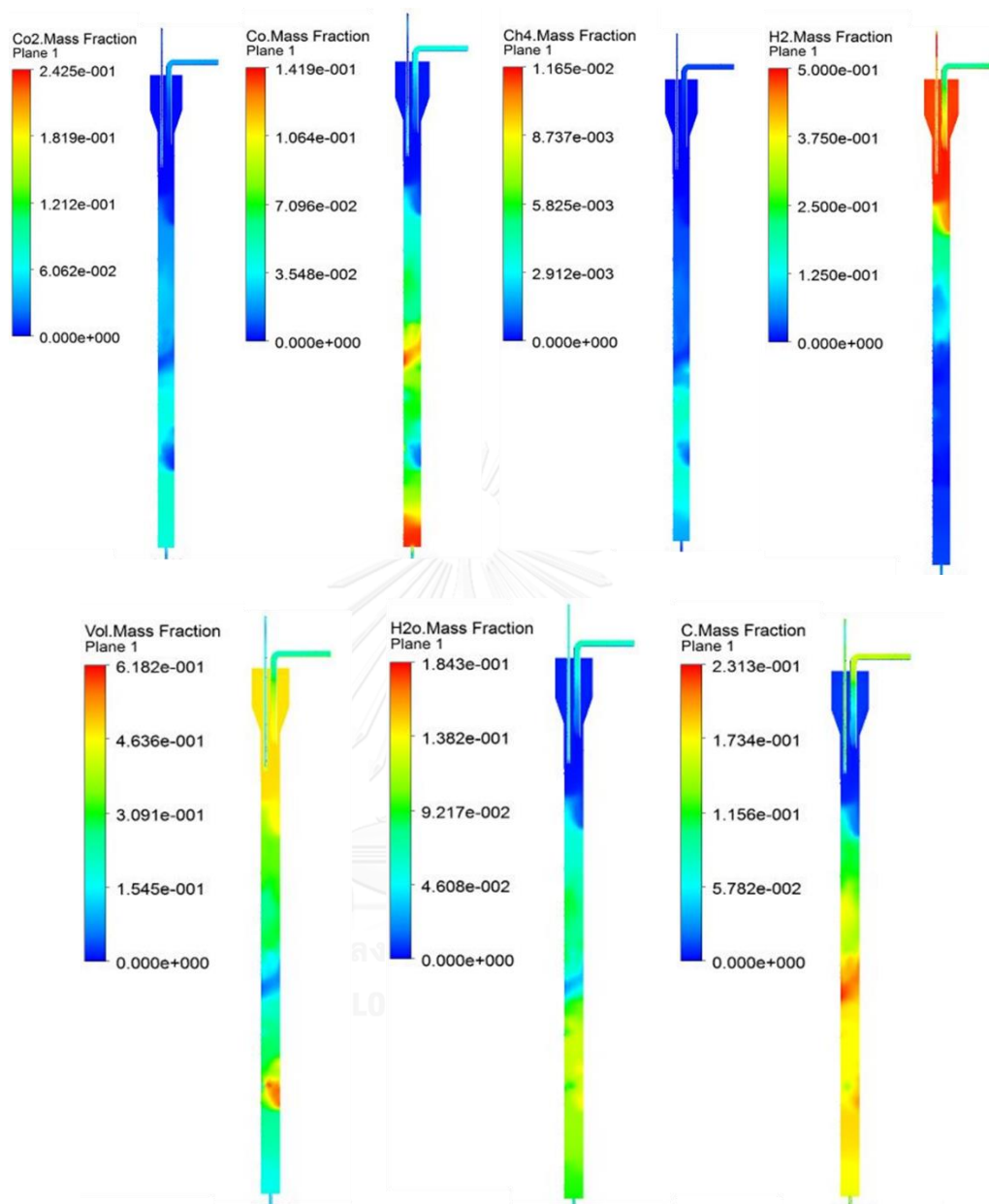
**Fig.D-2 Contour of product distributions at pyrolysis temperature of 500℃**
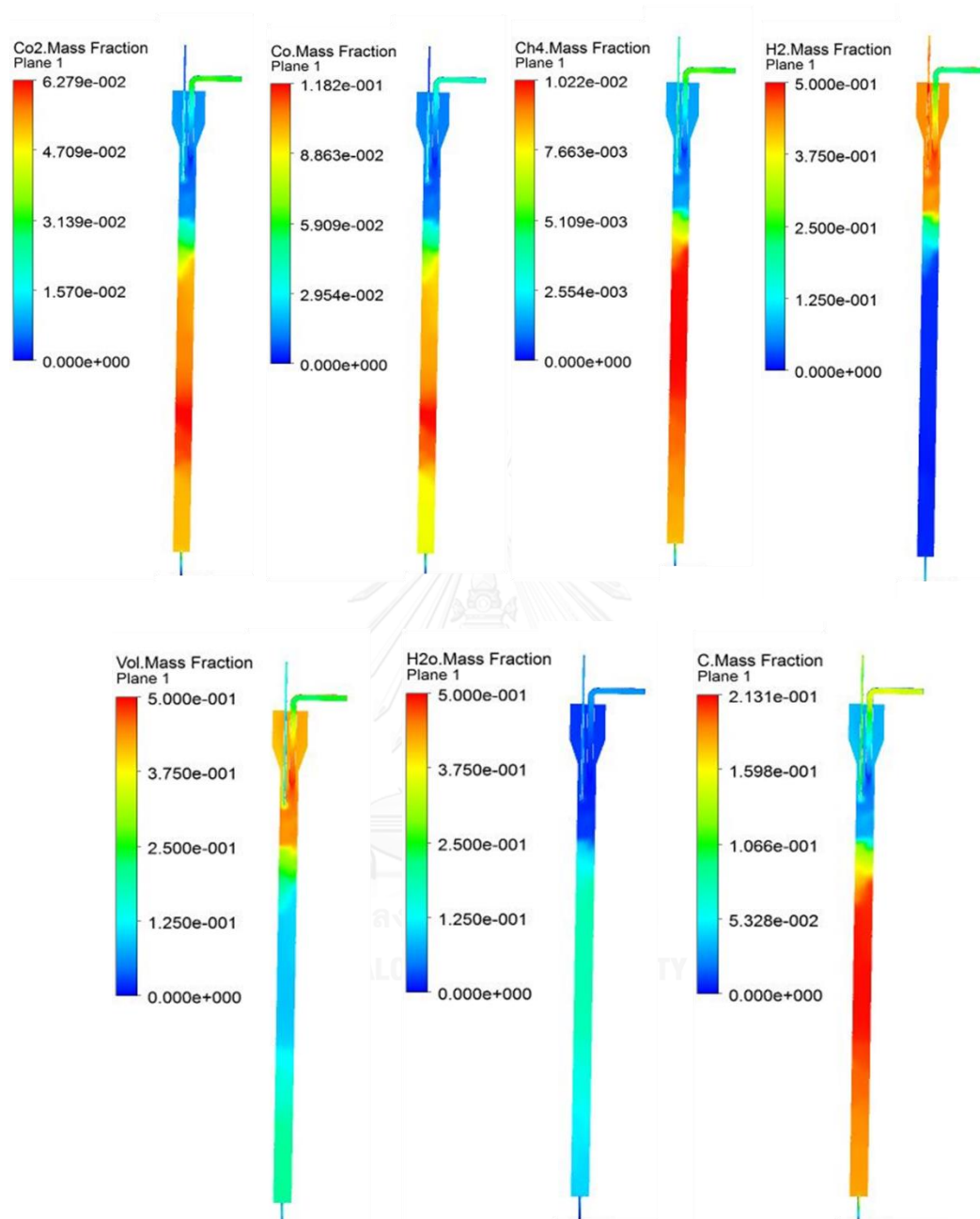
**Fig.D-3 Contour of product distributions at pyrolysis temperature of 600℃ (2 L/min)**
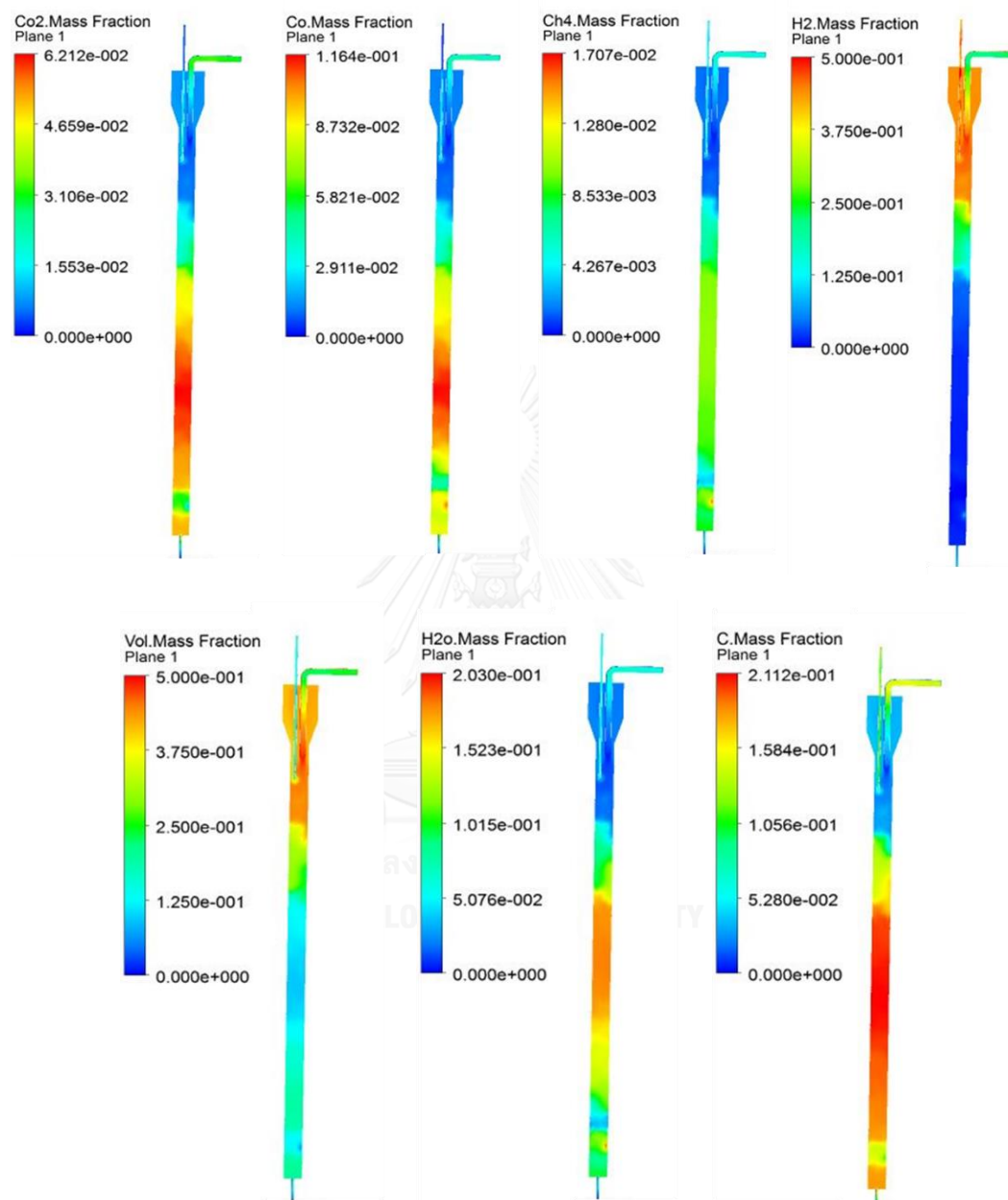
**Fig.D-4** Contour of product distributions at pyrolysis temperature of 600℃ (3 L/min)
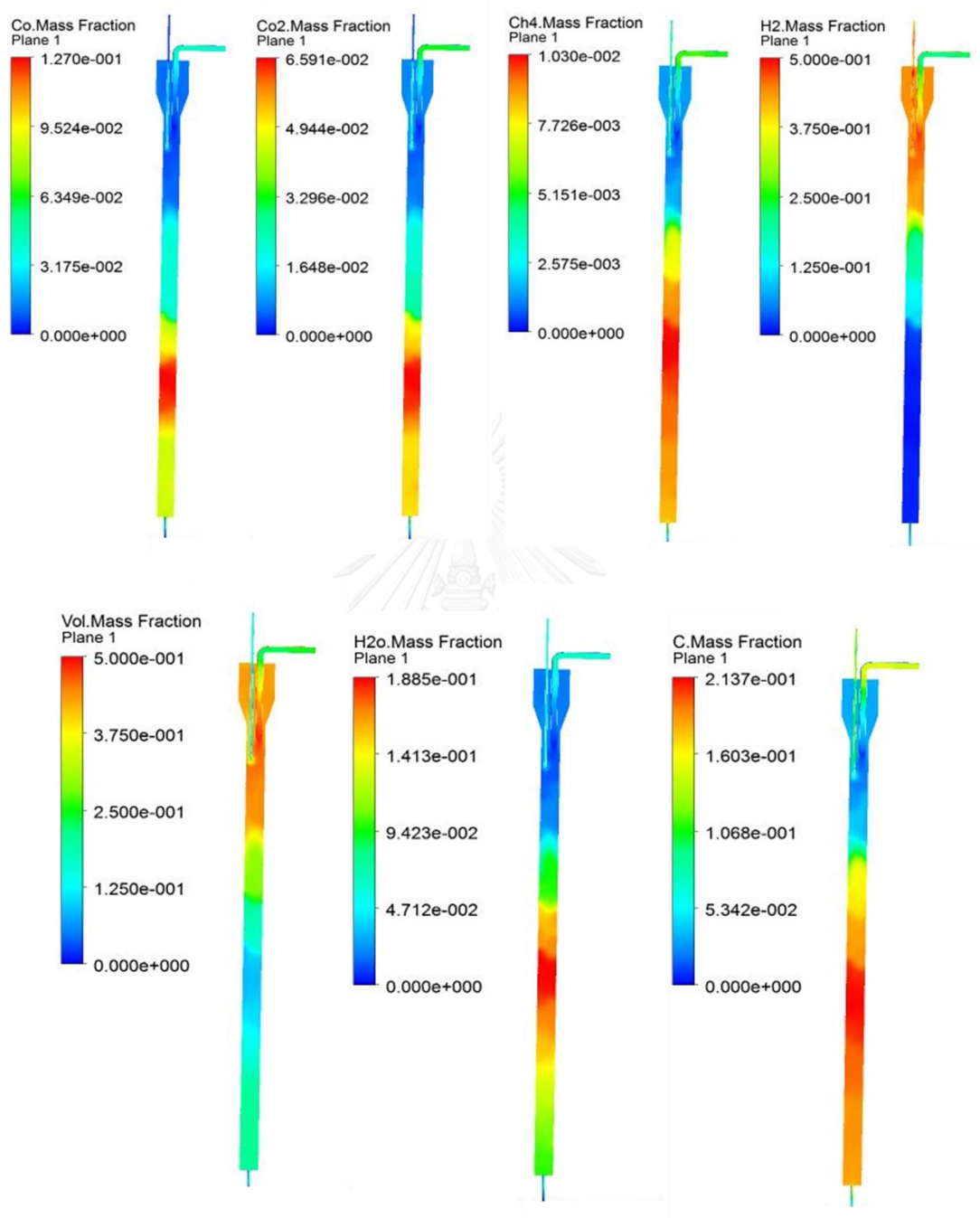
**Fig.D-4** Contour of product distributions at pyrolysis temperature of 600°C (4 L/min)
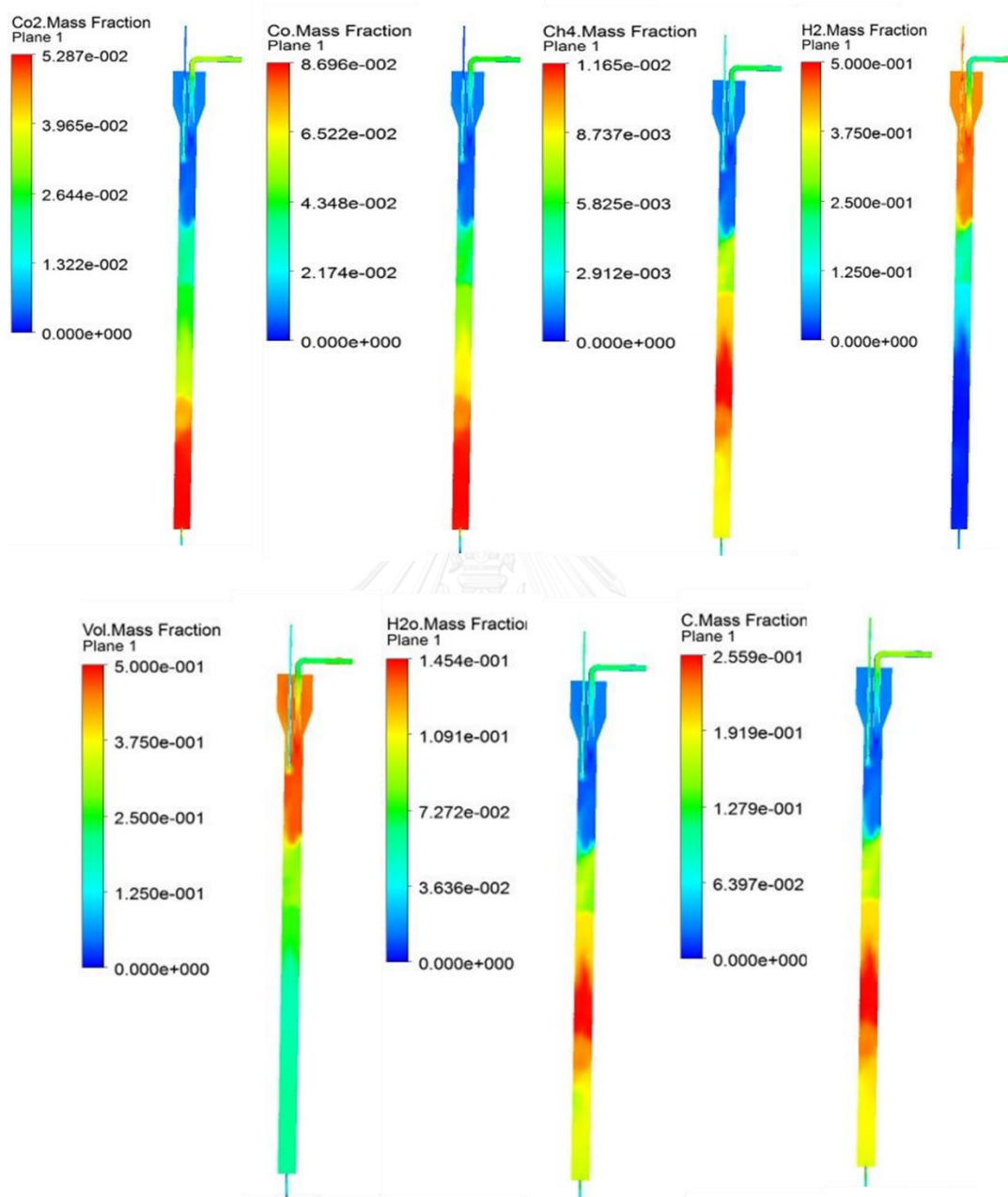
Fig.D-5 Contour of product distributions at pyrolysis temperature of 700°

**Appendix E**

**Characteristic of Catalysts and chars**
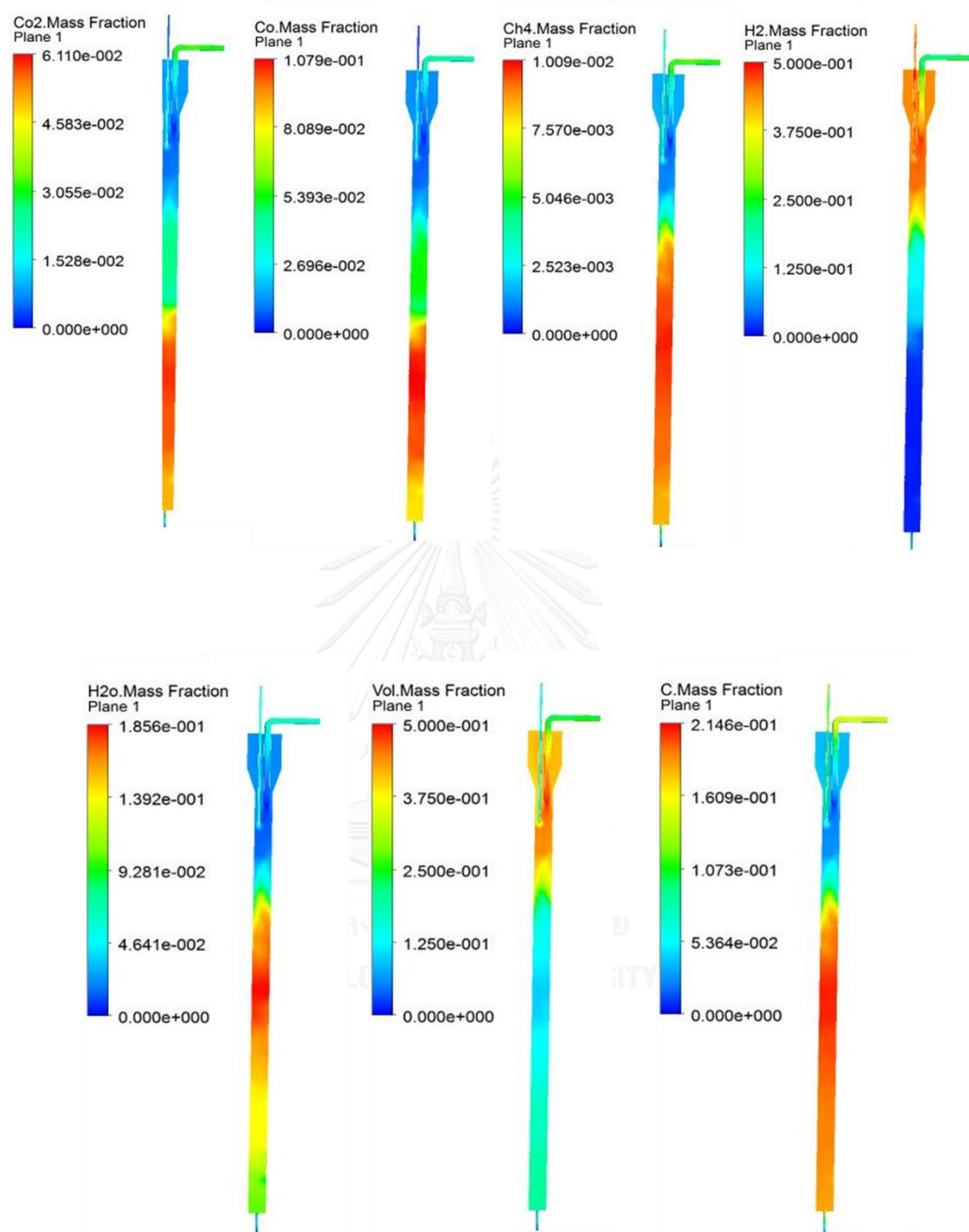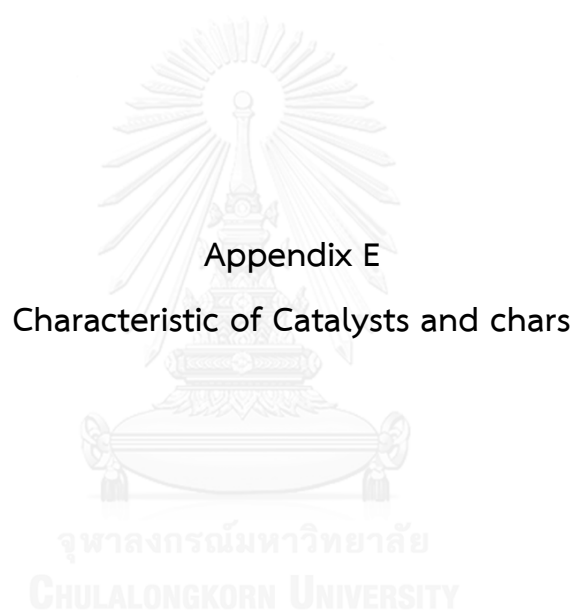
**Fig. E-1** TGA analysis of the M/AC catalysts (granule)
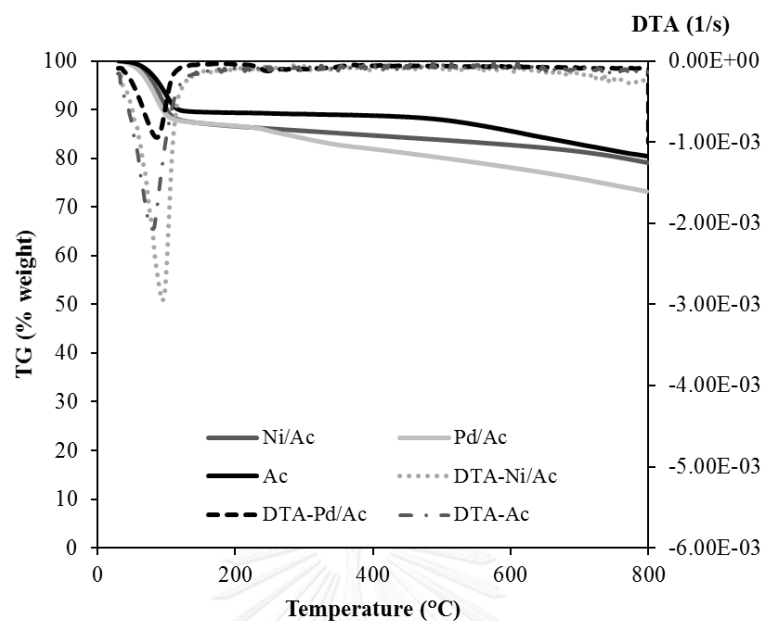


**Fig. E-2** TGA analysis of char from fast pyrolysis by drop tube reactor at 400°C
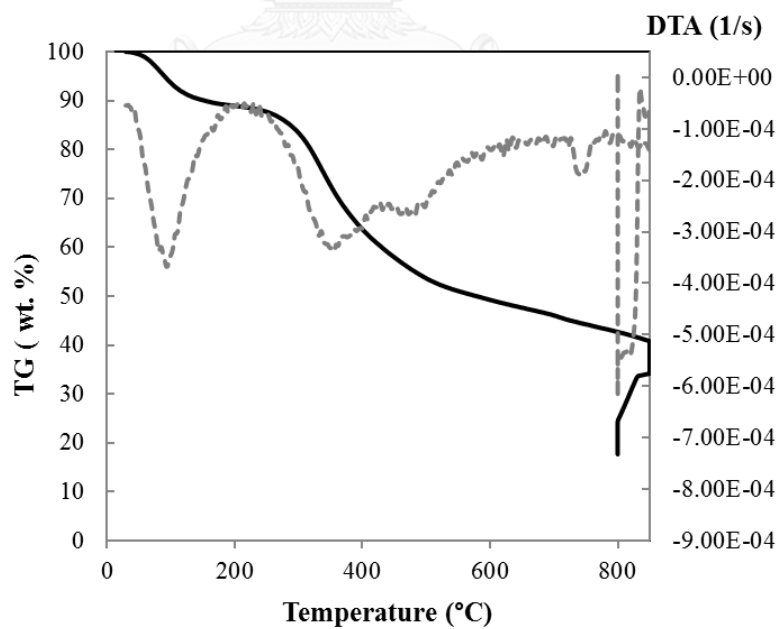
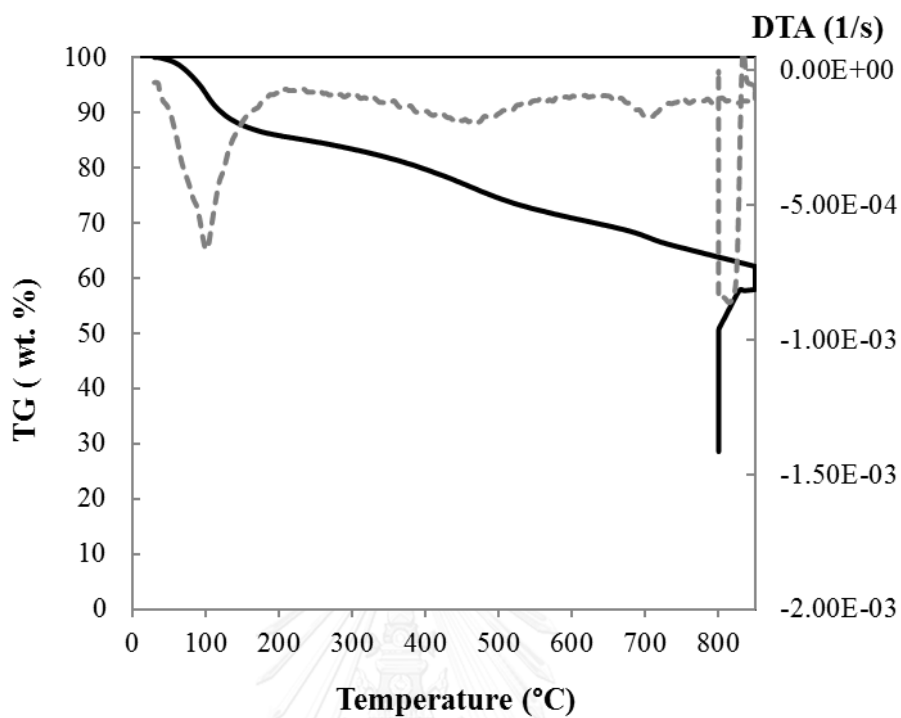**Fig. E-3** TGA analysis of char from fast pyrolysis by drop tube reactor at 500°C
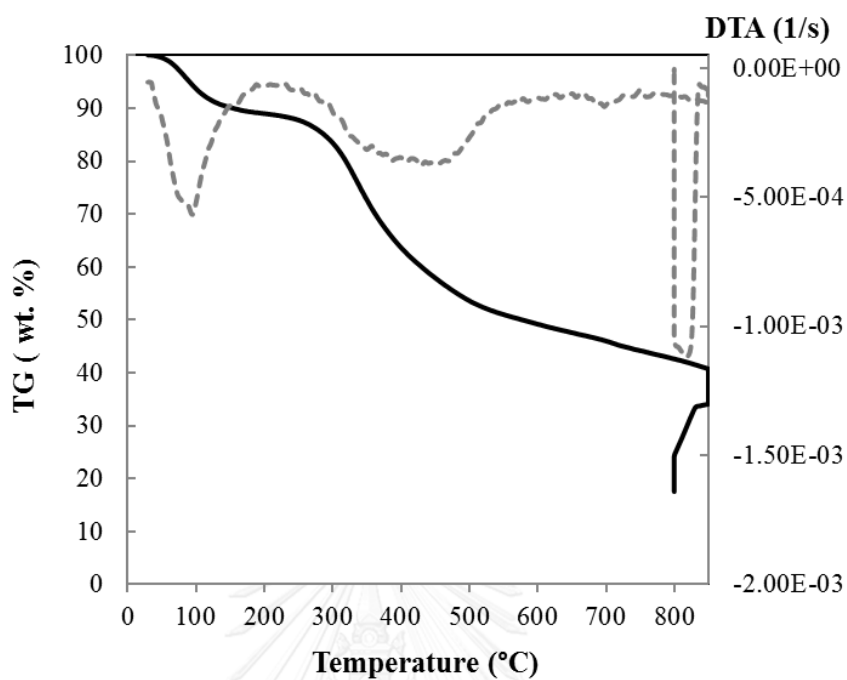


**Fig. E-4** TGA analysis of char from fast pyrolysis by drop tube reactor at 600°C
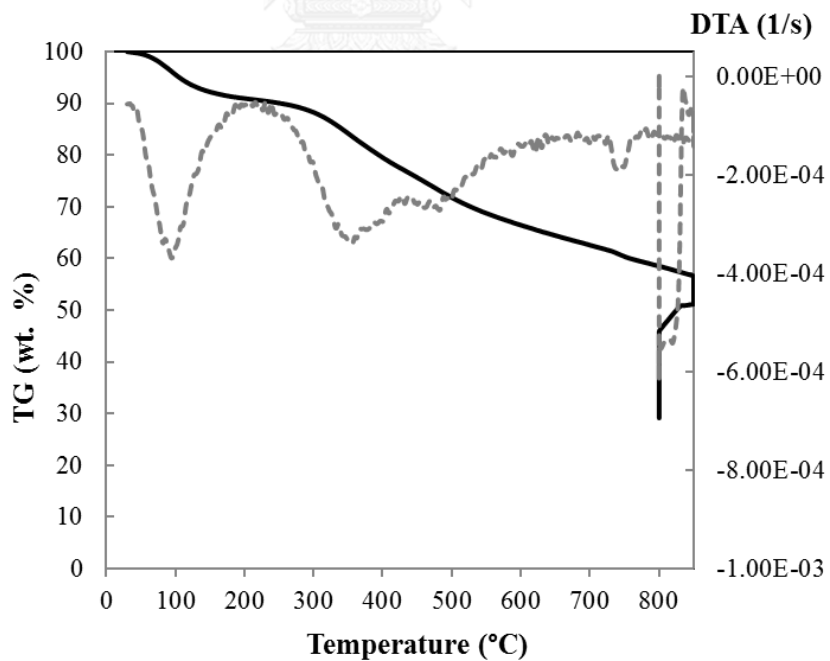
**Fig. E-5** TGA analysis of char from fast pyrolysis by drop tube reactor at 700℃



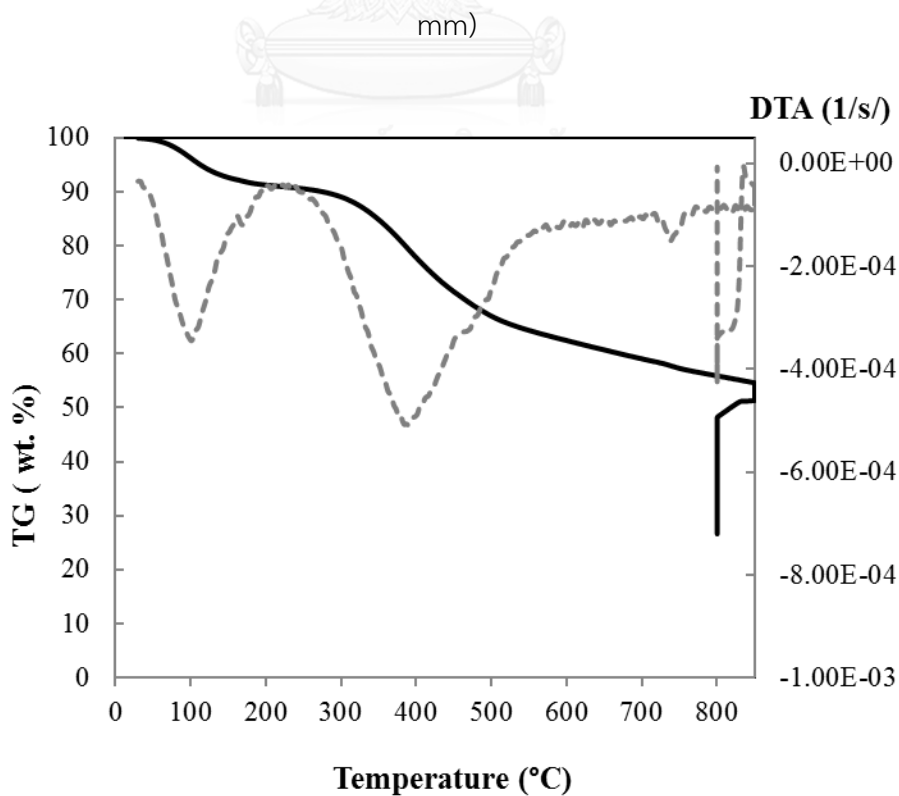**Fig. E-6** TGA analysis of char from fast pyrolysis by drop tube reactor at 600℃ (<125 mm)

**Fig. E-7** TGA analysis of char from fast pyrolysis by drop tube reactor at 600°C (0.425-0.850 mm)
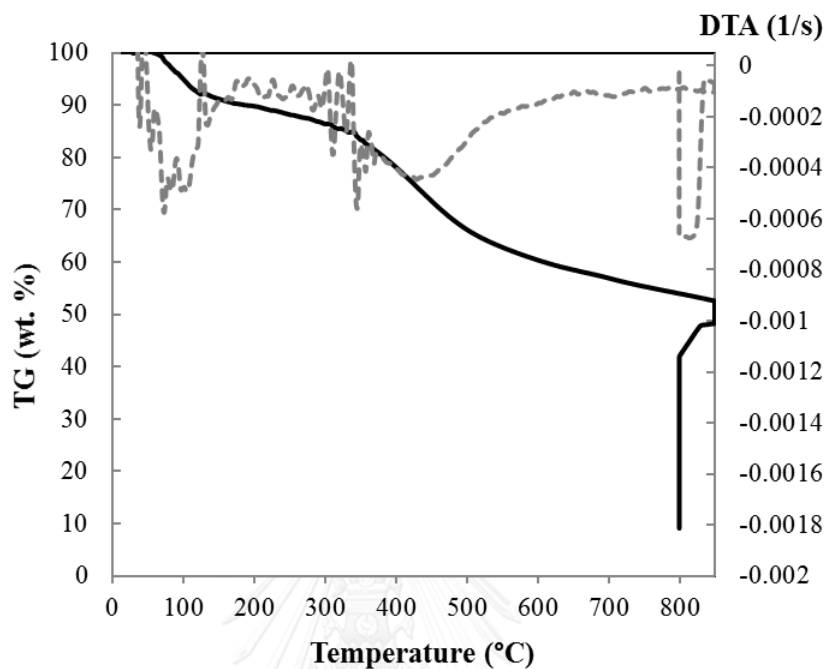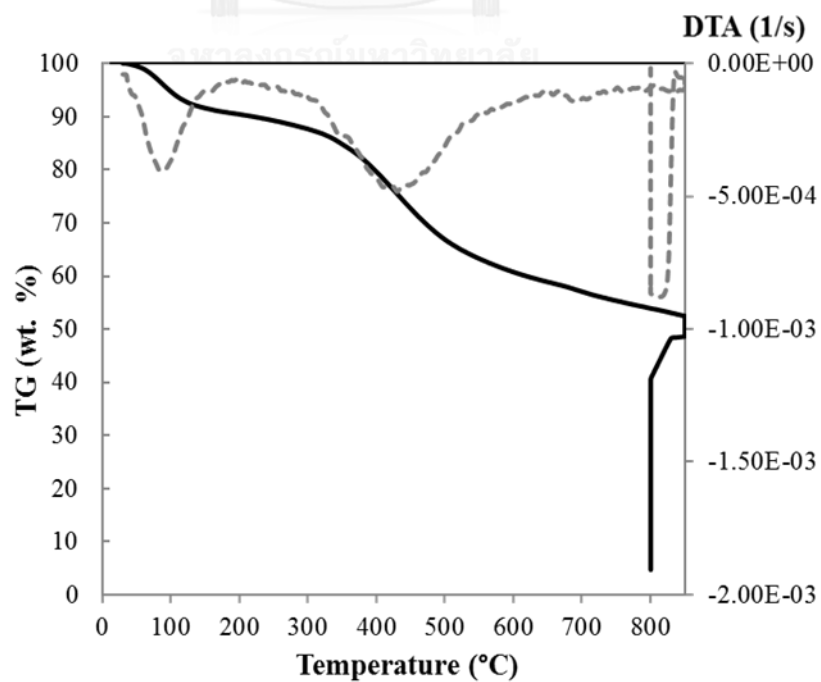


**Fig. E-8** TGA analysis of char from fast pyrolysis by drop tube reactor at 600°C (0.850-2.0 mm)

# VITA

Prangtip Kaewpengkrow was born in Bangkok, Thailand, on February 15th, 1986. After finishing high school in 2004, she entered the University in King Mongkut's Institute of Technology Ladkrabang, Thailand. In May of 2007 she completed a Bachelor of Science in Environmental Resources Chemistry. In September, 2011, she completed at Chulalongkorn University in Master degree of Engineering (Environmental Engineering).

Publications:

Kaewpengkrow, P., Atong, D., Sricharoenchaikul, V. 2014. Effect of Pd, Ru, Ni and ceramic supports on selective deoxygenation and hydrogenation of fast pyrolysis Jatropha residue vapors. Renewable Energy, 65(0), 92-101.

Kaewpengkrow, P., D. Atong, and V. Sricharoenchaikul, Catalytic upgrading of pyrolysis vapors from Jatropha wastes using alumina, zirconia and titania based catalysts. Bioresource Technology, 2014. 163(0), 262-269.

Kaewpengkrow, P., D. Atong, and V. Sricharoenchaikul, Selective catalytic fast pyrolysis of Jatropha residue with metal oxide impregnated activated carbon for upgrading bio-oil. International journal of hydrogen energy, 2017. 1-13

Kaewpengkrow, P., D. Atong, and V. Sricharoenchaikul, Effect of Metal Oxide/Alumina on Catalytic Deoxygentation of Biofuel from Physic Nut Residues Pyrolysis. International journal of hydrogen energy, 2017. (Article in press)

Permanent Address:

159/3 Kheharomklao 64

Klongsongtonnoon, Ladkrabank

Bangkok, Thailand 10520